1-1-2011

Isolation And Analysis Of Peptides Binding To Helix 69 Of E. Coli 23 S Rrna From M13 Phage Display

Moninderpal Kaur
Wayne State University

ISOLATION AND ANALYSIS OF PEPTIDES BINDING TO HELIX 69 OF *E. coli* 23 S rRNA FROM M13 PHAGE DISPLAY

by

MONINDERPAL KAUR

DISSERTATION

Submitted to the Graduate School

of Wayne State University,

Detroit, Michigan

in partial fulfillment of the requirements

for the degree of

DOCTOR OF PHILOSOPHY

2011

MAJOR: CHEMISTRY (BIOCHEMISTRY)

Approved by:

_____

Advisor Date

_____

_____

_____

_____

DEDICATION

To the love and support of my family

ACKNOWLEDGEMENTS

I thank Waheguru for all the perseverance He has bestowed on me for accomplishing this task and thus, the realization of my parents dream.

I thank my husband Amritpal Dhadiala for his never ending support, optimism and love. I am so fortunate to have him as my other half and a great friend. I am indebted to the love of my lovely daughter and son whose smiles are always there for me. I thank my parents and parents-in-law for their prayers and warm wishes. I would also like to thank my sisters and brother and my brothers-in-law and sisters-in-law for their continuous encouragement. I am blessed to have such a wonderful support system in my life.

I am grateful to have Dr. Christine Chow as my Ph.D advisor. She has a great passion for mentoring students in the scientific field. I am so thankful to her for believing in me and inspiring me for achieving my goal. I admire her deep scientific knowledge. I would like to keep seeking her advice on science related topics in future. I would like to thank my committee members Dr. Andrew Feig, Dr. Claudio Verani, and Dr.Alok Dutta for their insightful suggestions, critical comments and encouragement for my thesis work.

I thank Dr. Brain Shay and Dr. Lew Hryhorczuk for their help and training in Mass Spectrometry. I thank Nestor Ocampo for his kind help with computer related issues. I also thank Sharon Kelley, Melissa Barton, Erin Scully, Beverly Jacobs, Bernie Miezik and Deebie McCreless for their kind help in the paperwork issues.

I would like to say thank you to Dr. Edvin Klosi and Dr. Chamile Rupasinghe from Dr. Spaller's lab for sparing their valuable time in synthesizing peptides for me and Dr. Kris Ann Baker and Dr. Ash A. Saraiya from Dr. Phil Cunningham's group for teaching me the use of DNA sequencer.

Over the past years, I got the opportunity of working with wonderful labmates and friends. I thank Dr. Mei Li for her valuable friendship, laughs and helpful suggestions. I also thank Dr. Sanjaya Abeysirigunawardena, Dr. Santosh Mahto, Dr. Anne-Cécile E. Duc, Dr. Keshab Rijal, Srividya Pattabiriman for their endless support and I am so happy to state that they prove the age old saying that "friends in need, are friends in deed". I also thank Dr. Pei-Wen Chao, Dr. Yu-Cheng Chang, Dr. Tek Lamichhane, Dr. Dinuka Abeyderra and Dr. Papa Nii Asare-Okai for being great coworkers. I extend my gratitude to my past lab mates and friends for their warm support: Dr. Jean-Paul Desaulniers, Dr. Mina Sumita, and Dr. Jason W Kieltyka for their helpful conversations, and suggestions in the beginning years of my lab work.

Last but not the least, I would like to thank Wayne State University for providing me the opportunity of working in its research facilities.

TABLE OF CONTENTS

LIST OF TABLES

LIST OF FIGURES

CHAPTER 1

Introduction

1.1. Impact of antibiotic resistance on current drug research

Most microbes (bacteria or fungi) produce secondary metabolites that work as antibiotics, which serve as defense strategies in crowded environments (Levy, S.B., 1994). Discovery of the penicillin family of antibiotics facilitated progress of the so-called golden era of these drugs (1940-1960), at which time present-day antibiotics were identified. Unfortunately, during the same time period, antibiotic resistance also evolved due to environmental pressures of antibiotic overuse and the rapid growth ability of bacteria (Benveniste, R. *et al*., 1973; Overbye, K.M. *et al*., 2005). Antibiotic resistance in bacteria results from their ability to oppose the inhibitory (bacteriostatic) or killing (bacteriocidal) effects of antibiotics (Vakulenko, S.B. & Mobashery, S., 2003).

Antibiotic resistance has been a major driving force behind the discovery of new antibiotics. The first drug-resistant strains of pathogenic bacteria appeared predominantly in hospital settings, where the use of the antibiotics was most prevalent (Levy, S.B., 1998). In the 1930s and 1940s, the sulfonamide-resistant *Streptococcus pyogenes* (Levy. S.B., 1982; Coonan, K.M. *et al*., 1994) and the penicillin-resistant *Staphylococcus aureus* (Forbes, G.B., 1949) strains emerged in London military and civilian hospitals. Soon after, strains of *Mycobacterium tuberculosis* that were resistant to streptomycin also appeared (Crofton, J. *et al*., 1948). The enteric bacteria species, namely *Escherichia coli* (*E. coli*) (Cavalli, L.L *et al.*, 1952), *Shigella* and *Salmonella* (Watanabe, T. *et al.*, 1961), developed resistance to multiple drugs in the late 1950s

and 1960s, causing severe problems to people in developing countries. The threat of these bacterial species was not realized by the industrialized nations until the appearance of ampicillin-, chloroamphenicol-, and tetracycline-resistant *Haemophilus influenzae* and ampicillin-resistant *Neisseria gonorrhoeae* (Klingeren, B.V *et al*., 1977; Elwell, L.P. *et al*., 1977) strains in the 1970s. These pathogens caused untreatable respiratory and genitourinary diseases. In developing countries, overuse of antibiotics, poor sanitation conditions, and lower health-care funds further fueled the emergence of the antibiotic-resistant bacterial species (Okeke, I.N. *et al*., 1999).

Since the 1980s, the presence of multiple-drug-resistant (MDR) bacteria or the so-called “superbugs” caused a tough dilemma faced by modern medicine, since these organisms make drug therapy more expensive and sometimes unsuccessful. The superbugs include the well-known pathogens methicillan-resistant *Staphylococcus aureus* (MRSA), vancomycin-resistant enterococci (VRE), and drug-resistant *Escherichia coli*, *Pseudomonas aeruginosa*, *Stenotrophomonas maltophilia*, *A. baumannii*, and *Burkholderia cepacia* (Wright, G.D., 2007). In the case of *Staphylococcus aureus* strains present in the United States and United Kingdom, 40-60% are methicillin-resistant (MRSA). These MRSA strains are also showing resistance to vancomycin (Weigel, L.M. *et al*., 2003). In parts of Asia and China, some strains of *E. coli* that cause urinary tract infections have also become multiple-drug-resistant (MDR), including resistance to fluoroquinolones (Wang, H. *et al.,* 2001). Resistance in pneumococci, which causes severe ear infections and pneumonia in children worldwide, continues to rise. Individuals who were first resistant to penicillins have now acquired resistance to the macrolides and tetracyclines in many parts of the world (Schrag, S.J.

et al., 2004). The emergence of MDR strains has raised the health-care costs in United States from $150 million to $30 billion per year since the occurrence of the drug resistance has gone beyond the hospitals (Rubin, R.J. *et al*., 1999; Phelps, C.E, 1989).

The above-mentioned drug-resistance problems and their economic impact on society lead to the question of how the bacteria acquire resistance. Drug resistance is mainly achieved through transmittance of mobile genetic elements, such as bacteriophages, plasmids, naked DNA, or transposons that have genes for supplying bacteria with different resistance mechanisms (Hall, R.M. *et al.*, 1999; Nandi, S. *et al.*, 2004; Clewell, D.B. *et al.,* 1986). The resistance mechanisms present in these organisms are numerous and vary among different species (summarized in Figure 1.1). Some of the mechanisms are directed towards altering the antibiotic structures, such as using β-lactamase enzymes that inactivate penicillins and related compounds (Vakulenko, S.B. *et al*., 2003; Mingeot-Leclercq, M. *et al*., 1999). Another class of mechanisms involves pumping the antibiotics from the bacterial cell through efflux, which includes the tetracyclins and fluoroquinolones (Schweizer, H.P., 2003). A third mechanism involves modification of the antibiotic targets such as the ribosome, or metabolic enzymes for DNA metabolism or cell-wall synthesis, which makes the drug incapable of inhibiting important functions of the bacterial cell (Prammananan, T. *et al*., 1998) (Figure 1.1).

The impact of antibiotic resistance on the modern therapeutic world has obliged scientists to think deeply at the molecular level for the discovery and development of new antibiotics. For the discovery of novel drug leads, structure-based drug design (SBDD) and combinatorial library approaches gained success in the early 1990s and

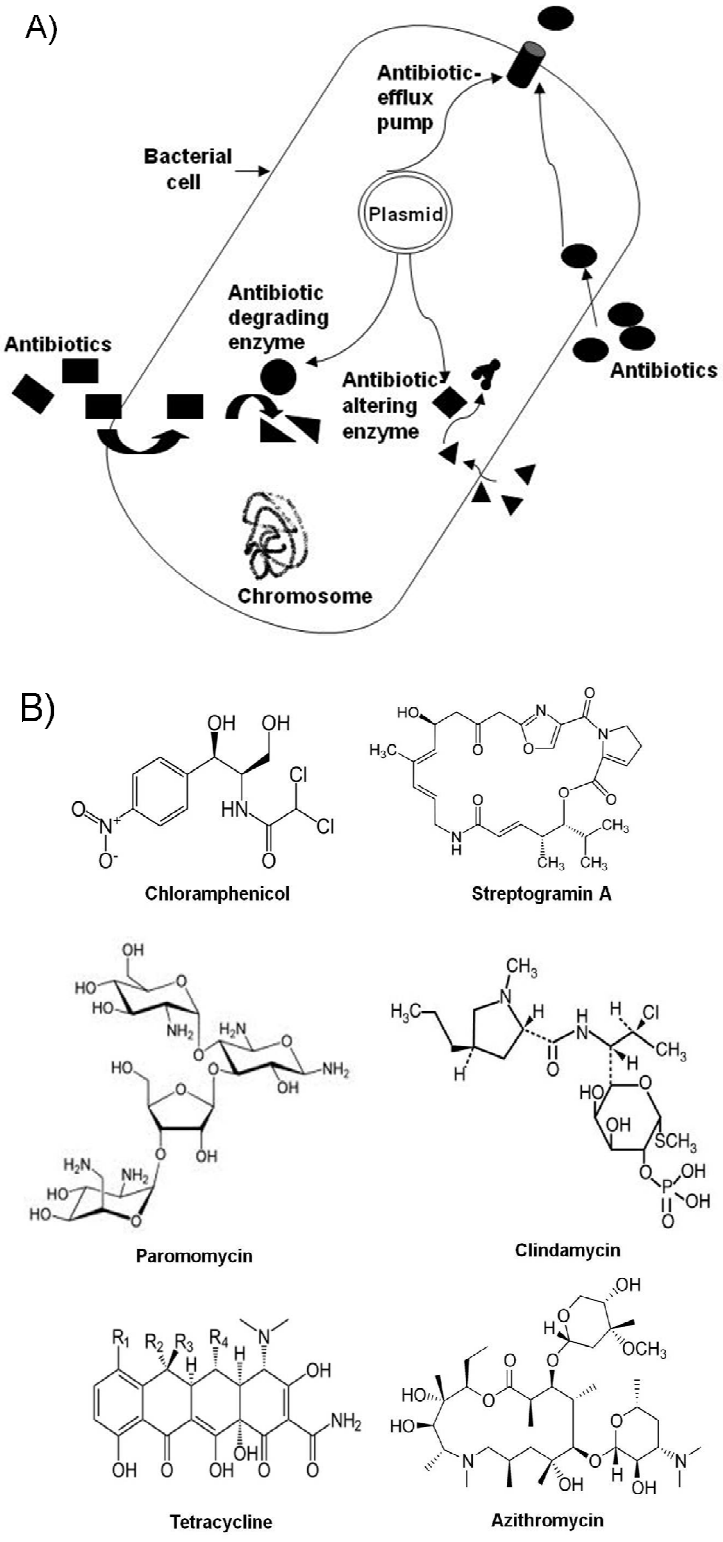

Figure 1.1.A) Some of the general mechanisms adopted by the bacterial cell for defending itself against environmental stress such as antibiotics are shown. B) The chemical structures of some antibiotics hindering protein synthesis are shown.

both practices are an integral part of the entire drug-discovery process. A wealth of genomic, proteomic, and structural information on pathogenic bacteria has further helped to streamline this process by providing information for new targets. The influence of SBDD has been clearly exhibited in the area of AIDS, in which five protease inhibitors have been designed based on the structural data of HIV-1 protease (Roberts, N.A. *et al*., 1990; Erickson, J., *et al*., 1990; Dorsey, B.D. *et al*., 1994).

Structure-based drug design involves multiple steps before an optimized lead compound goes into phase I trials. In the first step, a target with a potential binding site is selected. For example, the antimicrobial drug targets should have an essential role in the pathogen, be present only in the pathogen, and be able to be inhibited by a small molecule. Next, the binding site of the target should be a well-defined pocket with a variety of possible hydrogen-bond donors and acceptors, hydrophobic features, and size of a molecular surface. Examples in this category include the active sites of enzymes (Enyedy, I.J. *et al*., 2001), RNA secondary structural features (Lind, K.E. *et al*., 2002), and various protein-protein interactions. After selection of the target site, its structure is resolved by one of the three major methods: X-ray crystallography, NMR, or homology modeling. The compounds from a database are arranged into the well-defined pocket of the structure. After that, they are categorized based on their steric and electrostatic interactions with the target spot. The finest compounds are tested with the biochemical assays. In the second step, the structure of the compound (from the first cycle with micromolar inhibition *in vitro*) with the target is determined. The structure is then studied to reveal the sites on the compound to be optimized in order to raise its effectiveness. In later cycles, the optimized lead compound is synthesized with

improved features; the structure determination of the new target-lead complex is carried out and thus, after quite a few cycles, the optimized compound generally demonstrates an increase in binding and specificity towards the target (Anderson, A.C., 2003).

Some of the common experimental methods of high-throughput screening for finding the lead compound is applying combinatorial chemistry, in which thousands of compounds can be tested for biochemical assays (Lind, K.E. *et al*., 2002), the molecular-biology-based phage display (Smith, G.P. *et al*., 1997), mRNA library (Lipovsek, D. *et al*., 2004), ribosome display (Lipovsek, D. *et al*., 2004), and SELEX (Osborne, S.E. *et al*., 1997; Ellington, A.D. *et al*., 1990). The computer-aided methods for high-throughput screening are divided into three classes: inspection, virtual screening, and *de novo* generation. In the first section, known molecules that bind to the target site, such as in enzymes and in protein-nucleic acid interactions, are altered to become inhibitors by exploiting their complementary interactions in the target site (Roberts, N.A. *et al*., 1990; Dorsey, B.D. *et al*., 1994; Varney, M. *et al*., 1992; Chan, D. *et al*., 2001). In the second method of virtual screening, the molecules from available databases of small molecules are positioned at the target site and scored based on their calculated properties within the target site. In the *de novo* category, the small motifs of the molecules such as benzene rings, carbonyl groups, amino groups are arranged in the target site and scored. The final compounds created from the study are synthesized and tested for their binding properties. One of the computer softwares available for this type of virtual screening is DOCK (Kuntz, I. *et al*., 1982); ADAM (Mitzutani, M. *et al*., 1994) and others for *de novo* generation are LUDI (Boehm, H., 1992) and GRID (Goodford, P., 1985). All of these techniques aim to narrow the drug discovery timeline

by grading the promising lead compounds from active to nonactive, and decreasing the compounds required for synthesis.

Based on these criteria, in the discipline of developing effective antimicrobials, the bacterial ribosome is a fully validated antibacterial target, since it fulfills most of the requirements for a good target. It is targeted by half of the known antibiotics, such as aminoglycosides, macrolides, ketolides, and tetracyclines (Hansen, J.L. *et al*., 2002; Carter, A.P. *et al*., 2000). These antibiotics halt the ribosome's cellular function of protein synthesis by interacting with the ribosomal RNA rather than its related proteins. The common aminoglycoside antibiotics work as antibacterials by binding mainly to the bacterial decoding center (30S subunit, A-site rRNA), which is structurally different from the human decoding center (Lynch, S.R. *et al*., 2003). High-resolution crystal structures of the ribosomal subunits with antibiotics bound to them are a major achievement in the structural biology field (Wimberly, B.T. *et al*., 2000; Carter, A.P. *et al*., 2000; Ban, N. *et al*., 2000; Nissen, P. *et al*., 2000). Structural information for the ribosomal subunit is enhanced by the X-ray structures of smaller model systems such as the A site (Agalarov, S.C. *et al*., 2000; Fourmy, D. *et al*., 1996; Wimberley, B.T. *et al*., 1999).

The selectivity of the antibiotics for bacterial over eukaryote ribosomes is clearly apparent from structural knowledge. One case is the higher affinity of paromomycin for the bacterial A-site rRNA over the corresponding eukaryotic A site, as well as decreased affinity for a variant with methylation at A1408, which gives resistance to the antibiotic (Fourmy, D. *et al*., 1998). The high-resolution structure of paromomycin with the A-site rRNA fragment shows the role of water-mediated contacts, which could not be observed in the ribosome structures (Vincen, Q. *et al*., 2001). Thus, structural

information based on smaller model systems gives relevance to the biochemical and resistance data (Ogle, J.M. *et al*., 2001).

The present RNA structural data of the ribosomal subunits and its complexes with the antibiotics, such as aminoglycosides, allowed computational scientists to design and use drug-discovery models for new compounds. Attempts for designing neamine analogs as new antibacterials were lead by researchers at Wayne State University and a company named RiboTargets (Russell, R.J. *et al*., 2003). These compounds showed enhanced activity against several pathogenic bacteria, but were not able to reach the clinical level status. Another attempt was made by the company Vernalis Ltd., in which the target of interest was the A site or the decoding center located in the 30 S subunit of the ribosome (). Over one million compounds were screened against this target and 34 were shown to have the potential as leads for a novel antibacterial.

For possible new antibiotics against the 50S subunit of the ribosome, the available structure of chloramphenicol bound to the *D. radiodurans* bacterial ribosome and those of the chloramphenicol analogs was used (Johansson, D. *et al*.; 2005). The main aim was to design linker compounds between chloramphenicol and dinucleotides of the P-loop in 23 S rRNA of the 50 S subunit. With the use of the molecular dynamics simulations, Johansson and coworkers chose six compounds for synthesis, and one compound was verified through RNA-footprinting to be more effective than the parent chloramphenicol.

As structural genomics, bioinformatics, and computational power keeps advancing, more accomplishments in structure-based drug design are expected to follow. Since the emergence of antibiotic resistance is inevitable, clear rethinking of

strategies for preserving the useful life of the antibiotics calls for altering the behavior of both patients and physicians in their consumption.

1.2. The ribosome: its organization and cellular tasks

Each living cell in an adult human body has about a billion proteins that are continuously being degraded; therefore, a continuous production of these proteins is needed. The enormous task of synthesizing the proteins from the DNA genetic code is called translation and is performed by an intricate apparatus composed of ribosomes, messenger RNA (mRNA), transfer RNAs (tRNA), and various protein factors (Yonath, A., 2009). The ribosome is a complete ribonucleoprotein assembly that is the key player in the process of translation. All ribosomes are composed of two unequal subunits with their own defined functions. The small subunit makes available the path along which the mRNA advances, the decoding center for codon-anticodon interactions, and the mechanistic features for controlling translation fidelity. The large subunit contains the site for peptide-bond formation between the two amino acids and the exit tunnel for the nascent protein (Green, R. *et al*., 1997). These organelles have a molecular weight of about 2.5 MDa in bacteria and about 4 MDa in higher living beings (Davidovich, A. *et al*., 2009).

Usual mammalian cell contains over a million ribosomes and a bacterial cell has on the order of 100,000 ribosomes. The ribosomal RNA (rRNA) has the capacity of catalyzing peptide-bond formation between two amino acids, thus giving ribosome the distinction of being a ribozyme (Yonath, A. 2003). Ribosomes from all kingdoms of life have maximum sequence conservation in the functional regions, such as the decoding

center and the peptidyl-transferase center (PTC) (Ban, N. *et al*., 2000; Schluenzen, F. *et al*., 2000). The non-ribosomal participants of the translation process include the mRNA chain which carries the genetic information from the DNA (Brenner, S. *et al*., 1961), and the tRNAs which transport the cognate amino acids to the ribosome (Hecht, L.I. *et al*., 1959).

The two unequal subunits of the ribosome associate during the initiation step of protein synthesis through an intricate network of intermolecular bridges and work cooperatively during the elongation process of translation (Bashan, A. et al., 2003) (Figure 1.2.A). Both subunits are made of RNA and proteins. The entire ribosome in bacteria has a sedimentation coefficient of 70 S and in eukaryotes has a sedimentation coefficient of 80 S. In bacteria, the small subunit is designated as 30 S and has one RNA chain (16 S) of about 1500 nucleotides and 20-21 proteins (Schmeing, T.M. *et al*., 2009). The large subunit in bacteria is assigned as 50 S and has two RNA chains (23 S and 5 S) of about 3000 nucleotides and different 31-35 proteins and 120 nucleotides, respectively (Schmeing, T.M. *et al*., 2009) (Figure 1.2.B). The intersubunit surface of the ribosome is composed of rRNA and is occupied with tRNAs during translation. The anticodons of tRNAs form base pairs with codons on the mRNA in the 30 S subunit. Their 3'-CCA ends, which carry the growing polypeptide chain and incoming amino acid, contact the 50 S subunit. The PTC, where peptide bond formation is catalyzed, is on the 50 S subunit. This function shows that unlike protein enzymes, RNA is the main participant in the protein synthesis (Schmeing, T.M. *et al*., 2009).

A)

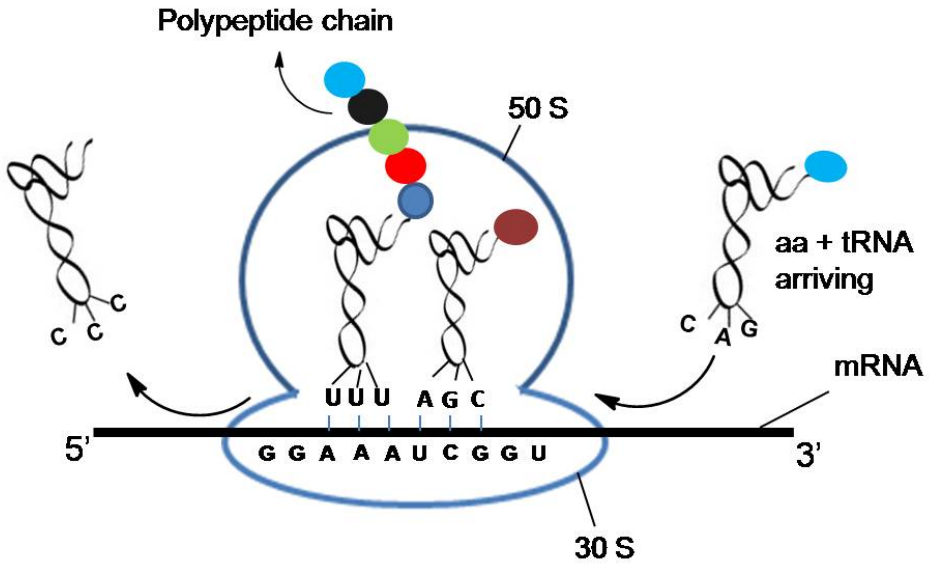

B)

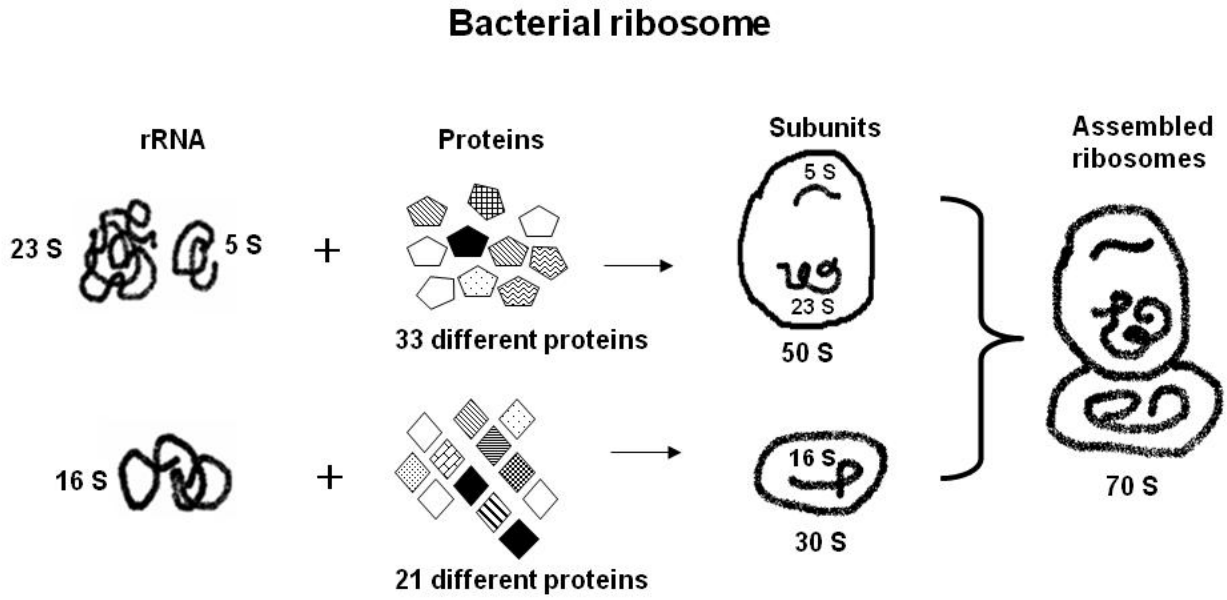

Figure 1.2. A) The schematic of ribosome showing the two subunits 50 S and 30 S, mRNA, tRNAs with their amino-acids and the growing polypeptide chain is depicted. B) The assembly of the bacterial ribosome from its large (50 S) and small (30 S) subunits with their respective rRNAs and proteins is shown.

The proteins mostly occupy the peripheral globular domains of the ribosome with their elongated loops or terminal extensions passing through rRNA interior. Thus, they seem to carry out the role of stabilizing the rRNA tertiary structure (Klein, D.J. *et al*., 2004). There are a few examples of proteins that appear to play a dynamic role in ribosome function. The L7/L12 stalks of the proteins L7 and L12 appear to be involved in tRNA translocation in the large subunit (Kothe, U. *et al*., 2004). The proteins S5, S6, and S12 are believed to help with mRNA (Ogle, J.M. *et al*., 2002).

Outstanding progress has been made in the field of ribosomal crystallography to learn about the function of ribosomes at the atomic level. Most of the existing ribosome crystal structures are from eubacteria *Deinococcus radiodurans* (D50S; Harms, J. *et al*., 2001), *Thermus thermophilus* (T30S, Schluenzen, F. *et al*., 2000; Wimberly, B.T. *et al*., 2000 and T70S, Yusupov, M.M. *et al*., 2001), the archaeon *Haloarcula marismortui* (H50S; Ban, N. *et al*., 2000), and the bacteria *Escherichia coli* (70S, Schuwirth, B.S. *et al*., 2005). Additional crystal structures include functional complexes of the small subunit with mRNA (Kaminishi, T. *et al*., 2007) and tRNAs (Selmer, M. *et al*., 2006) or modified tRNAs, (Dunham, C.M. *et al*., 2007), the large subunit with non-ribosomal secondary factors, such as the trigger factor (Baram, D. *et al*., 2005; Schluenzen, F. *et al*., 2005), and 50S with the ribosomal recycling factor (Pai, R.D. *et al*., 2008). Extensive studies of the bacterial ribosome through crystallography have contributed immensely to the comprehension of the universal process of protein synthesis. It has provided insight into the important issues concerning ribosome of the eukaryotic kingdom and revealed the different approaches for the development and improvement of ribosomal antibiotics.

Ribosomes are responsible for the conversion of the genetic information carried by the mRNAs into specific sequences of amino acids. Although the events of the translation process are universally conserved, major differences exist in the detailed mechanism of each phase. The translation in bacteria engages relatively few factors as compared to the complex process in eukaryotes (de Cock, E. *et al*., 1999). Bacterial translation on the ribosome is divided into four main phases, namely, initiation, elongation, termination, and ribosome recycling. In bacteria, specific protein factors are involved in the various stages of the initiation (McCutcheon, J.P. *et al*, 1999; Carter, A.P. *et al*., 2000), elongation (Stark, H. *et al*., 1997; Agrawal, R.K. *et al*., 1998), termination (Rawat, U.B.S. *et al*., 2003; Klaholz, B.P. *et al*., 2003; Klaholz, B.P. *et al*., 2004), and ribosome recycling (Pai, R.D. *et al*., 2008).

The third phase of translation, which is relevant to this thesis work, is termed termination, since it leads to the end of protein synthesis (Figure 1.3). This process takes place on the ribosome as a response to a stop codon in the A site. The codons UAG, UAA, and UGA are known as stop codons. This process is assisted by various release factors (RFs). There are two classes of RFs: class I, a codon-specific RF, and class II, a nonspecific RF (RF3) in bacteria (Nakamura, Y. *et al*., 2000). These RFs have tripeptide anticodons, Pro-Ala-Thr in RF1 and Ser-Pro-Phe in RF2 that determine the RF identity and the stop codon on the mRNA (RF1 for UAG/UAA and RF2 for UGA/UAA). After encountering the respective stop codon, the RFs relay the signal from the mRNA stop codon present in the A site to the PTC, where they are believed to trigger hydrolysis of the peptidyl tRNA (Freistroffer, D.V., *et al*., 1997; Kisselev, L.L. and Buckingham, R.H., 2000). Following the release of polypeptides by RFs, the ribosomal

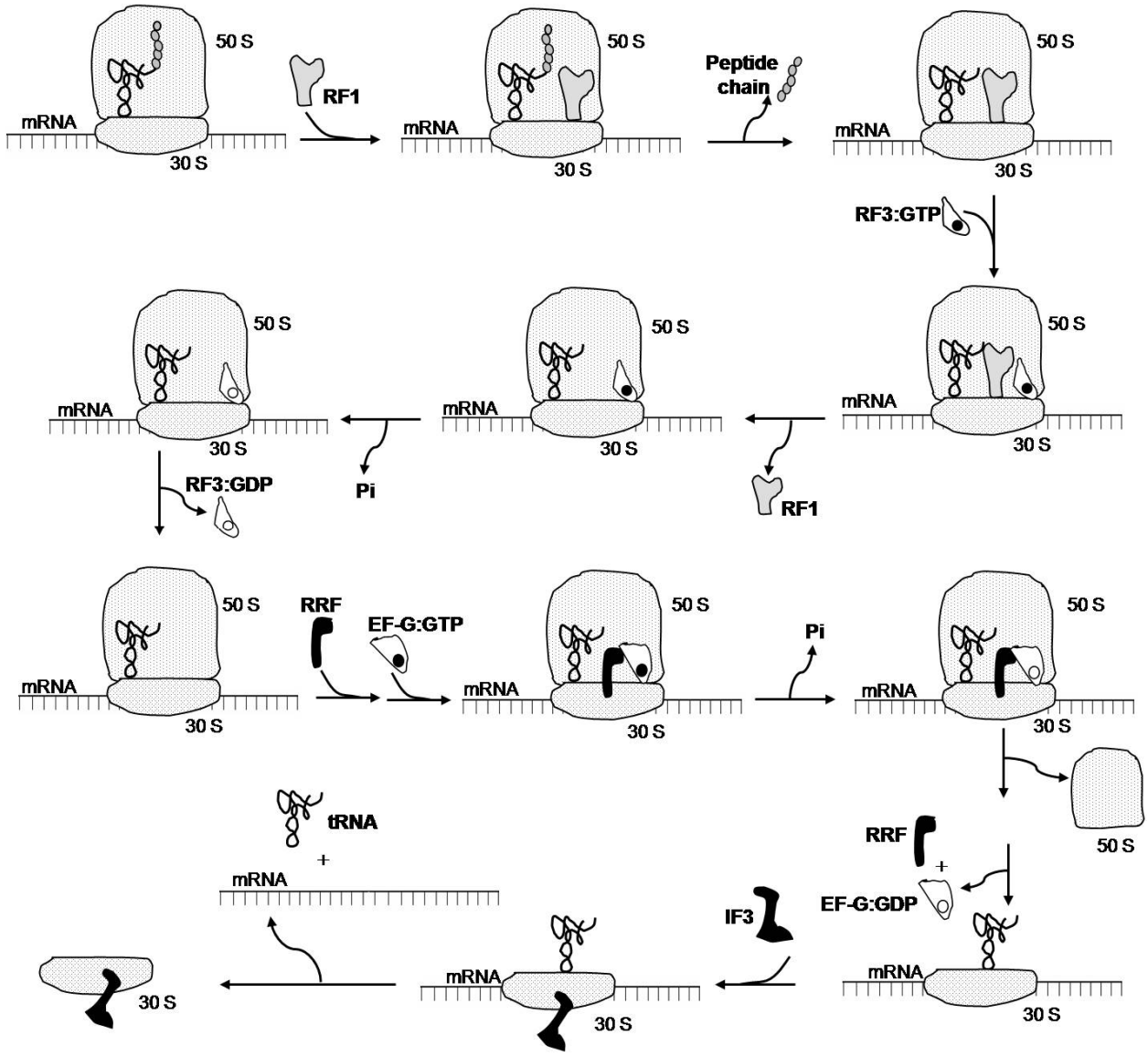

Figure 1.3. The termination of translation and the recycling of ribosome are shown. The RFs assist in peptide release and RRF together with EF-G helps in recycling of the ribosome. The RF = release factor, RRF = ribosome recycling factor, EF-G:GTP = elongation factor G with GTP.

complex of deacylated tRNA (in the P site), class I RF (in the A site) and mRNA are left behind. Thereafter, RF3 helps to dissociate RF1 or RF2 from the ribosome in a GTP-dependent manner (Milman, G. *et al*., 1969; Grentzmann, G. *et al*., 1994; Karimi, R., *et al*., 1999).

In the fourth phase of translation of ribosome recycling, the ribosome recycling factor (RRF), acts together with EF-G to cause dissociation of the 50 S and 30 S subunits (Figure 1.3). Crystal structures of RRF with *E. coli* 70 S ribosomes show the factor binding to a crevice involving the PTC. Upon binding of RRF, the tip of helix 69 (H69) in the 23S rRNA of large subunit shifts away from the small subunit and towards RRF by 8 Å, causing disruption of an important intersubunit bridge called B2a (Pai, R.D. *et al*., 2008). Disruption of this major contact between the two subunits reveals a key role of RRF in dissociation of the 70 S ribosome. Initiation factor 3 (IF3) is also required helps in recycling of ribosomes by acting on post-termination ternary complexes after the dissociation of 50 S subunits. It catalyzes the dissociation of deacylated tRNA from the partial P site of the 30 S subunits (Karimi, R. *et al*., 1999).

1.3. Antibiotics targeting the 50 S and 30 S subunits

The small (30 S) and large (50 S) ribosomal subunits are proven targets for many of the known antibiotics in pathogenic bacteria. A few of the inhibitory modes of the antibiotics studied crystallographically include: (i) improper coding at the decoding center by aminoglycoside antibiotics, such as paromomycin (Brodersen, D.E. *et al*., 2000), (ii) restriction of the ribosomal movement by spectinomycin, hygromycin B, or edeine (Brodersen, D.E. *et al*., 2000; Carter, A.P. *et al*., 2000; Pioletti, M. *et al*., 2001), (iii) obstruction of tRNA binding at the decoding center by paromomycin and tetracycline (Brodersen, D.E. *et al*., 2000; Pioletti, M. *et al*., 2001) or PTC by chloramphenicol or sparsomycin, and (iv) blockage of the protein exit tunnel by macrolides and ketolides (Schluenzen F. *et al*., 2001; Hansen, J.L. *et al*., 2003; Schluenzen, F. *et al*., 2001). It is clear from the given examples that the antibiotics target the well-established functional

centers of the ribosome. Some examples of antibiotics are summarized in table 1.1.

Table1.1. Various antibiotics targeting important functional regions of large and small subunits of ribosome are given. The classes of few of the antibiotics are given in parentheses.

Antibiotics	Target site	(PDB) ID
Anisomycin	A-site crevice, LS#	1K73
Blasticidin S	P loop of 23 S RNA, LS	1KC8
Sparsomycin	CCA-end of P-site substrate, LS	1M90
Virginiamycin M (Streptogramin A)	A and P-sites near PTC, LS	1N8R
Chloramphenicol (Phenicol)	PTC#, tRNA binding site in A-site, LS	1NJI
Clindamycin (Lincosamides)	A and P-sites in PTC, LS	1YJN
Linezolid (Oxazolidinones)	PTC, A-site tRNA binding site, LS	3CPW
Azithromycin (Macrolide)	Peptide exit tunnel between PTC and proteins L4 and L22, LS	1M1K
Paromomycin (Aminoglycoside)	Decoding region, SS	1IBK
Hygromycin *(Aminoglycoside)*	Top of h44 (A, P, and E-site tRNAs), SS#	1HNZ
Tetracycline	Head of 30 S and h27 switch region, SS	1HNW, 1I97
Edeine	Binding site of mRNA and two subunits, SS	1I95

#: LS = large subunit, SS = small subunit, PTC = peptidyl transferase center.

The 50 S or the large subunit of the ribosome is mainly responsible for peptide-bond formation in the PTC and channeling of the newly formed peptide chain through the exit tunnel (Ban, N. *et al*., 2000). Antibiotics that target the PTC can be classified into two categories. The first includes antibiotics that bind or disrupt peptide-bond formation (Schluenzen F, *et al*., 2004) and the second contains those that hinder the PTC or substrate motions (Harms,J. *et al*., 2004). Some of the known drugs binding to the PTC are chloramphenicol, puromycin, clindamycin, tiamulin, sparsomycin, and

streptogramin A (Schluenzen, F. *et al*., 2001; Harms,J. *et al*., 2004; Schluenzen F, *et al*., 2004; Bashan, A. *et al*., 2003).

The first antibiotic of the large subunit studied crystallographically was chloramphenicol, which works by blocking the A site as it binds to the PTC. Antibiotics interact with the active-site crevice or the exit-tunnel crevice by inserting their aromatic groups in the hydrophobic interiors of these motifs. The streptogramins are unique among the ribosomal antibiotics since they consist of two components, streptogramin A and B, which act synergistically. Quinopristin, a streptogramin B compound, binds and blocks the ribosomal exit tunnel; whereas, dalfopristin, a streptogramin A compound, binds directly within the PTC and affects the occupancy by both the A- and P-site tRNA molecules. Upon binding of these drugs, the PTC undergoes a substantial conformational change causing the post-antibiotic obstruction of protein synthesis (Harms, J.M. *et al*., 2004). The pleuromutilin class of antibiotics, tiamulin is a powerful inhibitor of protein synthesis.

The 30 S or the small ribosomal subunit is involved in two primary functions. The first is to monitor accuracy in the decoding process, in which matching of the aminoacyl tRNA with the codon of the mRNA at the A site is carried out. The second is to participate in the process of translocation, in which it works with the 50 S subunit to move tRNA and mRNA precisely by one codon at a time. The 30 S subunit is the target of a significant number of antibiotics, such as tetracyline, ediene, aminoglycosides, pactamycin, and cyclic peptides (viomycin and capreomycin) (Poehlsgaard, J. *et al*., 2005).

A plethora of antibiotics targeting the ribosomal RNA, few of which have been mentioned, bind to the functional centers of the ribosome. Developing a deeper understanding of their binding mechanisms at the molecular level will aid in designing compounds with an enhanced antimicrobial activities and reduced antibiotic resistance.

1.4. Secondary and tertiary structures in rRNA

In order to study the binding interactions of antibiotics and the ribosome, it is important to have a good understanding of the chemical structures of the compounds and targets. The primary sequence of the RNA determines the types of the secondary structures that in turn outline the tertiary structures. The RNA present in the cell has an A-form helix stabilized by pairing between bases on opposite strands and by stacking of adjoining bases. Any perturbation of the standard duplex structure leads to the formation of various secondary structures, such as single-base bulges, multiple-base bulges, hairpin loops, internal loops, duplexes, mismatch loops, and three-stem or four-stem junctions (Chow, C.S. *et al*., 1997) (Figure 1.4.). The single-base bulges are formed when the unpaired nucleotide in the duplex either stacks in the duplex or is exposed to the solution. The multiple-base bulges result from more than one base unpaired in the duplex. The base bulges often lead to an expansion of the deep groove of the RNA strand, thereby forming potential protein or small-molecule binding sites (Weeks, K.M. *et al*., 1991). The internal loops are formed by having one or more unpaired bases on each strand of the duplex. The three-stem or four-stem junctions are formed by the connection of three or more helical stems, and common example of four-stem junction is seen in tRNA.

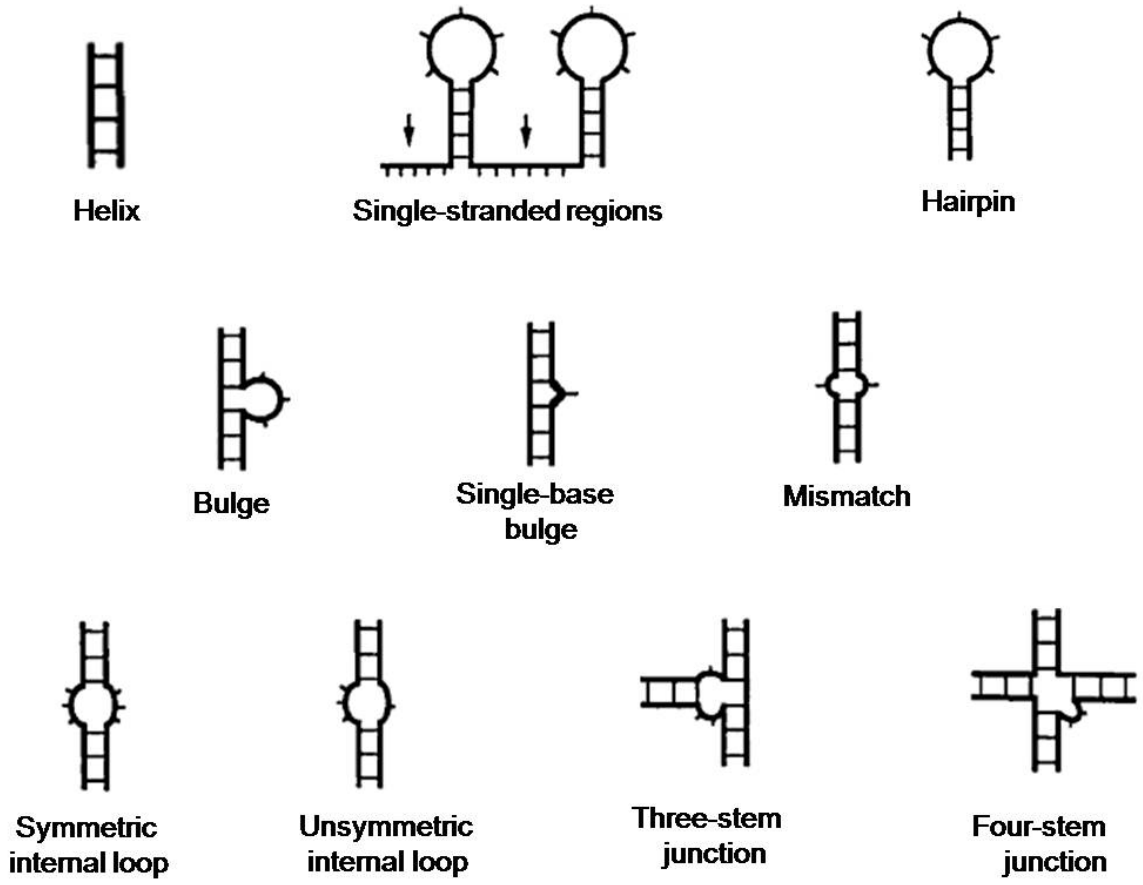

Figure 1.4. The different secondary structures adopted by the RNA in the ribosome are shown.

The rRNA has a vast array of these secondary structures that serve as unique recognition sites for a wide variety of substrates. The secondary structures of the rRNA also engage in additional interactions to form tertiary arrangements such as tetraloops, A-minor motifs, pseudoknots, and cross-strand purine stacks. The tetraloops are formed when four-base loops cap the double-helical strands in rRNA. These tetraloops exhibit invariant to highly variable sequences, depending upon their position in the molecule. The A-minor motif is the most commonly found long-range tertiary interaction in the large subunit. The A-minor motif occurs by the insertion of shallow groove edges of adenines into the shallow groove of the neighboring helices, most likely C-G base pairs.

The adenines then form hydrogen bonds with the 2'-OHs of those pairs (Lescoute, A. & Westhof, E., 2006). The main function of the A-minor motif appears to be stabilization of the interactions between the RNA helices or between loops and helices, and to influence the conformations of junctions and tight turns. A wide range of secondary and tertiary interactions exist within the ribosome, which will not be discussed in detail. The secondary structure map of 16 S rRNA is shown in Figure 1.5.

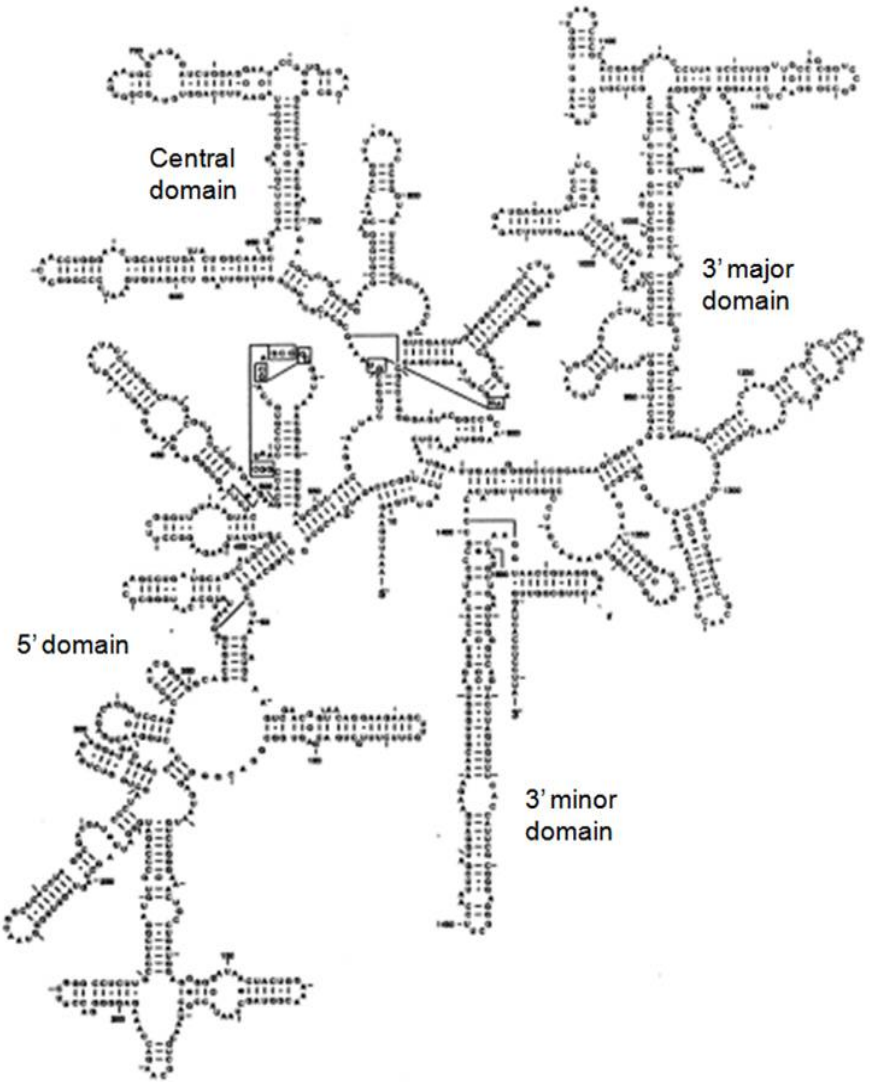

Figure 1.5. The secondary structure of 16 S rRNA of 30 S subunit illustrating the four main domains is shown (Gutell, R.R., 1993).

The large subunit (50 S) of the bacterial ribosome catalyzes peptide-bond formation in the PTC and holds the site for binding factors responsible for initiation, elongation, and termination phases of protein synthesis. The crystal structure of the large subunit of *H. marismortui* at 2.4 Å (Ban, N. *et al*., 2000) revealed that the secondary structure of 23 S rRNA could be divided into six large domains. The base pairs stabilizing the helices by at least two hydrogen bonds are clear and in addition, the secondary structures such as base triples, tetraloops, and cross-strand purine stacks are also recognized (Ban, N. *et al*., 2000) (Figure 1.6).

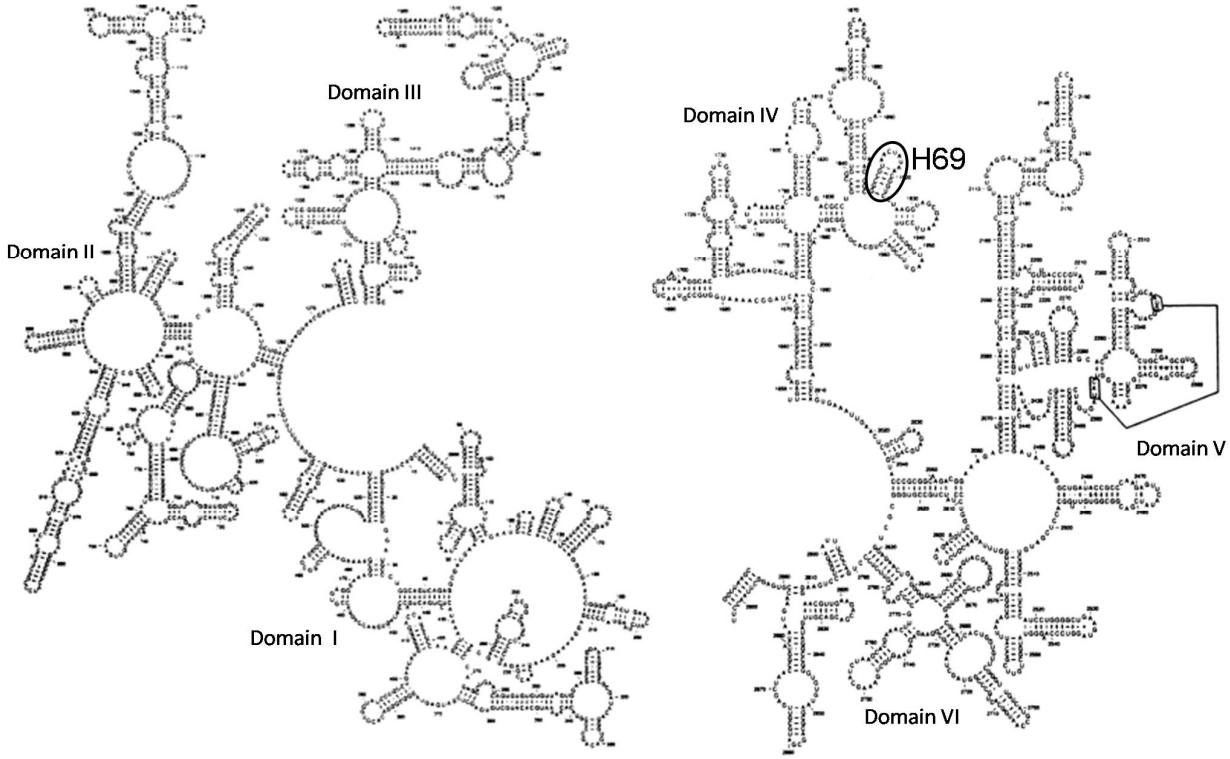

Figure 1.6. The secondary structure of 23 S rRNA of 50 S subunit is shown in which the six major domains are labeled, and the location of H69 is highlighted (Gutell, R.R. & Fox, G.E., 1988).

The secondary structure of 23 S rRNA encloses a central loop that is closed by a terminal stem, and 11 more stem-loops emerge from this central loop (Figure 1.6). Domain I is present in the back of the large subunit and helices 1 to 25 (H1-25) span the back region of domain I. This domain forms a globular structure behind the L1 protein region.

Domain II is observed to be the largest of all the domains and its three protrusions reach the subunit interface side of the particle. One of the protrusion having helices 42-44 (H42-44) form part of L7/L12 stalk and interact with the elongation factors. Helix 38 (H38) forms the second protrusion and the longest unbranched stem of the subunit. The third protrusion is made of helices 32 to 35.1 (H32-35.1), and the loop of helix 34 (H34) interacts directly with the small ribosomal subunit (Culver, G.M. *et al*., 1999).

Domain III occupies the bottom region of the subunit. It makes more contacts with domain II, with only modest contacts with domains I, IV, and VI, and hardly had any contact with domain V. For domain IV, most of it faces the intersubunit area of the large subunit and forms a diagonal patch of flat surface. It connects to domains III and V in the back of the particle.

Domain V is packed in between domains IV and II and is considered to be closely engaged in peptide-bond formation. Helix 75 (H75) forms the binding site for L1 protein, helices 80 to 88 (H80-88) form the central protuberance region and helices 89 to 93 (H89-93) widen towards domain VI and stabilize the elongation-factor binding region of the ribosome.

Domain VI is the smallest domain of the 23 S rRNA and includes the sarcin-ricin loop (SRL, stem-loop 95). This loop is required for factor binding and its conformation is stabilized through interactions with domain V and by proteins (Correll, C.C. *et al*., 1998). This loop is also seen to be exposed to solvent through nucleotide protection studies. Although the 23S rRNA is organized into six domains at the secondary structure level, the tertiary structure of the domains is stabilized by common elements such as pseudoknots, tetraloop-tetraloop interactions, and base triples (Westhof & Fritsch, 2000). Therefore, these interactions stabilize the contacts of sequences present in different parts of the secondary structure of 23 S rRNA (Figure 1.6).

1.5. Significance of helix 69 in the ribosome

1.5.1. Positioning of helix 69 at the subunit interface

Helix 69 (H69) is located in domain IV of the 50 S subunit with its loop portion being universally conserved. It is a 19-nucleotide hairpin loop (residues 1906-1924 by *E. coli* numbering) with three post-transcriptionally modified nucleotides, namely pseudouridine (Ψ) at positions 1911, 1915, and 1917 (Bakin and Ofengand, 1993). The pseudouridine at 1917 is methylated at its N3 position (Kowalak, J.A. *et al*., 1996). The secondary structure of H69, uridine, pseudouridine, and methylated-pseudouridine are shown in Figure 1.7.

A)

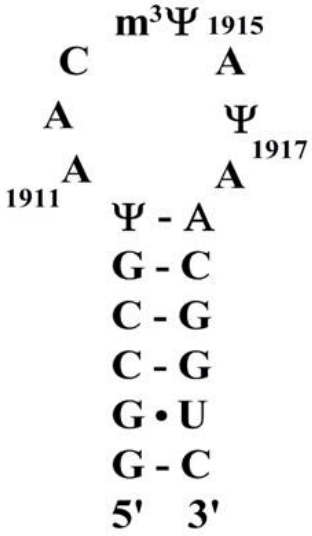

E. coli H69

B)

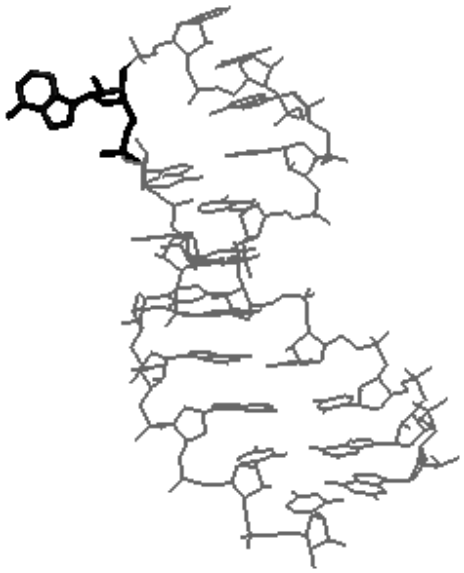

E. coli H69

C)

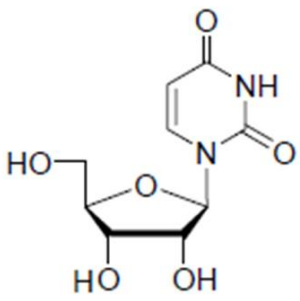

Uridine (U)

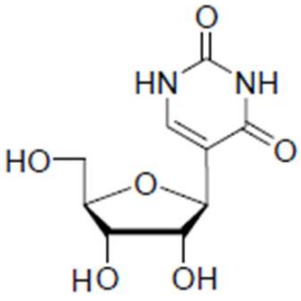

Pseudouridine (Ψ)

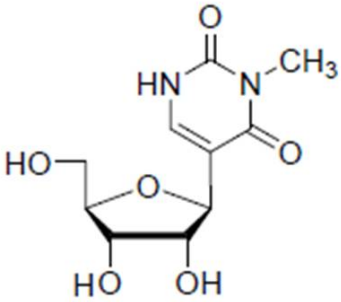

3-Methylpseudouridine ($m^3\Psi$)

Figure 1.7. A) The secondary structure of *E. coli* helix 69 (H69) is shown with its pseudouridine (Ψ) residues at 1911, 1915, and 1917 and a G•U mismatch in the stem region. The 1915 pseudouridine is methylated at N3 position.B) The crystal structure of H69 (1906-1924) in 70 S *E.coli* ribosome, with its A1913 (black) flipped out of the loopregion (PDB ID = 2J01) is presented. C) The chemical structures of uridine, pseudouridine and 3-methylpseudouridine are shown.

H69 is positioned in the interface of the two subunits and forms the major RNA-RNA bridge B2a that is found to be very flexible (Figure 1.8) (Harms et al., 2001; Yonath, 2002a, b). H69 was reasonably disordered in the X-ray crystal structures of the 50 S subunit (Ban *et al*., 2000; Bashan *et al*., 2003). These bridges are formed from components belonging to both subunits and it may adopt different conformations in the associated ribosome and the free ribosome.

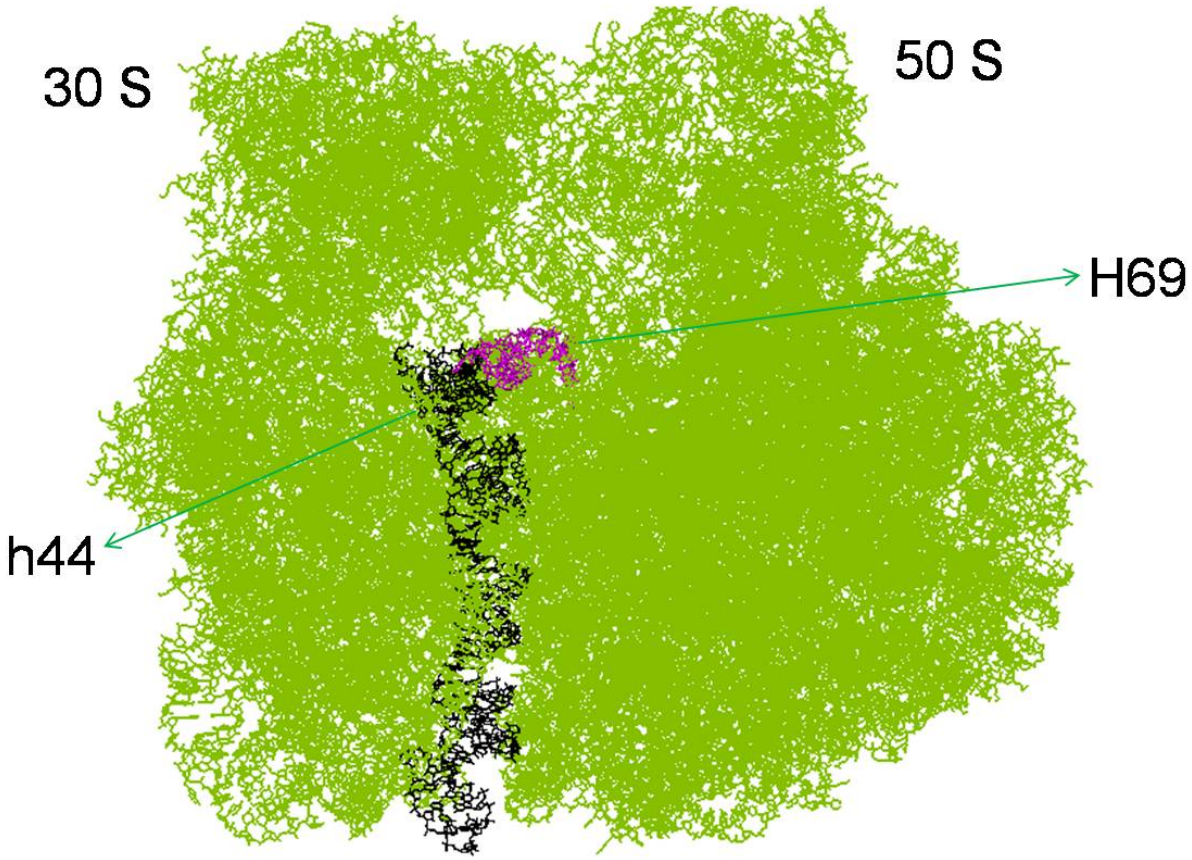

Figure 1.8. The components of RNA-RNA bridge b2a, h44 of 30 S subunit and H69 of 50 S subunit, are shown. The PDB ID for 50 S subunit = 2AW4 and for 30 S subunit = 2AVY (Schuwirth, B.S. *et al*., 2005).

In the 70 S ribosome crystal structure of *Thermus thermophilus*, it is very clear that the loop of H69 associates with the shallow groove of the D stem of the A-site

tRNA, and the shallow groove of its stem contacts the minor groove of the D stem of the P-site tRNA during protein synthesis. Simultaneously, it is also shown to be interacting with the shallow groove of h44 at the decoding region (Yusupov, M.M. *et al*., 2001).This structural data is supported by the previous cross-linking studies, in which it is clearly indicated that H69 contacts the decoding region at positions 1408-1411 and 1518-1520 of 16 S rRNA (Mitchell, P. *et al*., 1992). Since H69 interacts with both A-site and P-site-bound tRNAs, it can be deduced that H69 may be involved in the translocation process. It can be further hypothesized that the flexibility of H69 may be important for the proper functioning of the ribosome.

In a crystal structure of the *E. coli* 70 S ribosome at 3.5 Å, the molecular details of interactions of H69 with h44 are clearly described, suggesting a role for H69 in subunit association (Schuwirth, B.S. *et al*., 2005). Residues Ψ1911 and A1919 were shown to form a reversed-Hoogsteen base pair that is bridged by the 2'-OH of A1918, forming an A-A dinucleotide platform. This interaction moves A1919 close to the U1406/U1495 bases of h44 in the small subunit. Residue A1912 stacks on A1918 and forms a reversed-Hoogsteen base pair with Ψ1917. A1912 also projects into the shallow groove of the C1407/G1494 base pair in h44 of 16S rRNA (Schuwirth, B.S. *et al*., 2005).

The involvement of specific nucleotides of H69 in subunit association is encouraged by the fact that methylations at A1912 and A1918 as a result of DMS (dimethyl sulfate) modification studies were shown to interfere with subunit association and thus proper functioning of 70 S ribosome (Maivali, U. *et al*., 2004). These studies suggest that H69 has a dynamic character and might also participate in translocation (Yusopov, M.M. *et al*., 2001; Bashan, A *et al*., 2003; Klaholz, B.P. *et al*., 2004; Liiv, A. *et*

al., 2005). It was suggested in early reports that H69 might act as a molecular crane in transferring tRNA from A to the P site since it is difficult to visualize the movement of tRNA through RNA-packed interface without some simultaneous structural change (Ortiz-Meoz, R.F. & Green, R., 2010; Yonath, A. *et al*., 2003; Yonath, A. *et al*., 2004); however, recent studies refute this hypothesis (Ali, I.K. *et al*., 2006).

1.5.2. Mutational studies of helix 69

The high-resolution crystal structures of the ribosome have placed H69 at a functionally relevant area where it forms the RNA-RNA bridge B2a with h44 of the small subunit. Therefore, H69 is of utmost interest for mutational analysis through site-directed mutagenesis or complete deletion from the ribosome. Interestingly, in one of the earlier genetic studies for investigating the role of rRNA in preserving the accuracy of translation (O'Connor & Dahlberg, 1995) mutations were recovered in the loop region of H69. The mutations that were pulled out included a deletion of A1916, the insertion of two consecutive A residues between A1916 and U1917 and a C to U change at 1914 (Figure 1.9). These mutations promoted the readthrough of stop codons and showed increasing levels of both +1 and -1 frameshifting at the *trpE91* frameshift site. It was suggested that the mutations of the loop residues of H69 may have disturbed the precision of the codon-anticodon interaction by changing the conformation of the decoding center in 16S rRNA across the subunit interface (O'Connor & Dahlberg, 1995). Site-directed mutagenesis of the loop of H69 lead to mutants A1912G and A1919G, which were inactive during *in vitro* protein synthesis and under-represented in the polysomes (Liiv, A. *et al*., 2005). Also, mutant Ψ1917C had a strong growth phenotype and general depletion of the polysome pool (Liiv, A. *et al*., 2005). In addition,

the point mutations at A1912G, A1919G, and Ψ1917C strongly affected the translational activity both *in vivo* and *in vitro (*Ali, I.K. *et al*., 2006) (Figure 1.9).

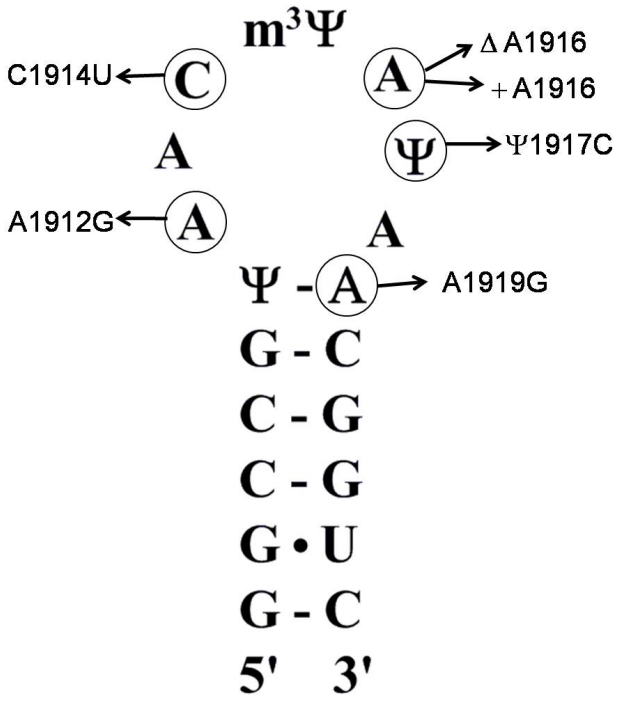

Figure 1.9. The mutations observed at different nucleotides of H69 are summarized in which mutations ΔA1916, +A1916, and C1914U promoted readthrough of stop codons and increased + 1 and – 1 frameshifting. The mutations A1912G, A1919G, and Ψ1917C affected the *in vivo* and *in vitro* translational activity (O'Connor & Dahlberg, 1995; Liiv, A. *et al*., 2005).

The mutational studies were also carried out for deciphering the importance of three pseudouridines (Ψs) in H69. The single synthase RluD, accountable for insertion of Ψs at the 1911, 1915, and 1917 positions in H69, was deleted. Its deletion led to a strong growth defect, and defective RluD led to impaired ribosome assembly (Raychaudari, S. *et al*., 1998; Sivaraman, J. *et al*., 2004). In another genetic mutational study in the loop region of H69, functional variants were attained through the randomization of the H69 loop. Residues A1912 and U1917 were found to be highly

important for the ribosome function and an A1915-ribosome mutant demonstrated fragile subunit association, weak A-site tRNA binding, and a severe growth phenotype and low translational fidelity (Hirabayashi, N. *et al*., 2006). In another study, single substitutions were introduced from positions 1912 to 1919 of H69. In a cell-free translation elongation assay, the mutated ribosomes had strongly reduced activity in the synthesis of the poly(Phe), but the peptidyl transferase activity was not affected in a puromycin-based assay. The A1919C and ΔH69 50 S subunit variants had the most severe *in vitro* reassociation efficiency and a mutation at A1919 also destabilized the dipeptidyl-tRNA in the A site (Kipper, K. *et al*., 2009). In general, mutations at loop positions of H69 affect the initiation factor-dependent 70 S initiation complex formation, ribosomal processivity *in vitro,* and lead to reduction of 50 S subunits in polysomal fractions *in vivo* (Kipper, K. *et al*., 2009). Therefore, the mutational studies on H69 clearly indicated its important role in subunit association and in various translation events.

1.5.3. Contacts of helix 69 (h69) with protein factors

Structural evidence has shown that H69 is involved in both peptide release and ribosome recycling by contacting release factors (RF) and ribosome recycling factor (RRF). The cryo-EM structures of release factor 2 (RF2) with 70 S reveal that the domain 2/4 of RF2 fits into a structure formed by protein S12, helix 18, and helix 44 of the small subunit and H69 of the large subunit (Klaholz, B.P. *et al*., 2003; Rawat, U.B.S. *et al*., 2003; Petry, S. *et al*., 2005). In cryo-EM studies of release factor 3 (RF3) bound to 70 S ribosome, the C-terminal domain of the RF3 contacts the loop of H69. As RF3 moves from an open to closed conformation, the tip of H69 moves slightly into the P site

because of absence of tRNA. This illustrates that H69, being present close to the rotation center of 30 S subunit, could be a major player for the structural transition of the ribosome and tRNA translocation (Klaholz, B.P. *et al*., 2004).

During later stages of protein translation, H69 has been observed to contact RRF. RRF together with elongation factor G (EF-G) disassembles the post-termination complex of mRNA, deacetylated tRNA, and the ribosome into their independent parts (Peske, F. *et al*., 2005; Zavialov, A.V. *et al*., 2005). While learning the molecular details of the mode of action of RRF through hydroxyl-radical probing studies, it was noticed that amino acids R129 and R132 of domain I of RRF come in close proximity with nucleotides 1907 and 1908 of H69 (Lancaster, L. *et al*., 2002). Later, cryo-EM reconstructions of a similar complex of *E. coli* 70S ribosome and RRF revealed that the loop residues of H69 contact highly conserved amino acids E122-R133 of RRF, and the loop itself shows some movement upon RRF's binding (Agrawal, R.K. *et al*., 2004).

A 3.3 Å crystal structure of domain I of RRF bound to *D. radiodurans* 50 S subunit demonstrated that binding of RRF disturbs the position of H69 (Wilson, D.N. *et al*., 2005). Nonetheless, this structure does not provide the insight into the separation of the two ribosomal subunits upon RRF binding. In a recent crystal structure of *E. coli* RRF or *T. thermophilus* RRF bound to *E. coli* 70 S ribosome, the tip of the H69 was observed to be moving away from the small subunit towards RRF by 8 Å, following the disruption of bridge B2a between two subunits (Pai, R.D. *et al*., 2008) (Figure 1.10). The movement of H69 implicated an ordered-to-disordered change upon RRF binding to the ribosome. RRF amino acids H23, V20, and S17 that lie on α-helix 1 in domain I interacted with the shallow groove nucleotides C1914 and Ψ1917. Thus, weakening of

bridge B2a due to RRF binding may play an important physiological role towards ribosome recycling (Pai, R.D. *et al*., 2008).

A) B)

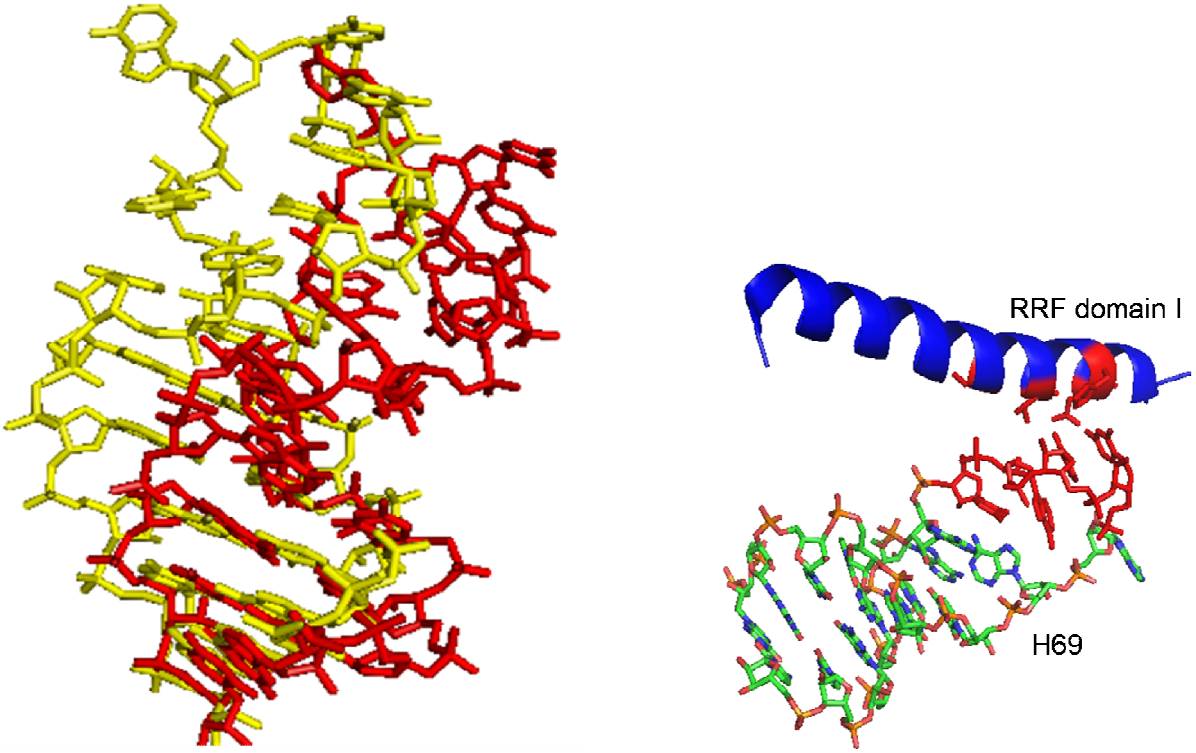

Figure 1.10. A) The overlapping images of H69 without RRF (red) and H69 bound to RRF (yellow) from *E. coli* are shown. PDB ID for red image = 2AW4 (Schuwirth, B.S. *et al*., 2005) and for green image = 2QBE (Borovinskaya, M.A. *et al*., 2007). B) The amino acids of domain I of RRF (red) making contacts with nucleotides of H69 (red) are shown.

In another structural study of aminoglycoside (gentamicin or paromomycin) inhibition of bacterial ribosome recycling, H69 was seen to move away from subunit interface upon RRF binding. But when aminoglycosides bind at the base of H69 stem (after h44 was saturated with the antibiotics) and RRF at the same time, H69 was not able to move away from h44 in bridge B2a. At this stage, the presence of aminoglycosides stabilized the intersubunit bridge B2a leading to obstruction of

ribosome recycling (Borovinskaya, M.A. *et al*., 2007). In summary, the above observations indicate that H69 plays a dynamic role through protein-assisted steps of translation.

1.5.4. Consideration of helix 69 (H69) as a drug target

The sequence of H69 has been shown to be a highly conserved moiety of ribosome in all three kingdoms of life, bacteria, archaea and eukaryotes (Cannone *et al*., 2002). More than 88% of the stem residues of H69 are conserved. However, when the sequences of H69 are compared between the bacteria (*E. coli*) and eukaryotes (*H. sapiens*), there are some visible differences between them (Figure 1.11). The first difference is that the 1915 position in *E. coli* is a methylated pseudouridine, whereas in humans it is not; secondly, the base at the 3' end of the loop is an A for *E. coli* and a G for *H. sapiens*; and thirdly, *H. sapiens* have two extra pseudouridines in the stem region of the hairpin. In *E. coli,* the native helix 69 has two pseudouridines (Ψ) at positions 1911 and 1917 (Bakin, A. *et al*., 1993) and an *N*3-methylated pseudouridine ($m^3\Psi$) at position 1915 (Kowalak, J.A. *et al*., 1996).

Considering the role played by H69 in subunit association of the ribosome during protein synthesis, the highlighted sequence differences of H69 between human and bacterial H69, and the dynamics of H69 when RRF binds ribosome, it is very attractive to consider H69 as novel antibacterial target. Additionally, through the study of chemical probes, it has been shown that in free 50S subunit, H69 nucleotides are strongly cleaved by hydroxyl radicals at most positions (Merryman, C. *et al*., 1999). Furthermore, H69 is exposed in the cell in the unassembled form of 50S and could be targeted by means of small molecules.

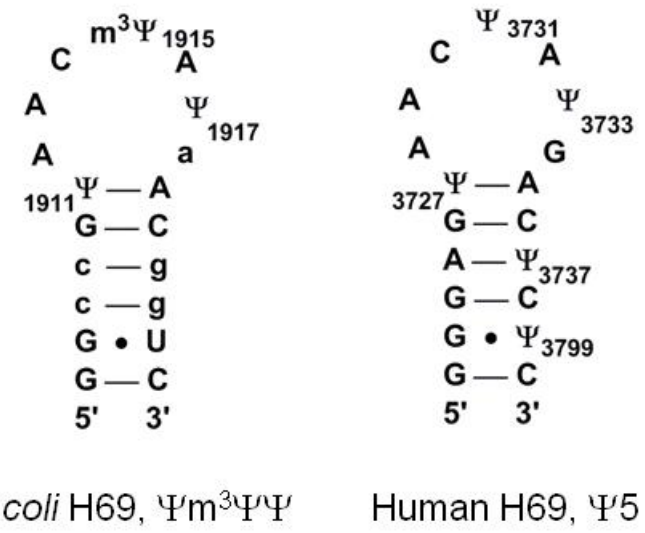

Figure 1.11. The sequences of the *E. coli* and human analogs of H69 are shown for comparison (referred to as $\Psi m^3\Psi\Psi$ and $\Psi 5$, respectively). Ψ is pseudouridine and $m^3\Psi$ is 3-methylated pseudouridine. The nucleotides in upper case letters in *E. coli* H69 sequence have >95% conservation and the lower case letters have 88-95% conservation in three kingdoms (Cannone, J.J. *et al*., 2002).

1.6. Thesis statement: goals and approaches

Bacterial ribosomes are composed of a large 50 S subunit having 23 S rRNA, 5 S rRNA, and over 30 proteins and a small 30 S subunit containing 16 S rRNA and about 20 proteins. The entire 70 S ribosome is formed by the combination of the 30 S and 50 S subunits through a network of intermolecular bridges. These intersubunit bridges are twelve in number and most of them involve rRNA (Yusupov, M.M. *et al*, 2001). The RNA-RNA contacts are centrally located and are in direct contact with the tRNA binding sites, whereas the protein contacts are on the outside of the ribosome (Yusopov, M.M. *et al*., 2001). The region of the ribosome under investigation in this study is helix 69 (H69), which occupies a large surface area of the RNA-RNA bridge called B2a. H69 is located in domain IV of the 23 S rRNA and consists of nucleotides 1906-1924.

H69 has been assigned a number of different roles due to its presence at the interface region of the ribosome. In addition to contacting the small subunit during mRNA decoding, H69 also contacts both the A- and P-sites tRNAs (Yusopov, M.M *et al*., 2001; Schuwirth, B.S. *et al*., 2005). These structural interactions implicate the involvement of H69 in translocation during protein synthesis (Bashan, A. *et al*., 2003; Liiv, A. *et al*., 2005; Sumita, M. *et al*., 2005; Yonath, A. *et al*., 2004; Yusopov, M.M. *et al*., 2001; Schuwirth, B.S. *et al*., 2005). Many groups have also ascertained H69's role between the 30 S decoding site and GTPase-related elements of the 50 S subunit (Bashan, A. *et al*., 2003; Cochella & Green, 2005; Frank, J. *et al*., 2005). Mutational studies have also established participation of H69 in ribosomal accuracy. A genetic selection for rRNA mutations increasing frameshifting and stop-codon readthrough identified three mutations in the loop of H69 (O'Connor & Dahlberg, 1995).

There are structural data showing H69 to be taking part in both peptide release and ribosome recycling. The cryo-EM models of release factors (RF1 and RF2) bound to 70 S ribosome indicate that domain II of the RFs comes in very close proximity to H69 (Klaholz, B.P. *et al*., 2003; Petry, S. *et al*., 2005; Rawat, U.B.S. *et al*., 2003). In alternate RF3-bound conformations of 70S ribosome, the loop of H69 assumes different structures after contacting the C-terminal domain of RF3 (Klaholz, B.P. *et al*., 2004). In crystal structures of the both *E. coli* and *T. thermophilus* ribosome recycling factor (RRF) bound to *E. coli* ribosomes, the loop of H69 is observed to be moving away from h44 of the small subunit, thereby interrupting a significant contact between the two subunits, which is bridge B2a (Pai, R.D. *et al*., 2008).

From the above-cited roles of H69 in various ribosomal functions, it is quite clear that H69 is a highly flexible multitask feature of the ribosome. Owing to the emergence of antibiotic resistance and the notable structural differences between the bacterial and human H69, this helix could be considered as a novel antibacterial target. H69 could be targeted in bacteria with some ligand or small molecule such as a peptide or DNA/RNA aptamer to interfere with the naturally occurring intersubunit contacts. The main idea behind this project was to isolate small peptides that specifically bind to H69 by using a phage-display peptide library. Phage-display libraries have already been used to isolate peptides and proteins that bind to antibodies or receptors and also to study protein interactions with DNA (Jamieson, A.C. *et al*., 1994; Wu, H. *et al*., 1995).

Phage display is a biological system that facilitates the cloning and rapid selection of peptides from large combinatorial libraries (Smith, G.P. & Petrenko, V.A., 1997). In comparison to the chemical combinatorial approach, the advantages of phage display lie in its simplicity and replicability. The phage display library is a heterogeneous mixture of phage clones, each carrying a different foreign DNA insert and therefore displaying a different hybrid peptide on its surface. An *in vitro* selection process called affinity selection, or biopanning, allows rapid identification of peptide ligands from this library (Lowman, H.B., 1997). Biopanning is carried out by incubating the phage peptide library with immobilized target (in this case H69) then removing the unbound phages and eluting the target bound phages. The eluted phages are amplified in cells to yield a large crop of progeny phages and subjected through additional binding/amplification cycles to enrich the pool in favor of the best binding sequences (Smith, G.P. & Petrenko, V.A., 1997; Arap, M.A., 2005). After three to four rounds of selection, the

amino-acid sequences of foreign DNA inserts of preferred RNA-binding phages are determined through DNA sequencing. Eventually, high-affinity peptides are cloned or synthesized so that they can be studied individually.

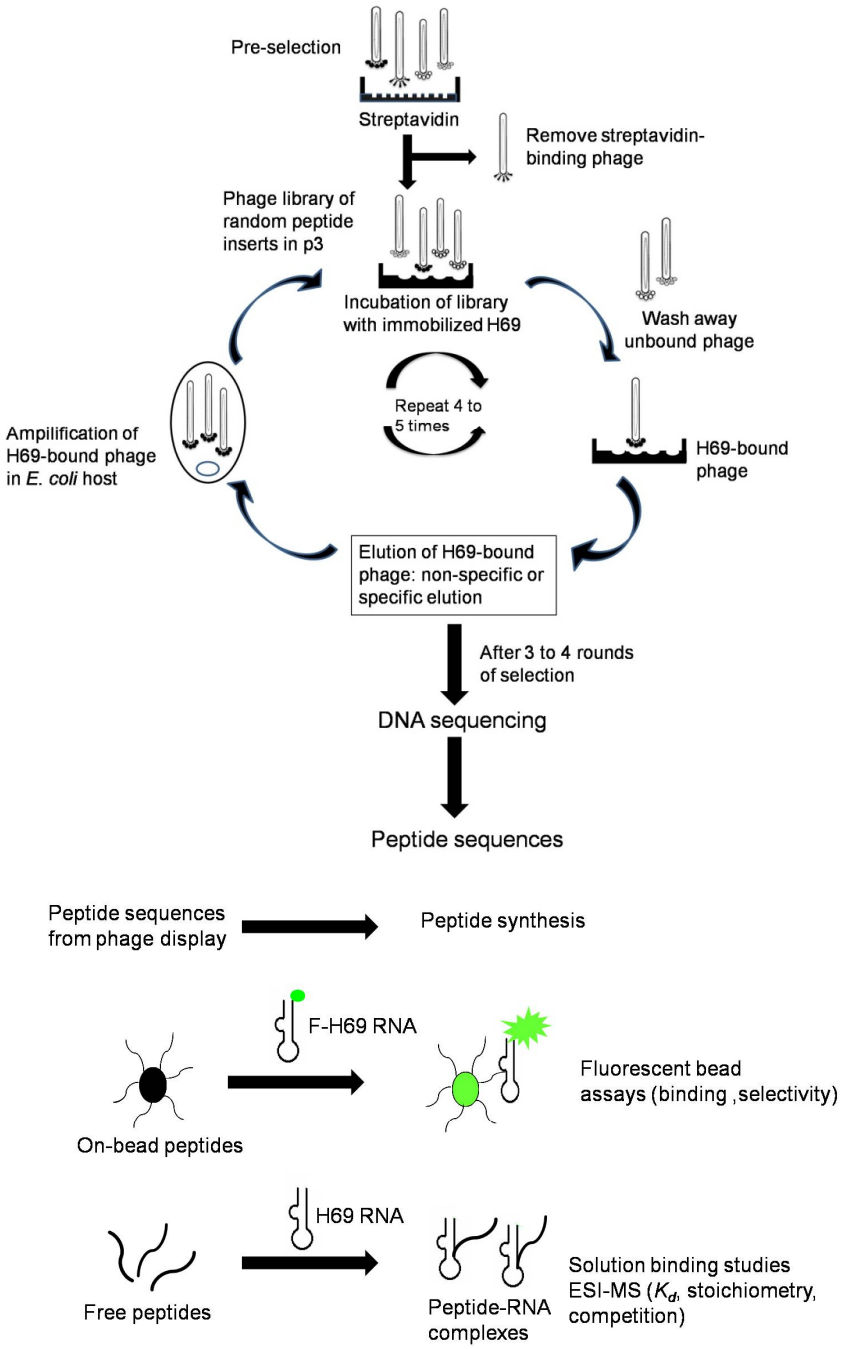

Figure 1.12. The overview of the project is shown. The H69 was targeted with phage library and later the selected peptide sequences were subjected to binding analysis.

To identify the preferred H69-binding peptides, the Ph.D.-7 Phage Display Peptide Library™ was chosen for selection. This phage library is based on a combinatorial library of random heptapeptides fused to a surface-exposed minor coat protein (pIII) of M13 phage, which is present in five copies at one end of the phage particle (Marvin, D.A., 1998). Thus, each phage displays five copies of one particular fused peptide. The library contains approximately 2×10^9 independent phage clones. The displayed heptapeptides are expressed at the N-terminus of pIII. A short spacer (Gly-Gly-Gly-Ser) is present between the peptides and the wild-type pIII sequence.

After the selection of a particular peptide sequence, further studies with the selected peptides involved the chemical synthesis of the peptides and later studies of binding mechanisms through biophysical methods. Binding studies included electrophoretic gel mobility shift assays (EMSA), on-bead peptide libraries using high-throughput fluorescence assays, Fe-EDTA reactions, in-line probing techniques, and electrospray ionization (ESI) mass spectrometry (MS). After all these analyses to determine binding affinities and selectivities of the selected peptides, they may be refined as antimicrobial drug leads, in the future, using peptidomimetic chemistry.

CHAPTER 2

Isolation of peptides binding to helix 69 of *E. coli* 23 S rRNA employing an M13 phage-display library

2.1. Phage-display libraries

2.1.1. Peptides as ligands for RNA

Phage-display libraries are composed of a collection of phage particles in which the foreign peptides or proteins are expressed along with the phage coat proteins. The phage is a single-stranded DNA virus that infects a number of gram-negative bacteria. This technology was first pioneered by George Smith (Smith, G.P., 1997). The formation of the phage library is achieved by integration of the nucleotide sequence encoding the peptide or protein to be displayed into the phage genome as a fusion in the gene responsible for a phage coat protein. This fusion makes certain that the assembled phage particles display the foreign peptide or protein together with the coat protein (Smith, G.P. & Scott, J.K., 1993). This physical link between the phenotype and the genotype of the expressed protein and the replicative ability of the phage are ideal features of the phage-display technology (Smith, G.P., 1985). The filamentous phage particles frequently used for display purposes are known as Ff, and include strains M13, f1, Fd and ft. The M13 strain is an *E. coli*-specific filamentous phage about 1 μm long and 5-7 nm in diameter (Marvin, D.A., 1998) (Figure 2.1). The major coat protein p8 (50 amino acids) together with four other minor coat proteins, p3, p6, p7, and p9, package a circular, single-stranded DNA of about 6400 nucleotides to make the complete phage particle (Marvin, D.A., 1998). The viral mass is 16.3 MDa and consists of approximately

2700 copies of p8. The proteins p7 and p9 cap one end of the particle and are present in either three or five copies; whereas, the other end is capped by proteins p3 and p6, which are also present in either three or five copies (Arap, A.M., 2005). The structural stability of the phage particle comes from the contribution of all five coat proteins, but p3 is necessary for host cell recognition and infection (Armstrong, J. *et al*., 1981).

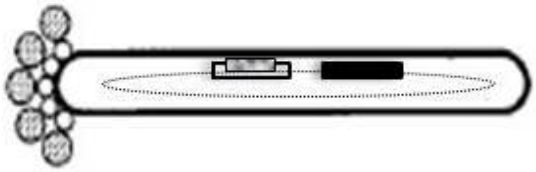

Figure 2.1. The filamentous M13 phage particle is shown in which the dashed line inside the phage represents the single-stranded DNA, with the segments encoding proteins p8 and p3 are shown by black and white boxes, respectively. The hatched segment within the white box represents for the foreign coding sequence merged into the p3 coat protein. The black oval shows the p8, which is the major coat protein, the small white circles at one end of the particle represent the N-terminal domains of the five p3 molecules, and the hatched circles on the p3 white circles show the peptides specified by the foreign coding sequences.

The polypeptides fused to the M13 coat proteins are displayed on the surface of the phage, on the condition that the fusion protein passes through the M13 phage assembly apparatus and does not influence the viability of phage particle itself (Russel, M., 1995). Applying simple molecular biology techniques, diverse phage-displayed libraries can be constructed (Sidhu, S.S. *et al*., 2000). The procedure for selection of peptides of desired binding properties from the library pool involves binding to an immobilized target, and then ascertaining the sequence of the selected peptide from the sequence of the enclosed DNA (Figure 2.2). Currently, optimized molecular techniques

enable the construction of phage-display libraries having >10^{11} unique DNA sequences (Sidhu, S.S. *et al*., 2000).

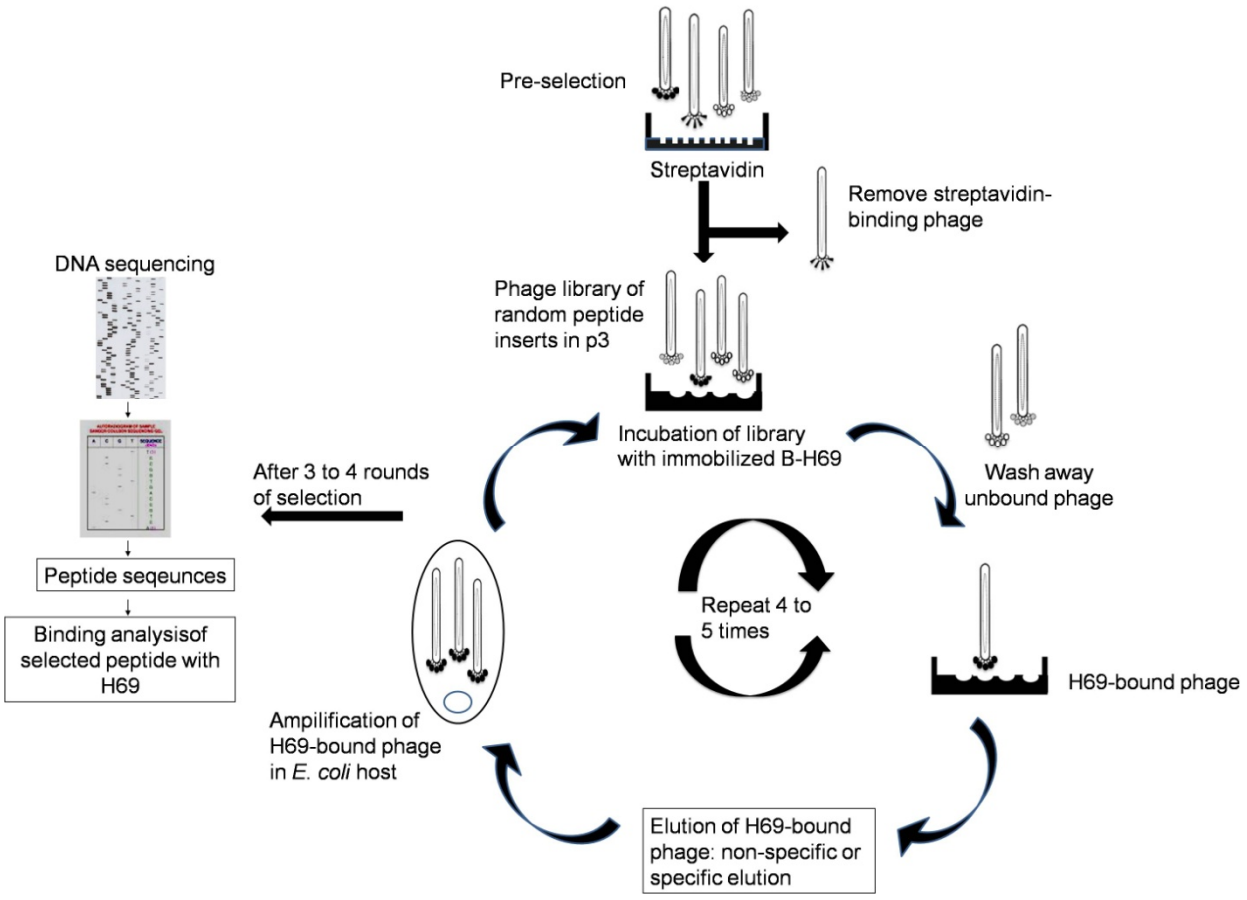

Figure 2.2. The generalized scheme of steps for selection of peptide ligands employing a phage-display library is shown, in which the immobilized target is biotin-labeled H69 RNA.

The use of phage display depends on the efficiency with which the peptides are displayed on the phage surface. The intensity of exhibition of different peptides depends on both the length and the sequence of the peptide. In polyvalent display, hundreds or thousands of copies of small peptides (<8 residues) can be displayed per phage particle (Liu, G. *et al*., 1996); whereas, larger proteins (>100 residues) are displayed in

monovalent format of one copy or less per phage particle (Lowman, H.B. *et al*., 1991; Sidhu, S.S. *et al*., 2000).

The initial design of phage display was the N-terminal fusion to the p3 or p8 coat proteins in the phage genome, but their use was limited because the function of the coat protein was compromised (Devlin, J.J *et al*., 1990; Cwirla, S.E. *et al*., 1990; Nakayama, G.R. *et al*., 1996). Later, to overcome this problem, hybrid phage-display systems were developed. In one system, the displayed fusion protein was present as an additional component of a phage coat that had all of the five coat proteins of wild-type. The fusion gene was added to a complete phage genome such that the expanded genome had two versions of the coat proteins, the wild type and the copy of the fused protein to be displayed (Smith, G.P., 1993). On the other hand, hybrid display was also accomplished with a phagemid-based system. A phagemid is a plasmid containing DNA sequences that are packaged into phage particles and these vectors have the M13 origin of replication and a phage packaging site in addition to the plasmid propagation elements (Azzazy & Highsmith, 2002). The phagemid has a coat protein gene that has the sequence of the foreign peptide to be displayed along with that coat protein. The progeny phage contains the wild-type coat proteins from the helper phage and the fusion coat protein from the phagemid. Consequently, the foreign protein or the peptide is displayed on the phage surface, surpassing the harmful effects of the fusion with the assistance of the helper-derived, wild-type coat proteins (Mead, D.A. & Kemper, B., 1988).

With the help of these hybrid display systems, large proteins are readily displayed as N-terminal fusions with p3 or p8 (Sidhu, S.S. *et al*., 2000) or with p7 and

p9 (Gao, C. *et al*., 1999). Also, C-terminal display has been realized with p6, p3, and p8 (Fuh, G. *et al*., 2000; Fuh & Sidhu, 2000). Most of these display formats are successful because the fusion protein stays as the minor component of the phage coat and does not interfere with the phage viability.

Some other types of phage have been employed as vehicles for constructing the libraries such as lambda and T7 (Gupta, A. *et al*., 2003; Danner, S. & Belasco, J.G., 2001). The M13 phage is an excellent cloning vehicle since the foreign sequences are accommodated easily by the formation of longer phage particles. But their nonlytic propagation mechanism requires that all the components of the phage coat be exported through the bacterial membrane. As a result, only the proteins capable of surviving this export are displayed (Marvin, D.A., 1998). This limitation is avoided by using the lytic phage lambda and T7 in which the capsid assembly takes place entirely in the cytoplasm before the disruption or lysis of the cell (Danner, S. & Belasco, J.G., 2001). Moreover, studies are showing that the T7 and lambda phage can tolerate the display of relatively large proteins in a polyvalent manner (Zucconi, A. *et al*., 2001).

Phage-display technology has been widely applied in the area of antibody engineering and further development of the phage-originated peptides into viable diagnostic reagents. Examples of diagnostic reagents include the *scFv*-alkaline phosphatase fusion protein, which was used to identify luteovirus in sap extracts from infected plants (Harper, K. *et al*. 1997). Phage-displaying antibody libraries are regularly used against immobilized antigens (Marks, J.D. *et al*. 1991; Malmborg, A.C. *et al*. 1996) or antigens in solution (Hawkins, R.E. *et al*. 1992). Peptides selected through phage display have also played a role as agonists and antagonists of the receptors (Doorbar,

J. *et al*. 1994). Phage-display libraries have been applied for mapping antibody epitopes by inserting the DNA fragments responsible for parts of the protein antigen into the phage coat proteins. Random-phage libraries displaying the antigenic peptides are then used for discovering the monoclonal and polyclonal antibody epitopes (Hill, H.R. & Stockley, P.G., 1996; Cortese, R. *et al*. 1994). The M13 phage libraries have been successfully applied in the field of proteins such as the insulin-like growth factor-binding protein 1, vascular endothelial growth factor (Sidhu, S.S. *et al*., 2000).

2.1.2. Peptide-RNA interactions: important examples

The secondary structure elements of RNA such as hairpins (stem-loops), bulged residues, and pseudoknots in the regular A-RNA conformation generate binding pockets for small molecules such as peptides (Chow, C.S. & Bogdan, F.M., 1997; Ye**,** X. *et al*., 1995). These structural features help in the accessibility of the deep groove of the RNA, which is otherwise narrow and unreachable for the peptides. Their presence helps in the widening of the RNA deep groove as observed in important examples of adaptive binding of arginine-rich peptide motifs of viral and phage proteins. These peptides include HIV-1 Rev peptide binding with the IIB hairpin of RRE (Battiste, J.L. *et al*., 1996), boxB hairpin of bacteriophage λ bound to an N-terminal peptide (Legault, P. *et al*., 1998), and P22 N-peptide boxB RNA complexes (Cai, Z. *et al*., 1998). These complexes follow induced fit-phenomenon, since both the RNA and the peptide undergo conformational changes upon binding.

Arginine-rich peptides (ARM) are 10-20 amino acids in length and bind RNA with the same specificity as the parent protein (Lazinski, D. *et al*., 1989). These peptides are

observed to form a variety of secondary structures such as α helices, β hairpins, or extended conformations, depending on the peptide sequence and the RNA site. One notable example of an arginine-rich peptide motif binding to RNA is the BIV-1 TAR RNA-Tat peptide complex (Figure 2.3). Upon binding of the 17-residue Tat peptide as a β hairpin, the deep groove of the TAR RNA is widened (Ye, X. *et al*., 1995). The widening of the groove is associated with bulging out of two uridine bases, U10 and U12. U10 forms a U10•(A-U) base triple with the A13-U24 base pair, and this base triple forms a suitable peptide-binding pocket. Uridine 12 is extruded and not involved in peptide binding (Ye, X. *et al*., 1995; Puglisi, J.D. *et al*., 1995). The formation of the base triple results in twisting of the phosphate backbone between G9 and U10. The guanidinium group of arginine forms hydrogen bonds with the deep groove edge of G11 and phosphate oxygen in a forked conformation (Calnan, B.J. *et al*., 1991). Similarly, in the HIV 1 Rev-RRE RNA arrangement, the RRE RNA consists of a stem having the purine-purine base pairs and protruding adenine and uridine. The Rev peptide docks itself deeply in the widened deep groove of the RNA as an α helix.

Another example of an arginine-rich peptide interacting with RNA is the bacteriophage λ N-peptide/boxB RNA complex (Legault, P. *et al*., 1998) (Figure 2.4). This ARM peptide constitutes the first 22 amino acids of the N protein and binds RNA with the same specificity as the entire protein. This peptide binds with the boxB RNA in a bent α-helical conformation and does not interact with the RNA deep groove. Instead, it binds with the 5' end of the boxB stem and the first three residues of the loop due to the negative charge of the RNA (Legault, P. *et al*., 1998). The peptide binding results in widening of the deep groove of the RNA due to the presence of a sheared G•A

mismatch (Weiss, M.A. & Narayana, N., 1998). Peptide-RNA interactions lead to formation of a GNRA-like tetraloop from four nucleotides of the boxB RNA hairpin pentaloop. The looped out nucleotide makes a considerable number of contacts with the bound peptide (Cai, Z. *et al*., 1998) (Figure 2.4).

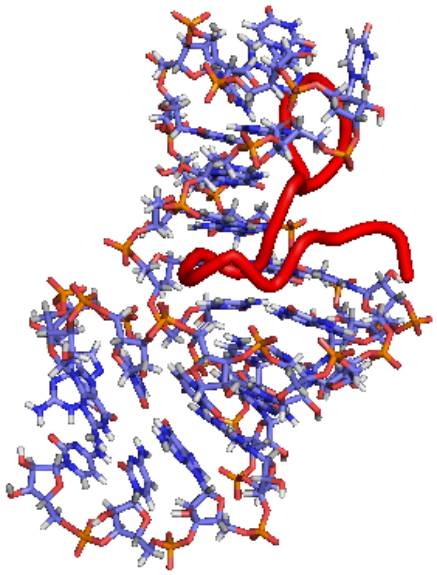

Figure 2.3. The 17-residue Tat peptide (in red) in complex with BIV TAR RNA is shown (PDB ID = 1BIV) (Ye, X. *et al*., 1995).

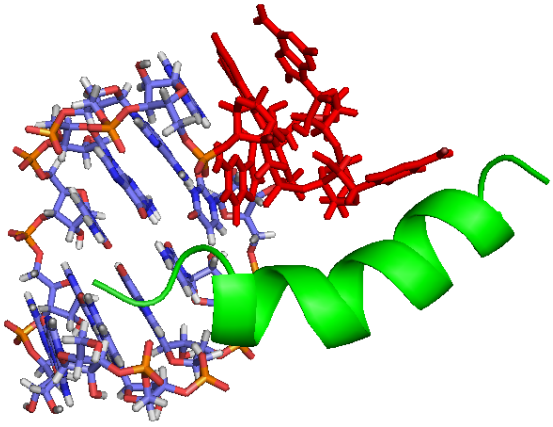

Figure 2.4. The bacteriophage λ N-peptide/boxB RNA complex showing the formation of GNRA-like tetraloop (in red) in the RNA. (PDB ID = 1A4T) (Cai, Z. *et al*., 1998).

Structure-based analysis of amino acids and nucleotide components of RNA-protein complexes has been performed to know the nature of the interactions at the atomic level using a JAVA-based program ENTANGLE (Allers, J. & Shamoo, Y., 2001). The examples in this study were taken from three different categories: i) tRNA synthetases; ii) ribosomal protein complexes and iii) viral protein complexes. It was observed that specific RNA recognition is largely through single-stranded structures such as stem-loops, bulges, and kinks, which take advantage of all RNA functional groups. It was also revealed that the RNA and protein motifs made contact through salt bridges (ionic interactions), van der Waals forces, and hydrogen bonds between bases and protein backbone amide and carbonyl groups. Sixteen percent of the H bonds to RNA bases involved protein amide groups and 17% were with the carbonyl groups. Purine N-1 and pyrimidine N-3 positions were well utilized in all of these RNA-protein interactions, since they are readily available in single-stranded regions of RNA. Non-base interactions involved the ribose 2' OH for interacting with carbonyl oxygen atom of the polypeptide backbone. In this case, the 2'-OH group helps for distinction of RNA from DNA for RNA-binding peptides and proteins. Out of the twenty amino acids, arginine was found to have the most contacts with all four bases of RNA. It was speculated that since the guanidium group of arginine is ionized at physiological pH, it forms pentadentate hydrogen bonds with RNA, whereas its long aliphatic chain helps to tether it to the main protein chain (Allers, J. & Shamoo, Y., 2001).

Ribonucleoprotein complexes as observed in transcriptional elongation in viruses, RNA processing, and tRNA coding have conserved sequence peptide motifs. These peptide motifs include RNA shape-dependent recognition by the double-stranded

RNA-binding motif (dsRBM), RNA sequence- and shape-dependent recognition by an RNA-recognition motif (RRM), RNA recognition by zinc fingers (Zif), and arginine-rich peptide motifs (ARMS).

RNA shape-dependent recognition by dsRBM is a stretch of 70 to 75 amino acids with a conserved $\alpha\beta\beta\beta\alpha$ protein topology. These motifs are present in a variable number of copies and up to five in *Drosophila melanogaster* staufen (Ramos, A. *et al*., 2000). These are categorized into two groups, depending on the presence of the catalytic domain in the protein (Fierro-Monti, I. *et al*., 2000). In the first category, the catalytic domain of RNA-dependent protein kinase (PKR) works in affiliation with this motif (Green, S.R. & Mathews, M.B., 1992; Patel, R.C. & Sen, G.C., 1992). The dsRNA-specific adenosine deaminases ADAR 1 and 2, in which the adenosines are converted to inosine, also represent the same category (Bass, B.L. & Weintraub, H., 1988). In the second category, the dsRBM proteins are missing the catalytic domain. Examples from this category are the transcription-related nuclear factor (NF90) family (Corthesy & Kao, 1994), trans-activation region (TAR)-RNA-binding protein (TRBP) (Benkirane, M. *et al*., 1997), vaccinia virus E3L protein (Romano, P.R. *et al*., 1998), and the RNAi/miRNA pathways-related RDE4/R2D2/HYL1 proteins (Tabara, H. *et al*., 2002; Liu, Q. *et al*., 2003).

The crystal structures of a dsRBM from *Xenopus laevis* RNA-binding protein (Xlrbpa2) complexed with a 10-bp dsRNA reveals that dsRBM interacts along one face of the RNA duplex through both α helices and a $\beta1$-$\beta2$ loop. The main interactions of the dsRBM with RNA are with the 2' OH and phosphate oxygens of two consecutive shallow grooves separated by a deep groove (Ryter, J.M. & Schultz, S.C., 1998) (Figure

2.5). The structures of two other related complexes of dsRBM-dsRNA complex of *Drosophila* staufen dsRBM3 with an RNA hairpin and that of *Escherichia coli* RNaseIII dsRBM with dsRNA show that dsRBMs recognize the RNA A-form helix through their loops 2 and 4 (Ramos, A. *et al*., 2000; Blaszczyk, J. *et al*., 2004).

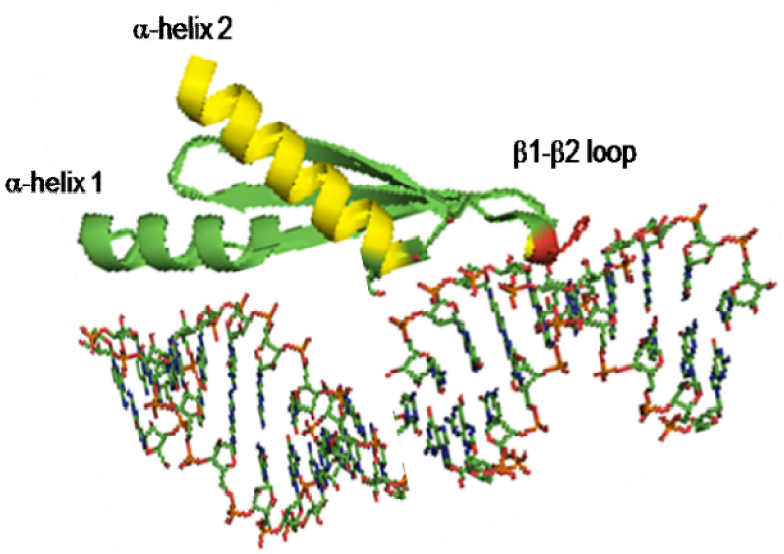

Figure 2.5. The dsRBM (double-stranded RNA-binding motif) of *Xenopus laevis* (Xlrbpa2) with its α helix 1, the β_1-β_2 loop, and the α helix 2 identifying the shape of dsRNA (Ryter, J.M. & Schultz, S.C., 1998, PDB ID = 1DI2).

RNA sequence- and shape-dependent recognition by an RNA-recognition motif (RRM) or RNA-binding domain (RBD) is the most common small protein motif of approximately 90 amino acids. RRM or RBD has a protein topology of $\beta\alpha\beta\beta\alpha\beta$, forming a four-stranded β-sheet against two α helices (Clery, A. *et al*., 2008). The β sheet is mainly involved in the recognition of single-stranded RNAs. RRMs bind several nucleotides, starting from a minimum of two in CBP20 RRM (Mazza, C. *et al*., 2002) and nucleolin RRM2 (Johansson, C. *et al*., 2004) to a maximum of eight in U2B" RRM1 (Price, S.R. *et al*., 1998). The bases of these RNA nucleotides are oriented parallel to

the β sheet plane and often contact the conserved hydrophobic amino-acid side chains (Clery, A. *et al*., 2008) (Figure 2.6).

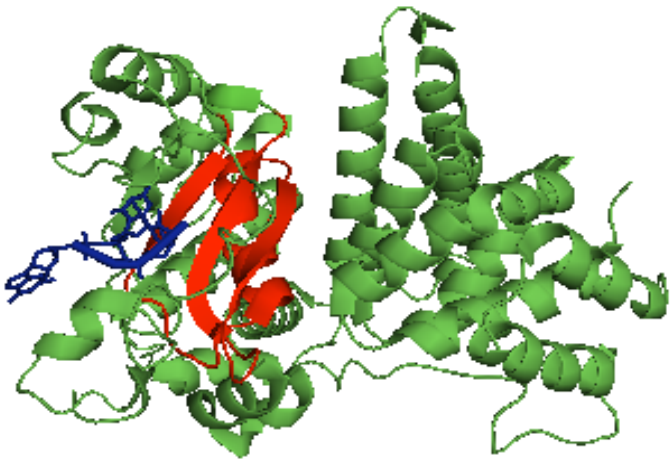

Figure 2.6. The RNA-recognition motif (RRM) of CBP20 in complex with m7GpppG (7-methyl-G(5')ppp(5')G is presented above (Mazza, C. *et al*., 2002, PDN ID = 1H2T). The m7GpppG is shown in blue.

In prokaryotes and viruses, approximately 80 proteins having one RRM motif have been identified (Maruyama, K. *et al*., 1999), whereas in eukaryotes, the RRM is the most common protein motif and more than 6000 RRM motifs have been recognized (Bateman, A. *et al*., 2002). In eukaryotes, the RRMs are often present as multiple copies of two to six RRMs (Oberstrass, F.C. *et al*., 2005). A few examples of RRMs include two RRM motifs of the sex lethal protein of *Drosophila melanogaster*, RRM1 of spliceosomal protein U1A (Handa, N. *et al*., 1999), and the poly (A)-binding protein (PAPB), in which RRM-containing proteins bind to more than three nucleotides and can distinguish longer single-stranded RNAs (Deo, R.C. *et al*., 1999).

Zinc-finger motifs displaying a ββα protein fold are common DNA-binding motifs (Pavletich & Pabo, 1991; Wolfe, S.A. *et al*., 2000). In the ββα protein fold, the β hairpin and α-helix are held together by a Zn^{2+} ion. They bind to specific bases in the DNA

major groove through protein side chains of the α helix (Pavletich, N.P. & Pabo, C.O., 1991). The first evidence of zinc finger binding to RNA came in crystal structure of the CCHH-type zinc finger of transcription factor IIIA (TFIIIA) with a 61-nucleotide fragment of 5S rRNA (Pelham, H. & Brown, D., 1980). CCHH-type zinc fingers have two modes of RNA-binding strategies; first, they interact non-specifically with the backbone of double helix and second, they recognize bulged-out bases of the structurally rigid elements. In the case of the zinc finger of TFIIIA bound to RNA, the F5 α helix recognizes dsRNA by contacts through basic amino acids to the RNA sugar-phosphate backbone, and the F4 α helix interacts with a bulged guanosine through the side chain of amino acids at the N-terminus (Lu, D. *et al*., 2003).

2.1.3. Phage display and RNA

2.1.3.1. Phage display with RNA: early examples

RNA has the capacity of folding into complex three-dimensional shapes, and its participation in many biological processes makes it more intriguing to learn its mode of binding with small molecules (Thomas, J.R. & Hergenrother, P.J., 2008). This knowledge can help in understanding the basic principles of nucleic-acid recognition involved in various natural processes. Advanced crystal structures of RNA-protein complexes and new combinatorial tools have led to the successful designing of peptides and small-molecule RNA binders (Carter, A. P. *et al*., 2000). The multiplicity of shapes of RNA gives the possibility of designing ligands with high affinities and specificities; however, RNA often rearranges itself in proper conformation after ligand binding. Thus,

the RNA target site may not be well defined without the ligand (Cheng, A.C. *et al*., 2001).

As mentioned in Section 2.1.1., phage display is a molecular biology-based technique for selecting peptide ligands for targets such as proteins, enzymes, and RNA (Lowman, H.B. 1997). The high diversity of the libraries allows the discovery of specific and high-affinity ligands for the target. A phage-display library based on the RNA recognition motif 1(RRM1) of U1A protein was one of the first peptide libraries to be targeted against the U1 snRNA hairpin binding site (Laird-Offringa, I.A. & Belasco, J.G., 1995). The library was constructed by inserting the N-terminal U1A domain (1-101 amino acids) into a phage-display vector. In order to determine which amino-acid residues were important for binding with U1 snRNA, nine key amino acids were partially randomized. After the selection, four of the nine amino acids were essentially appearing in all of the sequenced clones. Further analysis at position 49 showed that upon binding, the long side chain of leucine 49 (present in the β2-β3 loop of the RRM domain) was helping the protein to lock into the U1 snRNA loop. Also, one peptide sequence was found to bind to the U1 snRNA with two-fold higher affinity than the wild-type RRM. Thus, the phage library proved to be an efficient *in vitro* method of clarifying RNA-binding affinity of specific RNA-binding proteins (Laird-Offringa, I.A. & Belasco, J.G., 1995).

A random phage-display library was also used for selecting peptide ligands against the triply methylated, 17-nucleotide anticodon stem and loop (ASL^{Phe}) domain from yeast $tRNA^{Phe}$ (Agris, P.F. *et al*., 1999). The ASL^{Phe} (containing three of the five modifications Cm_{32}, Gm_{34}, m^5C_{40}) formed a five base-pair stem and a seven-membered

loop as its secondary structure. The 15-amino-acid peptide phage library used for selection had no preset restraints on the phage coat proteins, and the phage clones were sequenced after the fourth and fifth rounds of selection. The high-affinity peptides identified contained nonpolar aliphatic and aromatic amino acids. Tryptophan was the common aromatic amino acid present in the peptide sequences, but was not located in the center of the sequence. Serine was a frequent polar residue present at the N- and C-terminal positions of the peptide sequence. Fluorescence and circular dichroism spectroscopies were utilized for determining the binding constants of the peptides (Agris, P.F. *et al*., 1999). One of the peptides was further tested for inhibition of aminoacylation of the tRNA by its phenylalanyl-tRNA synthetase (FRS). The results indicated that the selected peptide bound to the tRNA effectively and had the ability to recognize the modifications as simple as methylations (Mucha, P. *et al*., 2001).

2.1.3.2. Phage library with zinc fingers

Another example of a phage library targeted towards RNA involved a zinc finger (ZF) library. The zinc-finger module, as mentioned earlier, is a widely studied motif with DNA-binding properties (Elrod-Erickson, M. *et al*., 1998; Turner J. & Crossley M., 1999). Following the discovery of DNA interactions, the binding of zinc fingers to RNA was also assessed (Blancafort, P. *et al*., 1999). A phage-displayed zinc finger (ZF) library was designed based on interactions of the Zif268-DNA model. Zif268 is mouse transcription factor and has three ZF domains, ZF1, ZF2, and ZF3 which bind to double-helical DNA (Pavletich, N.P. & Pabo, C.O., 1991). In the phage-display library, the middle ZF region (ZF2) was randomized while keeping the other two ZFs intact. Then, oligonucleotides

were designed in which the middle DNA triplet that binds to ZF2 was replaced with a variety of RNA triplets. The other two flanking DNA helices used to anchor the two flanking fingers, ZF1 and ZF3, were retained. Selection using this library against an RNA duplex having rG-C, rC-G, rA-U, and rU-A as the middle base pairs failed to capture any ZF phage. In contrast, when a selection was performed with an RNA duplex having rG-A as the middle base pair, ZF phage were selected after the fourth round. Specificity of binding of ZF phage clones for the G•A base pair within RNA triplets was tested by substituting with other base pairs. Only the RNA triplet with a C•A base pair was found to have significant affinity for this ZF clone. The NMR structure of ZF with the rG-A RNA duplex suggested that the interaction of ZF selected for RNA from the library was similar to that of ZF2 in Zif268-DNA complex. The rG-A base pair widened the deep groove of the RNA and made it more accessible for the α helices of the phage zinc finger (Blancafort, P. *et al*., 1999).

Combinatorial RNA-binding, zinc-finger libraries based on randomized α helices were also utilized to illustrate the amino acids required for binding TFIIIA ZF4 to 5S rRNA. It was observed that the RNA-binding zinc fingers also make use of a recognition helix for binding into the RNA deep groove (Friesen, W.J. *et al*., 1997). Similarly two-finger proteins recognizing 5S rRNA and the HIV-1 Rev response element (RRE) IIB were identified using the phage library based on TFIIIA finger 4 libraries (Friesen, W.J. & Darby, M.K., 1998)

2.1.3.3. Phage library with randomized α helix

The phage-display methodology has been applied to reduce the size of the binding domain of the Z-protein having a three α helical groups interacting with the F_c part of the immunoglobulin IgG_1 (Braisted, A.C. & Wells, J.A., 1996). The small binding motifs are simple to synthesize and more compliant for learning the basis of the protein function. The crystal structure of the complex (protein A and the IgG) showing the contacts of the protein part were from helices 1 and 2 but not 3; however, upon deleting helix 3, the affinity of the protein was reduced >105 fold. Therefore, the contacts of helices 1 and 2 were improved systematically by employing phage display and structure-based design to get a K_d of 43 nM (Braisted, A.C. & Wells, J.A., 1996).

The Z-domain of protein A (immunoglobulin binding staphylococcal protein A) was presented on M13 phage (Djojonegoro, B.M. *et al*., 1994). The phagemid libraries based on the peptide representing the first two helices of the Z-domain were assembled. These libraries contained the exoface, interface and intraface regions of the Z-domain. The best binder of the exoface library was considered as starting point for the intraface library and then the best peptide from that library was used as basis for the interface library. From this approach of sequential phage display, a peptide about half the size of its parent protein was selected having the same affinity as wild-type Z-domain (Braisted, A.C. & Wells, J.A., 1996).

In a different study regarding the three α-helical Z-domain of the staphylococcal protein A, phage libraries were constructed based on this domain (Nord, K. *et al*., 1997). They were prepared by randomization of 13 residues present at the two α helices involved in Fc-binding activity of the wild-type domain by employing either NNG/T or

(C/A/G)NN degeneracy strategies. Then, biopanning was performed against targets Taq DNA polymerase, human insulin, and a human apolipoprotein A-1 variant. The selected peptides were studied through SDS-PAGE and CD spectroscopy, and it was observed that the peptides had similar secondary structure to the native Z-domain. The binding analysis of these peptides resulted in micromolar dissociation constants (K_d) for their targets (Nord, K. *et al*., 1997).

2.2. Rationale of the project

Phage-display libraries were utilized in this project to select peptide ligands against the target RNA, helix 69 (H69) of *E. coli*. The rationale was to identify peptides as possible drug leads and to develop small molecules, as alternatives to aminoglycosides, as preferential binders for the ribosomal RNA target (Scheunemann, A.E. *et al*., 2010). The peptides also provide information regarding the nature and the spatial orientation of the functional groups in H69 RNA that are important for drug targeting. In addition, small peptides carved out of the RNA-binding domain of a complex protein have been shown to recognize its specific RNA site in the absence of extensive parent protein structure with almost the same affinity (Jiang, F. *et al*., 1999). There are examples in the literature supporting peptides as drug leads such as those designed for platelet glycoprotein IIb/IIIa (McDowell, R.S. *et al*., 1994) and another being advanced for rheumatoid arthritis (Adalimumab, 2003). In earlier studies aimed at learning about the chemistry of protein binding sites of antibodies, peptides gave information about the contributing functional motifs of the proteins (Benguri, D.R. *et al*., 2001). We hope to gain similar information with RNA targets by the use of peptides.

Phage-display techniques are well established with adequately laid out protocols that are easy to follow. Phage display is a viable choice because it utilizes the chemical and structural diversity of peptide libraries. The power of using phage-display libraries lies in the ability of rapid peptide-library construction with high diversity, affinity selection, amplification for enrichment of high-affinity peptides, and analysis of results (Smith, G.P. *et al*., 1997). Phage-display libraries have been widely used to isolate peptides and proteins that bind to antibodies or receptors, but also to study protein interactions with DNA/RNA (Marks, J.D. *et al*., 1991; Malmborg, A.C. *et al*., 1996). An example already mentioned is the phage-display library based on RRM1 (RNA recognition motif) of the U1A protein, which was one of the first peptide libraries to be targeted against the U1 snRNA hairpin binding site (Laird-Offringa, I.A. *et al*., 1995).

The target in this study is H69. H69 is a 19-nucleotide hairpin present in domain IV of bacterial 23 S rRNA (residues 1906-1924). This RNA has three post-transcriptionally modified pseudouridines (Ψ) at positions 1911, 1915, and 1917, with the pseudouridine at 1915 being methylated at N3 (Bakin, A. & Ofengand, J., 1993; Kowalak, J.A. *et al*., 1996). H69 rRNA has been chosen as a novel antibacterial target because this is the major constituent of the intersubunit bridge B2a in the ribosome (Yusopova, M.M. *et al*., 2001). This bridge is formed during the association of the two ribosomal subunits in the functional center of the ribosome. H69 is the element participating with the small subunit decoding region at helix 44 (h44). The region of the large subunit harboring hairpin H69 has been shown to be protruding from the 50 S subunit (Merryman, C. *et al*., 1999). The main idea behind this project was to obtain

phage-selected peptides as potential inhibitors of this rRNA bridge B2a, which could then lead to disruption of protein synthesis in bacterial pathogens.

2.3. Phage display library for selection

For selecting peptides against bacterial H69 in this project, the Ph.D.-7 Phage Display Peptide Library™ was chosen. This random peptide library is based on M13 filamentous bacteriophage and contained approximately ~2.8 x 10^9 independent phage clones amplified once to yield ~70 copies of each sequence in 10 μl of the supplied phage library solution. The random, foreign, seven amino-acid peptides were expressed along the N-terminus of the minor p3 coat protein with a copy number of three to five at one end of the phage particle. The first residue of the mature protein is the first randomized position. Then, the peptide is followed by a short spacer (Gly-Gly-Gly-Ser) and the wild-type p3 sequence.

2.4. Materials and methods

2.4.1. General materials

The materials included H69 RNA (5'-GGCCGΨAACm^{3}ΨAΨAACGGUC-3'), which was custom synthesized at Dharmacon Research Inc., (Lafayette, CO). The 3-methylpseudouridine (m^{3}Ψ) in the H69 sequence was synthesized by Helen Chui in our lab (Chui, H.M. *et al*., 2002). H69 was biotinylated at the 5' end following the procedure given in the 'Oligonucleotide biotin-labeling kit' from Amersham Life Science, Inc., (Piscataway, NJ). The enzyme polynucleotide kinase (PNK) was obtained from New England Biolabs (Ipswich, MA) and iodoacetyl-LC-biotin was purchased from Pierce

Biotechnology (Rockford, IL). The Ph.D.-7™ and Ph.D-12™ phage display library kits were purchased from New England Biolabs (Ipswich, MA). The kits included phage display library solution in TBS (50 mM Tris-HCl, pH 7.5; 150 mM NaCl) with 50% glycerol, *E. coli* ER 2738 host strain in 50% glycerol solution, streptavidin (lyophilized), biotin (10 mM, pH 7.0), -96 g3 sequencing primer (5'-CCCTCATAGTTAGCGTAACG-3',1 pmol/μL) and -28 g3 sequencing primer (5'-GTATGGGATTTGCTAAACAAC-3',1 pmol/μL). Streptavidin-coated plates (Reacti-Bind-streptavidin coated polystyrene 96-well plates from Sigma) were used for immobilizing the biotinylated RNA. The solutions used for biopanning experiments included LB medium (for 1 L: 10 g Bacto-tryptone, 5 g yeast extract, 5 g NaCl), agarose top (for 1 L: 10 g Bacto-tryptone, 5 g yeast extract, 5 g NaCl, 1 g $MgCl_2 \bullet 6H_2O$), TBS (50 mM Tris-HCl pH 7.5, 150 mM NaCl), PEG/NaCl (20% {w/v} polyethylene glycol-8000, 2.5 M NaCl), TBST (50 mM Tris-HCl, pH 7.5; 150 mM NaCl, 0.1% Tween-20), buffer A (10 mM Tris-HCl pH 7.5, 10 mM $MgCl_2$, 50 mM NaCl, 1 mM dithiothreitol), buffer B (0.2 M glycine-HCl pH 2.2, 1 mg/mL BSA), TBS with 0.02% sodium azide (final concentration), and equilibrated phenol solution (pH > 8). Isopropyl β-D-1-thiogalactopyranoside (IPTG), 5-bromo-4-chloro-3-indolyl-b-D-galactopyranoside (X-gal), tetracycline, bovine serum albumin (BSA), phenol solution and Tween-20 were purchased from Fisher Scientific (Pittsburgh, PA).

IPTG/Xgal stock solution was prepared in 25 mL ethanol by adding 1.25 g of IPTG (final concentration of 0.2 M) and 1 g of Xgal (final concentration of 0.1 M) and was stored in dark at -20 °C. The tetracycline stock solution was prepared by adding 20 mg in 1 mL of ethanol (final concentration of 0.045 M) and stored in dark at -20 °C. The LB/IPTG/Xgal plates used for growing the phage plaques had LB medium (1 L) and 15

g/L agar. The solution was autoclaved and after cooling to <70 °C, I mL of IPTG/Xgal stock solution was added to give final concentration of IPTG as 0.2 mM and Xgal as 0.1 mM. The LB/tet plates were prepared by adding 15 g/L agar to LB medium (I L), and then the solution was autoclaved. After cooling the solution to <70 °C, 1 mL tetracycline stock solution was added (final concentration of tetracycline was 0.02 mg or 0.045 mM).

The T4 polynucleotide kinase (PNK) was purchased from New England Biolabs (Ipswich, MA). Bacto agar and bacto tryptone were obtained from Difco (Detroit, MI). Acrylamide, bis-acrlyamide, ammonium persulfate, glycine-HCl, urea, *N*,*N*,*N*′,*N*′-tetramethyl-ethane-1,2-diamine (TEMED) and yeast extract were bought from Sigma (St. Louis, MO). Tris, NaCl, KCl, $MgCl_2$, EDTA, HEPES, dithiothreitol (DTT), sodium azide (NaN_3) and glycerol were bought from Fisher Scientific (Pittsburgh, PA). Sequitherm EXCEL II DNA sequencing kit was obtained from Epicentre Biotech (Madison, WI). Long range gel solution for sequencing was from Cambrex Bioscience (Rockland, ME).

2.4.2. Biotin-labeling of RNA

Helix 69 rRNA (H69), the target in this selection procedure, was biotinylated at its 5' end using a modified protocol provided by the 'Oligonucleotide biotin-labeling kit' (Amersham Life Science, Inc. 1995). H69 was first phosphorothiated at the 5' end using a kinase reaction and then biotinylated in the coupling reaction as shown in Figure 2.7. The modifications in the procedure were: i) for the kinase reaction, the RNA solution was first boiled and immediately placed on ice, ii) the amount of enzyme polynucleotide kinase (PNK) for the kinase reaction was increased to 5 μl, iii) after the kinase reaction

was completed, the reaction mixture was dried for 2 h or until it was almost dry, iv) the incubation time of the coupling reaction was increased to 1.5 - 2 h, v) after coupling was completed, 500 µl of ddH_2O was added and then dried in speed-vac, and vi) no ethanol precipitation was performed and samples were resuspended in ddH_2O for gel purification.

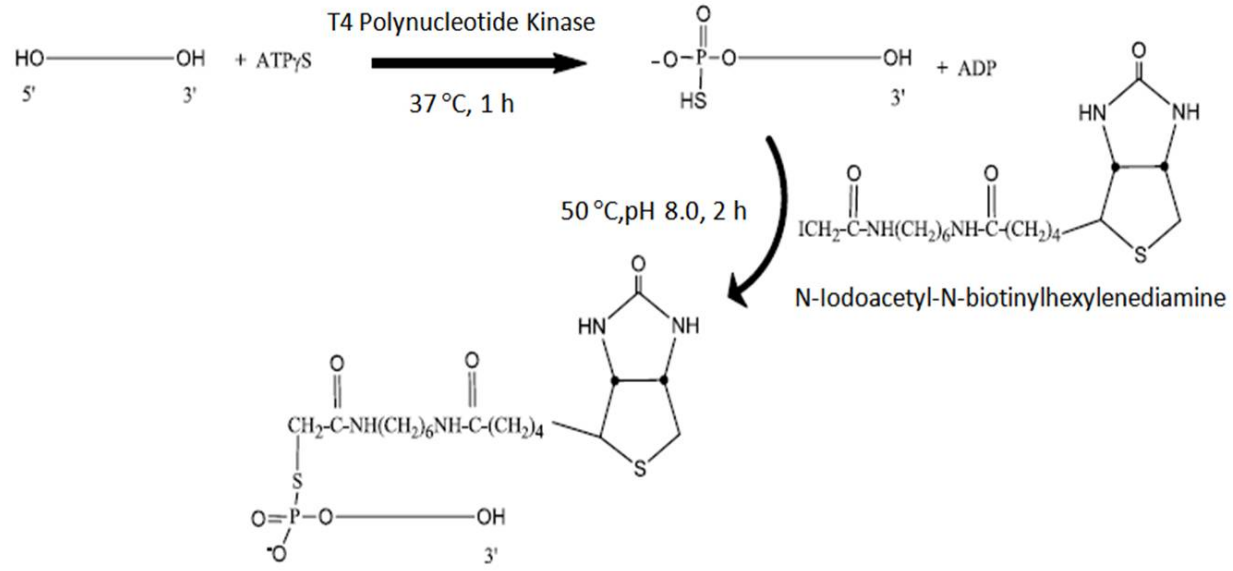

Figure 2.7. The biotinylation reaction scheme for 5'-biotin labeling of H69 consisting of kinase reaction with polynucleotide kinase and coupling reaction with N-Iodoacetyl-N-biotinylhexylenediamine is summarized.

2.5. Biopanning, or affinity selection, of peptides

2.5.1. On-plate, one-step selection

In the first attempt of biopanning or affinity selection, the process of selection and biopanning was carried out as given in the protocol provided by NEB (Ph.D-7™ kit) with minor modifications. During the first level of stringency, performed in the first round, the biotinylated H69 RNA (50 pmoles) was incubated overnight at 4 °C with gentle shaking in one well of the streptavidin-coated microtiter plate, in 150 µL buffer A (10 mM

Tris-HCl, 10 mM $MgCl_2$, 50 mM NaCl, 1 mM DTT). The binding solution was then poured off and the well was blocked with 3 mg/ml BSA for 1.5 h at 4 °C. Subsequently, the well was washed with TBST (50 mM Tris-HCl, 150 mM NaCl, pH 7.5 and Tween-20 0.1%) 6-8 times. Phage solution (10 µL of the original library in 100 µL of buffer A, 2 x 10^{11} pfu where pfu is plaque forming unit) was pipetted into a well having no immobilized target RNA and incubated for 1 h at RT with gentle shaking for pre-screening of the library. The phage library was later removed and added to the well having the immobilized target RNA for 1 h incubation at RT, with gentle shaking. After 1 h, the library was discarded and the unbound phage was washed with TBST (10-12 times). The bound phage were eluted with 100 µL of 0.2 M glycine-HCl (pH 2.2) containing 1 mg/mL BSA and neutralized immediately with 15 µL 0.1 M Tris-HCl, pH 9.0. The eluate was titered and amplified in ER2738 cells for use in subsequent rounds of panning.

In the next level of stringency, performed in the second round, the phage were incubated with 20 pmoles of biotinylated H69 RNA , the well was blocked with 5% non-fat dry milk, and washed with TBST buffer having Tween-20 concentration of 0.3%. The amplified phage library from first round was incubated for 30 min., at RT with the target RNA. For removing unbound phage, the timing of the even washes was 30 sec. and for odd washes was 3 min., and 12 washes were carried out.

In the third level of stringency, performed in the third round, the concentration of biotinylated H69 RNA was reduced to 10 pmoles, blocking of the well having immobilized RNA was conducted using 3% BSA. The amplified phage library from second round was incubated with target RNA for 15 min. at RT with gentle shaking. For

removing unbound phage, the timing of the even washes was 30 sec. and for odd washes was 3 min. and 14 washes were carried out. For the fourth round of the selection, target RNA was immobilized in two separate wells of the streptavidin-coated plate in order to carry out specific and non-specific elution for the bound phage. The specific elution was carried out with 30 pmoles of H69 RNA in TBST buffer, whereas the non-specific elution was performed with 100 µl of 0.2 M glycine-HCl (pH 2.2) containing 1 mg/ml BSA and neutralized immediately with 15 µL 0.1 M Tris-HCl, pH 9.0. The other experimental conditions were kept the same as third round. The conditions for selection are summarized in Table 2.1.

In the second attempt of screening, several changes were made in the screening procedure. The procedure for selection was carried out under similar conditions as the first attempt, but with the addition of tRNA (90 pmoles) and biotin (0.1 mM) during the third and fourth rounds as competitiors during incubation of the library with H69. The conditions of screening for the second attempt are summarized in Table 2.2.

Table 2.1. Conditions of biopanning summarized during the first attempt of selection for H69.

Biopanning rounds	[B-H69][a] pmoles	B-H69 binding time	B-H69 binding buffer	Blocking buffer	Number of washes	Wash buffer
Round 1	50	4 h at RT or O/N at 4 °C	Buffer A[b]	3% BSA	8	TBS[d] w/ 0.1% Tween-20
Round 2	20	4 h at RT or O/N at 4 °C	Buffer A[b]	5% non-fat dry milk	10	TBS[d] w/ 0.1% Tween-20
Round 3	10	4 h at RT or O/N at 4 °C	Buffer A[b]	3% BSA	12	TBS[d] w/ 0.1% Tween-20
Round 4	10	4 h at RT or O/N at 4 °C	Buffer A[b]	3% BSA	12	TBS[d] w/ 0.1% Tween-20

Phage binding buffer	Phage binding time	Number of washes	Wash buffer	Phage elution time	Elution buffer
TBS[d] w/ 0.1% Tween-20	60 min.	12	TBS[d] w/ 0.1% Tween-20	10 min.	Buffer B[c]
TBS[d] w/ 0.1% Tween-20	30 min.	12 (3 min. even & 30 s odd washes)	TBS[d] w/ 0.3% Tween-20	10 min.	Buffer B[c]
TBS[d] w/ 0.1% Tween-20	15 min.	14 (3 min. even & 30 s odd washes)	TBS[d] w/ 0.5% Tween-20	10 min.	Buffer B[c]
TBS[d] w/ 0.1% Tween-20	15 min.	14 (3 min. even & 30 s odd washes)	TBS[d] w/ 0.5% Tween-20	10 min.	Buffer B[c] & 30 pmoles H69 in 100 µL TBS[d] for specific elution

a) B-H69: 5'-biotinylated fully modified H69
b) Buffer A: 10 mM Tris-HCl pH 7.5, 10 mM $MgCl_2$, 50 mM NaCl, 1 mM DTT
c) Buffer B: 0.2 M glycine-HCl pH 2.2, 1 mg/ml BSA
d) TBS: 50 mM Tris-HCl (pH 7.5), 150 mM NaCl

Table 2.2. The biopanning conditions in second attempt of selection for H69.

Biopanning rounds	[B-H69][a] pmoles	B-H69 binding time	B-H69 binding buffer	Blocking buffer	Number of washes	Wash buffer
Round 1	50	4 h at RT or O/N at 4 °C	Buffer A[a]	3% BSA	8	TBS[b] w/ 0.1% Tween-20
Round 2	20	4 h at RT or O/N at 4 °C	Buffer A[a]	5% non- fat dry milk	10	TBS[b] w/ 0.1% Tween-20
Round 3	10	4 h at RT or O/N at 4 °C	Buffer A[a]	3% BSA	12	TBS[b] w/ 0.1% Tween-20
Round 4	10	4 h at RT or O/N at 4 °C	Buffer A[a]	5% casein sol.	14	TBS[b] w/ 0.1% Tween-20

Phage binding buffer	Phage binding time	Number of washes	Phage binding buffer	Phage elution time	Elution buffer for non-specific elution
TBS[c] w/ 0.1% Tween-20	60 min.	12	TBS[c] w/ 0.1% Tween-20	10 min.	Buffer B[c]
TBS[c] w/ 0.1% Tween-20	30 min.	12 (3 min. even & 30 s odd washes)	TBS[c] w/ 0.3% Tween-20	10 min.	Buffer B[c]
TBS[c] w/ 0.1% Tween-20 and 90 pmoles tRNA & 0.1 mM biotin	15 min.	14 (3 min. even & 30 s odd washes)	TBS[c] w/ 0.5% Tween-20 and 90 pmoles tRNA & 0.1 mM biotin	10 min.	Buffer B[c]
TBS[c] w/ 0.1% Tween-20and 90 pmoles tRNA & 0.1 mM biotin	15 min.	14 (3 min. even & 30 s odd washes)	TBS[c] w/ 0.5% Tween-20 and 90 pmoles tRNA & 0.1 mM biotin	10 min.	Buffer B[c]

a) Buffer A: 10 mM Tris-HCl pH 7.5, 10 mM $MgCl_2$, 50 mM NaCl, 1 mM DTT
b) TBS: 50 mM Tris-HCl (pH 7.5), 150 mM NaCl
c) Buffer B: 0.2 M glycine-HCl pH 2.2, 1 mg/ml BSA

2.5.2. Phage amplification and titering

After performing the particular round of biopanning with the target, a small amount of the eluted phage library or eluate (~1 μL) was set aside for carrying out titering of the unamplified eluate. The rest of the eluate was stored at 4 °C for next day amplification. An overnight culture of ER2738 in LB-tet was set up. On next day, the overnight culture of ER2738 was diluted in 1:100 ratio in LB medium (200 μL to 20 mL of culture) in a 250 mL Erlenmeyer flask and the remaining stored unamplified eluate was added to the diluted culture. Then, the flask was shaken vigorously at 37 °C for 4.5 h. After shaking, the culture was transferred to a centrifuge tube (50 mL) and spun for 10 minutes at 10,000 rpm at 4 °C. The process was repeated by transferring the supernatant to a fresh 50 ml centrifuge tube and re-spun. Then, the upper 80% supernatant (~ 16 mL) was pipeted to another fresh 50 mL centrifuge tube and 1/6 volume of PEG/NaCl was added to the solution. The phage was then allowed to precipitate at 4 °C for overnight.

On the next day, the PEG solution was precipitated for 15 minutes at 10,000 rpm at 4 °C, the supernatant was carefully decanted while leaving the pellet. The pellet was suspended in 1 ml TBS and the suspension was transferred to a centrifuge tube. It was spun for 5 minutes at 4 °C to remove residual cells and the supernatant was transferred to second centrifuge tube. Then 1/6 volume of PEG/NaCl was added to the tube and the tube was incubated on ice for 15-60 minutes. After that step, the tube was centrifuged for 10 minutes at 4 °C. The supernatant was discarded and after brief re-spinning, the remaining supernatant was removed. Finally, the pellet was suspended in

200 μL of TBS, 0.02% NaN_3 solution. The tube was centrifuged for another 1 minute to completely eliminate any insoluble matter. The supernatant was then transferred to a new tube and labeled as amplified eluate.

The titering of the phage eluate (unamplified or amplified) is the procedure to count the number of phage particles present in the eluate of the library after every round of selection. Each phage particle is represented by the "plaque" or hole formation on the LB/IPTG/Xgal plate. These plaques are formed due to the growth of the individual phage in a bacterial host cell suspended in the top agar lawn. The M13 phage is nonlytic phage so the plaques are due to diminished growth of the bacterial cells. Therefore, the number of viruses in the aliquot added to the plate is equal to the number of plaques that appear. The phage plaques of the M13 library used in this project were blue in color due to the presence of IPTG/Xgal. During the titering procedure firstly, 10-fold dilutions of the phage-display library in LB medium were prepared as given in the Table 2.3.

Table 2.3. The series of dilutions prepared for unamplified and amplified phage libraries after each round.

DILUTIONS	DILUTION FACTOR
10 μL given library solution + 90 μl LB	10^1
10 μL 10^{-1} dilution + 90 μL LB	10^2
10 μL 10^{-2} dilution + 90 μL LB	10^3
10 μL 10^{-3} dilution + 90 μL LB	10^4
10 μL 10^{-4} dilution + 90 μL LB	10^5
10 μL 10^{-5} dilution + 90 μL LB	10^6
10 μL 10^{-6} dilution + 90 μL LB	10^7
10 μL 10^{-7} dilution + 90 μL LB	10^8
10 μL 10^{-8} dilution + 90 μL LB	10^9

10 µL 10^{-9} dilution + 90 µL LB 10^{10}

The culture of ER2738 cells was set up by inoculating a single colony of ER2738 in 5-10 mL of LB medium. The solution was incubated with shaking until mid-log phase (OD_{600} ~ 0.5) was achieved. Meanwhile, the agarose top was melted in the microwave and equilibrated at 45 °C until ready for use. Then, the LB/IPTG/Xgal plates were pre-warmed at 37 °C until ready for use. Once the culture reached the mid-log phase, 50 µL was dispensed into microcentrifuge tubes (one for each dilution) already having 450 µL of melted agarose on top. Later, 1 µL solution from each dilution was added to the labeled microcentrifuge tubes, vortexed quickly, and added on the pre-warmed LB/IPTG/Xgal plate. The plates were divided into 2-4 sections for plating different dilutions on the same plate. The agarose top was spread evenly by tilting the plate. The plates were allowed to cool for 5 minutes, inverted, and incubated overnight at 37 °C. On the next day, the plaques were counted on plates having ~10^2 plaques. The number of the plaques was multiplied by the dilution factor for that plate to get the phage titer in plaque forming units (pfu) per µL.

2.5.3. Phage DNA purification

After the blue plaques were observed on the plates, each one of them represented a single DNA sequence to be purified by automated sequencing. The purification started with setting up an overnight culture of ER2738 in LB-Tet medium from a single colony. The next day, the culture was diluted in 1:100 in LB medium. Using a pipette tip, a blue plaque was picked up and transferred to centrifuge tube having 1 mL of diluted culture of ER2738. The tube was then incubated at 37 °C for 4.5-

5 h with vigorous shaking. Later, the mixture was centrifuged at 10,000 rpm for 5 minutes. The supernatant (~ 800 μL) was transferred to a new tube; 400 μL of 20% PEG-NaCl was added and carefully mixed by vortexing the solution. After vortexing, the solution was incubated at room temperature for 10 minutes and then centrifuged at 10,000 rpm for 10 minutes. The supernatant was removed and the pellet was dissolved in 70 μl TE buffer (10 mM Tris-HCl, pH 7.3; 1 mM EDTA). For DNA extraction phenol-chloroform extraction was carried out. An equilibrated solution of phenol (70 μL, pH > 8) was added, mixed properly by vortexing and then centrifuged at 10,000 rpm for 2 min. The lower phenol layer was removed very carefully and the supernatant was combined with 70 μL $CHCl_3$. After another centrifugation step, the lower $CHCl_3$ layer was discarded. Then, 7 μL of 3 M NaOAc and 100% cold ethanol (175 μL) were added to the supernatant and the solutions were stored at - 20 °C overnight. The next day, the sample was centrifuged at 15,000 rpm for 15 min, and after removing the supernatant, the pellet was washed with 500 μl of 70% ethanol. The pellet was then dried in the speed-vac and dissolved in 30 μl ddH_2O.

2.5.4. DNA sequencing

The phage DNA was sequenced using the LI-COR sequencer (Lincoln, Nebraska). The protocol for this sequencer comprised of four parallel PCR reactions (dATP, dTTP, dGTP, dCTP) for deciphering the DNA for each phage plaque. The reagents for the sequencing reactions were obtained from Sequitherm EXCEL II DNA sequencing kit (Epicentre Biotechnologies, Madison, WI). Each PCR reaction consisted of phage DNA template (0.6 μL) as purified in the above given protocol, premix solution

for each dNTP (1 μl), and 700 M13-96 rev primer (5'-CCCTCATAGTTAGCGTAACG-3') (LICOR) for M13 phage (0.96 μl). The premix solution for each PCR reaction included 3.5X sequencing buffer (0.4 μl), Taq DNA polymerase (0.05 μl) and dNTP (0.5 μl). The sequencing PCR protocol was designed as 1 cycle for 2 min at 94 °C, 29 cycles for 15 sec at 94 °C, 49.3 °C for 25 sec, and 72 °C for 25 sec, 1 cycle for 2 min at 72 °C, followed by holding at 4 °C. The reactions were performed in special PCR 0.2 ml tubes and after the PCR reaction was completed, loading dye (1 μl from the same kit) was added to each tube to discontinue the reaction. The samples were analyzed on 6% denaturing polyacrylamide gels with 7 M urea. Prior to loading the samples on the gel, the samples were denatured by heating for 5 min at 95 °C and then quick cooling on ice. After pre-running the gel for 20 min, the samples were loaded (0.6 μl for each lane) and the gel was run for 2.5 h at 12,000 V for every 25 cm gel.

2.5.5. Peptide synthesis

After the peptide sequences were identified, the peptides were chemically synthesized by Dr. Edvin Klosi and Dr. Chamila Rupasinghe using the micro TentaGel S-NH_2 beads by standard F-moc solid phase peptide synthesis procedure (Atherton, E. & Sheppard, R.C., 1989). The peptide beads were washed thoroughly with DMF and stored in DMF at 4 °C before use. In addition, the free peptides with C-terminal amidation were synthesized by following the standard F-moc solid phase peptide synthesis.

The peptide solutions were prepared in Millipore water and the solutions were quantified using the LavaPep peptide quantification kit (Fluorotechnics Pty. Ltd., 2006)

since the peptide lacked UV active amino acids such as tyrosine, tryptophan and phenylalanine. This kit has epicoccone dye, a fluorescent reagent that binds to lysine, histidine and arginine amino acids in the peptide sequence. The kit consists of two solutions named as part A that is dilute DMSO/acetonitrile solution of dye and part B that is bicarbonate buffer with SDS and acetonitrile. The dye fluoresces using a 540 ± 10 nm excitation filter and 630 ± 10 nm emission filter. For preparation of standard peptide curve, solutions of peptide HPVHHYQ-NH_2 in water were prepared in four-fold dilutions ranging from 40 ng/mL to 0.655 mg/mL. The working solution was prepared by mixing water, part A and part B in 8:1:1 ratio (the amount of solution depends on number of samples). For measuring fluorescence in 96-well microtiter plate, 50 µL of working solution was incubated with 50 µL of each HPVHHYQ-NH_2 peptide dilution in individual wells. Similarly a blank was prepared by adding 50 µl working solution and buffer /water (50 µL) in one well. For measuring peptide concentration of unknown concentration, 50 µL of that solution and 50 µL of working solution were added in another well. All the samples were incubated at room temperature in dark for 60 minutes. After recording the fluorescence readings using excitation wavelength of 540 nm and emission wavelength of 630 nm, the blank reading was subtracted from all the readings of solutions. A plot of log of fluorescence versus log of peptide concentration was generated using the linear fit. The equation obtained from the linear fit was then used for determining the concentration of peptide with unknown concentration.

2.6. Results and discussion

2.6.1. First screening using a seven-mer phage library on streptavidin-coated plates

The commercial Ph.D.-7™ (New England Biolabs) library was employed against H69 as target RNA and four rounds of selection were carried out. To obtain peptides specifically binding to H69 and for reducing the background nonspecific selection, the stringency of each round was increased at various steps. The conditions (discussed in chapter 3) were found to be successful for pulling out peptides having moderate affinity for the target H69 RNA. Stringency mainly refers to the scale at which high affinity peptides for the target are favored over low affinity or low specificity peptides.

Initial trials suggested that if stringency was too high, then no peptides would be selected. Stringency had to be lowered in order to get enough phage for the following rounds. The first step of each round was immobilization of biotinylated H69 (B-H69) on the streptavidin-coated plates. The concentration of B-H69 (in μM) used for immobilization was decreased with each round starting from 0.33, and decreasing to 0.2, 0.13, and 0.13 for respective rounds (Barrett, R.W. *et al*. 1992). Thus, the total number of pmoles of RNA on the surface was 50, 20, 10, and 10, respectively. The higher amount of the target for the first round will lead to the capturing of the peptides with a wide range of affinities for the H69 RNA. Lowering the amount of target for each round was carried out with the intention of obtaining a pool of peptides that have high affinity for the target.

Blocking buffers were applied in order to coat regions of the polystyrene plate that did not contain B-H69. The blocking reagents used during the selection were BSA (bovine serum albumin) and a non-fat dry milk solution. These two approaches were utilized since the presence of these soluble, globular, monomeric proteins without any characterized ligand-binding sites was expected to reduce the amount of non-specific

peptide binding. The peptides in the library should also have lower affinity for these proteins as compared to the target RNA. In addition, the binding times of the phage library were reduced for each successive round, from 60 to 15 minutes. With shorter binding times for each round, peptides with rapid on-rates (k_{on}) will be favored. After binding, the peptide library to the RNA for a specific amount of time, the unbound phage population was removed with washing buffer having increasing levels of detergent Tween-20. The presence of the detergent in the wash buffers helps to reduce nonspecific interactions between the phage and the target and/or blocking agents such as BSA. The Tween-20 concentration in the first round was low in order to have high elution of varied sequences of the phage library. It was increased from 0.1% in the first round to 0.5% in the fourth round. In order to obtain peptides with suitable k_{on} and k_{off} rates, the wash times and numbers were also varied. The time for even washes was three min and for the odd washes was 30 s for every round. This method was applied to enrich the pool of phage having faster on rates (k_{on}) and slower off rates (k_{off}). The elution time for the bound phage was kept at 10 min for each round, since a non-specific elution protocol was carried out in which the goal was to obtain all remaining peptides (0.2 M glycine-HCl, pH 2.2, 1 mg/ml BSA).

Selection of the phage library was also performed with a streptavidin-coated well with no immobilized target RNA. In all three rounds, the well was blocked with 3% BSA having 0.1 μg/mL streptavidin to complex with any biotin in BSA and elution of bound phage was carried out with 0.1 mM biotin in TBS for 30 min. The peptide sequences obtained for streptavidin as target are given in Table 2.4. The well-known consensus HPQ/L for the streptavidin ligands was obtained after sequencing five clones of control

experiment (Gissel, B. *et al*., 1995; Lam, K.S. & Lebl, M., 1992). This result validated the experimental conditions (blocking reagents, detergent strength in washing buffer, and binding and eluting times of the library) for four rounds designed for pulling out peptide sequences for control and target RNA.

Table 2.4. Peptide sequences for target RNA H69 obtained after three rounds.

Target H69 RNA				Control [b, c]	
Third round, non-specific elution[a]					
Peptide sequence	Frequency	Peptide sequence	Frequency	Peptide sequence	Frequency
SYYTSVS	1	NSPWLMT	1	TSPHPLT	1
STYTSVS	2	PNMQSQS	1	TRSHPLT	1
SHYTSVS	1	KLRWNQT	1	TPSHPLT	3
SYYTSVS	1	YRNTPLS	1		
VTDTSVS	1	APPPSPT	1		
VTYTSVS	1	PPARHRC	1		
ATYTSVS	1				
-TYTSVS	1				
SHLYYVS	1				

a) non-specific elution [0.2 M glycine-HCl (pH 2.2) containing 1 mg/ml BSA and neutralized immediately with 15 µl 0.1 M Tris-HCl, pH 9.0], b) the peptide sequences for control (streptavidin-coated well) where the familiar consensus of HPQ/L for streptavidin binding ligands is clearly seen, c) the consensus observed in the peptide sequences for both the target and the control is underlined.

For target RNA H69, the sequencing of ten clones gave a consensus of TSVS after the third round with non-specific elution. The sequencing of six other clones gave random sequences although three contained the S residue at positions 5 or 7 (Table 2.4). The elution of bound phage in the fourth round was carried out with two approaches: non-specific elution (low pH) and specific elution (higher concentration of

target RNA). When the sequencing of twenty phage plaques obtained after non-specific elution was performed, the peptide sequences of STYTSVS appeared eleven times and NQVANHQ appeared for five times (Table 2.5). For specific elution, twelve phage clones were sequenced out of which eight sequences were STYTSVS and four were NQVANHQ (Table 2.5). Interestingly, both STYTSVS and NQVANHQ peptide sequences appeared in the specific and non-specific elution methods of fourth round. Therefore, these two peptides were synthesized chemically for further binding studies with target H69 with different biochemical and bioanalytical assays such as the on-bead fluorescence assay, electrophoretic mobility shift assay (EMSA), electrospray ionization (ESI) mass spectrometry, and the in-line probing assay (Chapters 3, 4, and 5).

Table 2.5. The peptide sequences obtained after fourth round.

Target H69 RNA Fourth round			
Non-specific elution[a]		Specific elution[b]	
Peptide sequence	Frequency	Peptide sequence	Frequency
STYLYCA	1	STYTSVS	8
STYTSVS	11	NQVANHQ	4
PDYTSVS	1		
YYAAESL	1		
IRLPNHQ	1		
NQVANHQ	5		

a) the non-specific elution was carried out with 0.2 M glycine-HCl (pH 2.2) containing 1 mg/ml BSA and neutralized immediately with 15 µl 0.1 M Tris-HCl, pH 9.0, b) the specific elution was carried out three times higher concentration of the target RNA in order to compete with the bound phage.

2.6.2. Second screening using a seven-mer phage library and screening of a 12-mer phage library

The second selection attempt for searching peptides binding to H69 was aimed at finding a different set of peptide sequences. The stringency conditions were changed by adding some additional steps during the experiments. For example, to avoid selection against background materials like streptavidin and plastic of the 96-well streptavidin coated plates, the phage library was added to an empty well of the plate. After an hour of pre-screening with the well, it was removed and used for selection against H69. All the other conditions for selection in further rounds were kept the same except for adding tRNA (90 pmoles) and biotin (0.1 mM) in the third and fourth rounds as competitors during incubation of the library with H69. After the third round of selection, no consensus sequence was observed, but different peptide sequences were obtained as shown in Table 2.6.

The affinity selection for peptides against H69 was also performed using a commercial phage library displaying 12 amino-acid-long foreign peptides on its N-terminus (Ph.D.-12^{TM}). Three rounds of selection were carried out using similar conditions as applied for seven-mer phage library. After the third round of selection with non-specific elution for removing bound phage, 13 phage clones were sequenced and the peptide sequences are listed in Table 2.6. Further sequencing with the twelve-mer phage library was not actively pursued since the binding analysis of the peptides STYTSVS and NQVANHQ with the target H69 was started simultaneously and promising results were obtained (Chapter 3 and 4).

Table 2.6. Peptide sequences obtained from seven-mer library and twelve-mer library after three rounds.

Target H69 RNA Third round, non-specific elution[a]		Target H69 RNA Third round, non-specific elution[a]	
Peptide sequence	Frequency	Peptide sequence	Frequency
LSTLSYS	2	HVVSSSEFSGL	1
LSTLALY	1	GSSSYGPFLSDY	1
HPKYYLQ	1	IVASYFATATRT	1
MPKYYLQ	1	TASPLKQSRRP	1
ALKPPKY	1	QLCTLLHTCVPP	1
SLHSRPN	2	KQLTSPPQLNPV	1
SLDAPRS	1	GTPPMSPLVSRV	1
ILGAPRA	1	LRRRLEAESLRP	1
LHLEDFT	1	ATWSHHLSSAGL	2
FCSDFEL	1	HLQQIHRMHTMP	1
IMPHHTT	1	NGWWTASPGVPM	1
YAGPYQH	1	WPHNWWPHFKVK	2

a) = non-specific elution [0.2 M glycine-HCl (pH 2.2) containing 1 mg/ml BSA and neutralized immediately with 15 µl 0.1 M Tris-HCl, pH 9.0].

2.6. Conclusions

The phage-display technique was successfully carried out for selecting peptide sequences for target RNA H69. The library applied had heptapeptide sequences presented at the N-terminus of the p3 coat protein of the M13 phage particle. The N-terminus of the p3 protein is exposed to the cytoplasm resulting in easy availability of the peptides for the immobilized target. The consensus sequence obtained in the first attempt of biopanning after third round was TSVS. After the fourth round, the elution of

the bound phage was carried out by nonspecific elution (low pH conditions) and specific elution (three times higher concentration of target RNA). In case of non-specific elution, the peptide STYTSVS appeared for eleven times and peptide NQVANHQ appeared five times in addition to other peptide sequences. In the specific elution, only STYTSVS and NQVANHQ peptide sequences were obtained in the phage pool. The later was a unique sequence for which a consensus did not appear. Of note, however, was the fact that this sequence contained an abundance of amino acid residues that are also present in the ribosome recycling factor, RRF, and known to make contacts with H69.

The crystal structure of RRF bound to 70S ribosome shows the amino acids present on one face of α-helix 1 in domain 1 of RRF interacting with nucleotides of H69. The amino acids include serine 17 (S17) interacting with Ψ1917, valine 20 (V20) interacting with A1916 and $m^3\Psi$1915, histidine 23 (H23) and aspargine (N24) interacting with C1914 (Pai, R.D. *et al*., 2008). The presence of the similar amino acids in the RRF contacting H69 and the heptapeptide pulled out from the phage library give a validity to the optimized conditions of the selection employing phage-display library. Upon examining the peptide sequences from the selection, it was also noticed that polar, uncharged amino acids such as serine (S) and glutamine (Q) occurred in higher frequency.

The second attempt of the biopanning was performed with the same seven-mer library in order to get another set of peptide sequences. But the peptide sequences did not show any clear consensus and once more the peptide pool was dominated with polar, uncharged amino acids. In addition, selection with the twelve-mer library lead to peptide sequences having more polar, uncharged amino acids. The two peptide

sequences STYTSVS and NQVANHQ were chosen for binding analysis through electrospray ionization (ESI) mass spectrometry and the results are discussed in detail in the next chapter.

CHAPTER 3

Assays for validation of interactions of peptides with RNA

3.1. Introduction to Tentagel bead assay

After the selection of peptides for the target helix 69 (H69) using the phage-display method, preliminary binding studies of the peptides with RNA were pursued. The sequences of the chosen selected peptides were NQVANHQ and STYTSVS. A simple fluorescence-based assay using Tentagel beads was developed to obtain knowledge about the relative binding affinities of these peptides with H69. This assay was a modified version of the one-bead, one-peptide combinatorial assay developed originally by Lam and coworkers (Lam, K.S. *et al*., 1991). In their assay format, a large peptide library was first created on millions of Tentagel beads, in which each bead contained a single peptide sequence (six amino acids in length). The library was constructed using split-pool synthesis and represented a pool of possible random peptides in approximately equimolar proportion. After screening the library with a particular acceptor molecule, the next step was to pull out the RNA-bound beads. The acceptor molecules were linked to an enzyme (alkaline phosphatase) or fluorescein.

Complex formation between a particular peptide and the acceptor molecule caused intense staining or fluorescence of the beads, and the beads were observed with a low-power microscope. They were later removed for analysis of the peptide sequence. This assay has been widely applied for identifying novel peptide ligands against cell-surface receptors (Lau, D. H. *et al*., 2002), enzymes (Lam, K.S. *et al*., 1995), proteins (Udaka, K. *et al*., 1995), and antibodies (Pinilla, C. *et al*., 1994).

The one-bead one-peptide binding assay applied in this study differed from its original combinatorial selection by not using Tentagel bead peptide libraries for selection. Instead, the selection for peptide ligands for H69 RNA was performed using the phage-display library (Smith & Petrenko, 1997) as discussed in Chapter 2. Also, the conditions of the assay, such as type of blocking buffer, and incubation time of the beads and RNA, were changed, employing two tripeptides (K_L-K_D-N_L and R_L-K_D-V_D) and TAR RNA as the model system. These tripeptides were identified from a bead selection carried out by Hwang and coworkers (Hwang, S. *et al*., 1999) and were synthesized on the Tentagel beads. Later, the optimized assay conditions were applied to assess the binding of heptapeptide sequences against H69 with their target RNA.

Tariq Rana's group has successfully employed the one-bead one-peptide combinatorial assay against TAR RNA (a major target for anti-viral therapeutics) for discovering peptide ligands other than the natural Tat peptide. The TAR (transactivation response region) RNA is a 59-base stem-loop structure found at the 5' end of the 5' untranslated leader region of all the nascent HIV-1 viral mRNA transcripts. Replication of the HIV-1 virus requires the critical interaction of the TAR RNA with the Tat protein (transactivator protein) (Jones, K.A. *et al.*, 1994). The Tat binding site has been confined to a minimal RNA moiety within TAR RNA containing a hexanucleotide loop and three-nucleotide bulge (Cordingley, M.G. *et al*., 1990; Dingwall, C. *et al*., 1990; Weeks, K.M. *et al*., 1990). The binding of the Tat peptide to the TAR RNA is mediated through a 10 amino-acid basic α helix (rich in basic arginines and lysines) of the Tat peptide lying in the deep groove of the TAR RNA (Mujeeb, A. *et al*., 1994). This Tat-TAR interaction has been widely targeted by small molecules for developing anti-HIV

therapeutics. Examples of small molecules disrupting this Tat-TAR interaction include L-argininamide (Brodsky. A.S. *et al*., 1997), Tat-derived arginine-rich peptide mimics (Calnan, B.J. *et al*., 1991; Weeks, K.M. *et al*., 1991), oligocationic peptides (O'Brien, W.A. *et al*, 1996), peptoid Tat mimetics (Hamy, F. *et al*., 1997), D-Tat peptides (Huq,I. *et al*., 1997), and conjugates of the aminoglycosides with arginine (Litovchick, A. *et al*., 1999 & 2000).

A tripeptide combinatorial library of 24,389 members with both D- and L-amino acids was synthesized on Tentagel resin by Rana's group using split-pool synthesis (Hwang, S. *et al*., 1999). They were able to isolate tripeptides capable of binding specifically to the bulge region of the TAR RNA (Figure 3.2).

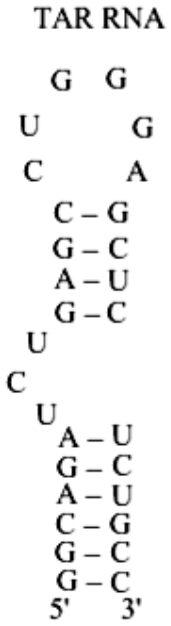

Figure 3.1. The sequence of TAR RNA used in Rana's group for selecting tripeptides binding specifically to the bulge region of the RNA (Hwang, S. *et al*., 1999).

In Rana's selection procedure, disperse red dye was covalently attached to the TAR RNA sequence having a bulge region. The labeled RNA sequences having the

bulge and the unlabeled RNA without the bulge were incubated in a suspension of the random peptide library beads. An unlabeled RNA sequence lacking the bulge region was added for selection of peptides specifically against the bulge region. The dye-TAR conjugate easily diffused through the beads, giving an evenly distributed red color to the translucent Tentagel beads. After the selection of colored beads from the library, a few tripeptide sequences were found to interact with the bulge region of the TAR RNA. One of the tripeptides, K_L-K_D-N_L, gave a dissociation constant of 420 ± 44 nM as compared to the wild-type Tat peptide (residues 48-57) that had a dissociation constant of 727 ± 74 nM. Thus, the tripeptide K_L-K_D-N_L showed even tighter binding with TAR RNA than the Tat peptide. Another tripeptide, R_L-K_D-V_D, gave a dissociation constant of 10,434 ± 594 nM, clearly indicating weaker binding with the TAR RNA.

To test the binding of the tripeptide K_L-K_D-N_L, Hwang and coworkers synthesized the peptide on Tentagel beads and incubated the dye-TAR conjugate with a suspension of the peptide beads. After incubation for 5 h at 4 °C, the beads turned red, confirming the binding of the TAR RNA with the tripeptide K_L-K_D-N_L. This simple fluorescence assay using disperse red dye provided useful information about the relative binding affinities of the TAR RNA binding ligands, although it did not represent the binding under true physiological conditions. Further NMR studies of the tripeptide K_L-K_D-N_L showed that the resonances of the bulge residues changed, specifying that the peptide specifically interacted with TAR RNA at the bulge region (Hwang, S. *et al*., 1999).

The TAR RNA and the two K_L-K_D-N_L and R_L-K_D-V_D tripeptide sequences were chosen as a model for our experiments. The changes in our assay included labeling the TAR RNA with fluorescein instead of disperse red dye, synthesis of the tripeptide

sequences K_L-K_D-N_L and R_L-K_D-V_D on Tentagel beads, and binding under different buffer conditions. The experimental conditions included washing, swelling, and blocking of the peptide beads with Superblock buffer (a commercially available buffer from Pierce Inc., IL). After blocking, the fluorescein-labeled TAR RNA (F-TAR RNA) was incubated with Tentagel beads. Later, the beads were viewed under a fluorescence microscope for analysis. The diagrammatic illustration of the assay is given in the Figure 3.2.

Similarly, the heptapeptide sequences NQVANHQ and STYTSVS for H69, selected from phage-display method (Chapter 2) were synthesized on Tentagel beads. The target RNA H69 was tagged with fluorescein (F-H69) for easy detection of the beads bound to RNA. Similar experimental conditions were applied with the NQVANHQ and STYTSVS Tentagel beads and F-H69. The different intensities of the fluorescing beads were interpreted to give a preliminary understanding of the relative binding affinity of these peptides for the target and unrelated RNA sequences. The Tentagel bead consists of polyethylene glycol attached to cross-linked polystyrene through an ether linkage, and combines the benefits of the soluble polyethylene glycol support with the insolubility and handling characteristics of the polystyrene bead (Quarrell, R. *et al*., 1996; McAlpine, S.R. *et al*., 1999).

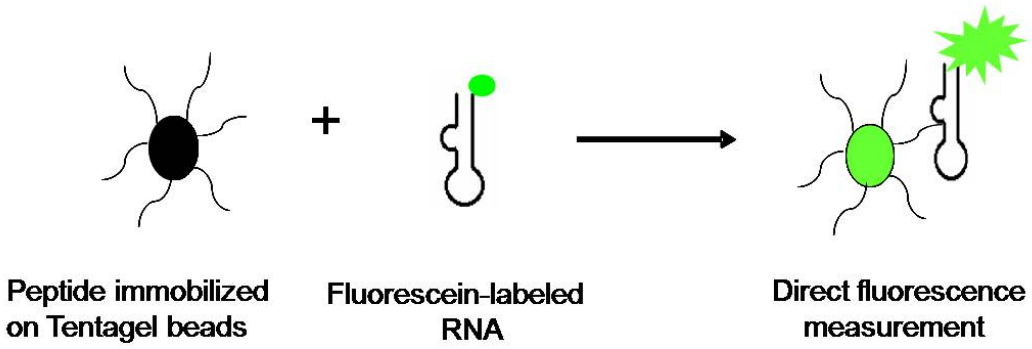

Figure 3.2. The schematic of the Tentagel bead assay is depicted, which is based on the fluorescence intensity of the Tentagel beads having a bound peptide-RNA complex.

3.2. Materials and methods

3.2.1. General materials

The fluorescein-labeled TAR RNA (Fl-5'-GGC AGA UCU GAG CCU GGG AGC UCU CUG CC-3') was purchased from IDT (Integrated DNA technologies, Coralville, IA). The F-TAR RNA was later gel purified by running on 20% polyacrylamide denaturing gels for ~ 2 h at 400 V. The RNA band was visualized by UV shadowing, excised and subjected to electroelution using Amicon Centrilutor^{TM} device and Centricon^{TM} YM-3 in 0.5 X TBE buffer (90 mM Tris-HCl, 90 mM boric acid, 2.5 mM Na-EDTA, pH 8.3) for 2 h. Then, the RNA was desalted and concentrated by centrifugation at 3000 rpm at 4 °C overnight with addition of water for further desalting. Finally, the RNA was stored in 10 mM HEPES buffer, pH 7.4. The final Fl-TAR RNA concentration was calculated by its absorbance value at 260 nm using Beer's law: $A = \varepsilon * C * l$, in which ε is the extinction coefficient of 268,900 $L^{-1}M^{-1}cm^{-1}$ for unlabeled TAR RNA, c is the concentration, l is the path length, and A is the absorbance at 260 nm. The secondary structure of the Fl-TAR RNA is given in Figure 3.3.

The nonspecific fluorescein-labeled RNAs used as controls in the experiments were theophylline-binding RNA (F-theophylline RNA, ε=296,160 M^{-1} cm^{-1}), 17-nucleotide substrate for the 38-nucleotide hammerhead ribozyme (S16-F, ε=162,300 M^{-1} cm^{-1}), GG dimer (F-GG, ε=21,600 M^{-1} cm^{-1}), and the A site of eukaryotic 18S rRNA (F-AS 18S rRNA, ε=258,100 M^{-1} cm^{-1}) as shown in Figure 3.3. All RNAs were renatured before use by heating and slow cooling.

A)

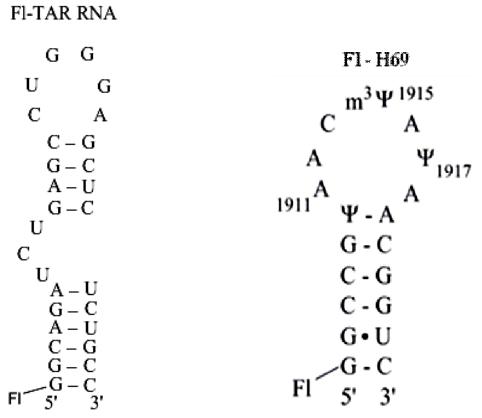

B)

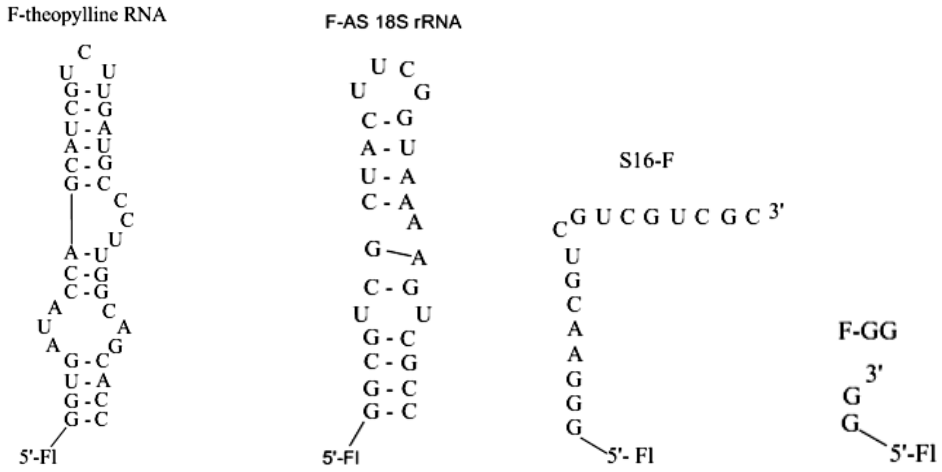

Figure 3.3. A) The sequences of the fluorescein-labeled TAR RNA and the fluorescein-labeled H69 as used in the experiments for the Tentagel bead assay are given. B) The sequences of the control RNAs are shown, where Fl stands for fluorescein.

RNA H69 was also fluorescein labeled using a 5'-amino-6-carbon linker H69 sequence [5'-NH_2-C6-GGCCGΨAAC(m^3Ψ)AΨAACGGUC-3']. The sequence of H69 is given in Figure 3.3. The labeling procedure included adding 20 µL or 0.0125 µmoles of the RNA, 3 µL of diiopropylethylamine, 15 µL of DMSO (dimethylsulfoxide), and 5 µL or 0.75 µmoles of fluorescein in DMSO to a 1.5 µL eppendorf tube. The eppendorf tube

was then placed in the shaker in reduced light and oscillated for 22-24 h. The reaction mixture was purified by directly running it on the 20% denaturing polyacrylamide gel (7 M urea) for ~ 2 h at 400 V. The RNA band was visualized by UV shadowing, excised and subjected to electroelution and desalting as described in the previous paragraph. The RNA was stored in 10 mM HEPES buffer, pH 7.4. The final RNA concentration was calculated using the extinction coefficient of 187,000 $L^{-1}M^{-1}cm^{-1}$ for H69 RNA. The RNA was renatured before use.

For the preparation of the Tentagel beads having peptides covalently attached to them, Tentagel S-NH_2 resin was employed (Tübigen, Germany). The sequences of the peptides synthesized on these beads were K_L-K_D-N_L, R_L-K_D-V_D, STYTSVS and NQVANHQ. The synthesis of the peptides was carried out by Edvin Klosi in Dr. Mark Spaller's lab.

3.2.2. Binding experiments utilizing F-TAR RNA and peptides on Tentagel beads

The first step for performing the assay was to optimize the conditions for the buffer required to block the beads (carrying peptide ligands) for reducing non-specific interactions. A few of the requirements for the most suitable buffer were to have minimal or no background fluorescence and no RNases activity. In Rana's group (Hwang, S. *et al*, 1999), the buffer used for all their bead assays was TK buffer (50 mM Tris-HCl, pH 7.4, 20 mM KCl, 0.1% Triton x 100). When this buffer was tested for background fluorescence in presence of our beads, we observed fluorescence. Therefore, this buffer was not continued for our assay. The other blocking buffers tested for the assay were "New blocking buffer" (0.1% BSA and 0.05% gelatin), Pierce "SuperBlock buffer"

(phosphate-buffered saline with 0.05% Tween-20 detergent from Pierce Inc., Rockford, IL) and HEPES binding buffer (50 mM HEPES, pH 7.4, 140 mM NaCl, 10 mM KCl, 1mM $MgCl_2$ and 1 mM $CaCl_2$). For background fluorescence, the beads were incubated with buffer and then visualized under the fluorescence microscope. To determine RNase activity in the buffer, the RNAs were incubated in each buffer and then run on polyacrylamide gels to see if degradation of RNA is visible. A ladder of RNA bands would indicate degradation of the RNA after incubation in the buffer.

The fluorescence microscope used in the visualization of the beads was Ziess fluorescence microscope (Tübigen, Germany) located in Dr. Marcus Fredrich's laboratory. The parameters for taking the images were: gamma (1.02), brightness (0.7-0.8), exposure time (30 sec), filter color (green), and binning (none). The microscope was equipped with Spot Advanced software, version 4.1.2 (Diagnostic Instruments, Inc.) for processing the images and the pictures were taken using 32-bit Pixel memory space.

After synthesizing the peptides on the beads, they were washed with water to remove the residual DMF (dimethylformamide). The beads were then blocked with Pierce SuperBlock buffer (500 µL) for two to three hours to avoid nonspecific interactions for further steps. Next, they were washed with ddH_2O (500 µL, X 3). A small quantity of the beads (~10-12) was extracted from the solution and 15 µl of 1 µM F-TAR RNA in 10 mM HEPES buffer was added to the beads. The suspension was then stirred in the shaker for one day at 4 °C. On the next day after the removal of the RNA, the beads were further incubated with more F-TAR RNA. This process was repeated for four consecutive days under the same conditions as described to attain maximum

fluorescence. At the end, the beads were washed with ddH_2O (500 µL, X 3) and then viewed under the fluorescence microscope. The above mentioned experimental conditions were optimized by my colleague Srividya Pattabiraman (Pattabiraman, S. 2006). For F-TAR RNA the peptides synthesized on the beads were K_L-K_D-N_L and R_L-K_D-V_D. The peptide K_L-K_D-N_L was reported by Rana's group to bind in the bulge region with high affinity, whereas R_L-K_D-V_D peptide was a very modest binder to TAR RNA (Hwang, S. *et al*, 1999).

3.2.3. ELISA assays of TAR RNA binding to peptides on Tentagel beads

As the name of the assay ELISA (Enzyme-Linked Immunosorbent Assay) suggests, the primary anti-FITC antibody was employed to perform this part of the colorimetric assay. A separate set of the experiments were executed for both K_L-K_D-N_L and R_L-K_D-V_D peptides selected for TAR RNA. The assay was carried out with the maximum fluorescing beads after a four-day incubation period and a schematic diagram of the assay is shown in Figure 3.4. Fifty µL of goat anti-FITC antibody (Biomed, Dedham, MA) was added to the beads in the ratio of 1:2000 using diluent (0.5% BSA in 10 mM Tris-HCl, 150 mM NaCl, 0.05% sodium azide) for 6 h in a shaker at 4 ºC. Afterwards, excess antibody was removed by washing with ddH_2O (500 µL, X 5). The resin was later incubated with a secondary antibody, namely rabbit anti-goat IgG conjugated with the enzyme alkaline phosphatase, in the ratio of 1:30,000 (using diluent as listed in the first step) for 6 h. Subsequently, the beads were washed with ddH_2O (500 µL, X 3) and then moved to BCIP solution (5-bromo-4-chloro-3-indolyl phosphate) (Promega, Madison, WI) (1.65 µL in 500 µL of diluents containing 100 mM Tris-HCl (pH

9.0), 150 mM NaCl, and 1 mM $MgCl_2$) for overnight incubation at 4 ºC. The beads attained a turquoise color as a result of the cleavage of the phosphate group from BCIP by the enzyme alkaline phosphatase. The beads were visualized under visible light and the turquoise-colored beads were removed manually. The control experiments for the assay involved the exclusion of the primary antibody, secondary antibody, or substrates from the procedure of the assay. The Ziess fluorescence microscope was used to view the beads, and in this case they were seen under visible light instead of UV light. The microscope used Spot Advanced software, version 4.1.2 (Diagnostic Instruments Inc., Sterling Heights, MI), for processing the images.

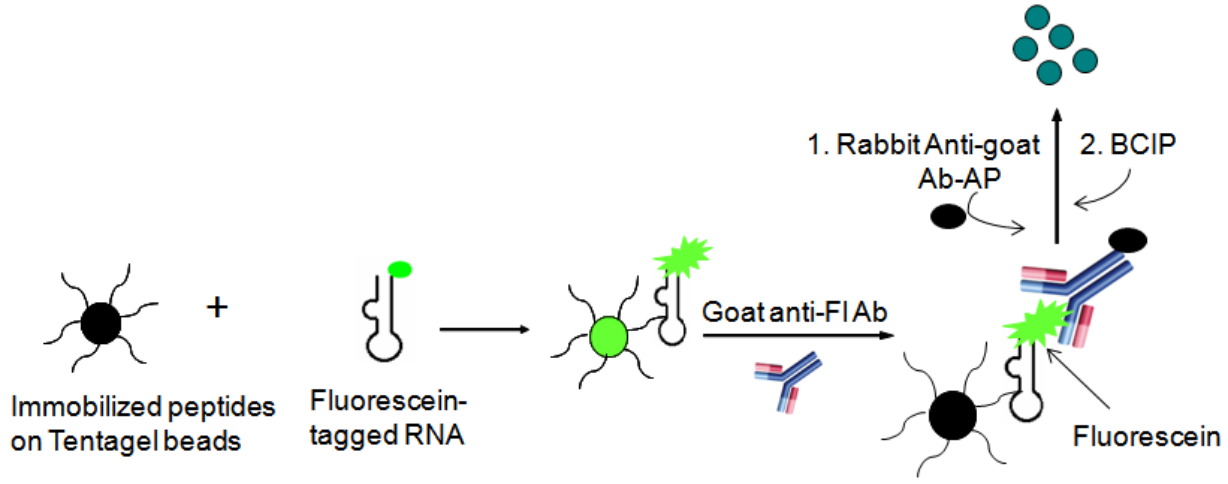

Figure 3.4. The generalized scheme for the ELISA experiment performed on fluorescing beads where Fl is fluorescein dye, Ab is antibody, AP is alkaline phosphatase enzyme and BCIP is 5-bromo-4-chloro-3-indolyl phosphate.

3.3. Results and discussion

3.3.1. Fluorescence assay for the F-TAR RNA and K_L-K_D-N_L and R_L-K_D-V_D peptides on Tentagel beads

The K_L-K_D-N_L peptide beads were first blocked with Pierce SuperBlock buffer, as it did not show any sign of causing RNA degradation and had very low background

fluorescence. Then, the peptide beads were incubated for four days as described in the Methods section with the F-TAR RNA. A fresh quantity of F-TAR RNA was added each day after removing the supernatant having the previous F-TAR RNA. The beads attained maximum fluorescence with this procedure after four days. The fluorescence was noticed to be distributed evenly throughout the beads. Similarly, the R_L-K_D-V_D peptide beads were also incubated for four days with the F-TAR RNA. The K_L-K_D-N_L peptide bead images as seen under the fluorescence microscope are shown in Figure 3.5.

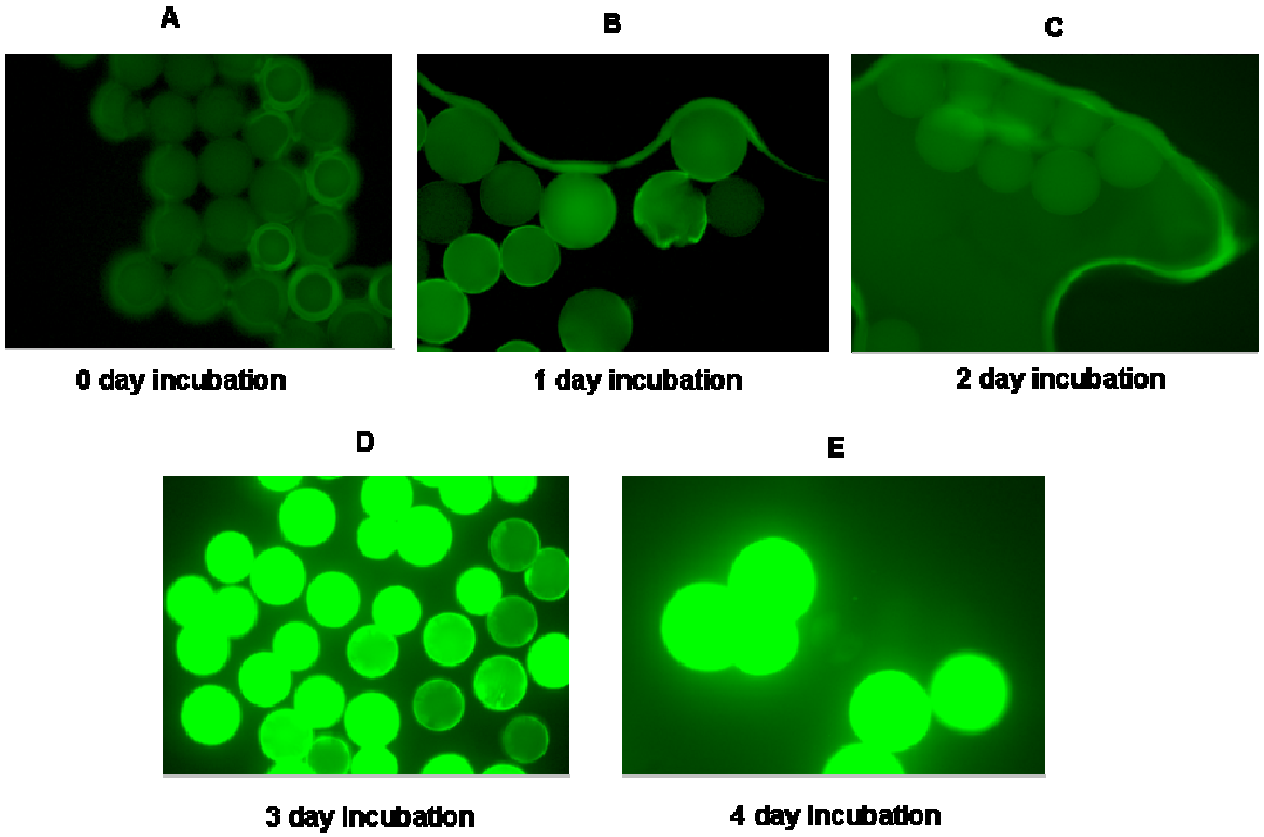

Figure 3.5. The above panels show the K_L-K_D-N_L peptide beads after incubation with F-TAR RNA for four days. The increase in the intensity of the peptide beads is clearly seen with the increasing incubation time.

The R_L-K_D-V_D peptide beads were also incubated with F-TAR RNA for four days. After visually comparing the beads of both peptides, it was observed that the K_L-K_D-N_L peptide beads were fluorescing more strongly as compared to R_L-K_D-V_D peptide beads. The beads of both peptides are seen side by side in Figure 3.6. (left panel). The weak fluorescence of the R_L-K_D-V_D peptide beads is observed when the beads having no peptides and the R_L-K_D-V_D peptide beads are mixed together (Figure 3.6., right panel). This qualitative observation was consistent with the results of the Rana's group bead assay, in which they have detected a stronger red color (from disperse red dye) for the beads having the K_L-K_D-N_L peptide (K_d = 420 ± 44 nM) as compared to the R_L-K_D-V_D peptide beads (K_d = 10,434 ± 594 nM) (Hwang, S. *et al*, 1999). The results clearly indicated that the F-TAR RNA was able to enter the bead interior and bind to the peptides. This assay was further carried out by synthesizing the peptide NQVANHQ and STYTSVS on Tentagel beads with F-H69, as described in Section 3.2.

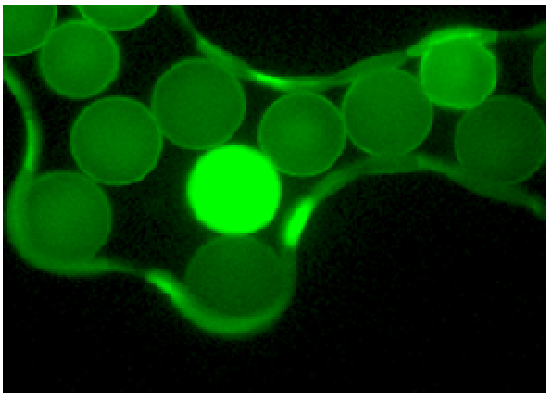

K_L-K_D-N_L beads + R_L-K_D-V_D beads

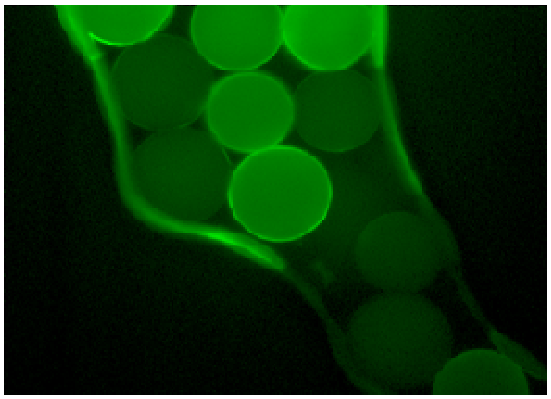

Beads (no peptide) + R_L-K_D-V_D beads

Figure 3.6. In the left panel, the difference in fluorescence intensity between the K_L-K_D-N_L peptide beads and the beads with R_L-K_D-V_D peptide is clearly seen. The brightest bead is the one having the K_L-K_D-N_L peptide. In the right panel, the comparison of the beads having no peptide and the R_L-K_D-V_D peptide beads is shown.

3.3.2. Determination of apparent dissociation constants

For determining the relative affinities of peptides to TAR RNA, the measurement of the apparent dissociation constant (K_d) was carried out from the fluorescence bead assay. The direct fluorescence intensity values were measured after a four-day incubation of the K_L-K_D-N_L peptide beads and the beads with R_L-K_D-V_D peptide. For the peptide K_L-K_D-N_L, the fluorescence intensity value reached the maximum plateau at less than 1 μM concentration of F-TAR RNA, whereas for the R_L-K_D-V_D peptide beads the plateau of the fluorescence intensity was reached at greater than 1 μM concentration of F-TAR RNA. After four days of successive incubation with F-TAR RNA, 10 micro-beads were selected for each set of concentrations of F-TAR RNA (ranging from 0.02 – 10 μM) and placed in 10 mM HEPES buffer in 96-well Costar plates. Each bead was 90 μm in size and had 90 pmole capacity for the ligand. Therefore, the concentration of the peptide on the beads was determined to be 9 μM/μL. After obtaining the fluorescence intensity value for each concentration of F-TAR RNA, the intensity value was converted to a fraction bound ratio using the following equation 3.1.

$$F_r = (F_o - F_i) / (F_o - F_f)$$

in which F_r is the fraction of RNA bound, F_o is the fluorescence intensity of the free RNA, F_i is the fluorescence intensity at any given concentration, and F_f is the fluorescence intensity at the final concentration of the experiment.

Assuming the simple binding mode of 1:1 for peptide and RNA, the apparent dissociation constant (K_d) for each peptide-RNA complex was acquired by fitting the data with quadratic equation (Equation 3.2.). The peptide concentration was the lower limit as the peptide was not free in the solution and its concentration was higher near

the beads. Kaleidagraph 4.0 was further used for curve fitting with following quadratic equation (Equation 3.2.):

((*K*$_d$ +[RNA]+[ligand]) – sqrt ((*K*$_d$ +[RNA]+[ligand])^ 2 – 4*[ligand] *[RNA]))/2*Const

The *K*$_d$ value calculated with the quadratic equation for K_L-K_D-N_L peptide with F-TAR RNA was found to be 120 ± 40 nM and for the R_L-K_D-V_D peptide with F-TAR RNA was found to be 6300 ± 500 nM. The plots representing the fraction of TAR RNA bound with the two peptides are given in Figure 3.7. The curve fit for the peptides was not ideal one for several reasons: i) these were not solution studies, ii) the direct calculation of the fluorescence intensity value from the beads may not be entirely consistent; and iii) the mixtures were non-uniform. The values calculated for the apparent dissociation constants for both peptides were different from the values obtained in Rana group's work (*K*$_d$ = 420 ± 44 nM for K_L-K_D-N_L and *K*$_d$ = 10,434 ± 594 nM for R_L-K_D-V_D). Nonetheless, the relative binding affinities of both peptides were in the same order as seen in Rana's work, in which the K_L-K_D-N_L peptide was shown to be having higher affinity for the TAR RNA than the R_L-K_D-V_D peptide (Hwang, S. *et al*, 1999). Our results suggest that this simple, cost-saving fluorescence method can be applied for determining the relative binding affinities for two or more ligands selected against a particular target.

The apparent dissociation constant and the number of binding sites (n) were also obtained applying the Hill equation. The *K*$_d$ value was obtained by the intercept of the plot. The following Hill equation (Equation 3.3.) used was:

log (B/([Peptide] – B)) = n (log[RNA]) – nlog*K*$_d$,

where B = ([peptide]* F_r) and [peptide] =(90 pmol/bead x 10 beads)/100 µl = 9 µM/µl.

A) B)

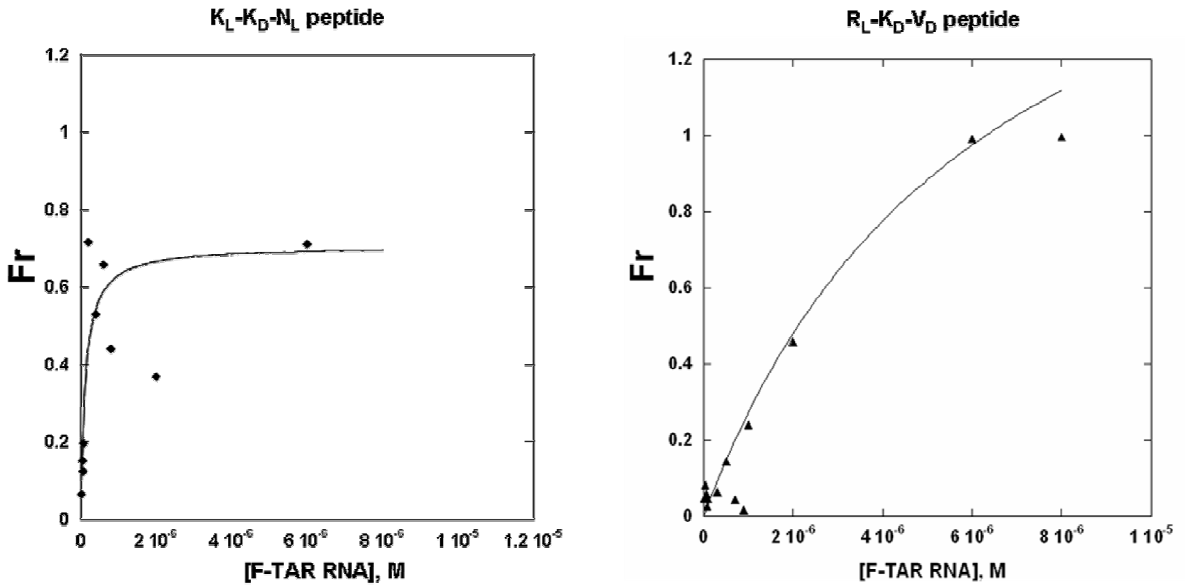

Figure 3.7. The plots of the fraction of TAR RNA bound with the two peptides K_L-K_D-N_L and R_L-K_D-V_D on beads in HEPES buffer at 4 ºC is shown. A) represents the K_L-K_D-N_L peptide giving the K_d of 120 ± 40 nM (R = 0.8), and B) stands for the R_L-K_D-V_D peptide with the K_d of 6300 ± 500 nM (R = 0.8).

After performing Hill analysis for the K_L-K_D-N_L peptide, a Hill constant of 1.0 was obtained and apparent dissociation constant of 320 nM was reached. For the second R_L-K_D-V_D peptide, a Hill constant of 0.9 was obtained and after fitting with Equation 3.3., the apparent dissociation constant calculated was 2,100 nM (Figure 3.8). The Hill constant suggested the presence of one binding site for the peptide with TAR RNA in both cases.

The values of the apparent dissociation constant obtained through our fluorescence assay for the two peptides and the TAR RNA and the ones calculated by the Rana's group are summarized in Table 3.1. Although we were not entirely satisfied with the outcome of these results, the relative binding affinities and approximate ranges of K_d*s* for the peptides could be assessed.

A) B)

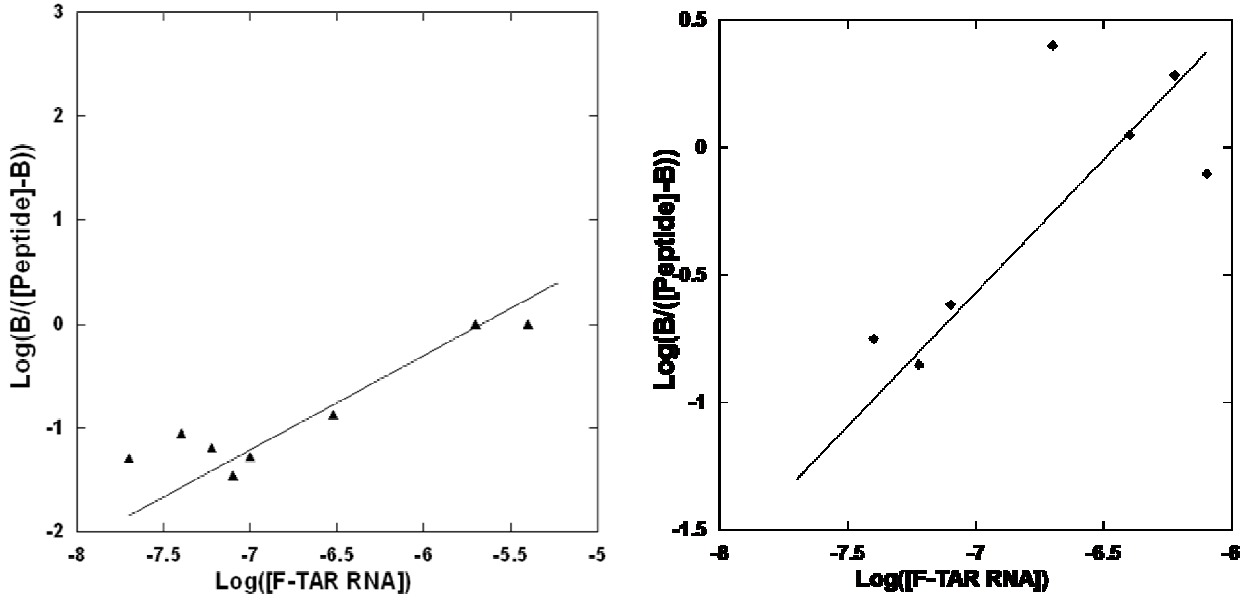

Figure 3.8. A) The Hill plot for K_L-K_D-N_L peptide binding to F-TAR RNA in HEPES buffer at 4 ºC is shown with [F-TAR RNA] between 0.2 to 10 μM (n =1.0, R = 0.9, K_d = 320 nM, B) The Hill plot for R_L-K_D-V_D peptide binding to F-TAR RNA in HEPES buffer at 4 ºC is shown with [F-TAR RNA] between 0.2 to 10 μM (n =0.9, R = 0.7, K_d = 2130 nM).

Table 3.1. Comparison of the various apparent dissociation constants values acquired for the two peptides for TAR RNA through our lab's fluorescence assay and the Rana group's assay.

Fluorescence assay		K_L-K_D-N_L peptide	R_L-K_D-V_D peptide
Equations applied	Quadratic equation	120 ± 40 nM	6,300 ± nM
	Hill equation	320 nM	2,100 nM
Rana's data (Hwang, S. *et al*, 1999)		420 ± 44 nM	10,434 ± 59 nM

3.3.3. Control and competition experiments

The control experiments for demonstrating the specificity of the peptides toward TAR RNA through the fluorescence assay included incubating the beads with K_L-K_D-N_L

and R_L-K_D-V_D peptides with free fluorescein and other unrelated RNAs such as F-theophylline RNA, F-GG, F-AS 18S rRNA, and F-substrate (Figure 3.3. B). The beads without any peptide were also incubated with free fluorescein to check if there is any interaction of the Tentagel beads themselves with the free dye. The images of the beads with K_L-K_D-N_L and R_L-K_D-V_D peptides and without peptides after incubation for four days with free fluorescein are given in Figure 3.8. The free fluorescein did not bind to the beads without any peptides or to the beads with peptides. No fluorescence was observed with these beads. It should be noted that a few anomalies were observed, as seen by a single bright control bead in Figure 3.9.B., so all such results need to be interpreted with some caution.

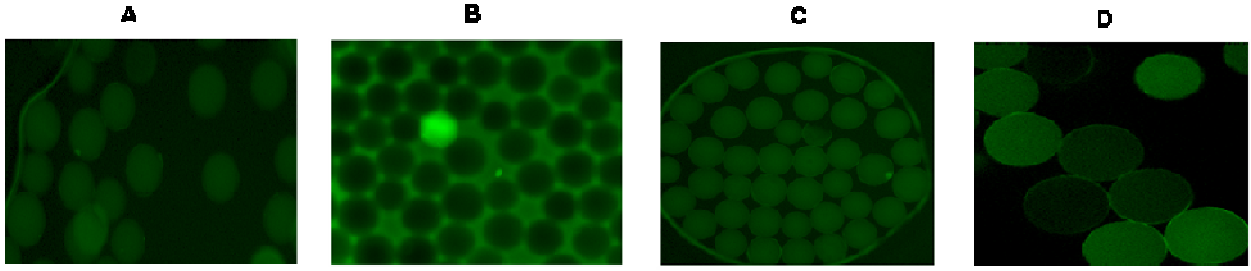

Figure 3.9. A) The beads without any peptides before incubation with free fluorescein and B) after incubation with free fluorescein are depicted in the pictures. C) The beads with K_L-K_D-N_L peptide before incubation and D) after the incubation with free fluorescein are shown in the images.

The control experiment with the unrelated RNAs such as F-theophylline RNA, F-GG, F-AS 18S rRNA, and F-substrate with the K_L-K_D-N_L and R_L-K_D-V_D peptides also demonstrated the same results as the free fluorescein. The beads were found not to interact with the unrelated RNAs, thus indicating specificity of the peptides for the TAR RNA. These results indicate success of this relatively simple fluorescence assay that can provide fairly accurate information about the “specificity” characteristic of these

peptides. The bead images of the K_L-K_D-N_L and R_L-K_D-V_D peptides with the control RNAs are shown in Figure 3.10.

The reversibility characteristic of the interaction of TAR RNA and the K_L-K_D-N_L peptide was tested through competition experiments. This experiment was performed by adding excess amount of unlabeled TAR RNA to the fluorescing K_L-K_D-N_L peptide beads. It was observed that after addition of 10 μM unlabeled TAR RNA as a competitor to the fluorescing beads the interaction between the K_L-K_D-N_L peptide and F-TAR RNA was either reduced or abolished. This demonstrated that the unlabeled TAR RNA competed with the previously bound F-TAR RNA for binding with the peptides, since the fluorescence of some of the beads was diminished or eliminated as shown in Figure 3.11., compared to the results in Figure 3.5. We did not attempt to use a high-fold competitor concentration due to the lack of availability of large quantities of the RNA.

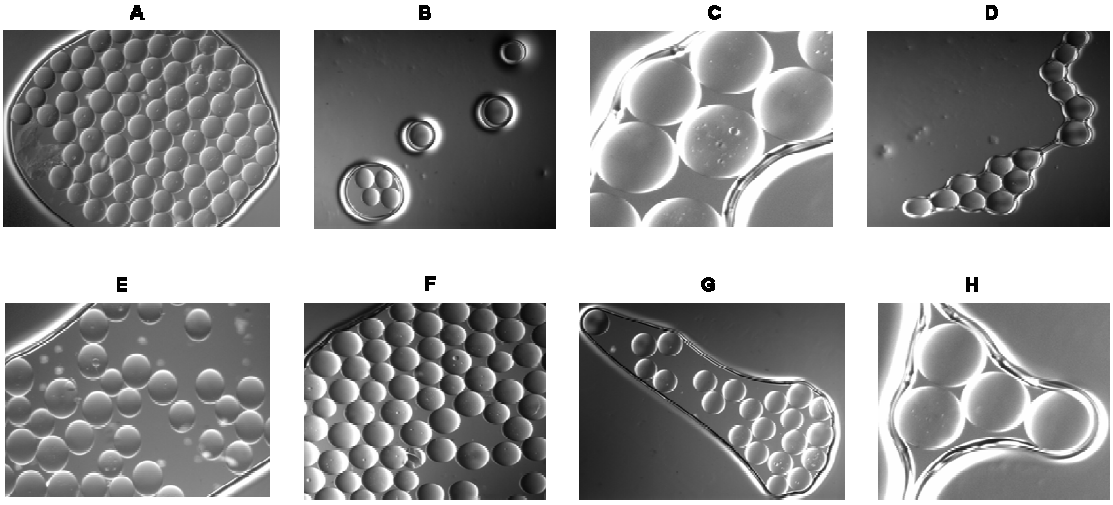

Figure 3.10. Beads with the peptide K_L-K_D-N_L with non-specific RNAs after four days of incubation are shown in A) F-AS 18S rRNA, B) F-GG, C) F-substrate, and D) F-theophylline RNA. The images of beads with the peptide R_L-K_D-V_D and non-specific RNAs such as F-AS 18S rRNA (E), F-GG (F), F-substrate (G), and F-theophylline (H) RNA are shown.

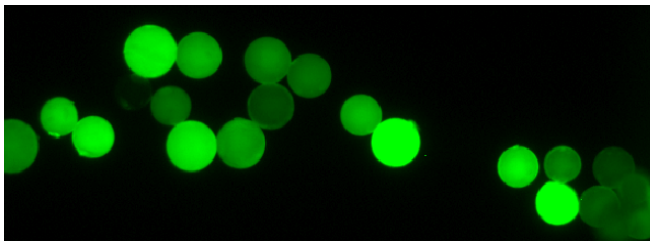

Figure 3.11. The beads with the peptide K_L-K_D-N_L incubated with 1 μM F-TAR RNA followed by the addition of unlabeled TAR RNA (10 μM) as a competitior are depicted. Some of the beads have diminished fluorescence intensity as compared to others.

3.3.4. On-bead ELISA assay for F-TAR RNA and K_L-K_D-N_L *peptide*

ELISA (Enzyme-Linked Immunosorbent Assay) with the fluorescing K_L-K_D-N_L peptide beads gave supplementary evidence for the interaction of this peptide with the TAR RNA. The procedure of the assay is outlined in Figure 3.4. This assay gave turquoise color to the beads by the addition of BCIP (5-bromo-4-chloro-3-indolyl phosphate) at the last stage of the assay. The turquoise color was evenly distributed all over the beads indicating homogeneous binding with the peptide K_L-K_D-N_L (Figure 3.12). The control experiments in this assay included lack of RNA or the antibodies to the different sets of experiments. As a result, no turquoise color was observed for those peptide beads (Figure 3.13) in the control experiments. The negative results of the control experiments confirmed specificity of the interaction of the TAR RNA and the K_L-K_D-N_L peptide and gave validity to the performance of this colorimetric assay.

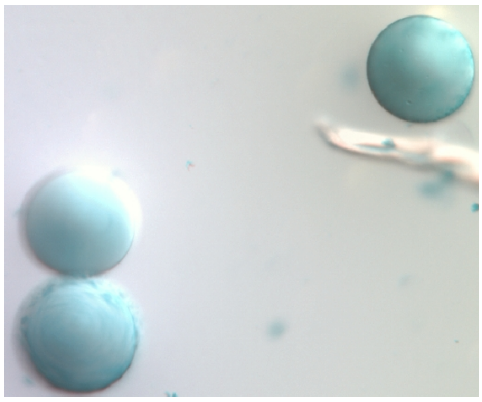

Figure 3.12. The image of the turquoise colored K_L-K_D-N_L peptide beads incubated with F-TAR RNA and subjected to ELISA is given.

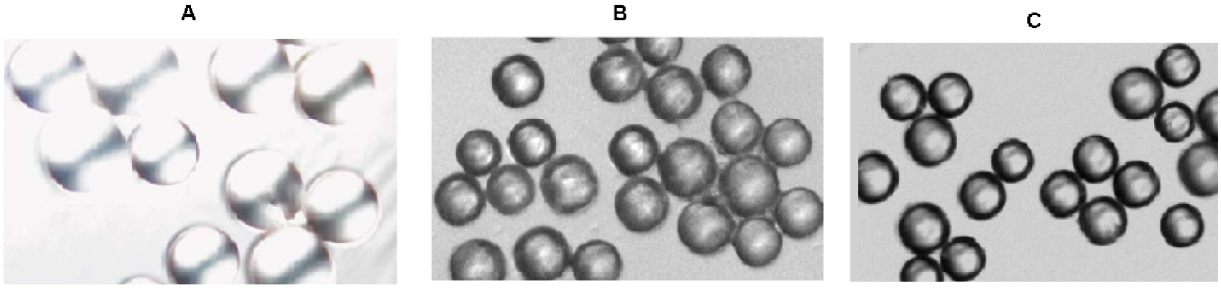

Figure 3.13. The ELISA control experiments with no addition of TAR RNA are shown in these pictures. A) ELISA experiments of K_L-K_D-N_L peptide beads with primary antibody, and substrate are shown. B) ELISA experiments of K_L-K_D-N_L peptide beads with secondary antibody conjugated to the enzyme and substrate are shown. C) ELISA experiments of K_L-K_D-N_L peptide beads with primary antibody, and secondary antibody conjugated to enzyme are shown.

3.3.5. Fluorescence assay for F-H69 and NQVANHQ and STYTSVS peptides on Tentagel beads

After optimizing the assay conditions for the TAR RNA and its peptides and observing positive results, similar experimental conditions were carried out with the phage-selected peptides NQVANHQ and STYTSVS for target RNA H69. These peptides were also chemically synthesized on the Tentagel beads. The initial steps

involved washing the peptide beads with water to remove residual DMF from the synthesis. Next, non-specific interactions with the beads were avoided by blocking the beads with 500 µL of 1 X “Pierce SuperBlock buffer” for 4 h. The beads were washed again with ddH_2O (500 µL x 3) before further use. These beads were incubated with fluorescein-labeled H69 (F-H69) at 1 µM concentrations for four days in the same manner as followed for F-TAR RNA. Peptide interactions with H69 were monitored with the measurement of the fluorescence intensity of the beads under the microscope. The higher or lower intensity of the fluorescence gave an idea about the relative binding affinity of the peptides with their target RNA H69. The fluorescence intensity of the beads having NQVANHQ peptide was slightly higher as compared to STYTSVS peptide beads indicating that NQVANHQ has stronger binding with H69 (Figure 3.14). These results were further verified with the higher precision method of ESI (electrospray ionization), in which direct titration experiments of the peptides with the H69 RNA were carried out (Chapter 4).

A)

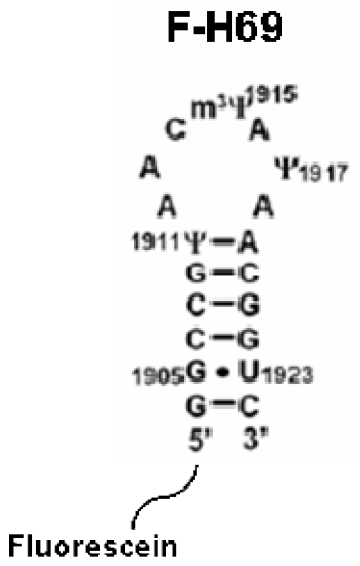

B)

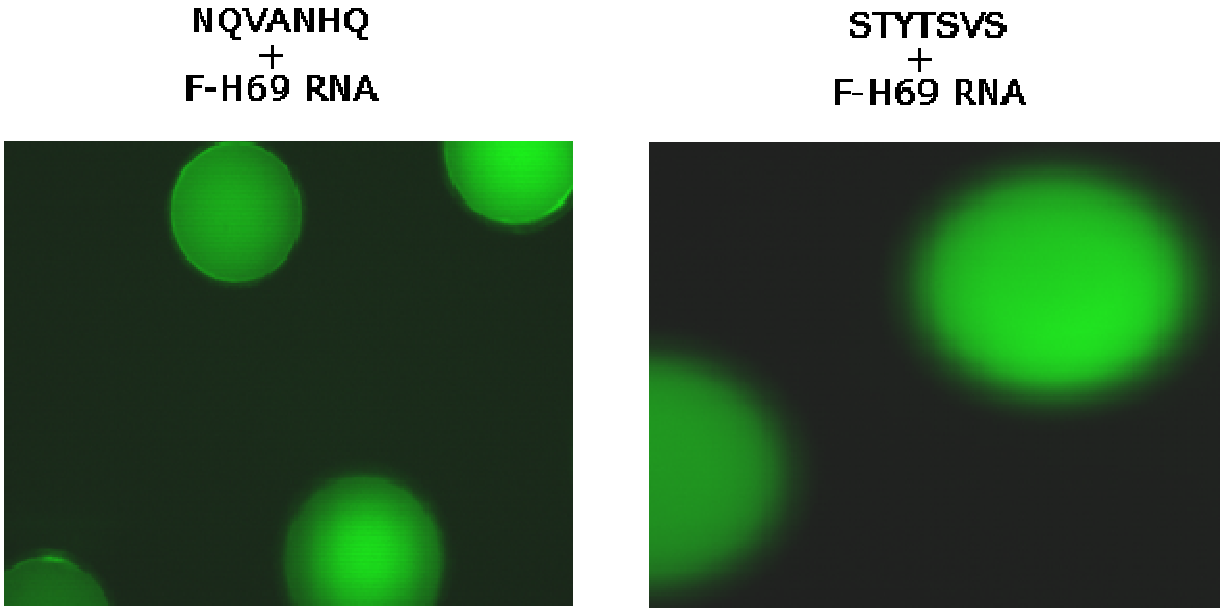

Figure 3.14. A) This panel shows the sequence of the target F-H69 being fluorescein labeled at the 5' end. B) The green fluorescent NQVANHQ peptide beads and STYTSVS peptide beads are observed after incubation with target F-H69.

The above assay was also performed with another kind of fluorophore called Quantum dots (Q-dots) that had an anti-fluorescein antibody attached to them. Q-dots are small inorganic particles of less than 10 nm in dimension (Goldman, E.R. *et al*, 2002). The main advantage of Q-dots is their bright fluorescence with prolonged photo stability that is tunable within the UV and IR range (Murray, C.B. *et al*., 1993). Q-dots were incubated with the mixture of peptide beads and F-RNA at concentrations as low as 1 nM. The images of the beads were monitored under the fluorescence microscope with an excitation wavelength at 430 nm and emission wavelength at 655 nm and the red color of the beads indicated that H69 is binding to the peptides. The results with Q-dots better illustrated that NQVAHNQ peptide has stronger affinity with H69 as

compared to peptide STYTSVS. These quantum dot assays were performed by Dr. Chamila Rupasinghe. The bead images are shown in Figure 3.15.

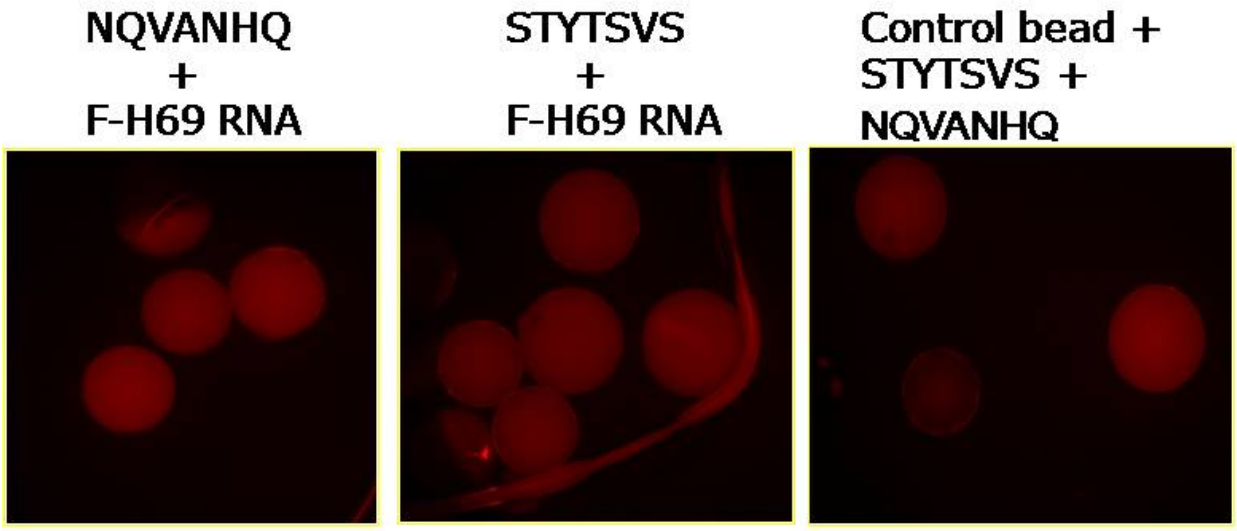

Figure 3.15. The images of NQVANHQ and STYTSVS peptide Q-dots recorded after they were incubated with F-H69. The higher intensity of red color of NQVANHQ beads indicates the same results as for fluorescein bead assay.

3.3.6. On-bead ELISA assay for H69 and peptides

In another scheme of validating the binding of the peptide with the target RNA H69, the above peptide bead assays were performed by employing antibodies. Antibodies against fluorescein (goat anti-Fl Ab) were practical since the H69 construct that was incubated with the peptide beads was fluorescein labeled. These antibodies were further reacted with rabbit anti-goat antibody conjugated with alkaline phosphatase enzyme. The enzyme further reacted with substrate BCIP, giving rise to a turquoise color on the peptide beads. The experiment was also repeated with biotin-labeled H69 (B-H69) instead of fluorescein H69. In this case, anti-biotin antibodies conjugated with enzyme alkaline phosphatase (anti-biotin Ab-AP) were used. The substrate used was

BCIP and turquoise colored peptide beads were seen. The general outline of the experiment is shown in Figure 3.16.

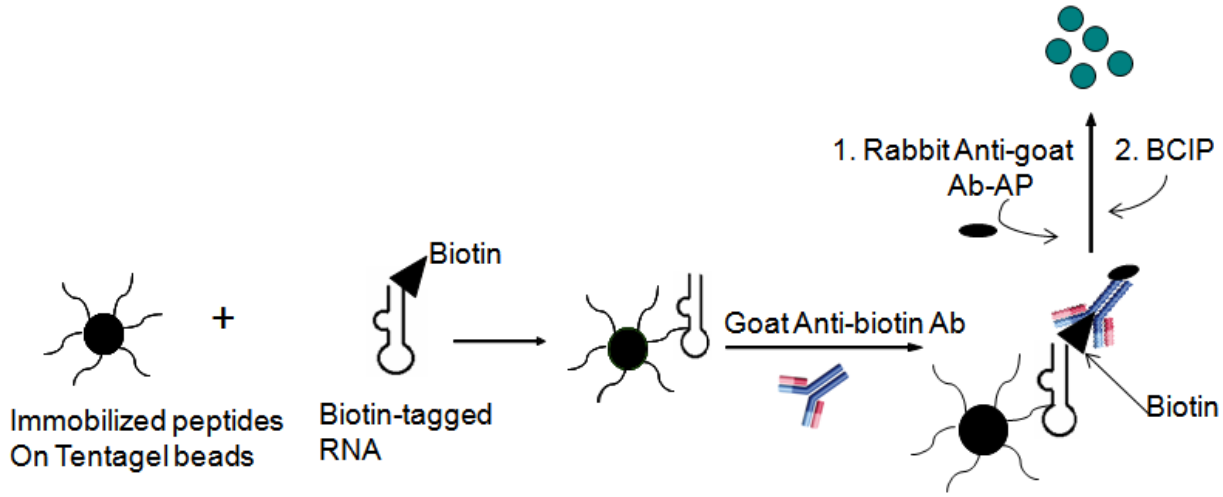

Figure 3.16. The fluorescein- or biotin-labeled RNAs are incubated with peptide beads and upon reaction with enzyme-conjugated antibodies and BCIP, turquoise color beads are seen, indicating the binding of the peptide with H69. Fl: fluorescein, Ab:antibody, AP: alkaline phosphatase, BCIP: 5-bromo-4-chloro-3'-indolyphosphate p-toluidine salt.

The turquoise color of the NQVANHQ peptide beads and STYTSVS peptide beads showed binding of RNA, although the relative affinities were not as apparent as with the Q-dot assay. In order to assess the role of the modified nucleotide pseudouridine (Ψ) present in the native H69, an additional H69 RNA having uridine (U) nucleotide instead of pseudouridine (Ψ) at positions 1911, 1915 and 1917 was synthesized. The unmodified helix 69 was biotin labeled (B-UUU) and incubated following the same procedure as explained in Section 3.3.3 for F-TAR RNA. The appearance of the blue color on the beads (Figure 3.17.) indicates binding of the peptide with the unmodified RNA, revealing that the pseudouridine (Ψ) nucleotides do to play a major role in binding selectivity of the peptide with the H69 under the given buffer conditions. Some non-specific binding of both peptides was seen with other RNAs such

as biotin-helix 17 (from the small subunit 16S RNA) to some extent and the beads itself. But upon comparing the intensity of the color of the beads, it was observed that the NQVANHQ peptide beads had higher affinity for modified H69. Overall, this assay was somewhat problematic and gave results that were difficult to quantify. The Q-dot method assay would be the preferred method for future studies.

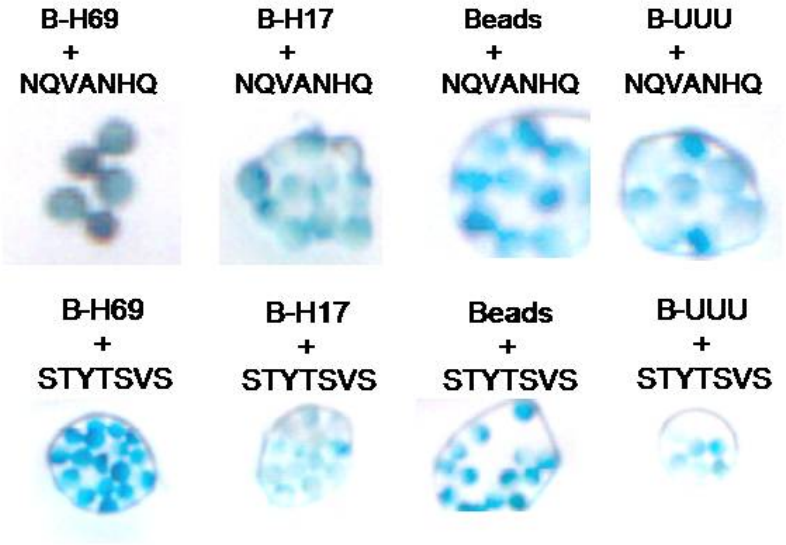

Figure 3.17. Comparison of the intensities of the color of beads is shown after performing the assay.

3.3.7. Affinity of NQVANHQ and STYTSVS peptide beads with control RNAs

Several control experiments were performed to demonstrate the specificity of the two peptides with the H69. First, the incubation of the free fluorescein dye with the NQVANHQ and STYTSVS peptide beads with free fluorescein indicated no interaction of the dye with the heptapeptides. Second, incubation of unrelated RNAs such as F-TAR RNA, and F-18 S RNA with the NQVANHQ and STYTSVS peptide beads was carried out. The two peptides did not reveal any binding interactions with F-18 S (human

A-site RNA), whereas the STYTSVS peptide beads showed some binding to F-TAR RNA. The images of the fluorescent beads taken under the fluorescence microscope are shown in Figure 3.18. The results of these control experiments showed that the binding of the NQVANHQ peptide was more specific for H69 than STYTSVS. This relative affinity was also verified by using ESI (Chapter 4 of this thesis and T. Wang, unpublished data).

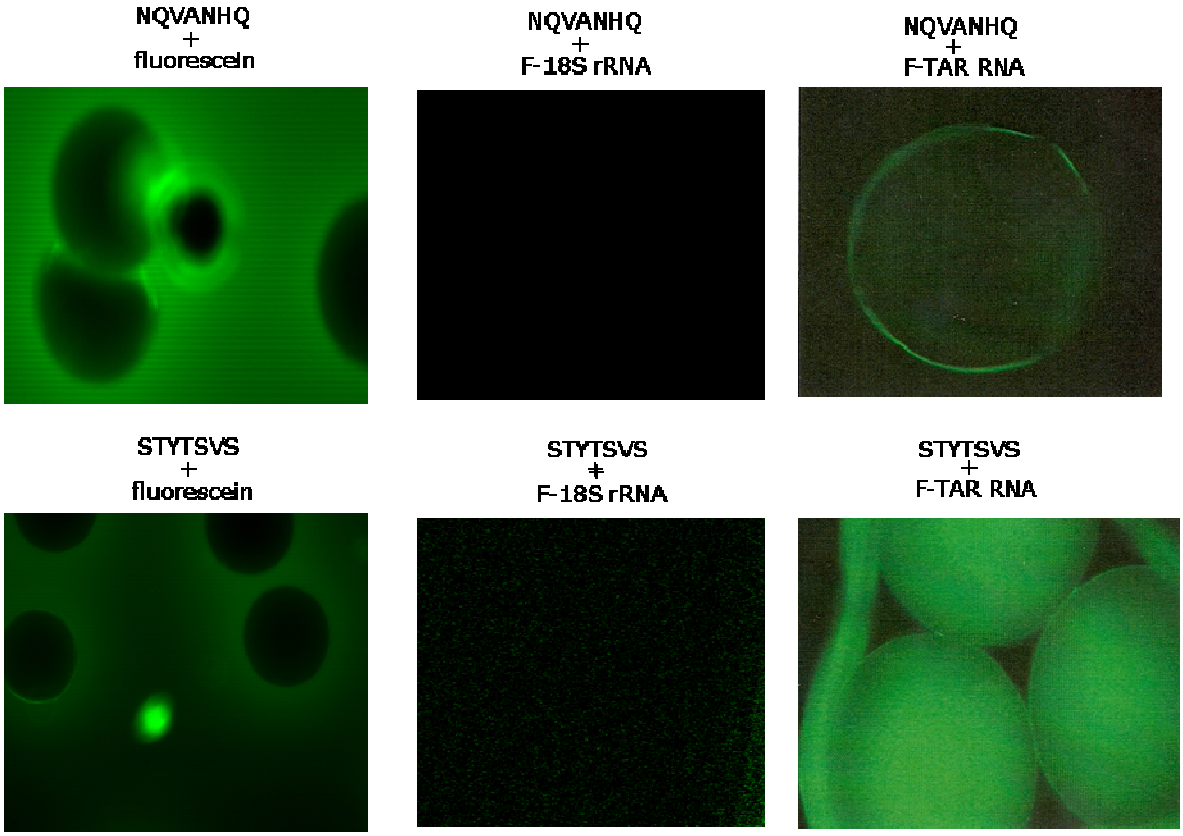

Figure 3.18. No fluorescent beads are observed with controls free fluorescein, human A-site RNA (F-18S RNA) and F-TAR RNA for NQVANHQ peptide. But non-specific binding is observed in case of STYTSVS peptide with F-TAR RNA.

3.4. Conclusions

TAR RNA and the two tripeptides selected by Rana's group, K_L-K_D-N_L and R_L-K_D-V_D, were used as a model system to develop the fluorescent Tentagel bead screening method.

This method was then applied to assess the relative binding affinities of the peptides selected by the phage display technology against target RNA H69. The K_L-K_D-N_L peptide had higher affinity for TAR RNA than the R_L-K_D-V_D peptide. The two peptides were covalently attached on the Tentagel beads and the TAR RNA was fluorescein labeled at its 5' end. This method had a relatively simple procedure to follow and was done at a reasonable cost. The peptide beads were incubated with F-TAR RNA and the beads gave green fluorescence once the TAR RNA interacted with the peptides. The fluorescence intensity of the beads was exploited to monitor the binding of the TAR RNA and the peptides. The green fluorescing peptide beads clearly indicated that the F-TAR RNA was able to enter the interior of the Tentagel beads and bind to the peptides. The K_L-K_D-N_L peptide beads were found to be fluorescing with more intensity as compared to the R_L-K_D-V_D peptide beads. These observations were consistent with the results acquired by Rana's group. The dissociation constants for the two peptides and the TAR RNA as reported in Rana's work for the K_L-K_D-N_L and R_L-K_D-V_D peptides were 420 ± 44 nM and 10,434 ± 54 nM, respectively (Hwang, S. *et al*, 1999). In our fluorescence-based assay, the dissociation constant calculated for the K_L-K_D-N_L peptide was 120 ± 40 nM and that for the R_L-K_D-V_D peptide was 6300 ± 500 nM. Although the values for the dissociation constants from our assay calculations vary considerably from the Rana group's values, the relative order of binding of the peptides was the same. The K_L-K_D-N_L peptide binds to TAR RNA with 25 times better affinity as compared to the R_L-K_D-V_D peptide.

The results of the ELISA experiments for K_L-K_D-N_L peptide beads further verified the fluorescence assay results. The K_L-K_D-N_L peptide was again validated to be binding with the TAR RNA, but the ELISA results of the R_L-K_D-V_D peptide were inconclusive. This assay

posed problems with the quantification of the binding interaction of the peptide; therefore, it was not considered to be that useful for future experiments.

For proving the specificity of the peptides for the TAR RNA, control experiments were performed. The peptides were not seen to bind to the free fluorescein or to unrelated RNAs, such as a theophylline aptamer, human A-site RNA, or ribozyme substrate. Upon performing a competition experiment with excess unlabeled TAR RNA, the green fluorescence of the peptide-F-TAR RNA beads was seen to either diminish or to be abolished. This observation indicated that the unlabeled TAR RNA competed with the F-TAR RNA for binding with the K_L-K_D-N_L peptide and that the binding of the peptide with the TAR RNA was reversible in nature.

After optimization of the assay conditions with the TAR RNA and its peptides, the next step involved using the same assay conditions for the NQVANHQ and STYTSVS peptides chosen for H69. The peptides were synthesized on the Tentagel beads and then incubated with F-H69. After four days of incubation, the fluorescence was observed to be evenly distributed within the beads for both peptide beads. But from the high fluorescence intensity of the NQVANHQ peptide beads, it was evident that the NQVANHQ peptide had good affinity for H69 RNA. The Q-dot assay verified this result and also showed a lower relative affinity of STYTSVS to H69 as compared to NQVANHQ. To check the specificity of the peptides with the H69 RNA, control experiments were carried out with the free fluorescein and several unrelated RNAs including F-TAR RNA and F-18S RNAs. There was no interaction detected between free fluorescein and the two peptide beads. The NQVANHQ peptide beads did not show any interaction with the F-TAR RNA or F-18S RNAs suggesting the specific nature of this peptide for H69. STYSTVS on the other hand, did show moderate affinity for at least one of the unrelated RNAs. The ELISA assay was also done with the

fluorescing NQVANHQ and STYTSVS peptide beads. There were some discrepancies detected with the ELISA assay results, so this was considered to be unreliable. Perhaps the reagents interacted nonspecifically with the bead components.

The Tentagel bead assay described provides a tool for quick testing of the binding of the newly discovered ligands for the target RNAs. The positive verification of the results of this Tentagel beads assay with ESI (electrospray ionization) technology as will be described in the next Chapter, gave powerful evidence of the dependability of this assay for preliminary knowledge of the relative affinities of new ligands for the RNA targets.

CHAPTER 4

Analysis of binding interactions of peptides with H69 RNA and variants using ESI-MS

4.1. Introduction

In this thesis work, ESI-MS (electrospray ionization mass spectrometry) has been applied to monitor complex formation between H69 and peptides NQVANHQ-NH_2 and STYTSVS-NH_2, and also for calculating the apparent dissociation constants (K_ds) of these peptides with H69 RNA and its variants. ESI-MS proved a convenient method to calculate stoichiometry and dissociation constants for these molecular complexes when conventional solution methods proved difficult for their characterization. In recent years, this technique has gained popularity for studying biological complexes having noncovalent interactions. The complexes of this nature are usually held together by noncovalent forces such as electrostatic interactions, hydrogen bonds, and hydrophobic interactions (Daniel, J.M. *et al*., 2002; Loo, J.A., 2000).

The ESI procedure originated from the work of Dole's group (Dole, M. *et al*, 1968), but it was coupled with mass spectrometry by Fenn's group at Yale University (Fenn, J.B. *et al*., 1989). This method allows, under appropriate conditions, the production of multiply charged ions from large molecules with little or no fragmentation and their advancement into the gas phase for direct mass analysis. The series of multiply charged ions gives rise to a series of peaks in the ESI spectra that is known as the charge-state distribution of each component in solution. High mass complexes are

easily detected due to the formation of highly charged species at relatively low mass-to-charge ratios (m/z) (Kebarle, P. *et al*., 1993). Most notably, since ESI is an extremely soft ionization technique, the strong covalent bonds and the weak noncovalent interactions between the molecules are preserved during their study.

The applicability of ESI-MS for studying noncovalent complexes started in the early 1990s. Ganem and coworkers in 1991, for the first time, detected the intact receptor-ligand complex between FK-binding protein and macrolide rapamycin, as well as the enzyme-substrate complex of lysozyme and N-acetylglucosamine through ESI-MS (Ganem, B. *et al*., 1991). Subsequently, this technique has been extensively applied for observation of protein-nucleotide and protein-ligand complexes. The first example in the category of protein-DNA complexes was reported by Cheng and coworkers, in which the homodimer of gene V protein from bacteriophage f1 and its complex with single-stranded DNA was observed by ESI-MS (Cheng, X. *et al*., 1996). In earlier studies of protein-RNA complex detection by ESI-MS, Cavanagh's group was successful in observing protonated molecules of dimeric NF-κB with its 31-nucleotide RNA aptamer. Peaks corresponding to protein-RNA complexes with a ratio of RNA aptamer to NF-κB protein dimer were detected (Cavanagh, J. *et al*., 2003).

One major question related to the validity of ESI-MS being applied for detection of noncovalent complexes is whether the complex structure in the gas phase is a true representation of the one that exists in solution phase. Much of the early work for this validation in ESI-MS was based on the studies performed on protein structure and conformation. The first demonstration to monitor a protein's solution conformation with this method was done by Chowdhury *et al*, in 1990 by using the well-studied protein

cytochrome C (Chowdhury, S.K. *et al*., 1990). A change in its charge distribution was observed as a function of solution pH, which correlated well with the protein's well-known conformational states in solution. In another study performed by Loo *et al*. in 1990, different solution conformations of a small protein ubiquitin with changing acetonitrile (organic solvent) content were displayed (Loo, J.A. *et al*., 1991). In contrast, the complexes of inhibitors with carbonic anhydrase, which interact through hydrophobic means, were extremely labile (Wu, Q. *et al*., 1997). Nonetheless, these studies demonstrated the ability to examine solution-phase structure of a macromolecule by ESI.

A few pioneering studies were performed in the area of oligonucleotide complexes. In the case of RNA-protein complexes, it was observed that the noncovalent complexes such as Tat peptide-TAR RNA (Sannes-Lowry, K.A. *et al*., 1997) and zinc finger human immunodeficiency virus (HIV) nucleocapsid protein NCp7-ψ-RNA (Loo, J.A. *et al*., 1998) were extremely stable in the ESI environment. Aminoglycosides such as neomycin are known to interact with RNAs primarily through charge-charge interactions. The neomycin-TAR RNA complexes were not observed to dissociate in the gas phase (Sannes-Lowry, K.A. *et al*., 1999). In the ESI spectrum, the multiple charge distribution represented by the m/z values, and the relative width of the m/z positions can be related to the structure or conformation of the solution-phase macromolecule.

For studies of small molecule-macromolecule complexes, such as aminoglycoside-RNA and peptide-RNA complexes, mass spectrometry is a sensitive and rapid method in comparison to the gel-based methods such as EMSA

(electrophoretic mobilbity shift assay) and footprinting. ESI-MS has been successfully employed to calculate binding constants (Sannes-Lowry, K.A. *et al*., 2000), the location of binding sites (Griffey, R.H. *et al*., 1999), and the binding specificity of aminoglycosides on the A-site rRNA (Hofstadler, S.A. *et al*., 1999). Although NMR and X-ray crystallography are powerful tools to acquire the three-dimensional structural information of macromolecules and their complexes with small molecules, milligram quantities of the samples are required (Fourmy, D. *et al*., 1998; Yusupov, M.M. *et al*., 2001). In the case of ESI-MS studies, only nanogram amounts of sample are required. When employing fluorescence-based methods, labeling of the target or ligand with an appropriate fluorophore is essential (Llano-Sotelo, B. *et al*., 1999); whereas, fluorophore labeling is not required for analysis by ESI-MS. The stoichiometry of the complexes can also be readily obtained through ESI-MS by knowing the molecular masses of the molecules involved in complex formation (Sannes-Lowry, K.A. *et al*., 1997).

Despite the advantages of ESI-MS, there are still some limitations in using this technique. For accurate measurement of the molecules and the complexes, very high purity samples are required. Pure samples are obtained through extensive dialysis, removing most of the nonvolatile counterions such as Na^+ and then precipitating the target in the presence of the desired volatile counterions (for example, NH_4^+). The most preferable buffers for analyzing RNA and small molecules is ammonium acetate, which is present in concentration ranges of 10 to 150 mM in the final solution. Ammonium acetate is preferred because like phosphate- and sulfate-based buffers, this compound

readily evaporates and does not form undesirable salt adducts in the gas phase with the analyte molecules (Iavarone, A.T. *et al*., 2004).

Regardless of these limitations, ESI-MS has been successfully applied for characterizing noncovalent complexes and estimating their apparent dissociation constants (K_d). The values of the apparent dissociation constants (K_d) obtained with ESI-MS correlate well with those determined from solution measurements in case of noncovalent complexes such as the src SH2-phosphopeptide system (Bligh, S.W.A. *et al*., 2003) , the antibiotic vancomycin binding to peptide ligands (Lim, H.K. *et al*., 1995), and aminoglycosides with A-site rRNA (Sannes-Lowry, K.A. *et al.*, 2000).

4.2. Electrospray ionization mass spectrometry (ESI-MS)

4.2.1. Basic principles of ESI-MS

Since the pioneering development of the electrospray ionisation (ESI) for mass spectroscopy by Fenn's group (Fenn, J.B. *et al*., 1989), it has been used as an active analytical tool in biology, biochemistry, and biomedical research. In the ESI-MS compounds are characterized by interpreting the mass spectrum, which typically shows a distribution of multiply charged ions that are separated according to their mass-to-charge ratio. Singly charged compounds represent their molecular weight as $(MW + H)^+$ in the positive ionization mode and as $(MW - H)^-$ in the negative ionization mode. ESI-MS works for the transfer of a large range of ions from the solution to the gas phase. The ions include the singly charged electrolytes Na^+ and Cl^-, group two ions Ca^{2+}, Sr^{2+}, and Ba^{2+}, bioorganic ions such as multiply protonated peptides and proteins

of molecular masses in the range of 100,000 Da, and multiply deprotonated negatively charged nucleic acids (Kebarle, P. *et al*., 1993).

The electrospray ionization inlet system is part of the mass spectrometer, which has a mass analyzer and detector. The electrospray ionization source, unlike other inlet systems, is a soft ionization inlet system that allows for the detection of complete non-fragmented compounds (analytes) (Figure 4.1).

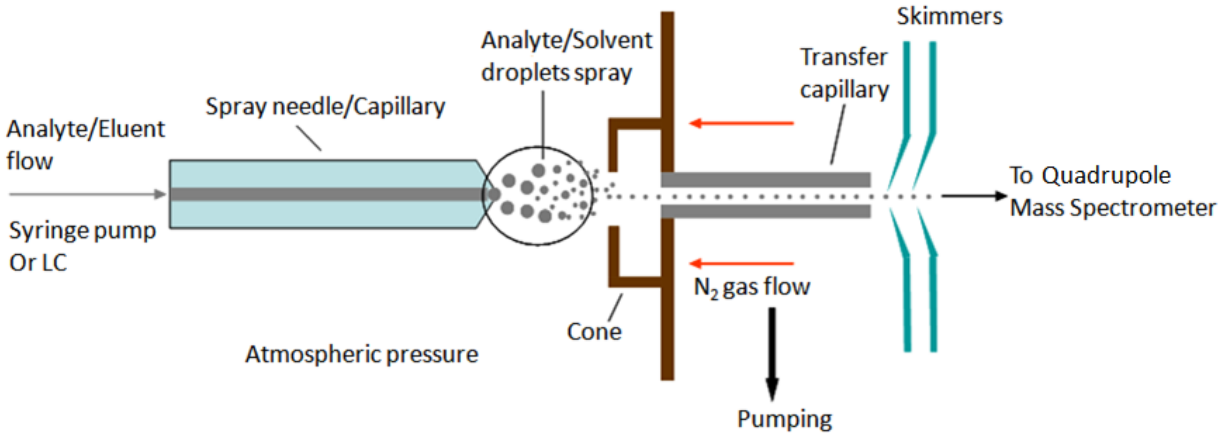

Figure 4.1. The principles of the electrospray ionization mass spectrometry (ESI-MS) are depicted in the above picture.

The steps involved in the formation of gas-phase analyte ions from solutions holding these ions can be divided into the following steps: a) formation of an aerosol of charged droplets at the capillary tip, and b) production of gas-phase ions from the very small charged droplets by the charge residue mechanism (CRM) or the ion evaporation mechanism (IEM) (Cole, B.R., 2000). For the formation of ions in ESI-MS, a high voltage is applied to the metal ESI capillary through which the sample solution is coming out. This leads to the electrophoretic movement of the ionic species in the sample solution under electric field strength of ~ 10^6-10^7 V m^{-1} (Pfeifer, R.J. *et al*., 1968). In the positive-ion mode, anions are driven inside of the metal ESI capillary,

whereas cations migrate away from the capillary, i.e., in the direction of the counter electrode. The positive ions at the surface of the liquid and the applied electric field cause a repulsive force that overcomes the surface tension of the emerging liquid. At sufficient high electric field strength, the liquid starts to emerge in shape of a cone also referred to as 'Taylor cone' (Taylor, J.R., 1964). Due to the presence of the high voltage difference between the ESI capillary and the counter electrode, oxidation reactions take place at the metal-solution edge of the ESI capillary such as H^+ production from water. In the negative-ion mode, the anions are attracted towards the counter electrode and the cations are driven inside of the ESI metal capillary. In this mode, reduction reactions may occur at the metal solution interface of the ESI capillary (Blades, A.T. *et al*., 1991). In both modes of ESI-MS, charge flow of the ions of same polarity is maintained by these electrochemical reactions. Similarly, at the counter electrodes where the ions of reverse polarity keep arriving, another electrochemical reaction is completed. The occurrence of this second electrochemical reaction completes the special kind of electrical circuit and thus, electrospray source has been considered as an unusual type of electrolytic cell, in which electrolysis maintains the continuous stream of charged droplets (Kebarle, P. *et al*., 2000).

The accumulation of excess charges on the surface of the droplets help to elongate the emerging liquid in the direction of the counter-electrode and the opposing force of surface tension of the liquid keeps the liquid droplet together. The balancing act of these two forces produces the dynamic Taylor cone at the tip of ESI capillary (Taylor, J.R., 1964). The theory behind the formation of gas-phase ions from the small, highly charged droplets is explained with the help of two principal mechanisms,

namely, charged residue model (CRM) (Dole, M. *et al*., 1968) and the ion evaporation mechanism (IEM) (Iribarne & Thomson, 1976; Thomson & Iribarne, 1979). In the CRM, proposed by Dole and co-workers (Dole, M. *et al*., 1968), a series of fission events eventually leads to the generation of final small droplets having one or more excess charges, but only a single analyte molecule. Due to the evaporation of the last few solvent molecules, the excess charges present will accumulate on the sites forming the most stable gas-phase analyte ion. In IEM, Iribarne and Thomson (Iribarne & Thomson, 1976; Thomson & Iribarne, 1979) reasoned that prior to decrease of the radius of the droplet below 10 nm (Rayleigh limit), the electric field on the surface of the charged droplets is high enough for emitting the solvated ions into the gas phase. In the IEM, the partitioning of the single solvated analyte ion carrying some of the droplet's charge is due to the desorption event.

Despite the controversy of the two major events leading to the formation of gas-phase ions in ESI-MS, a firm consensus has come forward that ionic structure of very large molecules, comprising multiply charged molecules, are formed due to the charge residue mechanism (CRM). The examples of these large molecules usually comprise the protein-protein complexes such as enzyme-substrate, and enzyme-product complexes (Fernandez de la Mora, J., 2000; Valentine, S.J., 1997; Shelimov, K.B. *et al*., 1997). These complexes are held together in the cellular environment with the strong covalent bonds as well as weak noncovalent interactions such as electrostatic interactions, hydrogen bonds, and hydrophobic interactions. Formation of the small gas-phase ions is favored by IEM, such as the simple stable alkali metal Na^+, K^+, Cs^+ ions. These ions are helpful for the production of ionized analytes from the species that

do not ionize in solution, but have polar groups such as sugars and glycols. In solutions of these molecules, these ions enter the gas phase with a solvated shell as $M^+(H_2O)_m$ when the solvent is water (since the IEM holds in early stages). As the solvent evaporates, the formation of ML^+ ions predominates (where L is sugar or glycol molecule) (Kebarle, P. *et al*., 2000; Gamero-Castaño, M., 2000). Therefore, ESI-MS has enabled the observation of molecular ions of intact noncovalent complexes under certain solvent conditions.

4.2.2. Applications of ESI-MS to nucleic acids

At present, mass spectrometry with the introduction of electrospray ionization has accelerated the studies of biological macromolecular complexes such as DNA and RNA duplexes, triplexes and quadruplexes in the field of nucleic acids. This chapter focuses on the study of RNA interactions with heptapeptides using ESI-MS. There is sufficient evidence provided by the literature for using this technique for characterizing nucleic acid complexes held together noncovalent forces. The first nucleic acid complex observed with ESI-MS was from the group of Ganem and coworkers, in which the duplex structure of two DNA strands formed by the noncovalent base pairing was clearly seen (Ganem, B. *et al*., 1991). It was reported that the relative abundance of the duplex versus single-stranded DNA was more for a GC-abundant 8-mer as compared to an AT-rich 8-mer. Another study by Doktycz and coworkers using an ion-trap quadruple mass spectrometer, pointed to the stability of the DNA duplex in the ESI experimental settings (Doktycz, M.J. *et al*., 1994). In their study, the 10-mer and 20-mer DNA duplexes were observed to survive the atmosphere/vacuum interface and

had lifetimes of hundreds of milliseconds in the gas phase. Bowers and coworkers not only studied the duplex formation of DNA strands, but also the different parameters of duplex formation such as strand length, effects of metal ions on the Watson-Crick base pairing, and quadruplex formation by using ESI-MS (Gidden, J. *et al*., 2005). In their results, they reported that the duplexs retained their helical structure on the ms time scale in the gas phase, and that DNA quadruplex formation was observed for G-C rich oligonucleotides in presence of ammonium ions.

Higher-order complexes of DNA were observed with ESI-MS in negative ion mode by Griffith and co-workers (Griffith, M.C. *et al*., 1995). They studied the binding of a 10-mer peptide nucleic acid (PNA) with 15-mer single-stranded DNA, in which triplexes consisting of two PNAs bound to one DNA strand were formed. These authors found that an AG-rich PNA strand was bound to a TC-rich DNA strand as a triplet. These studies helped to push forward the concept of PNAs as antigene and antisense agents

ESI-MS has been used extensively for probing the DNA-protein interactions. ESI-MS studies of RNA-protein interactions have been more challenging due to the innate difficulties of handling RNA and due to the presence of RNA nucleases. Despite these hurdles, interactions of HIV-TAR RNA with Tat peptide and Tat protein were successfully carried out (Sannes-Lowry, K.A. *et al*., 1997). Relative binding affinities between Tat peptide and TAR RNA and several mutants were differentiated with ESI competitive binding experiments by Sannes-Lowry's group. There was reduced affinity of the Tat peptide with the mutant TAR RNAs, consistent with the previous gel-mobility shift experiments (Roy, S. *et al*., 1990). It was quite evident from these studies that

specific interactions between the peptide and protein were maintained in the gas phase as compared to the solution-phase studies of the same TAR RNA and Tat peptide or Tat protein systems. ESI-MS was a convenient method to calculate peptide-RNA binding stoichiometries and binding constants (Sannes-Lowry, K.A. *et al*., 1997).

In a recent study, ESI-MS was employed for detecting cobalt (III)hexammine [$Co(NH_3)_6^{3+}$] binding to RNA hairpins having G•U and A•C wobble pairs, in addition to modified bases such as pseudouridine (Ψ) and 3-methyl-pseudouridine ($m^3\Psi$) (Kieltyka, J.W. *et al*., 2006). The pH-dependent binding studies of $Co(NH_3)_6^{3+}$ were performed with the 790 GU-loop RNA containing a G•U mismatch and 790 A•C-loop RNA having an A•C mismatch. At pH 5.3, only the -3, -4, and -5 charge states of the complexes were observed, whereas at pH 7.2, an additional charge state of -6 was also observed. This showed that lowering the pH of the solution resulted in simpler spectra by narrowing of the charge state envelope of the complex. Further, it resulted in three-fold decrease in the formation of the 1:1 complex for 790 GU hairpin with $Co(NH_3)_6^{3+}$ and an increase in the 1:2 complex, showing decreased specificity. This three-fold decrease of binding affinity was possibly attributed to the protonation of the base in the 790 GU hairpin leading to unfavorable interactions with $Co(NH_3)_6^{3+}$. In case of 790 A•C-loop RNA, a thirty-fold decrease in binding affinity of the $Co(NH_3)_6^{3+}$with the RNA hairpin was noticed. The decrease in binding affinity was probably due to the protonation of the mismatch site (A^+•C), and this mismatch site was a potential binding site of the metal complex with RNA. These studies revealed that the ESI-MS is a viable and sensitive technique for characterizing noncovalent interactions between RNA and the transition-metal complexes. The change in the binding affinity of the complexes

because of the pH change lead to the recognition of the potential ligand-binding sites of the RNA hairpins (Kieltyka, J.W. *et al*., 2006). Based on the previous studies, we believe that ESI-MS would be useful to characterize the interactions of peptides discovered through phage display with H69 RNAs.

4.3. Materials and methods

4.3.1. General materials

All the experiments were conducted on the Quattro LC tandem quadrupole mass spectrometer with electrospray ionization (ESI) inlet (Micromass, Manchester, UK). A quadrupole mass analyzer consists of four parallel rods applied with direct current (DC) and radio frequency (RF) voltage. The schematic of the Quattro LC is shown in Figure 4.2.

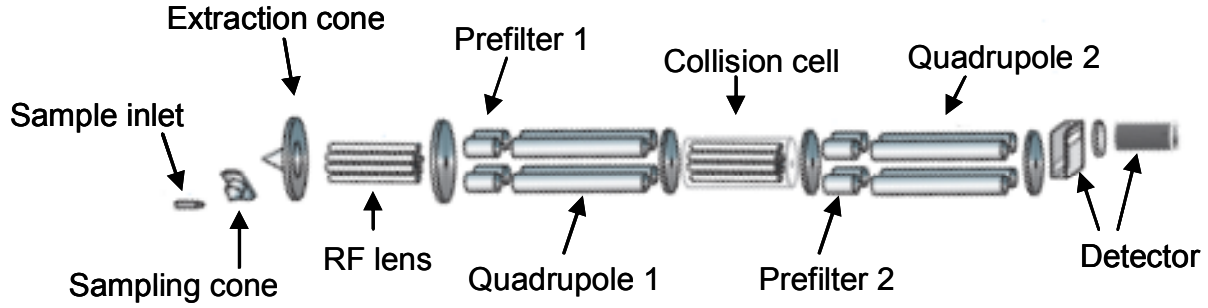

Figure 4.2. A general format of the Micromass Quattro LC mass spectrometer showing the main parts of the instrument is illustrated (Quattro LC User's Guide).

The ESI-MS experiments in this thesis were carried out with the Quattro LC tandem quadrupole mass spectrometer having electrospray ionization in the negative ion mode (Micromass, Manchester, UK). The operating conditions included a capillary

voltage of 2.5 kV, cone voltage of 50 V, extractor cone voltage of 2 V, RF lens voltage of 0.6 V, source block temperature of 100 °C, and a desolvation temperature of 120 °C. A flow rate of 6 µl/min was set for infusing the sample using a Harvard II syringe pump. The desolvation gas flow rate was set to be ~ 400 L/h and nebuliser gas flow rate of ~ 90 L/h was used. Since none of the RNA charge states were observed below the m/z value of 1200 and above the m/z value of 2500, the mass spectra were recorded from 1200-2500 m/z for every sample and 60-70 spectra were averaged. Before acquiring the data on the instrument, thorough cleaning of the sample cone and the lines was performed. The sample cone was cleaned by sonication (50% water, 45% methanol, 5% formic acid) for 20 minutes followed by rinsing with water and then drying with stream of nitrogen. The capillary tubing and the transfer lines were cleaned with the solution of 75% water and 25% 2-propanol.

The RNA oligonucleotides for ESI-MS study were chemically synthesized on a 1.0 µmole scale via phosphoramidite technique (Scaringe, S.A. *et al*., 1998) by Dharmacon, Inc. (Lafayette, CO). 3-Methylpseudouridine ($m^3\Psi$) was synthesized in our lab by Helen Chui, converted to its phosphoramidite form (Chui, H.M.-P. *et al*., 2002) and sent to the Dharmacon, Inc. for incorporation in the given RNA sequences (Figure 4.3.).

H69 [5'-GGCCGΨAAC($m^3\Psi$)AΨAACGGUC-3', modified, $\Psi m^3\Psi\Psi$]

UUU [5'GGCCGUAACUAUAACGGUC-3', unmodified]

U$\Psi\Psi$ [5'-GGCCGUAAC($m^3\Psi$)AΨAACGGUC-3'] and

ΨUΨ [5'-GGCCGΨAACUAΨAACGGUC-3']

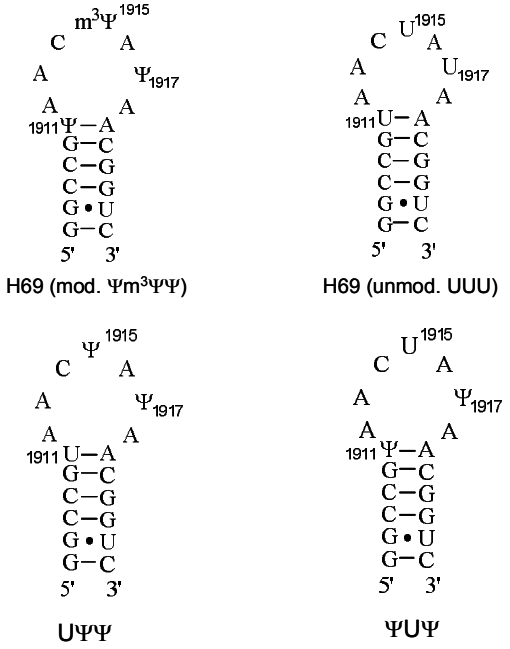

Figure 4.3. The sequences of H69 (mod. and unmod.), mutants of H69 (UΨΨ, ΨUΨ) that were employed for carrying out the binding studies with the peptides are shown.

The RNAs were recieved as 2'-O-ACE protected oligos and were deprotected by dissolving in 100 mM TEMED-acetic acid solution (pH 3.8) followed by incubation at 60 °C for 30 minutes. The RNAs were then dried in a speed-vac. Following deprotection, the RNAs were precipitated twice with 7.5 M ammonium acetate, pH 7.2. The precipitation was performed by adding 250 µl ammonium acetate solution and 750 µl of 200-proof cold ethanol. The samples were mixed properly and incubated at -80 °C for 45 to 60 minutes. After incubation the samples were centrifuged (10,000 rpm, 4 °C) for 30 minutes followed by cautious removal of the supernatant. The above procedure was carried out again and after removal of the supernatant the second time, 200 µl of cold ethanol was added to the RNA pellet. The RNA pellet was then dried in speed-vac, reconstituted in water and stored at - 20 °C. For the ESI-MS experiments, the RNAs were renatured in 15-30 µl aliquots of 100-200 µM RNA in 100 mM ammonium

acetate (pH 7.2) by incubating in heat block at 90 °C for 2 minutes. The heat block was switched off and the RNA solutions were gradually allowed to reach at room temperature (3 to 4 hrs). The concentrations of the RNA solutions were calculated from the UV-visible spectra by applying Beer's law. The extinction coefficients (ε) for the RNAs were calculated using the Schepartz Lab Biopolymer Calculator and their values were 187,000 L^{-1}•mol^{-1}•$cm^{-1}$for UUU (unmodified H69). The ε value acquired for UUU was also applied to the H69 ($\Psi m^3\Psi\Psi$), U$\Psi\Psi$, and ΨUΨ RNAs, since the Biopolymer calculator does not have values for the modified nucleotides.

The peptides NQVANHQ-NH_2 and STYTSVS-NH_2 with C-terminal amidation used in the ESI-MS experiments with RNA were synthesized by Chamila Rupasinghe in our lab using solid-phase peptide synthesis. The amidated peptides were generated and the chemical structures are given in Figure 5.4. The peptide solutions were prepared in Millipore water and the solutions were quantified using the LavaPep peptide quantification kit (Fluorotechnics Pty Ltd., Sydney, Australia, 2006) since the peptide lacked UV active amino acids such as tyrosine, tryptophan and phenylalanine. This kit has epicoccone dye, a fluorescent reagent that binds to lysine, histidine, and arginine amino acids in the peptide sequence. The kit consists of two solutions named as part A that is a dilute DMSO/acetonitrile solution of dye and part B that is bicarbonate buffer with SDS and acetonitrile. The dye fluoresces using a 540 ± 10 nm excitation filter and 630 ± 10 nm emission filter. For preparation of standard peptide curve, solutions of peptide HPVHHYQ-NH_2 in water were prepared in four-fold dilutions ranging from 40 ng/mL to 0.655 mg/ml. The working solution was prepared by mixing water, part A and part B in 8:1:1 ratio (the amount of solution depends on number of

samples). For measuring fluorescence in a 96-well microtiter plate, 50 µl of working solution was incubated with 50 µl of each HPVHHYQ-NH_2 peptide dilution in individual wells. Similarly a blank was prepared by adding 50 µl working solution and buffer/water (50 µl) in one well. For measuring peptide concentration of unknown concentration, 50 µl of that solution and 50 µl of working solution were added in another well. All the samples were incubated at room temperature in the dark for 60 minutes. After recording the fluorescence readings using an excitation wavelength of 540 nm and emission wavelength of 630 nm, the blank reading was subtracted from all the readings of solutions. A plot of log of fluorescence versus log of peptide concentration was generated using the linear fit. The equation obtained from the linear fit was then used for determining the concentration of peptide with unknown concentration. The concentration of STYTSVS-NH_2 was calculated by measuring its absorbance at 280 nm. The extinction coefficient (ε) used for tyrosine (Y) was 1200 AU/mmol/ml.

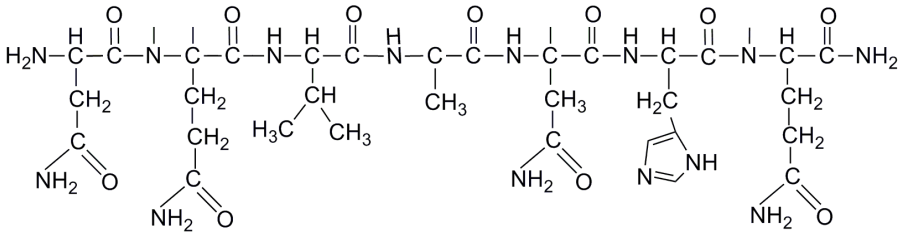

NQVANHQ-NH_2

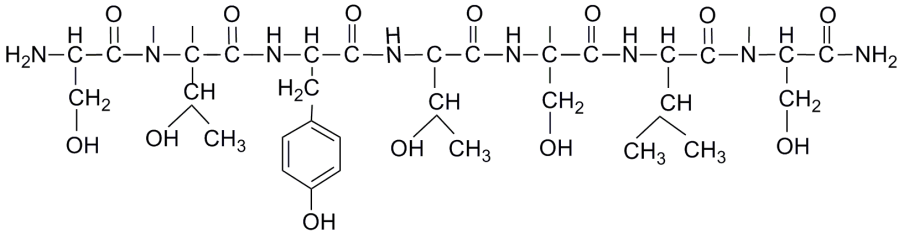

STYTSVS-NH_2

Figure 4.4. The chemical structures of the peptides NQVANHQ-NH_2 and STYTSVS-NH_2 are shown.

4.3.2. ESI-MS data analysis

The optimized conditions for the binding studies in this thesis for the ESI-MS samples were typically 50 µl volume having final concentrations of 1-3 µM RNA, 150 mM ammonium acetate, pH 5.2 or pH 7.0, 25% 2-propanol and 0-120 µM peptide. The mixtures of the RNA and the peptide were equilibrated for 30 min at room temp before each measurement. In the spectra of the RNA, usually three charge states -3, -4 and -5 were observed, whereas in the spectra of the RNA-peptide complexes, the charge state of -4 was more dominant as compared to the -5 charge state. The formation of the complex between the RNA and the peptide did not change the charge states of the RNA as seen in the absence of the peptide. The formation of 1:1 complex between RNA and the peptide NQVANHQ-NH_2 was more as compared to 1:2 complex. An assumption regarding the ionization efficiencies of the free RNA and the RNA-peptide complexes was made in accordance with the literature (Hofstadler, S.A. *et al*., 1999 and 2001; Daniel, J.M. *et al*., 2002; Smith, R.D. *et al*., 1997; Sannes-Lowry, K.A. *et al*., 1997, 1999, 2000; Loo, J.A. *et al*., 1997 and 2000; Bligh, A.S.W. *et al*., 2003; Nesatyy, V.J., 2002). It has been shown previously that if the ligand is much smaller than the target biomolecule in mass, then the ionization efficiencies of the biomolecule and their complexes are considered same. In the present studies, the binding of the peptides to the RNA was presumed to not alter the ionization efficiency of the complex since the mass of the peptides are small compared to the RNA target (<10%). Thus, for all calculations, a correction factor for different ionization efficiencies was not used. Mass Lynx^{TM} 4.0 was applied for data collection and analysis. For calculation of the peak areas, the spectra were smoothed once from the full-width at half-height value using

the Savitzky-Golay method before integration (command for integration in the Mass Lynx^{TM} 4.0). In performing these experiments, it was assumed that the summed peak areas of the charge states of the free RNA, 1:1, and 1:2 complexes was comparative to the concentrations of the free RNA, 1:1, and 1:2 complexes in solution, respectively. This assumption was considered reasonable, since low concentrations of RNA and peptide were employed (Tang, L. *et al*., 1993; Sannes-Lowry, K.A. *et al*., 2000; Loo, J.A., 2000).

For calculating apparent dissociation constants, in much of the literature, the sum of the peak areas of all the observed charge states is generally taken into account (Sannes-Lowry, K.A. *et al*., 2000; Bligh, A.S.W. *et al*., 2003; Greig, M.J. *et al*., 1995; Rosu, F. *et al*., 2002; Loo, J.A. *et al*., 1997; Gabelica, V., 2003; Wendt, S. *et al*., 2003). Therefore, the peak intensities of free RNA ions, RNA-Na^+ and RNA-K^+ adduct ions in the -4, -5, and -6 charge states were summed up. Similarly, the peak intensities of the RNA-peptide complexes (including 1:1, 1:2) and their Na^+ and K^+ ion adducts were added up. The fraction of RNA bound was calculated by dividing the peak intensity of RNA-peptide complexes with summation of peak intensities of free RNA and RNA-peptide complexes. The apparent dissociation constant (K_d) was calculated by plotting the fraction of RNA bound versus the concentration of peptide and using a non-linear curve fitting quadratic equation (Equation 5.1.). This equation was applied because mainly 1:1 complex formation was observed at lower concentrations of the peptide and in a previous study carried out in our lab involving the calculations of the apparent dissociation constants of the transition metal complexes with the RNA, only this

equation gave suitable results for the K_ds out of many equations tried (thesis submitted by Jason W. Kieltyka, 2006)

Equation 4.1:

$$\frac{\sum RP^{n-}}{\sum R^{n-} + \sum RP^{n-}} = \frac{([R]_o + [P]_o + K_d) - (([R]_o + [P]_o + K_d)^2 - 4[R]_o[P]_o)^{0.5}}{2[R]_o}$$

In the above equation, $[R]_o$ is the total concentration of RNA, $[P]_o$ is the total concentration of peptide, ΣRP^{n-} is the total concentration of RNA-peptide complexes at given charge state or all charge states (depending upon which approach is used), ΣR^{n-} is the total concentration of free RNA at given charge state or all charge states (depending upon which approach is used). The Kalaidagraph™ software was employed to fit the data and apparent dissociation constants were calculated with the above quadratic equation.

In another approach, the apparent dissociation constant for the 1:1 complex was also calculated for the individual charge states of -4 and -5, where the peak areas of free RNA H69 with its salt adducts at individual charge state and the complexed RNA H69 at individual charge state with its salt adducts were summed together. The fraction of H69 bound to the peptide at a particular charge state was calculated by dividing peak intensity of the H69-peptide complexes with the summation of the peak intensities of the free RNA and the RNA-peptide complexes. The data was again analyzed using Equation 4.1. Similarly, the apparent dissociation constant for 1:2 complexes was determined at the -4 charge state. For some of the apparent dissociation constant calculations, the relative fraction of peptide-bound RNA was also calculated using equation 4.2:

$F_r = (F_0-F_i)/(F_0-F_f)$, Equation 4.2.

where F_r is the fraction of RNA bound, F_0 is the intensity of free RNA, F_i is the intensity at a given titration point, and F_f is the intensity at the end point of the titration. The data obtained after using equation 4.2 is marked with an asterisk (∗).

4.4. Results and discussion

4.4.1. ESI-MS binding studies with the NQVANH-NH_2 peptide and H69

In this work, experiments for studying the peptide-RNA complexes were carried out with different H69 RNA sequences (modified, $\Psi m^3\Psi\Psi$; unmodified, UUU; $\Psi U\Psi$; $U\Psi\Psi$) and the other criterion was to do the experiments at two different pH values of 7.0 and 5.2 for modified and unmodified H69 RNA. The titrations were carried out by keeping the H69 RNA concentration constant and varying the peptide concentrations. The dissociation constants for H69-NQVANHQ-NH_2 and UUU-NQVANHQ-NH_2 complexes was calculated at two pH values, one at physiological pH 7.0 and the other at pH 5.2. The two pH values were selected in accordance with the pH-dependent studies performed at pH 7.0 and at lower pH values by my colleague Dr. Sanjaya Abeysirigunawardena (Abeysirigunawardena, S. & Chow, C.S., 2008). The circular dichroism and UV melting data clearly indicated that an altered conformation of H69 existed at lower pH and that the protonated form of RNA at pH 5.5 had a slightly higher stability than the unprotonated form at pH 7.0. The apparent pK_a for H69 protonation was 6.3 and was calculated based on molar ellipiticity changes at different pH values. The CD experiments were also carried out with only the stem region of H69, excluding the loop residues, and no notable differences in structure were seen at pH 7.0 and pH 5.5. This led to the conclusion that the loop region plays important role in pH-

dependent conformational change of H69. Temperature-dependent NMR data further revealed that at the higher pH value, the loop residue A1913 is flipped out, leading to partial exposure of Ψ1915 and Ψ1917 to solvent, but at lower pH the loop residue A1913 is located inside the loop and protects the Ψ1915 and Ψ1917 from solvent exchange. Therefore, at higher pH the loop region was more dynamic and at lower pH had a higher degree of base stacking or stabilization. The structural changes observed with the lower pH conditions for isolated H69 construct were in accordance with the 50S structure given by Bashan and coworkers (Bashan, A. *et al*., 2003).

H69 has three uridine (U) residues modified to pseudouridine (Ψ) residues at positions 1911, 1915 and 1917 with Ψ1915 being methylated at N3 position. The role of the Ψ residues at 1911 and 1915 in binding of the peptide with the H69 was also investigated. For this purpose, two separate RNA H69 constructs having uridines instead of pseudouridine (Ψ) nucleotides at position 1911 and 1915, respectively, were synthesized (the other pseudouridine nucleotides being present in the sequence). The dissociation constants for the complexes of NQVANHQ-NH_2 peptide with these RNA constructs were also calculated with ESI-MS.

4.4.1.1. Experiments at pH 7.0 with H69 (modified, $\Psi m^3\Psi\Psi$)

Our first set of experiments was carried out with the H69 RNA derived from *E. coli* 23S rRNA with peptide NQVANHQ-NH_2 within a range of concentrations. For free RNA, three charge states (-3, -4, -5) were observed, with the -4 charge state being the dominant and -5 being the least dominant charge state. For the 1:1 complex of RNA and peptide, -4 and -5 charge states were detected, and the dominant charge state was

-4; whereas, for 1:2 complexes, only the -4 charge state was observed at higher concentrations. The calculated average molecular weights for all the charge states for the free RNA and its complexes with the peptide are summarized in Table 4.1.

Table 4.1. The calculated average molecular weights for the free H69 and its variants and their complexes with the peptide are listed as given by the MassLynx V4.0.

	H69 and its variants			
Species	Ψm³ΨΨ	UUU	UΨΨ	ΨUΨ
$[RNA - 3H^+]^{3-}$	1213.9	1211	1211	1211
$[RNA - 4H^+]^{4-}$	1517.6	1514.1	1514.1	1514.1
$[RNA - 5H^+]^{5-}$	2023.9	2019.2	2019.2	2019.2
$[RNA + NQVANHQ- 4H^+]^{4-}$	1720.3	1716.6	1716.6	1716.6
$[RNA + NQVANHQ- 5H^+]^{5-}$	1375.9	1373.1	1373.1	1373.1
$[RNA + 2NQVANHQ- 4H^+]^{4-}$	1922.5	1919.0	1919.0	1919.0

In one approach, the fraction of RNA bound with the peptide was calculated based on the sum of the total complexes, in which ΣRP^{n-} is the total intensity of RNA-peptide complex and their salt adducts, at all stoichiometries (1:1, 1:1 + 1:2) and the data was analyzed using Equation 4.1. The apparent dissociation constant (K_d) for the H69-peptide complex based on the sum of all the charge states, was 20 ± 3 μM. In another approach, the fraction of RNA bound in 1:1 complex was estimated based on the individual charge states of -5 and -4. The apparent dissociation constant (K_d) for the 1:1 H69-peptide complex obtained from the dominant -4 charge state was 11 ± 1 μM and for the less dominant -5 charge state was 16 ± 6 μM (Figure 4.5). The calculations for the errors in apparent dissociation constants were based on the standard deviation of average of two experiments. The accuracy of the ESI-MS is challenged by the presence of low fraction of the complex and no saturation conditions of the complex (*i.e.,* disappearance of the free species of RNA in favor of the RNA-peptide complex). The saturation conditions for our present RNA-peptide complex were not reached due

to the poor ionization efficiency of the RNA-peptide complex in which hydrophobic interactions likely dominated. Thus, only relative values of dissociation constants were obtained instead of the absolute values since the saturation was considered to be achieved when the fraction bound was found to become stationary. Applying this relative change and low signal-to-noise ratio (due to low fraction bound), the peaks were integrated for calculation of a dissociation constant at a known stoichiometry. The fraction bound was found to be low even at more than saturating concentrations, showing that the hydrophobic interactions are the major driving forces behind the complex formation.

The comparison of the values of the apparent dissociation constants (K_d) for the 1:1 complex at the -4 and -5 charge states shows that the -4 charge state is predominant among the two charge states for the 1:1 complex. Since the -5 charge states is not the major charge state for the 1:1 complex and the peaks are quite small, the error bars for the fraction of RNA bound plot of this charge states are high as compared to the 1:1 complex at -4 charge state. For the 1:2 complex of H69 and peptide at the -4 charge state, the apparent dissociation constant of 28 ± 6 μM shows that the formation of this complex is not as favorable in comparison to the 1:1 complex at the same charge state of -4 (Figure 4.6). The value of the collective calculation of the apparent dissociation constant of 20 ± 3 μM for the H69-NQVANHQ complex where all the charge states are summed for 1:1 and 1:2 complexes, represents the average of the apparent dissociation constant of 1:1 and 1:2 complexes (Figure 4.6). The ESI spectra for the free RNA and the complex formation as the peptide concentration increases from 0 to 120 μM are shown in Figure 4.7.

A)∗ B)

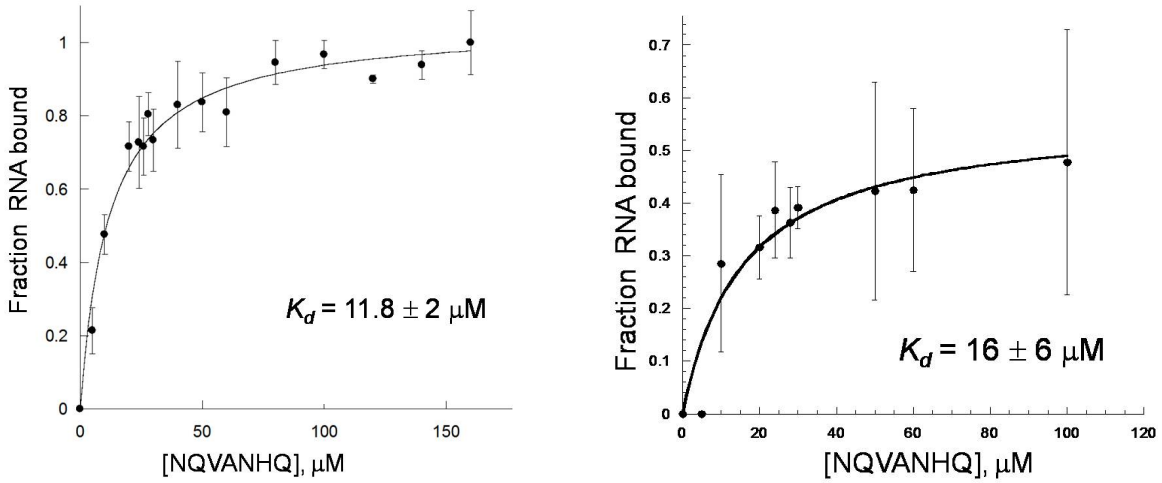

Figure 4.5. (A) The plot of fraction of H69 bound in 1:1 complex with the peptide NQVANHQ at -4 charge state and the K_d obtained with equation 4.1 after normalization with equation 4.2.∗ (B) The fraction of H69 bound in 1:1 complex with the peptide at -5 charge state. The values obtained for the K_d is the average of two separate experiments.

A) B)∗

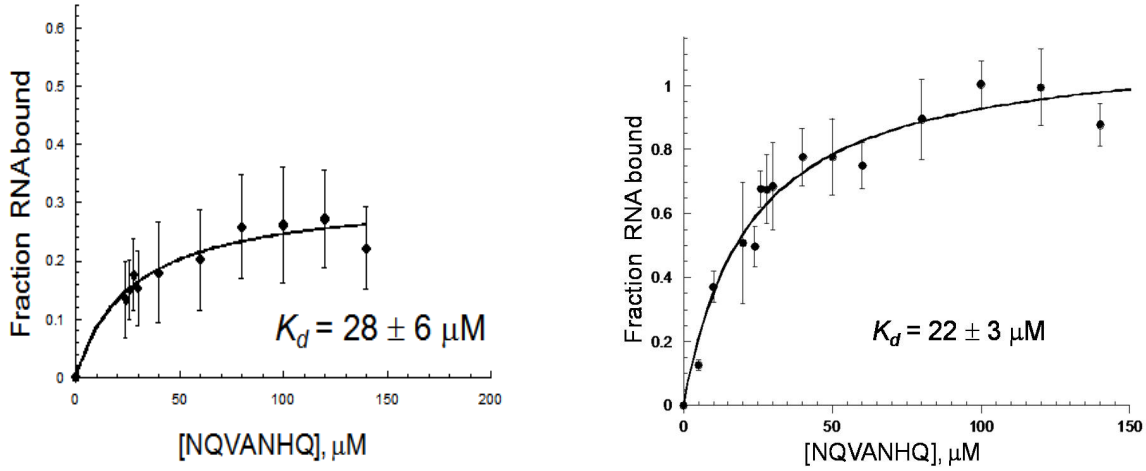

Figure 4.6. (A) This plot represents the H69 bound in 1:2 complex at -4 charge state with peptide NQVANHQ. (B) In this plot the fraction of H69 bound is the average of all charge states and the K_d shown is the average value of 1:1 and 1:2 complexes and is obtained after normalization with equation 4.2.∗ The values obtained for the K_d is the average of two separate experiments.

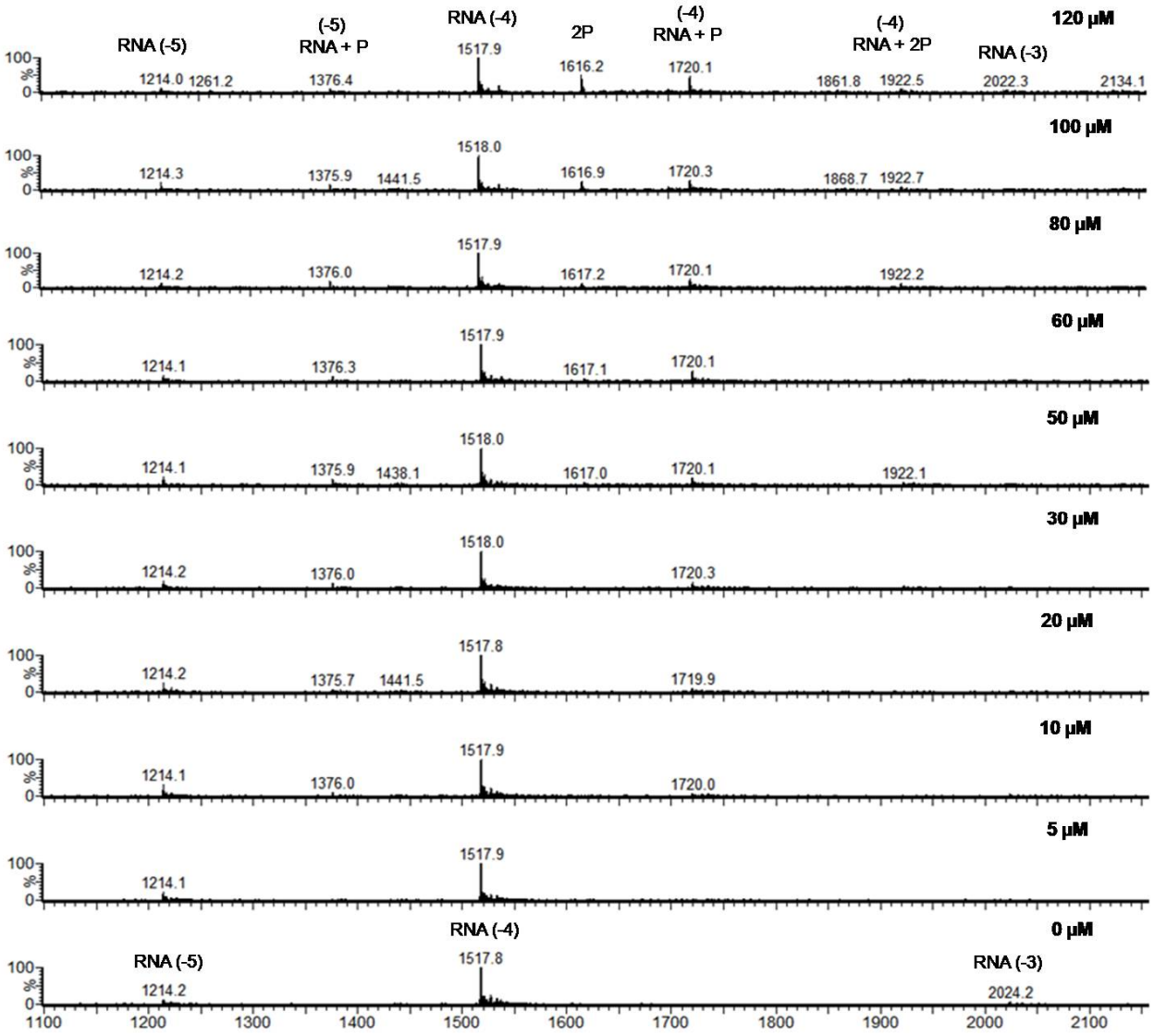

Figure 4.7. The spectra obtained from ESI-MS experiment at pH 7.0 showing the free RNA at -3, -4, -5 charge states; H69-NQVANHQ-NH_2 1:1 complex (RNA + P) at -5 and -4 charge states; H69-NQVANHQ-NH_2 1:2 complex (RNA + 2P) at -4 charge state and peptide dimer (2P).

4.4.1.2. Experiments at pH 5.2 with H69 (modified, $\Psi m^3\Psi\Psi$)

Based on the observed pH-dependent conformational changes for the H69 RNA (modified, $\Psi m^3\Psi\Psi$) (Abeysirigunawardena, S. & Chow, C.S., 2008), the binding studies for H69-NQVANHQ-NH_2 peptide were carried out at different pH values. At a pH value of 7.0, the apparent dissociation constant obtained for the 1:1 H69-NQVANHQ peptide complex at -4 charge state was 11 ± 1 μM, but when the ESI-MS experiments were carried out pH 5.2, the apparent dissociation constant for 1:1 complex increased to 34 ± 3 μM for the same charge state calculation (Figure 4.8.). The apparent dissociation constant changed to 31 ± 12 μM for the 1:1 complex at -5 charge state (Figure 4.8.). Since this charge state was less dominant for the H69-peptide complex, the error value for the apparent dissociation constant and the error bars were high. The three-fold increase in value of K_d for 1:1 complex at lower pH suggests weakening of the binding affinity of this peptide for H69. The structural change of H69 at lower pH value might be contributing to the decreased affinity of the peptide NQVANHQ-NH_2, although a pH-dependent change of the peptide cannot be ruled out. The observed pH-dependent changes occurred in the loop region of H69 where the residues were in a higher stacked conformation (Abeysirigunawardena, S. & Chow, C.S., 2008). Therefore, it is possible that one important binding site for this peptide is in the loop region that is lost due to change in pH value. An alternate explanation is that certain peptide functional groups are protonated at lower pH, which may also inhibit interactions with H69.

The comparison of free energy values (ΔG°) for H69 at two pH values (Table 4.2.) indicates that peptide seems to have slight preference for the thermodynamically less stable H69 conformer at pH 7.0 and reduced affinity for thermodynamically more

stable H69 structure at pH 5.2. The low and high pH-states for H69 were observed in 50S subunits and 70S ribosome crystal structures, respectively (Bashan, A. *et al*., 2003; Selmer, M. *et al*., 2006). The ESI spectra for the free RNA and the complex formation as the peptide concentration increases from 0 to 140 μM are shown in Figure 4.9.

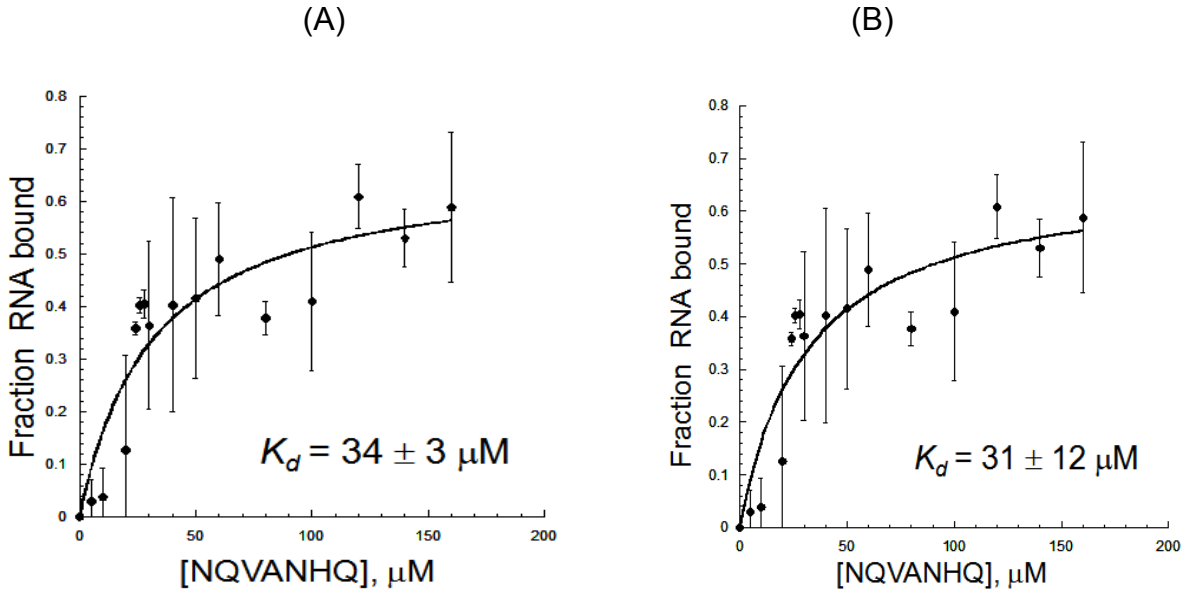

Figure 4.8. (A) This plot represents the curve fitting for calculation of apparent dissociation constant for 1:1 complex at -4 charge state for H69-NQVANHQ peptide complex at pH 5.2. (B) The calculation of apparent dissociation constant for 1:1 H69-NQVANHQ peptide complex at -5 charge state and at pH 5.2. The values obtained for the K_d is the average of two separate experiments.

Table 4.2. The apparent dissociation constants for the 1:1 H69-NQVANHQ-NH_2 complexes at the -4 charge state and at pH 7.0 and 5.2 and the free energy values for the H69 are summarized in tabular form.

RNA	K_d at pH 7.0 (1:1, RNA+NQVANHQ-NH_2)	ΔG^o at pH 7.0 (kcal/mol)[a]	K_d at pH 5.2 (1:1, RNA+NQVANHQ-NH_2)	ΔG^o at pH 5.2 (kcal/mol)[a]
E. coli H69 (mod. Ψm^{3}ΨΨ)	11 ± 1 μM	- 4.8	34 ± 3 μM	- 5.3

a = data from Abeysirigunawardena, S. & Chow, C.S., 2008.

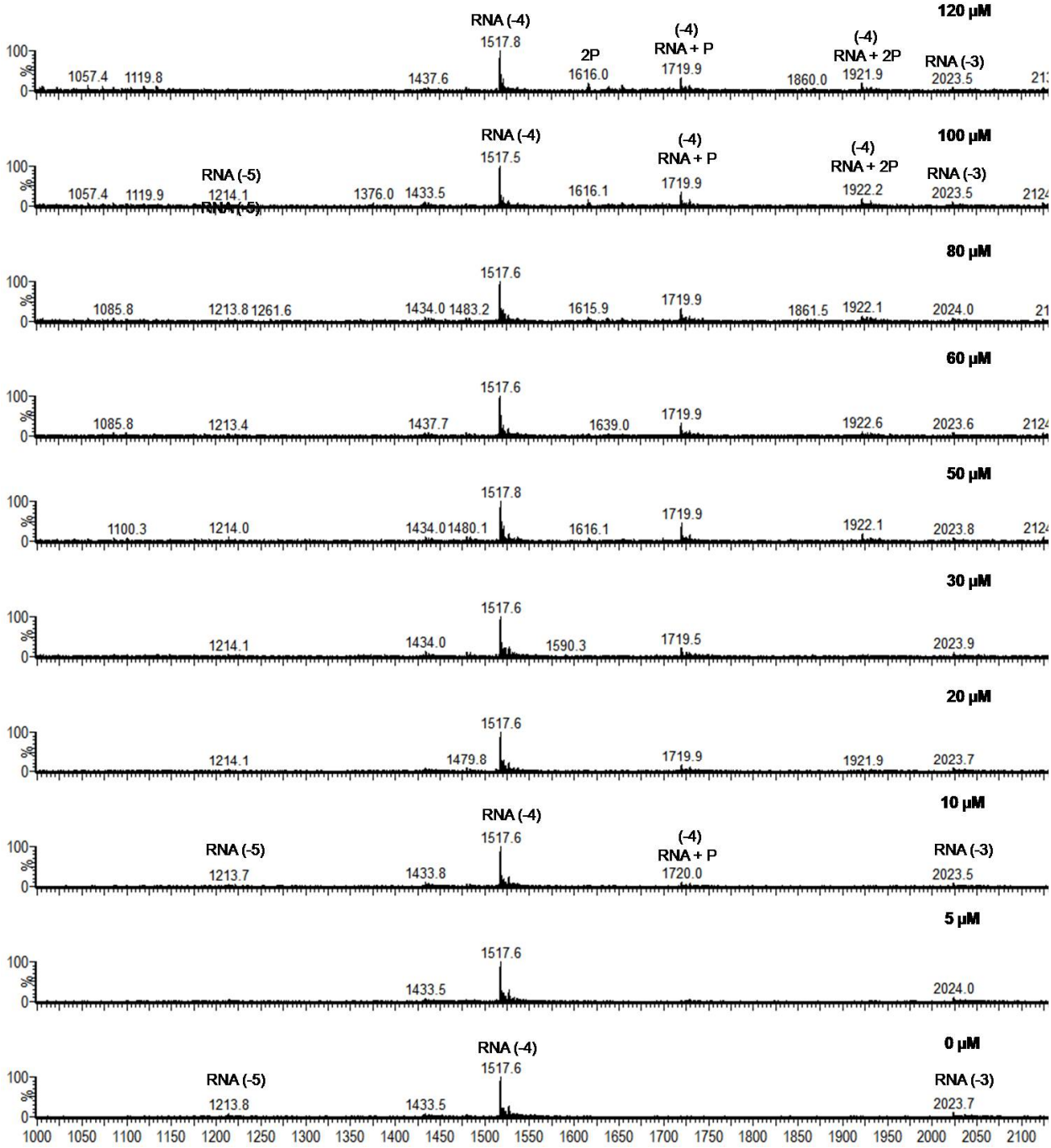

Figure 4.9. The ESI spectra at pH 5.2 showing the free H69 RNA at -3, -4, and -5 charge states and H69-NQVANHQ-NH_2 1:1 complex (RNA + P) at -5 and -4 charge states; H69-NQVANHQ-NH_2 1:2 complex (RNA + 2P) at -4 charge state and peptide dimer (2P).

4.4.1.3. Experiments at pH 7.0 with H69 (unmodified, UUU)

The fully modified *E. coli* H69 (mod. $\Psi m^3\Psi\Psi$) construct used above for phage selection and binding studies with peptide NQVANHQ-NH_2 has three pseudouridines (Ψ) at positions 1911, 1915 and 1917. The corresponding nucleotides in the 23S rRNA are post-transcriptionally modified from uridines to pseudouridines in bacteria (Raychaudhuri, S. *et al*., 1998). To study the effects of these pseudouridine residues on the binding of the peptide NQVANHQ-NH_2, a 19-nucleotide RNA construct having uridine (U) residues in place of the Ψ residues was synthesized. The construct is referred to unmodified UUU H69. The binding of the peptide NQVANHQ-NH_2 with UUU H69 was studied similarly through ESI-MS at pH 7.0 and 5.2. The experimental setup for performing the solution-based titrations for binding studies was the same as described for the modified H69. The titration was carried out with a range of concentrations for the peptide (0-120 μM). The apparent dissociation constant for the 1:1 complex for UUU-NQVANHQ-NH_2 was calculated based on the quadratic equation (Equation 4.1). The value of the dissociation constant obtained at the dominant -4 charge state for 1:1 complex of UUU-NQVANHQ-NH_2 at pH 7.0 was 19 ± 2 μM and at the less dominant -5 charge state for the same complex was 12 ± 3 μM (Figure 4.10).

As seen in the plots for the two charge states, the value of apparent dissociation constant at the -5 charge state is lower because the number of titration points available for plotting is fewer due to the low intensities in the MS spectra. The error bars plotted for the -5 charge state are also high compared to those of the -4 charge state. This result shows that the apparent dissociation constant for -5 charge state is less reliable

compared to that from the -4 charge state. The slightly higher value of the dissociation constant for the 1:1 UUU-NQVANHQ-NH_2 complex at pH 7.0 than the H69-NQVANHQ-NH_2 complex shows that the Ψ residues influence the K_d, (11 μM Vs. 19 μM for $\Psi m^3\Psi\Psi$ and UUU, respectively, at pH 7.0). This result is supported by the work of Meroueh and coworkers (Meroueh, M. *et al.*, 2000) in which the overall stabilities of UUU and $\Psi m^3\Psi\Psi$ H69 RNAs were identical at pH 7.0, but the overall structures differed, particularly in the loop region. The ESI spectra for the free RNA and the complex formation as the peptide concentration increases from 0 to 120 μM are shown in Figure 4.11.

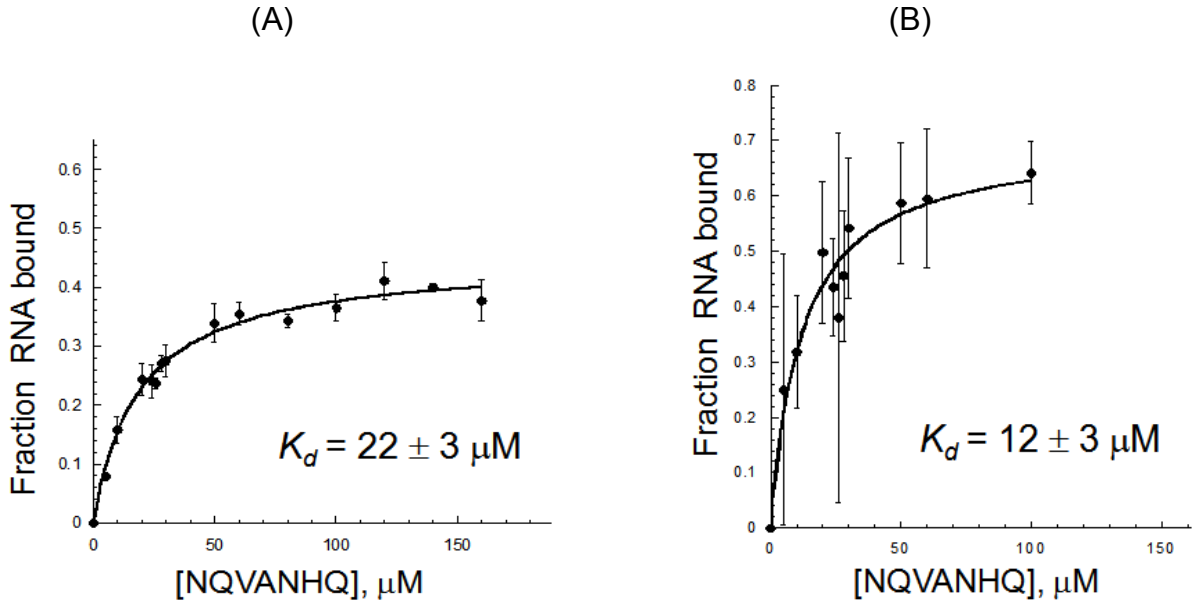

Figure 4.10. (A) This plot represents the curve fitting for calculation of apparent dissociation constant for 1:1 complex at -4 charge state for UUU-NQVANHQ peptide complex at pH 7.0. (B) The calculation of apparent dissociation constant for 1:1 UUU-NQVANHQ-NH_2 peptide complex at -5 charge state, pH 7.0. The values obtained for the K_d is the average of three separate experiments.

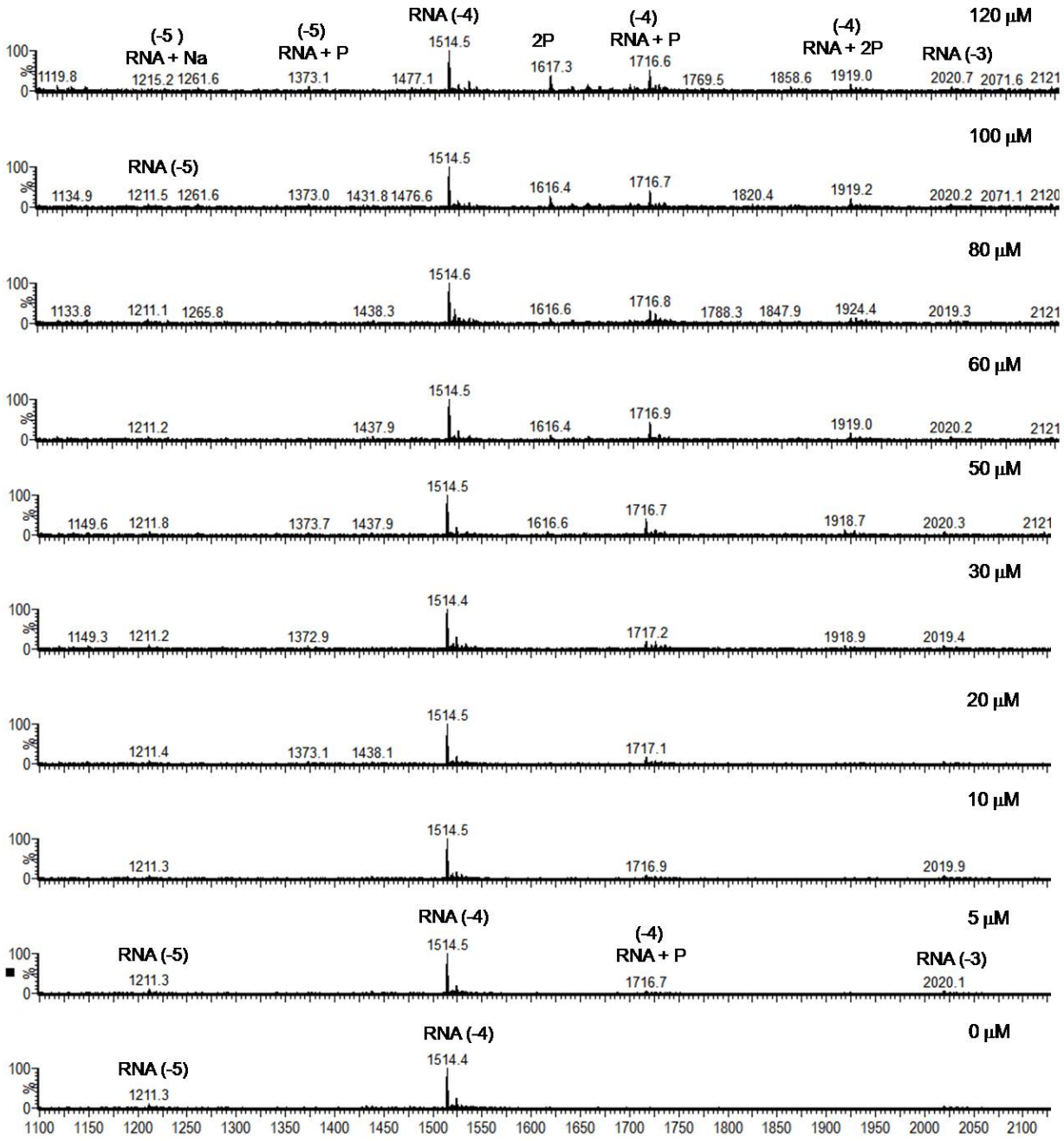

Figure 4.11. The ESI spectra at pH 7.0 showing the free UUU RNA at -3, -4, and -5 charge states and UUU-NQVANHQ-NH_2 1:1 complex (RNA + P) at -5 and -4 charge states; UUU-NQVANHQ-NH_2 1:2 complex (RNA + 2P) at -4 charge state and peptide dimer (2P).

4.4.1.4. Experiments at pH 5.2 with H69 (unmodified, UUU)

The binding experiments conducted with the modified H69 construct ($\Psi m^3\Psi\Psi$) and peptide NQVANHQ-NH_2 at pH 7.0 and pH 5.2 resulted in different values of the apparent dissociation constants for the complex. A similar approach was followed for the UUU-NQVANHQ-NH_2 complex for studying the effect of the pH on the binding of the peptide. The binding experiments of the UUU with peptide NQVANHQ-NH_2 at pH 7.0 gave the value of 19 ± 2 μM for the apparent dissociation constant (K_d) for 1:1 complex. The K_d value was lower for the modified H69 ($\Psi m^3\Psi\Psi$) and peptide complex, thus indicating the stronger binding of the peptide for the Ψ-containing RNA. ESI-MS experiments were carried out at pH 5.2 for UUU-NQVANHQ-NH_2 complex. The calculations for the 1:1 complex at -4 charge state gave a K_d value of 31 ± 3 μM and the plot is shown in Figure 4.12. Calculations for the -5 charge state were not possible.

This higher value of the apparent dissociation constant (K_d) at pH 5.2 indicates that the binding affinity of the peptide has decreased for the UUU RNA. This affect could be attributed to the fact that the peptide is undergoing some protonation event resulting in some unfavorable conformational change. The UUU RNA was shown to be unaffected by the change in pH. Although the difference of the free energy values of the UUU RNA at two pH values of 7.0 and 5.2 was almost negligible, the binding affinity of the peptide for the RNA was reduced (Table 4.3). This suggests that a change in the peptide conformation at the lower pH value might play a role in the reduction of the binding affinity for H69 RNA. The ESI spectra for the free RNA and the complex formation as the peptide concentration increases from 0 to 120 μM are shown in Figure 4.13.

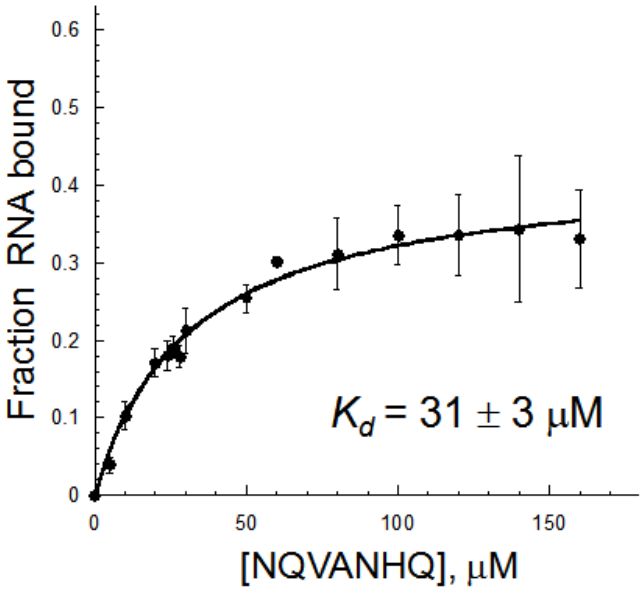

Figure 4.12. The value of the apparent dissociation constant for the 1:1 UUU-NQVANHQ-NH_2 complex is calculated at -4 charge state at pH 5.2. The values obtained for the K_d is the average of three separate experiments.

Table 4.3. The apparent dissociation constants for the 1:1 complex of the UUU-NQVANHQ-NH_2 complex at the -4 charge state at two pH values are summarized in the table.

RNA	K_d at pH 7.0 (1:1, RNA+NQVANHQ-NH_2)	$\Delta G°$ at pH 7.0 (kcal/mol)[a]	K_d at pH 5.2 (1:1, RNA+NQVANHQ-NH_2)	$\Delta G°$ at pH 5.2 (kcal/mol)[a]
E. coli H69 (unmod. UUU)	19 ± 2 μM	- 4.9	31 ± 3 μM	- 4.7

a : The free energy values of the UUU RNA at pH 7.0 and 5.2 are also presented (Abeysirigunawardena, S. & Chow, C.S., 2008).

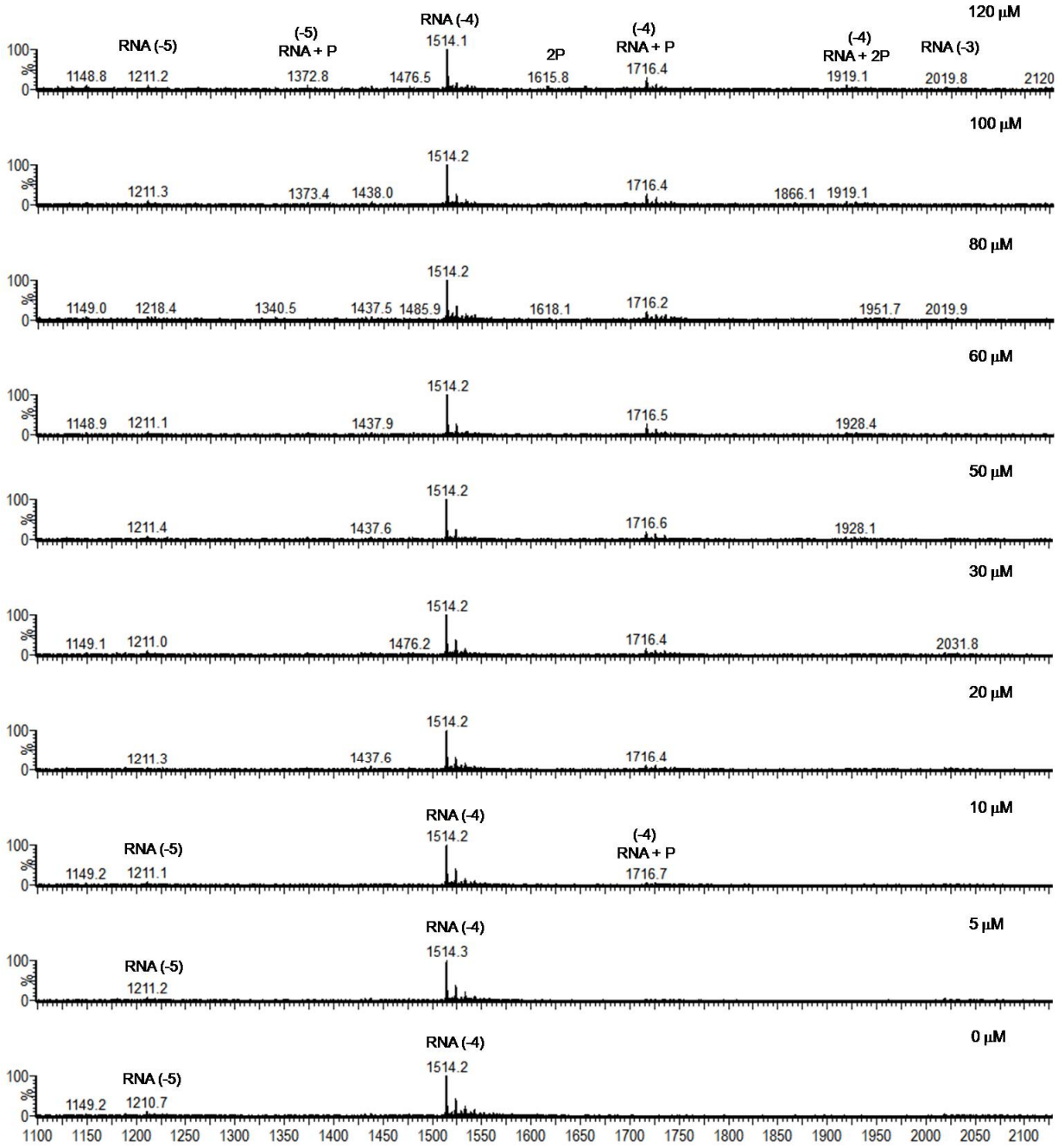

Figure 4.13. The ESI spectra at pH 5.2 showing the free UUU RNA at -3, -4, and -5 charge states and UUU-NQVANHQ-NH_2 1:1 complex (RNA + P) at -5 and -4 charge states; UUU-NQVANHQ-NH_2 1:2 complex (RNA + 2P) at -4 charge state and peptide dimer (2P).

4.5.2. The role of the pseudouridine residues in binding of H69 to NQVANHQ-NH_2

For studying the effect of the pseudouridine modifications on the binding behavior of the peptide NQVANHQ-NH_2 with H69 (modified, $\Psi m^3\Psi\Psi$), constructs with individual pseudouridine (Ψ) residues replaced with uridine ($U\Psi\Psi$, $\Psi U\Psi$) were synthesized. The ESI-MS experiments were performed by keeping the RNA concentration constant and varying the peptide concentration from 0 to 120 μM. The procedure for the experiments has been described in the ESI-MS data collection section.

4.5.2.1. ESI-MS with $U\Psi\Psi$

The apparent dissociation constant for the 1:1 $U\Psi\Psi$-NQVANHQ-NH_2 complex at -4 charge state and at pH 7.0 was calculated to be 28 ± 5 μM, as shown by the plot in Figure 4.14. The 2.5-fold higher value of the apparent dissociation constant for 1:1 complex of this RNA construct compared to the fully modified H69 ($\Psi m^3\Psi\Psi$) RNA indicates a role for Ψ1911 in the binding of peptide. This reduced affinity of the peptide towards $U\Psi\Psi$ is supported by the results of Meroueh and coworkers in which the effects of single Ψ residues on the structure and stability of the H69 were studied (Meroueh, M. *et al*., 2000). It was shown that the presence of the individual Ψ residues had unique local effects on the structure of the H69, and in different combinations, the Ψ residues had varying structural and stabilizing effects. The pseudouridine at 1911 position that forms the loop-closing base pair has a stabilizing effect on the structure of H69.

The K_d values for the H69, UUU and $U\Psi\Psi$ in complex with the peptide and the free energy (ΔG°) values for the individual RNA constructs are summarized in Table 4.4.

The free energy values are obtained from the literature (Abeysirigunawardena, S. & Chow, C.S., 2008). Comparison of the free energy values at pH 7.0 shows that the UΨΨ mutant is thermodynamically less stable than both fully modified H69 and unmodified UUU RNAs. The peptide has a reduced preference for binding to mutant, possibly due to an altered loop structure. The ESI spectra for the free RNA and the complex formation as the peptide concentration increases from 0 to 120 μM are shown in Figure 4.15.

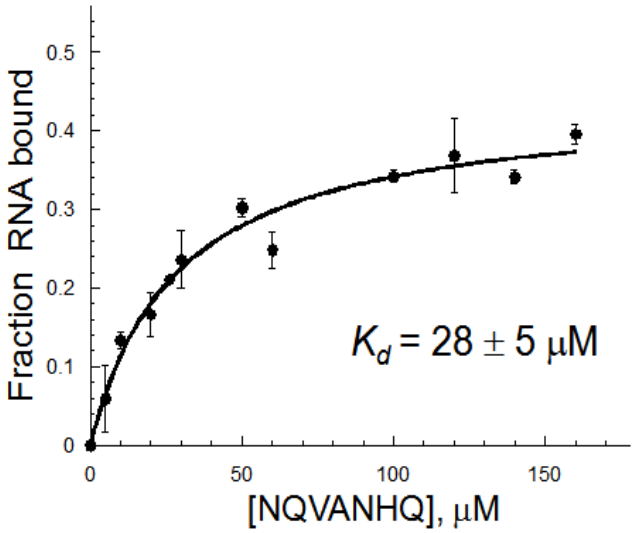

Figure 4.14. The fraction of UΨΨ RNA bound with the peptide NQVANHQ-NH_2 in 1:1 complex is shown and the K_d for the 1:1 complex is calculated from the dominant -4 charge state of the ESI-MS spectra. The values obtained for the K_d is the average of two separate experiments.

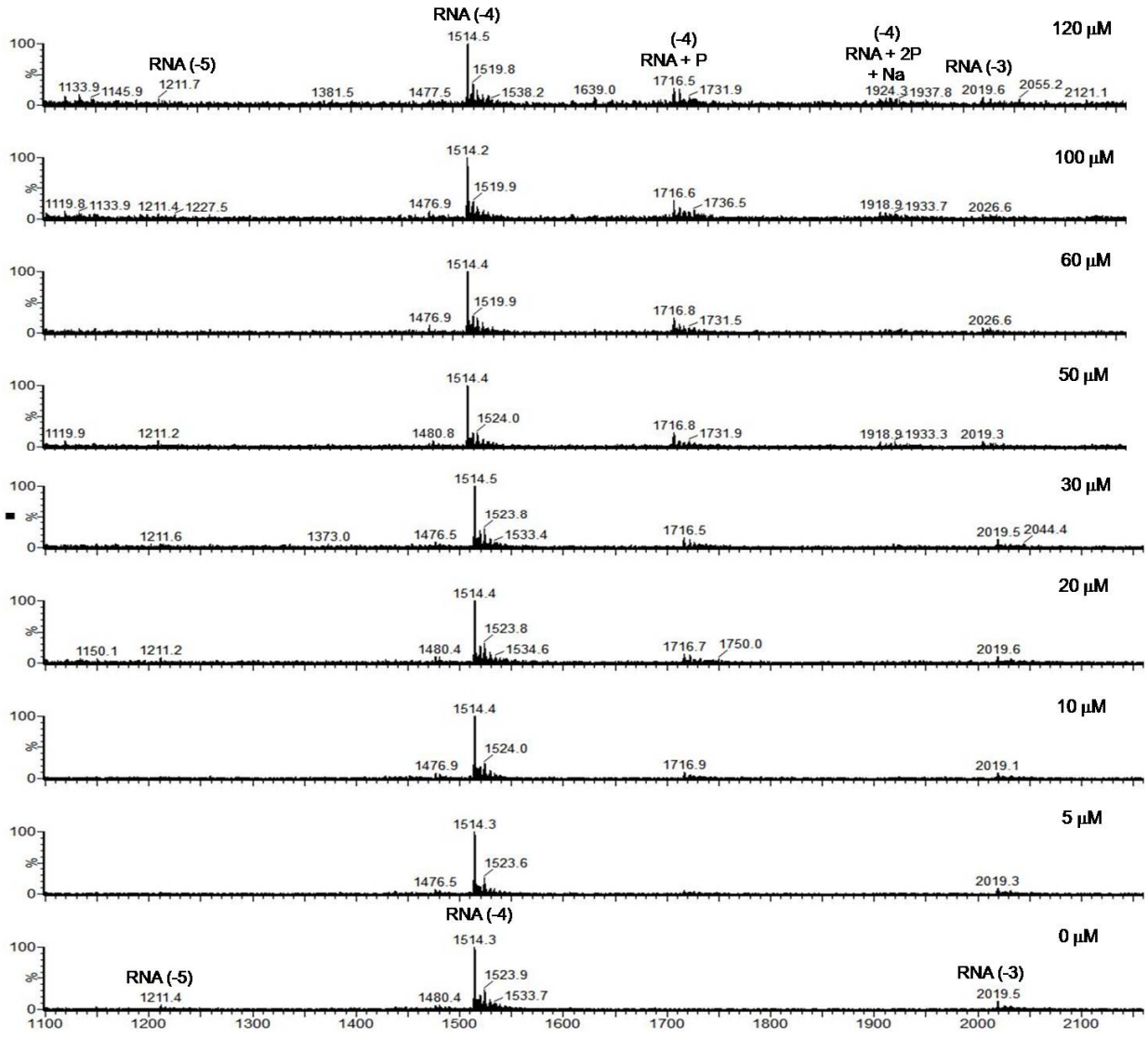

Figure 4.15. The ESI spectra at pH 5.2 showing the free UΨΨ RNA at -3, -4, and -5 charge states and UΨΨ-NQVANHQ-NH_2 1:1 complex (RNA + P) at -5 and -4 charge states; UΨΨ-NQVANHQ-NH_2 1:2 complex (RNA + 2P) at -4 charge state and peptide dimer (2P).

4.5.2.2. ESI-MS with ΨUΨ

The ESI-MS binding experiments for the ΨUΨ RNA with peptide NQVANHQ-NH_2 at pH 7.0 were completed using same approach as described above. After data collection, the ΨUΨ-NQVANHQ-NH_2 complex was analyzed for the -4 charge state and

the K_d was estimated to be 28 ± 4 μM as shown by the plot in Figure 4.16. This value is comparable to the UΨΨ RNA and 2.5-fold higher than the fully modified H69 RNA. This result shows that the peptide affinity for the RNA has been reduced as compared to the Ψm^{3}ΨΨ. In contrast to the UΨΨ RNA, the ΨUΨ RNA construct is thermodynamically more stable in comparison to the H69, UUU (Table 4.4). Even though the RNA acquires a stable thermodynamic conformation in the absence of Ψ1915, this conformation is less favorable for the binding of the peptide NQVANHQ-NH_2. The ESI spectra for the free RNA and the complex formation as the peptide concentration increases from 0 to 120 μM are shown in Figure 4.17.

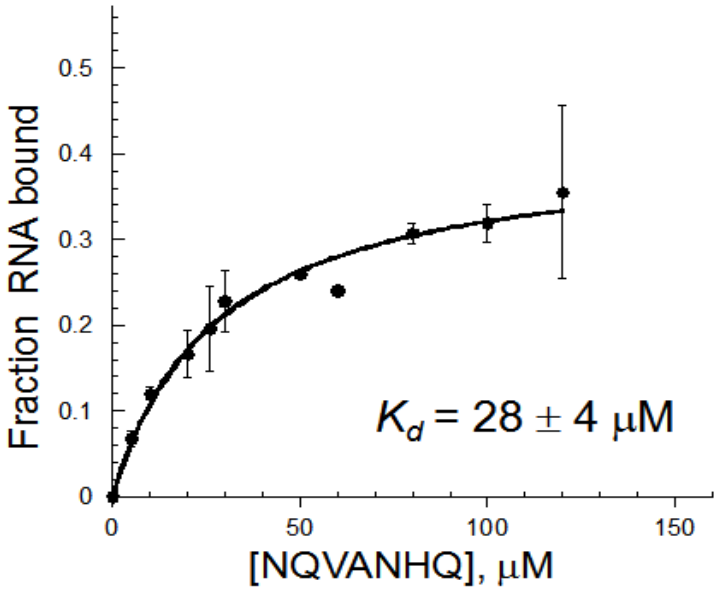

Figure 4.16. This plot represents the fraction of ΨUΨ RNA in complex with the peptide in 1:1 complex at pH 7.0. The K_d was calculated from -4 charge state of the ESI-MS experiments. The values obtained for the K_d is the average of two separate experiments.

Table 4.4. Comparison of the apparent dissociation constants (K_d) obtained for 1:1 complexes for H69, UUU and H69 mutants with peptide NQVANHQ-NH_2.

RNA	K_d at pH 7.0 (RNA + NQVANHQ-NH_2), 1:1	ΔG^o (kcal/mol)
E. coli H69 (mod. $\Psi m^3\Psi\Psi$)	11 ± 1 μM	- 4.8
E. coli H69 (unmod. UUU)	19 ± 2 μM	- 4.9
E. coli H69 mutants		
i) U$\Psi\Psi$	28 ± 5 μM	- 4.4
ii) ΨUΨ	28 ± 4 μM	- 5.3

4.5.3. Selectivity of NQVANHQ-NH_2 for H69

The preferential binding of peptide NQVANHQ-NH_2 with fully modified H69 ($\Psi m^3\Psi\Psi$) as compared to other RNAs was addressed by testing its binding for other RNAs such as helix 31, human H69 (referred to as Ψ5) and the A-site RNA (Figure 4.18). To compare the binding affinities of these RNAs for NQVANHQ-NH_2, ESI-MS experiments were carried as described above for H69. Helix 31, or h31, of *E. coli* 16S rRNA is located near the P site (where peptide bond formation takes place) and is considered to be closely involved in the translation process (Döring, T. *et al*., 1994; Selmer, M. *et al*., 2006; Korostelev, A. *et al*. 2006). The apparent dissociation constant (K_d) obtained at pH 7.0 for this RNA in a 1:1 complex with peptide NQVANHQ-NH_2 was 33 ± 10 μM (three-fold higher than H69) (Figure 4.19). This result shows that the peptide selected for H69 has lower affinity for an unrelated RNA at physiological pH.

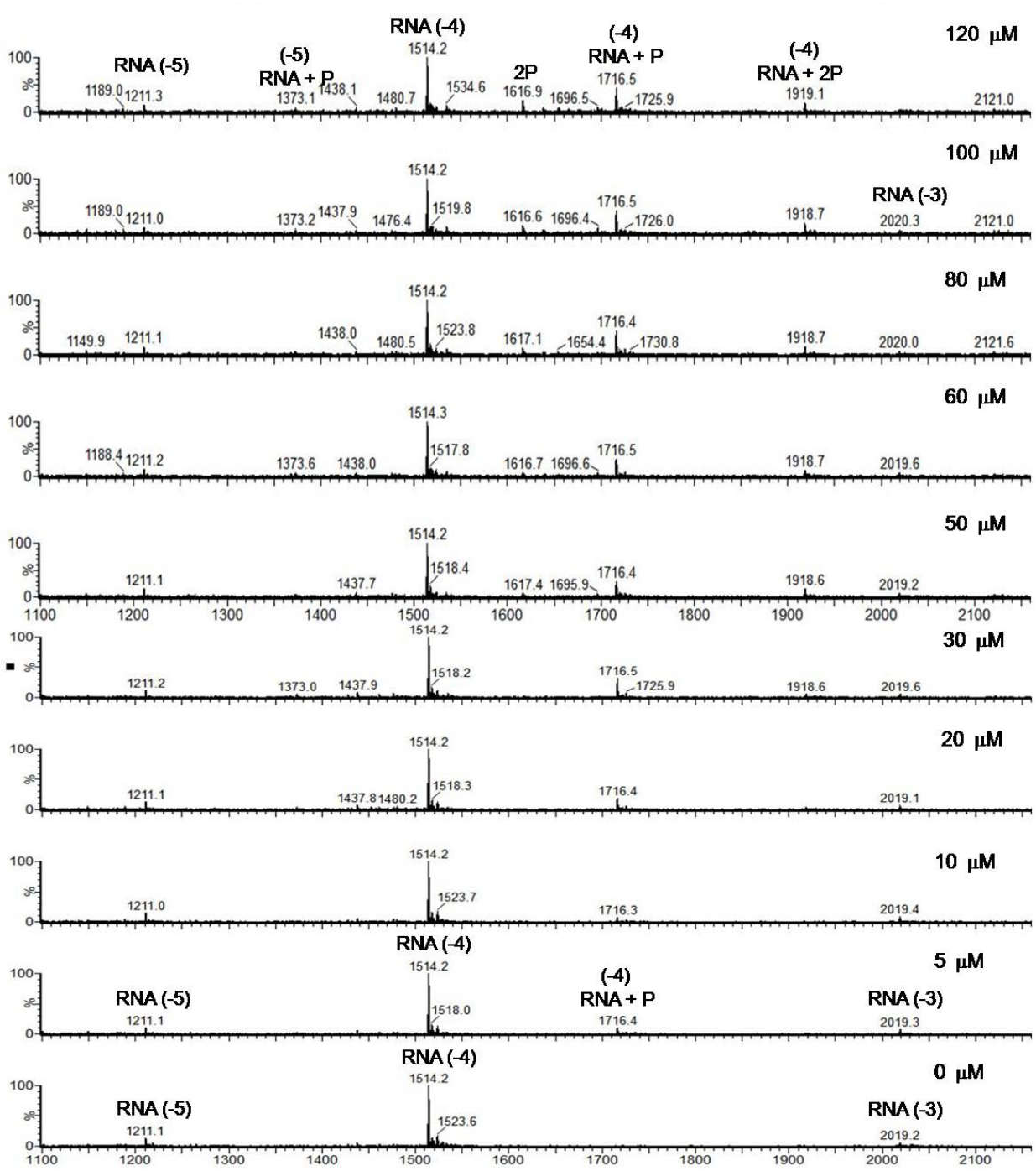

Figure 4.17. The ESI spectra at pH 5.2 showing the free ΨUΨ RNA at -3, -4, and -5 charge states and ΨUΨ-NQVANHQ-NH_2 1:1 complex (RNA + P) at -5 and -4 charge states; ΨUΨ-NQVANHQ-NH_2 1:2 complex (RNA + 2P) at -4 charge state and peptide dimer (2P).

The A-site RNA is part of the bacterial decoding region and is located in h44 of 16S ribosomal RNA of the small subunit. The A site is the location of codon-anticodon interactions in the ribosome and plays a very crucial role in the translation process. The K_d value for binding of this RNA in 1:1 complex with peptide NQVANHQ-NH_2 is 35 $\pm$ 5 μM, which is also three-fold higher than the fully modified H69 ($\Psi m^3\Psi\Psi$), again showing that the peptide prefers to bind to the RNA for which it was selected against.

The human sequence of the H69 (referred to as Ψ5) has five pseudouridine residues compared to three in the *E. coli* H69. The K_d value (50 $\pm$ 8 μM) obtained for this RNA is almost five-fold higher than the *E. coli* H69. This result shows that the peptide will have a higher preference for bacterial H69 over the human H69. This feature of the peptide is important if it is to be considered as a potential lead for new antibacterials. The apparent dissociation constants (K_d) obtained at pH 7.0 for these RNAs in 1:1 complexes with the peptide NQVANHQ-NH_2 are summarized in Table 4.5.

Table 4.5. Summary of binding constants (K_ds) of both related and unrelated RNAs with NQVANHQ-NH_2.

RNA	K_d at pH 7.0
E. coli H69 (mod.$\Psi m^3\Psi\Psi$)	11 $\pm$ 1 μM
Human H69 (Ψ5)	50 $\pm$ 8 μM
h31	33 $\pm$ 10 μM
A-site	49 $\pm$ 10 μM

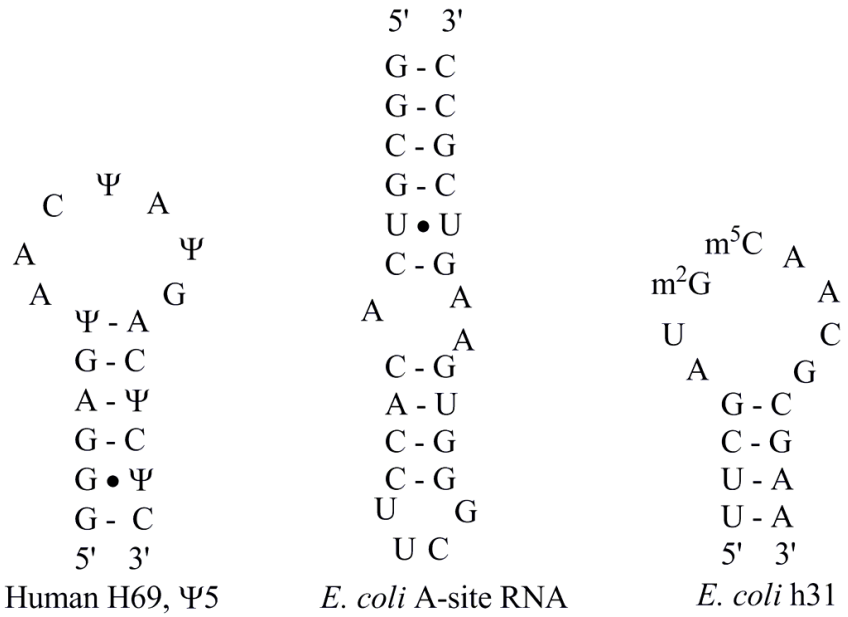

Figure 4.18. The secondary structures of human H69, *E. coli* A-site RNA, and *E. coli* h31 as used in the experiments are shown.

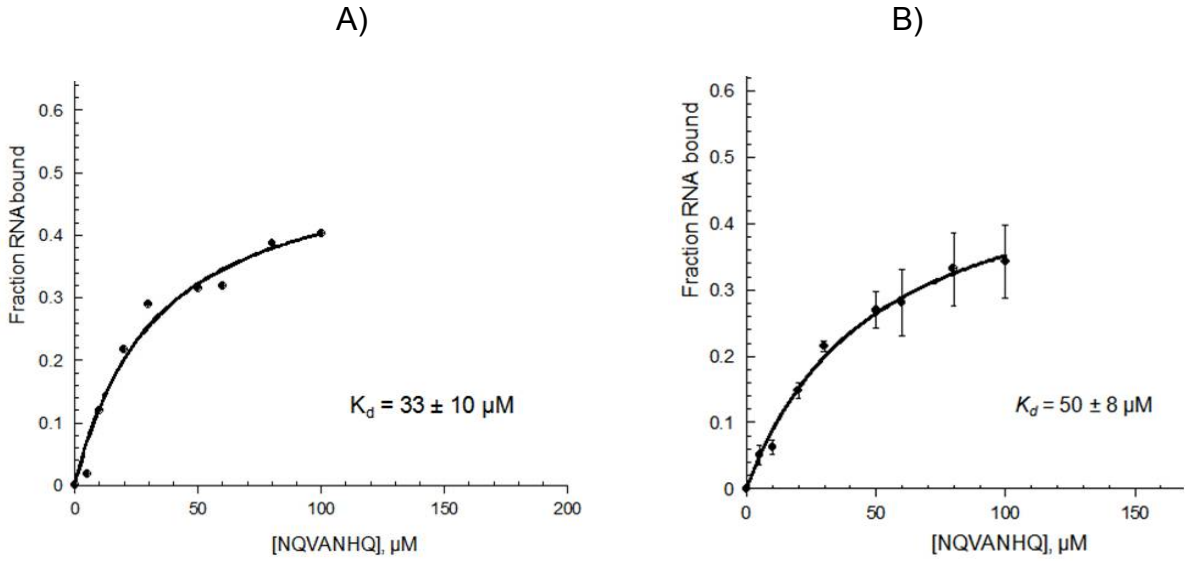

C)

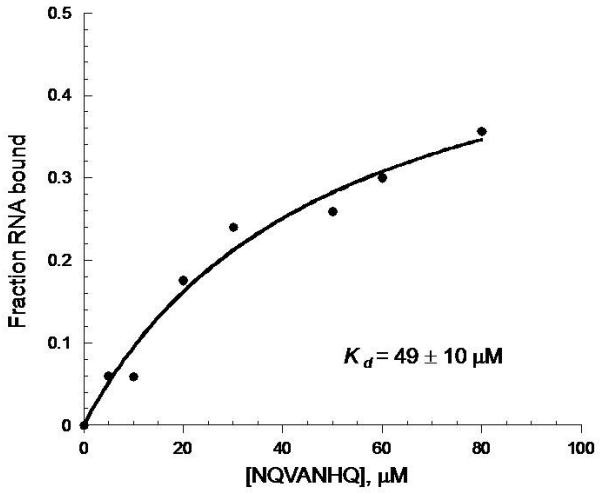

Figure 4.19. The plot of fractions of RNAs A) h31RNA, B) human H69 RNA, and C) A site bound to peptide NQVANHQ-NH_2 are depicted. For h31 and human H69, the K_ds were calculated at -4 charge state and for A-site RNA the K_d was calculated at -5 charge state.

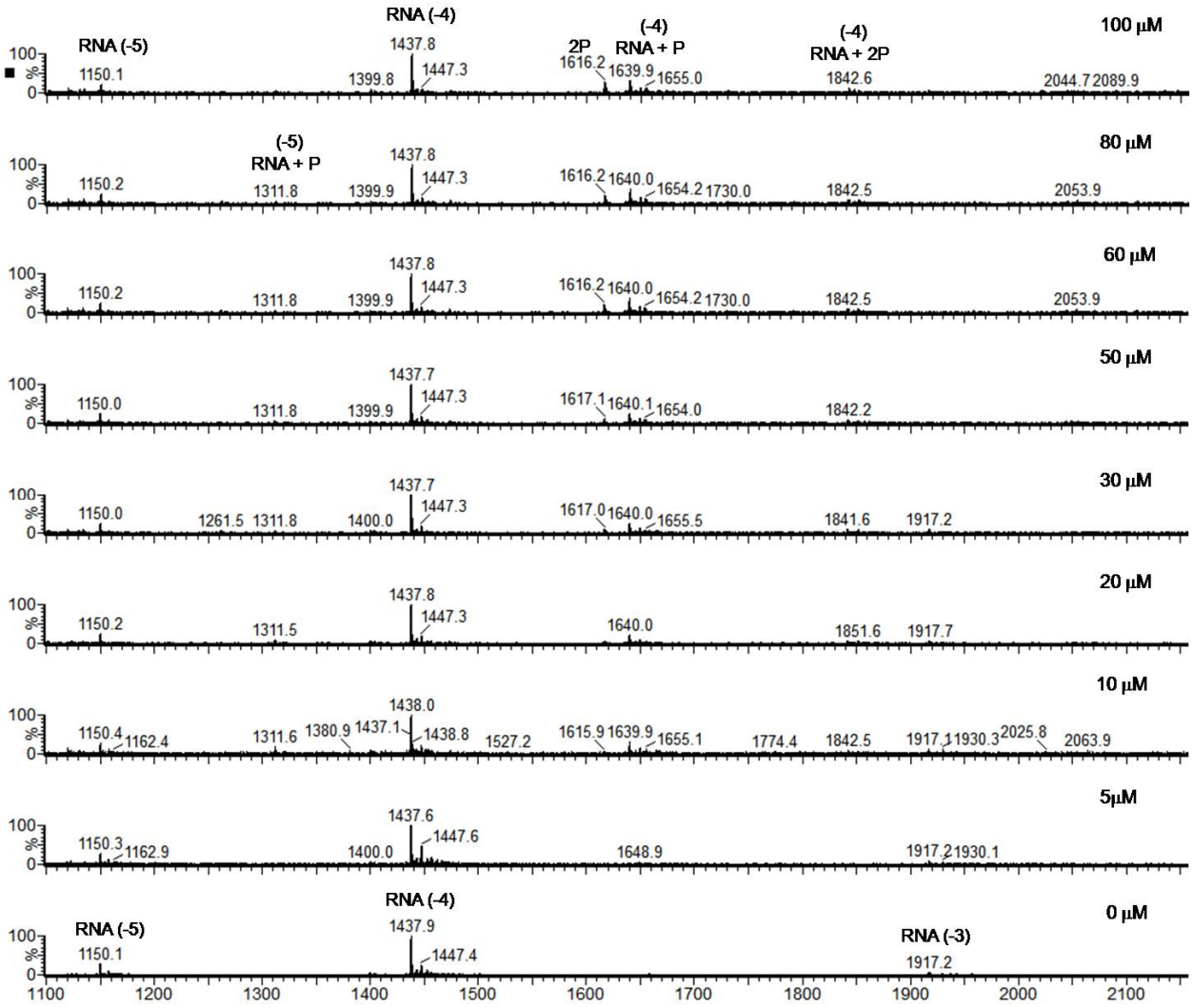

Figure 4.20. The ESI spectra at pH 7.0 showing the free h31 RNA at -3, -4 and -5 charge states and h31-NQVANHQ-NH_2 1:1 complex (RNA + P) at -5 and -4 charge states; h31-NQVANHQ-NH_2 1:2 complex (RNA + 2P) at -4 charge state and peptide dimer (2P).

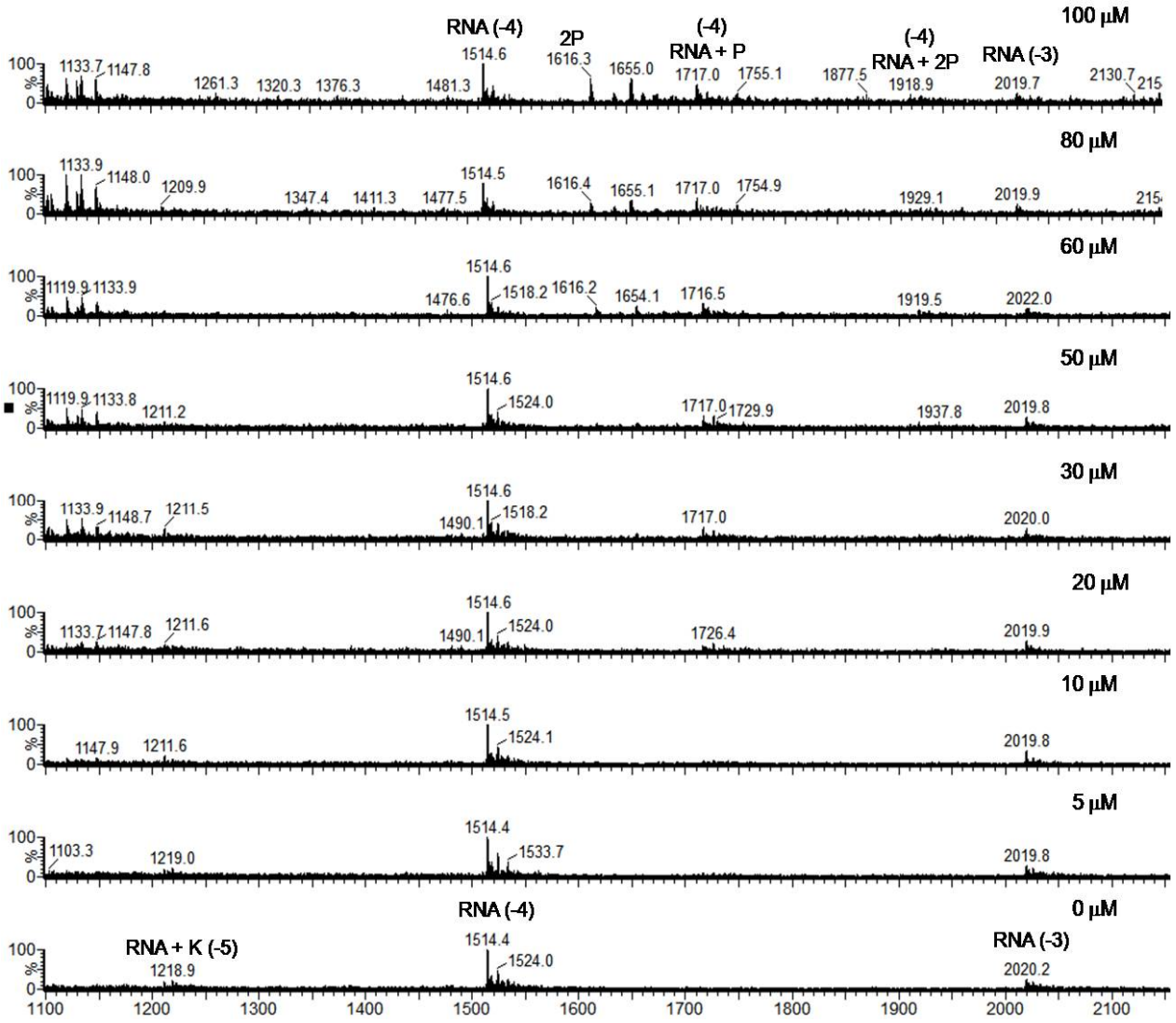

Figure 4.21. The ESI spectra at pH 7.0 showing the human H69 RNA at -3, -4, and -5 charge states and human H69-NQVANHQ-NH_2 1:1 complex (RNA + P) at -4 charge states; human H69-NQVANHQ-NH_2 1:2 complex (RNA + 2P) at -4 charge state and peptide dimer (2P).

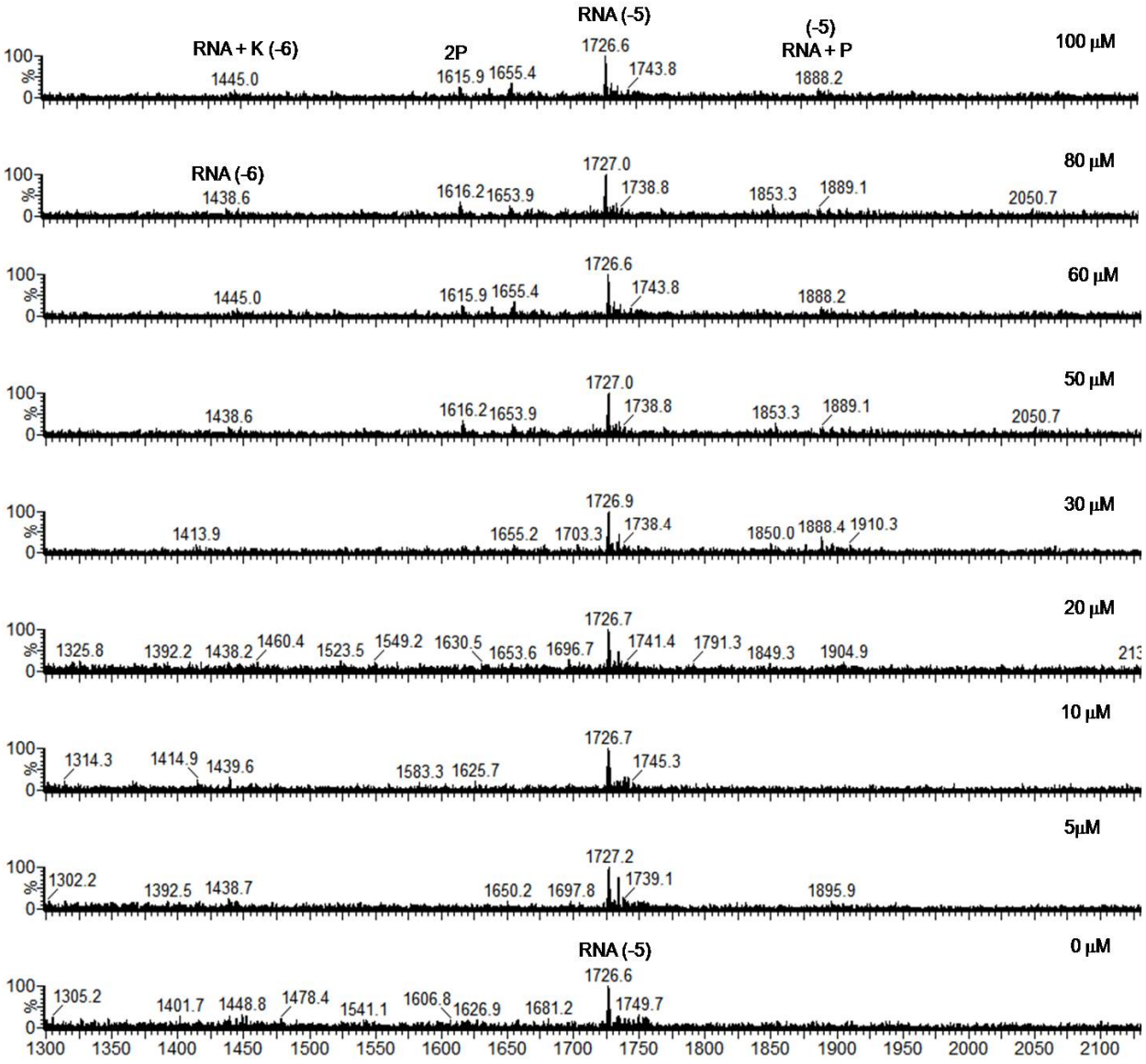

Figure 4.22. The ESI spectra at pH 7.0 showing the A-site RNA at -5 and -6 charge states and A site-NQVANHQ-NH_2 1:1 complex (RNA + P) at -5 charge states, and peptide dimer (2P).

4.6. Conclusions

In this chapter, binding studies of the heptapeptide NQVANHQ-NH_2 were conducted with modified H69 ($\Psi m^3\Psi\Psi$), unmodified H69 (UUU), as well as several mutants, U$\Psi\Psi$ and ΨUΨ RNAs. The technique applied for this study was electrospray ionization mass spectroscopy (ESI-MS). This method has been shown in the literature to provide reliable apparent binding constants (K_d*s*) for noncovalent complexes involving nucleic acids such as the Tat peptide-TAR RNA complex (Sannes-Lowry, K.A. *et al*., 1997) and aminoglycosides with the A-site rRNA (Sannes-Lowry, K.A. *et al*., 2000), and the antibiotic vancomycin binding to peptide ligands (Lim, H.K. *et al*., 1995).

For the ESI-MS experiments carried out in this study, the RNAs were ionized with the help of the organic solvent isopropanol and ammonium salts in the buffer systems. The apparent dissociation constants (K_d*s*) obtained for the 1:1 complexes of modified H69 ($\Psi m^3\Psi\Psi$)-peptide in this study was 11 ± 1 μM. This value represents moderately good binding affinity of the peptide for the target RNA H69 for which it was selected against. This value is comparable to that of aminoglycoside antibiotics binding to the A-site RNA (1 to 10 μM) (Wong, C.H. *et al*., 1992; Fourmy, D. *et al*., 1996; Wang, Y. *et al*., 1996; Sannes-Lowry, K.A. *et al*., 2000; Llano-Sotelo, B. et al., 2002; Kaul, M. *et al*., 2004). It should be noted that this interaction may be enhanced under more physiological buffer conditions, since the ESI-MS method is limited by ammonium acetate buffer in the absence of Na^+ or K^+. Unfortunately, due to the limited availability of the 'modified RNA', we were not able to carry out other binding experiments such as isothermal titration calorimetry or NMR spectroscopy, although such experiments will be done in the future.

Since the H69 RNA has three pseudouridine (Ψ) residues in its sequence, another RNA construct having uridine (U) residues in the place of pseudouridines was synthesized in order to assess the contribution of the modifications to peptide binding. This construct is referred to as UUU. The apparent dissociation constant (K_d) of 19 ± 2 μM was acquired for the 1:1 complex of UUU-NQVANHQ-NH_2. The increase in K_d value for the UUU RNA-peptide complex revealed the importance of the collective role played by the pseudouridines in binding of the peptide with fully modified *E. coli* H69.

The *E. coli* H69 has been shown to undergo a conformational change with the change in pH from 7.0 to 5.5 (Abeysirigunawardena, S. & Chow, C.S., 2008), thus, it was of interest to analyze the influence of pH change on the binding of the peptide with the RNA. The ESI-MS experiments for this study were carried out at pH 7.0 and pH 5.2. The apparent dissociation constant for the 1:1 complex of RNA and the peptide was reduced for both RNA sequences ($\Psi m^3\Psi\Psi$ and UUU) by three-fold upon lowering the pH. From these results, it could be concluded that either protonation of the RNA or the peptide structure influenced this change in binding of the two species. Until further experiments are done, we will not know the protonation site or specific contributions to the binding interactions.

In another effort to study the role of the pseudouridines (Ψ) in binding of the peptide, two RNA constructs, UΨΨ and ΨUΨ, were synthesized. In the UΨΨ RNA, the pseudouridine at position 1911 was replaced by uridine (U) and in the ΨUΨ RNA; the pseudouridine at position 1915 was replaced by uridine (U). The K_d for the 1:1 complex for the UΨΨ- NQVANHQ-NH_2 was 28 ± 5 μM and for the ΨUΨ-NQVANHQ-NH_2 was 28 ± 4 μM at pH 7.0. These values were 2.5-fold higher than the K_d for H69, suggesting

that the peptide binding site is located at or near the loop region containing the pseudouridines at positions 1911 and 1915. These results also reveal that even subtle differences in RNA stability or conformation due to the presence or lack of modifications can influence peptide binding. Such differences are important to consider when looking at species selectivity or possible changes that could lead to antibiotic resistance in future drug designs.

To establish the selectivity of the peptide for H69, the propensity of peptide-RNA complex formation with both unrelated and related RNAs was studied through ESI-MS experiments. The unrelated RNAs chosen were from the small subunit of the ribosome, namely, the A-site RNA and helix 31 and the related RNA was the human H69. The peptide had moderate affinity for the A-site RNA, helix 31, and the human H69, but with three-fold lower affinity than the target H69 RNA. This result suggests that the peptide has features that allow for generic RNA binding as well as specific binding for modified H69.

CHAPTER 5

Probing assays used for H69-NQVANHQ complex

5.1. Introduction

The phage display technique was successfully applied for pulling out peptides from the phage peptide library for H69. To quantitatively evaluate the binding interaction of NQVANHQ-NH_2 peptide with H69, several of the recognized biochemical assays were carried out. They included electrophoretic mobility shift assays (EMSA), Fe-EDTA cleavage reactions, and in-line probing assays.

EMSA was chosen since it is technically simple and relatively fast to perform. Typically, discrete bands corresponding to uncomplexed RNA/DNA and the complexed RNA/DNA are clearly resolved since the RNA/DNA in complex with protein or any other ligand migrate through the a nondenaturing polyacrylamide gel more slowly than the free RNA/DNA (Garner, M.M. & Revzin, A., 1981). This assay is widely utilized for studying binding of larger proteins to specific sites on DNA and serves as qualitative probe for DNA-protein interactions (Khanna, H. *et al*., 2006; Brunner & Wirth, 2006).

The Fe-EDTA reaction assay was selected in order to ascertain the binding site of the peptide on the H69 RNA. In this method, $[Fe(EDTA)]^{2-}$ is the reagent that is used for identifying the binding sites of nucleic-acid binding ligands (Brenowitz, M. *et al*., 2002). This reagent is prepared by adding appropriate amounts of ferrous ammonium sulfate solution to the EDTA (ethylenediaminetetraacetic acid) solutions and incubating with RNA. EDTA is a metal chelator that binds to Fe(II), which catalyzes a reaction to produce hydroxyl radicals. This reaction is widely known as the Fenton reaction

(Hertzberg, R.P. & Dervan, P.B., 1984). The hydroxyl radicals lead to strand scission of RNA through oxidative degradation of the ribose moiety (Tullius, T.D. & Dombroski, B.A., 1985). The reaction scheme is as follows:

$[Fe(EDTA)]^{2-} + O_2 \rightarrow [Fe(EDTA)]^{-} + O_2^{-}$

$[Fe(EDTA)]^{2-} + O_2^{-} + 2H^{+} \rightarrow [Fe(EDTA)]^{-} + H_2O_2$

$[Fe(EDTA)]^{2-} + H_2O_2 \rightarrow [Fe(EDTA)]^{-} + \bullet OH + OH^{-}$

$RNA + \bullet OH \rightarrow H_2O + RNA\ (\bullet C1' \text{ or } \bullet C4') \rightarrow RNA\ fragments$

$Fe(EDTA)]^{-} + e^{-} \rightarrow [Fe(EDTA)]^{2-}$

In the above reaction mechanism, i) the $[Fe(EDTA)]^{2-}$ oxidizes to $[Fe(EDTA)]^{-}$ and provides the electrons for reducing oxygen in the solution, ii) the reduced oxygen in solution forms highly reactive hydroxyl radicals through a hydrogen peroxide intermediate or if the hydrogen peroxide is added to the reaction, the free radicals are formed from hydrogen peroxide rather from oxygen in solution (Celander, D.W., 2000), iii) the hydroxyl radicals then react with a sugar carbon (C1' or C4') causing the backbone cleavage by a β-elimination reaction. The nucleotide strand scission occurs through two possible mechanisms, oxygen-dependent and oxygen-independent pathways. The oxygen-independent pathway occurs at pH 12 or higher (Stubbe, J. & Kozarich, J.W., 1987). In this study, the reaction is performed at neutral pH, thus, the reaction pathway is considered to be oxygen-dependent. The iron complex is recycled by the reduction of $[Fe(EDTA)]^{-}$ to $[Fe(EDTA)]^{2-}$ by ascorbate or dithiothreitol (DTT). The hydroxyl radicals are quenched with thiourea (Celander, D.W. & Cech, T.R., 2000).

$[Fe(EDTA)]^{2-}$ catalyzes the scission of the nucleic acid backbone without base or sequence distinction and without any preference for secondary structure of the

oligonucleotide under study (Latham, J.A. & Cech, T.R., 1989; Celander & Cech, 1990), but the reaction depends on the solvent accessibility of the nucleotides. If all of the nucleotides of the given sequence are solvent accessible, then the bands corresponding to each nucleotide will be visible on a polyacrylamide gel. However upon addition of a ligand such as a small molecule or protein, the cleavage pattern of the nucleic acid changes. This change occurs because the ligand binds at certain positions and hinders $[Fe(EDTA)]^{2-}$ from reacting at that position of the backbone of the nucleic acid. Thus, some bands on the gel corresponding to certain nucleotides may be absent or show less intensity due to the binding of the ligand.

In the inline-probing assay developed by Breaker and coworkers, the objective is to ascertain the binding site of a ligand on RNA such as the NQVANHQ peptide on H69 RNA. This assay takes advantage of the inherent self-cleaving property of RNA due to the presence of 2'-OH (Soukup, G.A. & Breaker, R.R., 1999). The reaction scheme explaining the reaction is summarized in Figure 5.1.

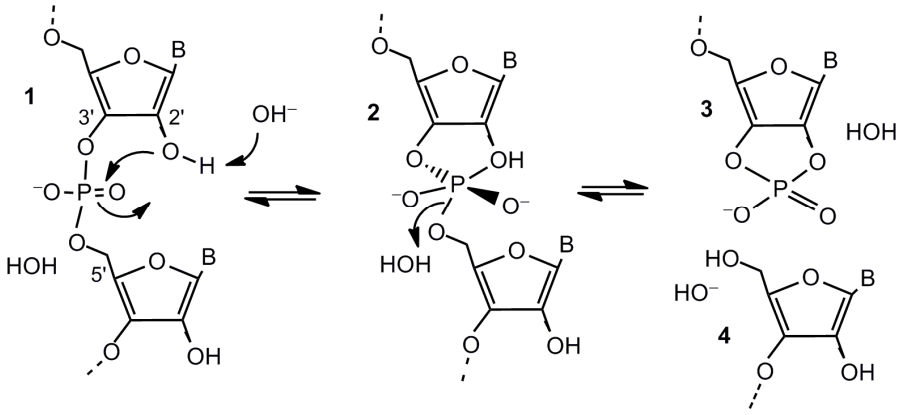

Figure 5.1. The mechanism for intramolecular phosphoester cleavage leading to RNA strand scission is shown. The reaction produces RNA fragments with 2',3'-cyclic phosphate (3) and 5'-hydroxyl termini (4) (Soukup, G.A. & Breaker, R.R., 1999).

The cleavage of the RNA strand in inline probing can be hindered due to the presence of a bound ligand. All of this information could be ascertained by running the reaction mixtures having RNA alone and RNA with peptide on polyacrylamide gels. The sequence of RNA appears as distinct bands, in which each band specifies a nucleotide. The intensity of the bands corresponding to the nucleotides with the bound ligand decreases with increasing concentrations of the ligand. The gels could then be quantified for ascertaining the binding constant of the complex.

5.2. Materials and methods

5.2.1. 3'- and 5'- ^{32}P labeling of RNA

The RNAs H69 and UUU were purchased from Dharmacon Research Inc., (Lafayette, CO) and were chemically synthesized at 1.0 μmole scale as described in Chapter 4. For conducting the EMSA and Fe-EDTA probing assays, H69 and UUU RNAs were radiolabeled at the 3'-end with pCp. For the 3'-^{32}P labeling of H69 the total reaction volume was kept at 30 μl. In a 2 ml centrifuge tube the following contents were added in final concentrations: 50 pmols of gel-purified RNA (modified, $\Psi m^3\Psi\Psi$ H69), 10% DMSO (dimethyl sulfoxide), 1X T4 RNA ligase buffer (50 mM Tris-HCl, 10 mM $MgCl_2$, 1 mM ATP, 10 mM dithiothreitol, pH 7.8 buffer), 10 mM ATP, 20 μCi/pmol [5'-^{32}P]-pCp (Perkin-Elmer, Waltham, MA), and 1 μL T4 RNA ligase (20 U/μL from New England Biolabs, Ipswich, MA). The mixture was incubated for 4 h at 4 °C. The RNA was then subjected to ethanol precipitation by addition of 25 μl of cold 4 M ammonium acetate (NH_4OAc), 5 μg $tRNA^{Phe}$, and 300 μl cold 100% ethanol. The reaction mixture was incubated again on dry ice for 1 h and then centrifuged at 12,000 x g at 4 °C for 20

min. The supernatant was removed immediately followed by another clean-up of RNA by adding 200 µl of 0.5 M NH_4OAc and 750 µl of cold ethanol. The mixture was again kept on dry ice for 1 h, centrifuged at 12,000 x g at 4 °C for 20 min. Finally, the pellet was washed with 500 µl cold ethanol and dried in speed-vac. The sample was later resuspended in 20 to 30 µl ddH_2O. The 3'-labeled RNAs were purified on 20% polyacrylamide gels, typically at 350 V for 4 h and the RNA bands were visualized under the Molecular Dynamics phosphoimager. The gel bands corresponding to RNA were excised and then electroeluted with 0.5 x TBE buffer (45 mM Tris, 45 mM boric acid, 0.5 mM EDTA, pH 8.2) at 200 V for 2 h in an Amicon Centrilutor™ (Beverly, MA) device. The RNAs were desalted with ddH_2O overnight by using a centrifuge and Centricon 3^{TM} (Amicon) devices. The RNAs were renatured in 10 mM Tris-HCl, pH 7.5 by heating to 90 °C for two minutes followed by slow cooling to room temperature. The A- and U-specific reactions and the aniline treatment for UUU RNA were performed as described by Peattie (Peattie, D.A., 1979).

For 5'-labeling of RNA, 50 pmole of RNA solution was incubated in 1X fresh polynucleotide kinase buffer (70 mM Tris-HCl, 10 mM $MgCl_2$, 5 mM dithiothreitol, pH 7.6), and 1 µl γ-^{32}P-ATP. The reaction mixture was vortexed at slow speed and spun down. Then, 30,000 U of polynucleotide kinase (PNK) enzyme (10,000 U/ µl from New England Biolabs, Ipswich, MA) were added. The mixture was heated at 37 °C for 30-45 min. Later, 10 µl of cold 7.5 M NH_4OAc (kept at 4 °C) was added. For removing excess salt and γ-^{32}P-ATP, a preloaded G25 column was used (Illustra, MicroSpins G-25 columns, GE healthcare) according to the manufacturer's protocol. The first ethanol precipitation was carried out by adding 25 µl of cold 7.5 M NH_4OAc (kept at 4 °C), 5 µg

$tRNA^{Phe}$, and 300 µl cold 100% ethanol. The centrifuge tube was incubated at –20 °C for one h followed by spinning at 13,000 rpm for 30 min at 4 °C. The supernatant was carefully removed and transferred to another centrifuge tube. The second ethanol precipitation was performed at –20 °C for one h by adding 750 µl cold ethanol, and 250 µl 7.5 M NH_4OAc. Finally, the sample was washed with 500 µl cold ethanol and placed in speed-vac for drying. The sample was later resuspended in 20 to 30 µl ddH_2O and 1 µl was used for scintillation counter.

5.2.2. Electrophoretic mobility shift assay (EMSA)

The EMSA experiments were performed in 5 µl of total reaction volume by adding 10,000 cpm of 3'-^{32}P-labeled H69 RNA with varying concentrations of peptide (0.2-200 µM), and 1X of reaction buffer. The reaction was incubated at 37 °C for 30 min. The sample having only RNA and no peptide was used as control. After incubation, 2 µl of loading buffer (0.1% bromophenol blue, 0.1% xylene cyanole FF, 20% glycerol) was added to each sample. Native polyacrylamide gels were used for separating the RNA-peptide complex from the RNA. Before loading samples on the non-denaturing gel, the gel was pre-run for 15 min. The samples were then loaded on native gels (5000 cpm per lane) and the gel was run at 250 V, at 4 °C for 2 h or at 300 V at RT for 2 h. The gel was then wrapped and exposed to a storage phosphor screen (Amersham Biosciences, Piscataway, NJ) at -20 °C overnight. The screen was then scanned with a Typhoon phosphorimager (GE Healthcare, Piscataway, NJ). The gel was then analyzed for complex formation. For optimizing the conditions of the experiments, the cross-linking of the gel (ratio of acrylamide to bisacrylamide) was varied between 19:1 to 60:1 and the

percentage of the gels was also varied between 8% and 20%. Another step towards optimization of the reaction conditions involved changing buffers for formation of the peptide-RNA complex. The following buffers used were: 0.1% TBST (50 mM Tris, 150 mM NaCl, and 0.1% Tween-20), TE buffer (10 mM Tris-HCl, pH 7.5, 70 mM NaCl, 0.2 mM EDTA, 0.01% NP-40, and 5% glycerol), and Hepes buffer (10 mM HEPES-KOH, pH 7.3, 100 mM KCl, 1 mM $MgCl_2$, 0.5 mM EDTA, and 0.01% Triton X-100). The reaction conditions were tested on the established model of A-site RNA and streptomycin (Fourmy, D., *et al*., 1996). The buffer used for this complex formation was Hepes buffer (10 mM HEPES-KOH, pH 7.3, 100 mM KCl, 1 mM $MgCl_2$, 0.5 mM EDTA, and 0.01% Triton X-100). The samples were prepared by adding 10,000 cpm of 3'-^{32}P-labeled A-site RNA with 1μl of varying concentrations of streptomycin (0.04, 0.4, 4, and 40 μM), 1X buffer and x μl of ddH_2O for a total reaction volume of 5 μl. the samples were then incubated at 37 °C for 30 min. After incubation, 2 μl of loading buffer (0.1% bromophenol blue, 0.1% xylene cyanole FF, 20% glycerol) was added to each sample. The samples were then loaded onto the native gel, in which the gel conditions were 15% native gel with 40:1 cross-linking and run at 250 V at 4 °C. The gel was then wrapped and exposed onto a storage phosphor screen (Amersham Biosciences, Piscataway, NJ) at -20 °C overnight. The screen was then scanned with a Typhoon phosphorimager (GE Healthcare, Piscataway, NJ).

5.2.3. Fe-EDTA cleavage reaction

For carrying out footprinting assays involving H69 and the peptides with $[Fe(EDTA)]^{2-}$, the following solutions were prepared: the $[Fe(EDTA)]^{2-}$ solution, sodium

ascorbate solution, and hydrogen peroxide solution. The $[Fe(EDTA)]^{2-}$ solution (1 M) in ddH_2O was freshly prepared fresh using $[(NH_4)_2Fe(II)(SO_4)_2 \bullet 6H_2O]$ (A.C.S.reagent, Baker & Adamson) in a 10 ml volumetric flask. The solution was kept in the dark until ready for use. A sodium ascorbate (1 M) solution was freshly prepared in a 10 ml volumetric flask. It was diluted with ddH_2O to make a 10 mM final stock solution. The hydrogen peroxide (H_2O_2) solution was freshly prepared as a 0.6% solution in ddH_2O from a 30% stock solution. The loading buffer for the experiment contained thiourea, bromophenol blue, xylene FF, formamide and glycerol. A 10 µl reaction was set up for each concentration of peptide. It contained 30,000 cpm of 3'-^{32}P-labeled H69 RNA, 1X binding buffer, and peptide solution from 0.2 to 200 µM concentration. The reaction mixtures were incubated for varying amounts of time. The binding buffers used were 0.1% TBST (50 mM Tris-HCl, 150 mM NaCl, 0.1% Tween-20) at pH 6.5 and 0.1% TBST at pH 7.5 and cacodylate buffer (50 mM NaCl, 20 mM Na cacodylate, pH 5.8). The samples were allowed to reach equilibrium at room temperature for 30 min. After incubation, H_2O_2 solution representing 0.06% final concentration, Fe/EDTA solution having final concentration of 2 mM $[(NH_4)_2Fe(II)(SO_4)_2 \bullet 6H_2O]$, and 4 mM Na_2EDTA, and sodium ascorbate having final concentration of 100 mM were added to the side of the centrifuge tube and spun down. The samples were incubated at 42 °C for 2 h. The reactions were then quenched by adding thiourea solution at final concentration of 10 mM. The loading buffer (2 µl) was added to all the samples. The samples were then loaded on high-resolution 20% polyacrylamide gels for analysis. The gels were prepared using plates 33 x 42 cm or 20 x 42 cm in dimensions with a 0.4 mm-thick spacer. The ratio of acrylamide:bisacrylamide used was 19:1 with 14 M urea. The gels

were run at 1800-2000 V (~20 mA of current) for 2-3 h and were analyzed using the phosphorimager (Typhoon, GE Healthcare).

5.2.4. Inline-probing assay

For inline-probing assay, the reactions were carried out under alkaline conditions using the buffer 50 mM Tris-HCl, pH 8.3, 20 mM $MgCl_2$, and 100 mM KCl. Samples with 30,000 cpm of the 5'-labeled H69 and 5 to 100 μM peptide concentrations were incubated in alkaline buffer (50 mM Tris-HCl, pH 8.3, 20 mM $MgCl_2$, and 100 mM KCl) at 25 °C for 20 h and in dark. After incubation, all the RNA samples were denatured by boiling for 1 min with 2 μl of formamide loading buffer (0.1% bromophenol blue, 0.1% xylene cyanole FF, 80% formamide, 20% glycerol). Before loading the samples on the 20% denaturing gel, the gel was pre-run for 20 min. Later, the reaction samples (50,000 cpm/each) were added to the long, thin (42 cm x 33 cm), denaturing (7 M urea) gel and the running buffer for the gel was 0.5x TBE buffer (900 mM Tris, 900 mM boric acid, pH 8.3, 25 mM Na_2EDTA). The gel was run for 3-4 h at 2800 V and later transferred onto a film, wrapped and exposed onto a storage phosphor sreen (Amersham Biosciences, Piscataway, NJ) at -20 °C overnight. The screen was then scanned on the Typhoon (GE Healthcare, Piscataway, NJ). The alkaline hydrolysis ladder of the labeled H69 was generated by incubation with 50 mM $NaHCO_3/Na_2CO_3$ (pH 9.0 at 23 °C) and 1 mM EDTA for 7 min at 90 °C (Knapp, G., 1989). The A- and U-specific reactions and aniline treatment of UUU RNA were carried out as described by Peattie (Peattie, D.A., 1979).

5.3. Results and discussion

5.3.1. EMSA for model system of A site RNA and streptomycin

The model system of A-site RNA and streptomycin for optimizing the EMSA conditions was adopted because streptomycin has been proven to bind to A-site RNA through a number of biochemical assays such as protection assays (Moazed, D. & Noller, H. F, 1987), crosslinking assays (Gravel, M. *et al*., 1987), and mutagenesis data (Pinard, R. *et al*., 1993; Melancon, P. *et al*., 1988). These conditions were employed because the H69 RNA and peptide were comparable in size to the A-site RNA and streptomycin system.

In the gel picture (Figure 5.4.), the bands corresponding to the complex formation between A-site RNA and streptomycin and the uncomplexed RNA are observed. Since the mobility of the molecules through polyacrylamide gels is partly based on their size, the bands for the A-site RNA-streptomycin complex move slower than the uncomplexed RNA. The lower bands on the bottom of the gel represent the uncomplexed RNA and the upper bands correspond to the complex between RNA and streptomycin. It is observed that increasing concentrations of streptomycin lead to darker bands for the complex as well as a gradual shift in the band for complex. From the shift in the location of the complex bands, it seemed that at 40 mM concentrations of streptomycin, the entire amount of RNA is in complex with streptomycin, although it was somewhat difficult to analyze due to the smearing of the bands. The chosen ionic conditions provided by the HEPES buffer appeared to be appropriate for stabilizing complex formation and the chosen matrix of a 15% polyacrylamide gel was also suitable for analyses of the RNA-drug complex. Streptomycin is known to bind to the A-site RNA

with an approximate K_d of > 400 μM (Gromadski, K.B. & Rodnina, M.V., 2004); thus, the estimated K_d from the EMSA shown here is in the appropriate range.

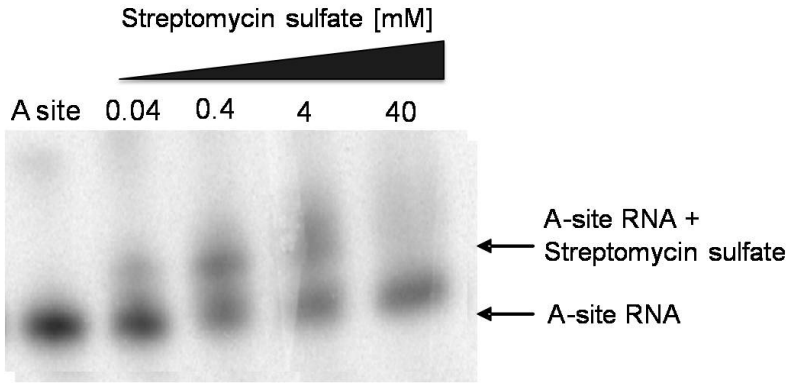

Figure 5.2. The picture of the native polyarylamide gel showing bands of the free A-site RNA and the A-site RNA complexed with streptomycin under the conditions described in the Materials and methods section is given.

5.3.2. EMSA for H69 and NQVANHQ-NH_2 peptide

After successfully monitoring the formation of A-site RNA and streptomycin complex through EMSA, similar assay conditions were applied for observing H69 and NQVANHQ-NH_2 peptide complex formation. A band corresponding to the uncomplexed RNA H69 was seen, but a band corresponding to complex of peptide and RNA was not detected (Figure 5.3). Many conditions of buffer, gel matrix (%, acrlyamide:bisacrylamide, etc.), ratios of peptide to RNA, incubation times, and loading conditions were tried, but unfortunately none were successful. One reason for not observing the band for complex was thought to be due to dissociation of the complex in the gel matrix. In order to overcome this issue, the native gels were prepared with different ratios of acrylamide to bisacrylamide. However, the band corresponding to the complex was still not observed. The gels were also run at different temperatures such

as at 4 °C and at room temperature, but there was no positive outcome. In order to change the ionic conditions during the complex formation, different buffer systems were tried, but again the bands representing the complex in the gels was not present. Surface plasmon resonance (SPR) experiments were also attempted, but poor results here suggested that the association/dissociation kinetics for the peptide-RNA complex (H69-NQVANHQ-NH_2) are not suitable for analysis by either method. After many attempts, this approach was abandoned.

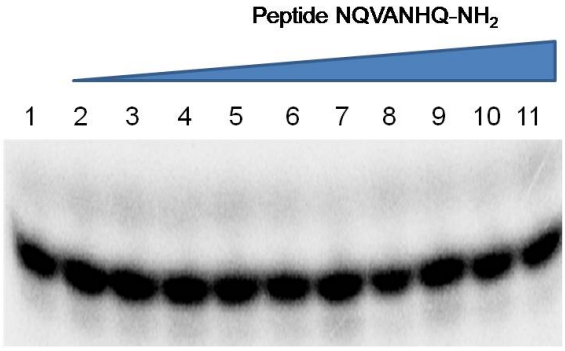

Figure 5.3. The native gel image of EMSA for detecting the complex between H69 and the peptide NQVANHQ-NH_2 is shown. Lane 1 is the control having only RNA H69, lanes 2-11 show RNA in the presence of increasing concentrations of peptide (350, 400, 450, 500, 600, 700, 800 μM, 1 mM, and 5 mM, respectively).

5.3.3. Fe-EDTA reaction results for H69 and NQVANHQ-NH_2 peptide

The probing reactions for studying the binding site of NQVANHQ-NH_2 peptide on H69 RNA employing $[Fe(EDTA)]^{2-}$ solutions were carried out in the buffer used for binding the phage library with H69 during biopanning (0.1% TBST: 50 mM Tris-HCl, pH 7.5, 150 mM NaCl, 0.1% Tween-20). The peptide concentrations used were 0.2, 2, 20, and 200 μM. The A and U sequencing reactions for determining the positions of bands were carried out with 3'-^{32}P-UUU RNA (unmodified H69) (Figure 5.4). In this assay,

some bands showed slight changes in the presence of peptide. However, this sort of trend was not observed at any particular position (Figure 5.5.) and the results were not reproducible, even under a variety of conditions that were tried. Thus, the Fe-EDTA assay was also determined to be unsuccessful.

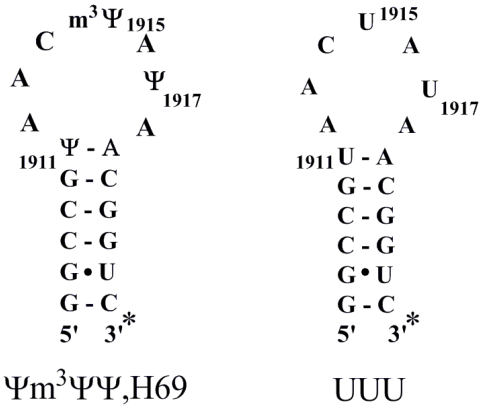

Figure 5.4. The secondary structures of H69 and UUU RNAs used in this assay are shown (∗ represents the ^{32}-P labeled end).

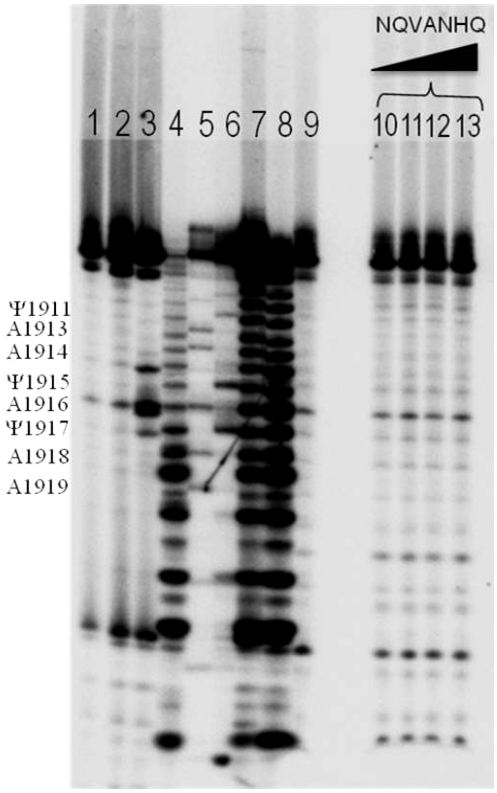

Figure 5.5. The gel image of the Fe-EDTA reaction performed with H69 and NQVANHQ-NH_2 peptide complex is shown. Lanes 1& 2 are the H69 RNA alone, lane 3 is UUU RNA, lane 4 is alkaline hydrolysis of H69, lane 5 is the A reaction, lane 6 is the U reaction, lanes 7 & 8 are the alkaline hydrolysis of H69, lane 9 is the Fe-EDTA reaction of H69 only, and lanes 10-13 represent RNA in the presence of increasing concentrations of NQVANHQ-NH_2 peptide (0.2, 2, 20, and 200 μM, respectively).

5.3.4. Results for inline-probing using H69 and NQVANHQ-NH_2 peptide

The presence of the 2'-OH group in the RNA makes it highly susceptible to self-cleavage under physiological conditions. The spontaneous cleavage of the phosphodiester linkages occurs through intramolecular transesterification reactions (Soukap & Breaker, 1999). This property of RNA is enhanced under acidic or alkaline conditions. The reaction mixtures for this assay were prepared under alkaline conditions. The varying concentrations of the peptide with 5' labeled H69, used in the reaction mixtures were: 5, 10, 20, 24, 26, 28, 40, 50, 60, 80, and 100 μM. RNase T1

enzyme digestion reactions were done to precisely ascertain the positions of guanine nucleotides in the sequence of H69. The reaction mixtures were run on thin polyacrylamide gels to view the different intensities of the bands of the RNA and the complex. The intensities of the bands of the complex reaction mixtures were expected to decrease at certain positions of the RNA sequence indicating the presence of bound peptide. However, this manifestation of decreased intensity of the bands at certain nucleotide positions was not noticed (Figure 5.7). Thus, the binding site of the peptide NQVANHQ-NH_2 was not determined through this assay. As with the other assays mentioned in this chapter, a variety of conditions were tried, but none were successful.

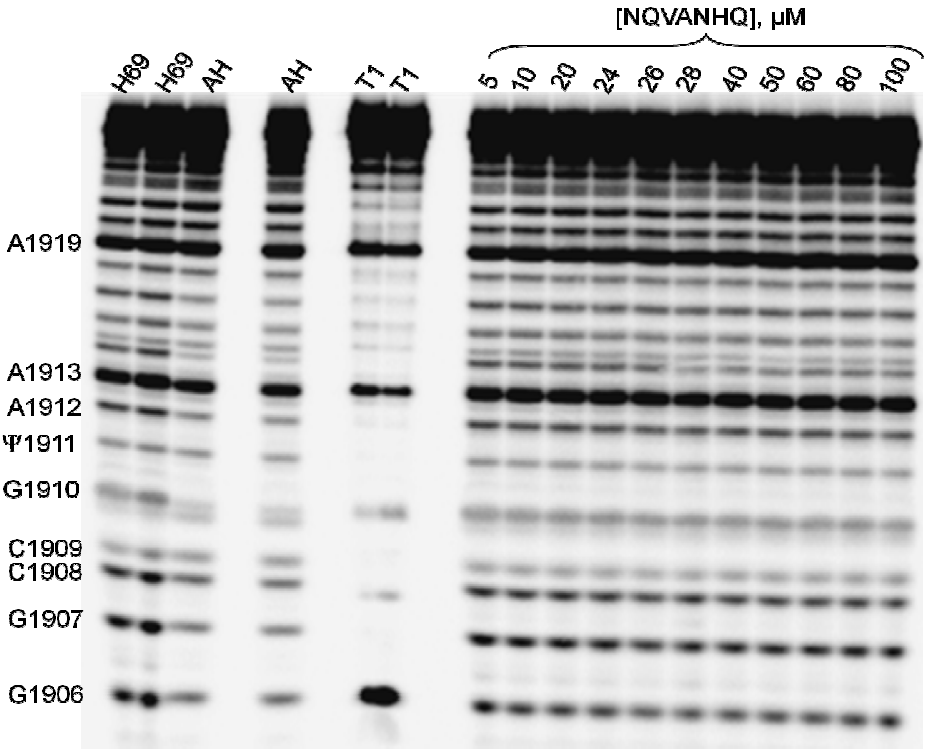

Figure 5.6. The gel image of the inline-probing assay of H69 and the reaction mixtures having varying concentrations of the peptide NQVANHQ, run on 20% thin polyacrylamide gel, is shown. AH = alkaline hydrolysis, T1 = RNase T1.

5.4. Conclusions

The gel shift assay is an established method for observing the complex formation for a variety of systems such as the TAR RNA-Tat peptide (Shah, K. et al., 1996), and DNA binding proteins (Garner, M.M. & Revzin, A. 1981). The assay was first optimized for the A-site RNA and streptomycin complex, and the complex of the RNA and the aminoglycoside streptomycin was observed. On the other hand, when the same gel conditions were applied for examining the H69 and peptide NQVANHQ complex, the gel bands corresponding to the complex were not observed. This could be attributed to fast on/off kinetics of binding of peptide to H69, as compared to the A-site RNA and streptomycin (complex involving electrostatic interactions), or the instability of the peptide-H69 complex in the gel matrix. In addition, previous work in the literature regarding the success of EMSA mostly involved charged small molecules or dye-like molecules with strong binding.

For determining the specific locations of binding of the peptide on the H69 hairpin, two recognized probing assays were performed, Fe-EDTA cleavage and the inline-probing assay. Unfortunately, despite many attempts, these assays were not successful in giving any conclusive or reliable information about the binding site of the peptide. As a result, the binding of the peptide NQVANHQ-NH_2 with H69 was monitored through electrospray ionization (ESI) mass spectrometry that was discussed thoroughly in the previous chapter.

Further experiments will be required to determine the binding site, such as more elaborate mass spectrometry experiments or NMR spectroscopy. Furthermore, the peptide is hydrophobic in nature and there is not much literature available describing

assays for studying hydrophobic peptides and RNA, therefore, new assays need to be developed for studying these kinds of interactions. Currently, work is in progress by another student in the laboratory to map the site of NQVANHQ-NH_2 binding on the 23 S rRNA in 50 S subunit.

CHAPTER 6

Conclusions and future directions

6.1. Conclusions

The problem of antibiotic resistance demands for the development of new antimicrobials. The ribosome is a well-known target for many antibiotics. The challenging work of ribosomal crystallography performed in Ada E.Yonath, Thomas A. Steitz, and Venkatraman Ramakrishnan labs was recognized worldwide when the Nobel Prize in Chemistry in 2009 was awarded to these scientists. Crystal structures of the ribosome and its subunits have led to the exploration of novel regions of bacterial pathogens as targets, in addition to the acknowledged ones such as A site of the decoding region (Tenson, T. *et al*., 2006). Helix 69 (H69) rRNA has been chosen as a target for the present thesis studies due to its location in the interface region of a functionally active ribosome. H69 is a 19-nucleotide stem-loop motif present in 23 S rRNA of large or 50 S subunit having pseudouridine (Ψ) at positions 1911, and 1915 and a methylated pseudouridine (Ψ) at position 1915. It is recognized to participate in many vital stages of translation such as subunit association, where it participates in an important RNA-RNA bridge B2a with h44 of small subunit, translocation of tRNAs, and ribosome recycling (Ortiz-Meoz, R.F. & Green, R., 2010; Yonath, A. *et al*., 2003; Yonath, A. *et al*., 2004; Kipper, K. *et al*., 2009; Klaholz, B.P. *et al*., 2004; Pai, R.D. *et al*., 2008). Mutational studies involving complete deletion of H69 made 50 S subunit variants to have most severe *in vitro* reassociation efficiency and mutations of loop residues influenced initiation factor dependent 70S initiation complex formation (Kipper,

K. *et al*., 2009, Ali, I.K. *et al*., 2006). In addition, H69 has been shown to be exposed in the cell in unassembled 50S subunit and could be targeted by small molecules (Merryman, C. *et al*., 1999). Therefore, based on the amplitude of functions involving H69 and its vital position in the ribosome, it fulfills the conditions for an antimicrobial target.

Phage-display methodology was employed in pursuit of finding small molecules such as peptides that could bind H69 and disrupt protein synthesis by interrupting the formation of intersubunit bridge in the ribosome. This molecular biology based tool has been successfully applied for identification of peptide agonists and antagonists for receptors (Pillutla, R.C. *et al*., 2002), recognition of targets for obstruction of tumour-specific angiogenesis (Trepel, M. *et al*., 2002), discovery of peptide drug candidates (Ladner, R.C. *et al*., 2004) and vaccine development (Wang & Yu, 2004). In this work, four rounds of selection were performed with different levels of stringency for experimental conditions such as amount of immobilized biotinylated H69 (target), the nature of the blocking solution, the binding time of phage library with the target H69, the number of washes, and the timings of odd and even washes. All of these conditions have been clearly described in Chapter 2. After sequencing phage clones of the fourth round, two peptide sequences dominated the phage pool, STYTSVS and NQVANHQ.

The NQVANHQ peptide was found to bind H69 RNA with a low micromolar dissociation constant. The later sequence was a unique sequence for which no consensus appeared, but it contained an abundance of amino acid residues that are also present in the ribosome recycling factor, RRF, and known to make contacts with H69 (Pai, R.D. *et al*., 2008). The crystal structure of RRF bound to 70 S ribosome

shows the amino acids present on one face of the α-helix 1 in domain 1 of RRF interacting with nucleotides of H69. The amino acids include serine 17 (S17) interacting with Ψ1917, valine 20 (V20) interacting with A1916 and $m^3\Psi$1915, histidine 23 (H23) and aspargine (N24) interacting with C1914 (Pai, R.D. *et al*., 2008). Thus, the conditions optimized for selection of peptides against H69 RNA and employing phage display were successful.

For preliminary evaluation of the binding affinity of these peptides with H69, fluorescence and enzyme-linked assays were applied. The peptide sequences NQVANHQ and STYTSVS were chemically synthesized on the Tentagel beads. These beads were incubated with fluoresecent-labeled H69 for fluorescence assay and biotin-labeled H69 for enzyme-linked assay. For the fluorescence assay, the fluorescence intensity of the NQVANHQ beads was observed to be higher than STYTSVS beads indicating that peptide NQVANHQ has higher affinity for H69 as compared to STYTSVS. The peptides NQVANHQ and STYTSVS were also probed with Quantum dots (Q-dots). The peptide beads were incubated with F-H69 and then with Q-dots (having anti-fluorescein antibody). The results of the Q-dots were in accordance with the green fluorescence beads and more clearly showed that peptide NQVANHQ had higher affinity for H69 as compared to STYTSVS.

The fluorescence-based assay was not very convenient due to the longer incubation times and high number of washing steps required for observing the results. In addition, the affect of the attachment of the peptide to the bead on the affinity of peptide to RNA was not resolved. Therefore, binding of NQVANHQ was further validated by using a more sensitive method, namely electrospray ionization (ESI) mass

spectroscopy. There is convincing evidence in literature for employing ESI-MS for detecting noncovalent complexes of biological nature (Sannes-Lowry, K.A. *et al*., 1999). ESI-MS is a speedy and reliable technique for assessing the stoichiometry and the apparent dissociation constants (K_d*s*) of complexes such as aminoglycosides neomycin and streptomycin bound with the TAR RNA, and tat peptide-TAR RNA complex. In this dissertation work, ESI-MS studies involved direct titration experiments in which the RNA (H69 and its variants) concentration was kept constant and lower than the expected K_d of the complex. The ESI-MS has some limitations due to the use of ammonium acetate buffer for its experiments since the presence of cations Na^+ and K^+ form abundant RNA adducts and this makes the RNA spectra difficult to interpret; however, studies have shown that the RNA-peptide complex is able to tolerate high concentrations of NH_4OAc.

The apparent dissociation constant obtained for the H69 and NQVANHQ-NH_2 was in the low micromolar range (11 $\pm$ 1 μM). This value is comparable to that of aminoglycoside antibiotics binding to the A-site RNA (1 to 10 μM) (Wong, C.H. *et al*., 1992; Fourmy, D. *et al*., 1996; Wang, Y. *et al*., 1996; Sannes-Lowry, K.A. *et al*., 2000; Llano-Sotelo, B. et al., 2002; Kaul, M. *et al*., 2004), as well as with H69 (8 μM) (Duc, A. thesis). However, this dissociation constant is to be considered relative rather than the absolute value since the fraction of the bound peptide was observed to be low even at more than saturating concentrations of peptide. The low observance of fraction bound also reveals that the key driving force behind the complex formation may be hydrophobic interactions. The stoichiometry of the interaction of this peptide with H69 was predominantly 1:1 suggesting the interaction to be relatively specific.

The ESI-MS experiments were also carried out with H69 variant UUU RNA (having uridines instead of pseudouridines at positions 1911, 195, and 1917) and peptide NQVANHQ-NH_2. The relative dissociation constant (K_d) obtained for UUU-NQVANHQ-NH_2 complex at 1:1 stoichiometry was 19 $\pm$ 2 μM. The higher value of K_d calculated for this complex revealed that the presence of all three pseudouridine residues positively contributes towards binding of this peptide to H69. To learn more about the role of individual pseudouridines at positions 1911 and 1915 towards binding of the peptide, ESI-MS experiments were performed with two H69 variants, UΨΨ and ΨUΨ. The apparent dissociation constant (K_d) calculated for UΨΨ was 28 $\pm$ 5 μM and for ΨUΨ was 28 $\pm$ 4 μM. The observed 2.5-fold decrease in the apparent dissociation constant for the 1:1 complex of RNA and the peptide suggests that the peptide binding site is located at or near the loop region containing the pseudouridines at positions 1911 and 1915. This also reveals that the presence or lack of modifications influences the RNA stability, which further influences the binding of peptide.

The effect of pH on the complex formation of H69 and UUU RNA with NQVANHQ-NH_2 peptide was studied at two different values, 7.0 and 5.2. The selection of the pH values was based on the pH-dependent conformational changes observed for the loop region of H69 (Abeysirigunawardena, S. & Chow, C.S., 2008). The three-fold decrease of the apparent dissociation constant for the 1:1 complex of RNA and the peptide indicated that either protonation of the RNA or the peptide structure influenced this change in binding of the two species. Until further experiments are done, we will not know the protonation site or specific contributions to the binding interactions.

For ascertaining the specificity of the peptide for H69, its binding affinity was tested with related RNA such as human H69 and unrelated RNAs such as helix 31 and A-site rRNA. The peptide showed three-fold lower affinity than the target H69 RNA for all these RNAs suggesting that the peptide has features that are suitable for developing it as a lead compound for novel antimicrobial.

For determining the binding site of the peptide on H69 RNA, various assays were employed such as EMSA, Fe-EDTA reaction, and inline-probing assay. Unfortunately, none of the assays gave reliable information about the binding site of the peptide. The presence of greater hydrophobic character, reduced electrostatic component and fewer hydrogen bonding moieties in the NQVANHQ-NH_2 peptide might have contributed towards the negative results of these assays. Further experiments will be required to determine the binding site, such as more elaborate mass spectrometry experiments or NMR spectroscopy.

6.2. Future directions

The NQVANHQ peptide selected for H69 employing phage-display library shows moderate binding with the target RNA. This could be attributed to the fact that since phage display technique involves live bacteria for amplification of phage, the peptide sequences (strongest binders) that will interfere with protein synthesis in bacteria and may not actually survive the selection process. Thus, the affinity and specificity of NQVANHQ peptide for H69 RNA needs to be improved by understanding the contribution of individual amino acid side chain functional groups through alanine scanning mutagenesis. The amino acid alanine is mostly used because of its small and

inert methyl functional group. In alanine scanning, this smallest chiral amino acid, alanine, is used to substitute each non-alanine residue one at a time. This process, if used with NQVANHQ, will result in six different variants of the parent peptide having alanine at desired positions. In addition, double-alanine scanning could be carried out for getting more insight into the roles of individual amino acid or to consider possible cooperative effects. The binding of the variant peptides could be monitored by ESI-MS or some other biochemical technique. The substitution of key amino acid residue(s) with alanine may cause diminished binding activity, thus relating to the important role of that particular amino acid(s) in the parent peptide. Therefore, alanine scanning will enable us to quickly determine each individual amino acid's contribution to the peptide's functionality.

Applying the peptidomimetic chemistry, different formats of the parent peptide NQVANHQ could be synthesized and characterized for their binding affinities towards H69. The examples include β-peptides (Gelman, M.A. *et al*., 2003), peptides having D-amino acids (Huq, I. *et al*., 1999), and peptoid-based sequence (Simon, R.J. *et al*., 1992). The binding affinity of these peptide sequences could be monitored using ESI-MS and compared with parent peptide NQVANHQ.

Another approach for improving the affinity of the peptides from phage library is the construction of peptide sequences with the help of split-pool peptide synthesis. In this approach, the knowledge from the alanine-scanning studies will be applied. The amino-acids whose removal in alanine scanning resulted in diminished activity will be kept constant. The amino-acids at other positions will be varied with all ninteen amino-

acids. Thus, peptide library will be generated which could then be used for further binding experiments for selecting the high affinity peptide.

REFERENCES

Abeysirigunawardena, S.C.; Chow, C.S. pH-dependent structural changes of helix 69 from *Escherichia coli* 23 S ribosomal RNA. *RNA*, **2008**, 14, 782-792.

Adalimumab (HUMIRA) for rheumatoid arthritis. *Medical Letters on Drugs and Therapeutics*, **2003**, 45, 25-27.

Agalarov, S.C.; Prasad, G.S.; Funke, P.M.; Stout, C.D.; Williamson, J.R. Structure of the S15,S6,S18-rRNA complex: assembly of the 30 S ribosome central domain. *Science*, **2000**, 288, 107-113.

Agrawal, R.K., Sharma, M.R., Kiel, M.C., Hirokawa, G., Booth, T.M., Spahn, C.M.T., Grassucci, R.A., Kaji, A., and Frank, J. Visualization of ribosome-recycling factor on the *Escherichia coli* 70 S ribosome: Functional implications. *Proceedings of the National Academy of Sciences USA*, **2004**, 101, 8900-8905.

Agrawal, R.K.; Heagle, A.B.; Penczek, P.; Grassucci, R.A.; Frank, J. EF-G-dependent GTP hydrolysis induces translocation accompanied by large conformational changes in the 70 S ribosome. *Nature Structural & Molecular Biology*, **1999**, 6(7), 643-647.

Agrawal, R.K.; Penczak, P.; Grassucci, R.A.; Frank, J. Visualization of elongation factor G on the *Escherichia coli* 70S ribosome: The mechanism of translocation. *Proceedings of the National Academy of Sciences USA*, **1998**, 95, 6134-6138.

Agris, P.F.; Marchbank, M.T.; Newman, W.; Guenther, R.; Ingram, P.; Swallow, J.; Mucha, P.; Szyk, A.; Rekowski, P.; Peletskaya, E.; Deutscher, S.L. Experimental models of protein–RNA interaction: isolation and analyses of tRNA(Phe) and U1

snRNA-binding peptides from bacteriophage display libraries. *Journal of Protein Chemistry*, **1999**, 18, 425-435.

Ali, I. K., Lancaster, L.; Feinberg, J.; Joseph, S.; Noller, H.F. Deletion of a conserved, central ribosomal intersubunit RNA bridge. *Molecular Cell*, **2006**, 23, 865-874.

Allers, J.; Shamoo, Y. Structure-based analysis of protein-RNA interactions using the program ENTANGLE. *Journal of Molecular Biology*, **2001**, 311, 75-86.

Amersham Life Science, Inc. Oligonucleotide Biotin Labeling Kit, 1995, Product Number US72350, pages 1-2.

Anand, M.; Valente, L.; Carr-Schmid, A.; Munshi, R.; Olarewaju, O.; Ortiz, P.A.; Kinzy, T.J. Translation elongation factor 1 functions in the yeast *Saccharomyces cerevisiae*. *The Ribosome Cold Spring Harbor Symposia in Quantitative Biology Volume LXVI*, **2001**, Cold Spring Harbor Laboratory Press, Cold Spring Harbor, 439-448.

Anderson, A.C. The process of structure-based drug design. *Chemistry & Biology*, **2003**, 10, 787-797.

Arap, M.A. Phage display technology- applications and innovations. *Genetics and Molecular Biology*, **2005**, 28, 1, 1-9.

Armstrong, J.; Perham, R.N.; Walker, J.E. Domain structure of bacteriophage fd adsorption protein. *FEBS Letters*, **1981**, 135,167-172.

Atherton, E., Sheppard, R.C. Solid Phase peptide synthesis: a practical approach, **1989**, IRL Press, Oxford, England.

Auerbach, T.; Bashan, A.; Harms, J.; Schluenzen, F.; Zarivach, R.; Bartels, H.; Agmon, I.; Kessler, M.; Pioletti, M.; Franceschi, F.; Yonath, A. Antibiotics targeting

ribosomes: crystallographic studies. *Current Drug Targets-Infectious Disorders*, **2002**, 2, 169-186.

Azzazy, H.M.E.; Highsmith, J.W.E. Phage display technology: clinical applications and recent innovations. *Clinical Biochemistry*, **2002**, 35, 425-445.

Bakin, A.; Ofengand, J. Four newly located pseudouridylate residues in *Escherichia coli* 23 S ribosomal RNA are all at the peptidyltransferase center: Analysis by the application of a new sequencing technique. *Biochemistry*, **1993**, 32, 9754–9762.

Ban, N.; Nissen, P.; Hansen, J.; Capel, M.; Moore, P.B; Steitz, T.A. Placement of protein and RNA structures into a 5 Å-resolution map of the 50 S ribosomal subunit. *Nature,* **1999**, 400, 841-847.

Ban, N.; Nissen, P.; Hansen, J.; Moore, P.B.; Steitz, T.A. The complete atomic structure of the large ribosomal subunit at 2.4 Å resolution. *Science*, **2000**, 289, (5481), 905-920.

Baram, D.; Pyetan, E.; Sittner, A.; Auerbach-Nevo, T.; Bashan, A.; Yonath, A. Structure of trigger factor binding domain in biologically homologous complex with eubacterial ribosome reveals its chaperone action. *Proceedings of the National Academy of Science USA,* **2005**, 102(34), 12017-12022.

Barret, J. F. & Hoch, J. A. Two-component signal transduction as a target for microbial anti-infective therapy. *Antimicrobial Agents and Chemotherapy,***1998**, 42, 1529-1536.

Barrett, R.W.; Cwirla, S.E.; Ackerman, M.S.; Olson, A.M.; Peters, E.A.; Dower, W.J. Selective enrichment and characterization of high affinity ligands from collections

of random peptides on filamentous phage. *Analytical Biochemistry*, **1992**, 204, 357-364.

Bashan, A.; Agmon, I.; Zarivach, R.; Schluenzen, F.; Harms, J.; Berisio, R.; Bartels, H.; Franceschi, F.; Auerbach, T.; Hansen, H.A.S.; Kossoy, E.; Kessler, M.; Yonath. A Structural basis of the ribosomal machinery for peptide bond formation, translocation, and nascent chain progression. *Molecular Cell*, **2003**, 11, 91-102.

Bass, B.L.; Weintraub, H. An unwinding activity that covalently modifies its double-stranded RNA substrate. *Cell*, **1988**, 55, 1089-1098.

Bass, S.; Greene, R.; Wells, J.A. Hormone phage: An enrichment method for variant proteins with altered binding properties. *Proteins*, **1990**, 8, 309-314.

Bateman, A.; Birney, E.; Cerruti, L.; Durbin, R.; Etwiller, L.; Eddy, S.R.; Griffiths-Jones, S.; Howe, K.L.; Marshall, M.; Sonnhammer, E.L. The Pfam protein families database. *Nucleic Acids Research*, **2002**, 30, 276-280.

Battiste, J.L.; Mao, H.; Rao, N.S.; Tan, R.; Muhandiram, D.R.; Kay, L.E.; Frankel, A.D.; Williamson, J.R. α-Helix-RNA major groove recognition in an HIV-1 Rev peptide-RRE RNA complex. *Science*, **1996**, 273, 1547-1551.

Bauer, G.; Berens, C.; Projan, S.J.; Hillen, W. Comparison of tetracycline and tigecycline binding to ribosomes mapped by dimethylsulphate and drug-directed Fe^{2+} cleavage of 16 S rRNA. *Journal of Antimicrobial Chemotherapy,* **2004**, 53, 592-599.

Benguri, D.R.; Dungu, B.; Thiaucourt, F.; du Plessis, D.H. Phage displayed peptides and anti-idiotype antibodies recognised by a monoclonal antibody directed

against a diagnostic antigen of *Mycoplasma capricolum* subsp. capripneumoniae. *Veterinary Microbiology*, **2001**, 81, 165-179.

Benkirane, M.; Neuveut, C.; Chun, R.F.; Smith, S.M.; Samuel, C.E.; Gatignol, A.; Jeang K-T Oncogenic potential of TAR RNA-binding protein TRBO and its regulatory interaction with RNA-dependent protein kinase PKR. *EMBO Journal*, **1997**, 16, 611-624.

Benveniste, R.; Davies, J. Aminoglycoside antibiotic-inactivating enzymes in actinomycetes similar to those present in clinical isolates of antibiotic-resistant bacteria. *Proceedings of the National Academy of Science USA*, **1973**, 70(8), 2276-2280.

Blades, A.T.; Ikonomou, M.G.; Kebarle, P. Mechanism of electrospray mass spectrometry: Electrospray as an electrolysis cell. *Analytical Chemistry*, **1991**, 63, 2109-2114.

Blancafort, P.; Steinberg, S.V.; Paquin, B.; Klinck, R.; Scott, J.K.; Cedergren, R. The recognition of a noncanonical RNA base pair by a zinc finger protein. *Chemistry & Biology*, **1999**, 6, 585-597.

Blaszczyk, J.; Gan, J.; Tropea, J.E.; Court, D.L.; Waugh, D.S.; Ji, X. Noncatalytic assembly of ribonuclease III with double-stranded RNA. *Structure*, **2004**, 12, 457-466.

Bligh, A.S.W.; Haley, H.; Lowe, P.N. Measurement of dissociation constants of inhibitors binding to Src SH2 protein by non-covalent electrospray ionization mass spectroscopy. *Journal of Molecular Recognition*, **2003**, 16, 139-147.

Boehm, H. The computer program, LUDI: a new method for the de novo design of enzyme inhibitors. *Journal of Computer-aided Molecular Design,* **1992**, 6, 61-78.

Borovinskaya, M.A., Pai, R.D., Zhang, W., Schuwirth, B.S., Holton, J.M., Hirokawa, G., Kaji, H., Kaji, A., Cate, J.H.D Structural basis for aminoglycoside inhibition of bacterial ribosome recycling. *Nature Structural & Molecular Biology*, **2007**, 14, 727-732.

Braisted, A.C.; Wells, J.A. Minimizing a binding domain from protein A. *Proceedings of the National Academy of Sciences USA*, **1996**, 93, 5688-5692.

Brenner, S.; Jacob, F.; Meselson, M. An unstable intermediate carrying information from genes to ribosomes for protein synthesis. *Nature*, **1961**, 190, 576-581.

Brenowitz, M.; Chance, M.R.; Dhavan, G.; Takamoto, K. Probing the structural dynamics of nucleic acids by quantitative time-resolved and equilibrium hydroxyl radical "footprinting". *Current Opinion in Structural Biology*, **2002**, 12, 648-653.

Brimacombe, R.; Atmadja, J.; Stiege, W.; Schüler, D. A detailed model of the three-dimensional structure of E. coli 16S ribosomal RNA in situ in the 30S subunit. *Journal of Molecular Biology*, **1988**, 199, 115-136.

Brimacombe,R. The structure of ribosomal RNA: a three dimensional jigsaw puzzle. *European Journal of Biochemistry*, **1995**, 230, 365-383.

Brink, M.F.; Ph.Verbeet, M.; A.de Boer, H. Formation of the central pseudoknot in 16S is essential for initiation of translation. *The EMBO Journal,* **1993**, 12, 3987-3996.

Brion, P; Westhof, E. Hierarchy and dynamics of RNA folding. *Annual Review of Biophysics and Biomolecular Structure,* **1997**, 26,113-37.

Brock, S.; Szkaradkiewicz, K.; Sprinzl, M. Initiation factors of protein biosynthesis in bacteria and their structural relationship to elongation and termination factors. *Molecular Microbiology*, **1998**, 29, 409-417.

Brodersen, D.E.; Clemons, W.M.; Carter, A.P.; Morgan-Warren, R.J.; Wimberly, B.T.; Ramakrishnan, V. The structural basis for the action of the antibiotics tetracycline, pactamycin, and hygromycin B on the 30S ribosomal subunit. *Cell*, **2000**, 103**,** 1143-1154

Brodsky, A.S.; Williamson, J.R. Solution structure of the HIV-2 TAR-argininamide complex. *Journal of Molecular Biology*, ***1997***, 267, 624-639

Brown. T.; Leonard, G.A.; Booth, E.D.; Kneale, G Influence of pH on the conformation and stability of mismatch base-pairs in DNA. *Journal of Molecular Biology*, **1990**, 212, 437-440.

Brunner, C.; Wirth, T. Btk expression is controlled by Oct and BOB.1/OBF.1. *Nucleic Acids Research*, **2006**, 34(6), 1807-1815.

Cai, Z.; Gorin, A.; Frederick, R.; Ye, X.; Hu, W.; Majumdar, A.; Kettani, A.; Patel, D.A. Solution structure of P22 transcriptional antitermination N peptide-boxB RNA complex. *Nature Structural Biology*, **1998**, 5, 203-212.

Calero, G.; Wilson, K.F.; Ly, T.; Rios-Steiner, J.L.; Clardy, J.C.; Cerione, R.A. Structural basis of m7GpppG binding to the nuclear cap binding protein complex. *Nature Structural Biology*, **2002**, 9, 912-917.

Calnan, B.J.; Biancalana, S.; Hudson, D.; Frankel, A.D. Analysis of arginine-rich peptides from the HIV Tat protein reveals unusual features of RNA-protein recognition. *Genes Development,* **1991**, 5, 201-210.

Calnan, B.J.; Tidor, B.; Biancalana, S.; Hudson, D.; Frankel, A.D. Arginine-mediated RNA recognition: the arginine fork. *Science*, **1991**, 252, 1167-1171.

Cannone, J.J.; Subramanian, S.; Schnare, M.N.; Collett, J.R.; D'Souza, L.M.; Du, Y.; Feng, B.; Lin, N.; Madabusi, L.V.; Muller, K.M. et al. The Comparative RNA Web (CRW) Site: an online database of comparative sequence and structure information for ribosomal, intron, and other RNAs**.** *BMC Bioinformatics*, **2002**, 3, 2-32.

Carter, A.P.; Clemons, W.M.; Brodersen, D.E.; Morgan-Warren, R.J.; Hartsch, T.; Wimberly, B.T.; Ramakrishnan, V. Crystal structure of an initiation factor bound to the 30*S* ribosomal subunit. *Science*, **2000**, 291, 498-501.

Carter, A.P.; Clemons, W.M.; Brodersen, D.E.; Morgan-Warren, R.J.; Wimberly, B.T.; Ramakrishnan, V. Functional insights from the structure of the 30S ribosomal subunit and its interactions with antibiotics. *Nature*, **2000**, 407, 340-348.

Cate, J.H.; Yusupov, M.M; Yusupova, G, Zh.; Earnest, T.N.; Noller, H.F X-ray crystal structures of 70*S* ribosome functional complexes. *Science*, **1999**, 285, 2095-2104.

Cavalli, L.L; Maccacaro, G.A Polygenic inheritance of drug-resistance in the bacterium *Escherichia coli*. *Heredity*, **1952**, 6, 311-331.

Cavanagh, J.; Benson, L.M.; Thompson, R.; Naylor, S. In line desalting mass spectroscopy for the study of noncovalent biological complexes. *Analytical Chemistry*, **2003**, 75, 3281-3286.

Celander, D.W. Probing RNA structures with hydroxyl radicals. *Current Protocol in Nucleic Acid Chemistry*, **2000**, 6.5.1.-6.5.6.

Celander, D.W.; Cech, T.R. Iron(II)-ethylenediaminetetraacetic acid catalyzed cleavage of RNA and DNA oligonucleotides: similar reactivity toward single- and double-stranded forms. *Biochemistry*, **1990**, 29, 1355-1361.

Chen, D. Z. *et al.* Actinonin, a naturally occurring antibacterial agent is a potent peptide deformylase inhibitor. *Biochemistry,* **2000***,* 39, 1256-1262.

Cheng, A.C.; Calabro, V.; Frankel, A.D. Design of RNA-binding proteins and ligands. *Current Opinion in Structural Biology*, **2001**, 11, 478-484.

Cheng, X.; Gale, D.C.; Udseth, H.R.; Smith, R.D. Charge state reduction of oligonucleotide negative ions from electrospray ionization. *Analytical Chemistry*, **1995**, 67, 586-593.

Cheng, X.; Gao, Q.; Smith, R.D.; Jung, K.; Switzer, C. Comparison of 3′, 5′- and 2′, 5′-linked DNA duplex stabilities by electrospray ionization mass spectrometry. *Chemical Communications*, **1996**, 747.

Cheng, X.; Harms, A.C.; Gondreau, P.N.; Terwilliger, T.C.; Smith, R.D. Direct measurement of oligonucleotide binding stoichiometry of gene V protein by mass spectrometry. *Proceedings of National Academy Sciences USA*, **1996**, 93, 7022-7027.

Chopra, I., Hodgson, J., Metcalf, B. & Poste, G. The search for antimicrobial agents effective against bacteria resistant to multiple antibiotics. *Antimicrobial Agents and Chemotherapy,* **1997**, 41, 497-503.

Chow, C.S.; Bogdan, F.M. A structural basis for RNA-ligand interactions. *Chemical Reviews,* **1997,** 97, 1489□1513.

Chowdhury, S.K.; Katta, V.; Chait, B.T. Probing conformational changes in proteins by mass spectroscopy. *Journal of American Chemical Society*, **1990**, 112, 9012-9013.

Chui, H.M.; Desaulniers, J.P.; Scaringe, S.A.; Chow, C.S. Synthesis of helix 69 of *Escherichia coli* 23S rRNA containing its natural modified nucleosides, $m^3\Psi$ and Ψ. *Journal of Organic Chemistry*, **2002**, 67, 8847-8854

Clery, A.; Blatter, M.; Allain, F.H. RNA recognition motifs: boring? Not quite. *Current Opinion in Structural Biology*, **2008**, 18, 290-298.

Clewell, D.B.; Gawron-Burke, C. Conjugative transposons and the dissemination of antibiotic resistance in *Streptococci*. *Annual Review of Microbiology*, **1986**, 40, 635-659.

Cochella, L., Green, R. An active role for tRNA in decoding beyond codon:anticodon pairing. *Science*, **2005**, 308, 1178-1180.

Cole, B.R. Some tenets pertaining to electrospray ionization mass spectroscopy. *Journal of Mass Spectrometry*, **2000**, 35, 763-772.

Cole, S.T., R. Brosch, et al. Deciphering the biology of *Mycobacterium tuberculosis* from the complete genome sequence. *Nature*, **1998**, 393, 537-544.

Coonan, K.M.; Kaplan, E.L. *In vitro* susceptibility of recent North American group A *streptococcal* isolates to eleven oral antibiotics. *The Pediatric Infectious Disease Journal*, **1994**, 13, 630-635.

Cordingley, M.G.; LaFemina, R.L.; Callahan, P.L.; Condra, J.H.; Sardana, V.V.; Graham, D.J.; Nguyen, T.M.; LeGrow, K.; Gotlib, L.; Schlabach, A.J. Sequence-specific interaction of Tat protein and Tat peptides with the transactivation-

responsive sequence element of human immunodeficiency virus type 1 in vitro. *Proceedings of the National Academy of Sciences USA,* **1990**, 87, 8985-8989.

Correll, C.C.; Freeborn, B.; Moore, P.B.; Steitz, T.A. Metals, motifs, and recognition in the crystal structure of a 5 S rRNA domain. *Cell*, **1997**, 91, 705-712.

Correll, C.C.; Munishkin, A.; Chan, Y.; Ren, Z.; Wool, I.G.; Steitz, T.A. Crystal structure of the ribosomal RNA domain essential for binding elongation factors. *Proceedings of the National Academy of Science USA*, **1998**, 95(23), 13436-13441.

Cortese, R.; Felici, F.; Galfre, G. et al. Epitope discovery using peptide libraries displayed on phage. *Trends in Biotechnology*, **1994**, 12, 262-7.

Corthe´sy, B.; Kao, P.N. Purification by DNA affinity chromatography of two polypeptides that contact the NF-AT DNA binding site in the interleukin 2 promoter. *Journal of Biological Chemistry*, **1994**, 269, 20682-20690.

Crick, F. Central dogma of molecular biology. *Nature*, **1970**, 227, 561-563.

Crofton, J.; Mitchison, D.A. Streptomycin resistance in pulmonary tuberculosis. *British Medical Journal*, **1948**, 2, 1009-1015.

Culver, G.M.; Cate, J.H.; Yusupova, G, Zh.; Yusupov, M.M.; Noller, H.F. Identification of an RNA-Protein bridge spanning the ribosomal subunit interface. *Science,* **1999**, 285, 2133-2135.

Cwirla, S.E.; Peters, E.A.; Barrett, R.W.; Dower, W.J. Peptides on phage: A vast library of peptides for identifying ligands. *Proceedings of the National Academy of Sciences USA*, **1990**, 87, 6378-82.

Daniel, J. M.; Friess, S.D.; Rajagopalan, S.; Wendt, S.; Zenobi, R. Quantitiative determination of noncovalent binding interactions using soft ionization mass spectroscopy. *International Journal of Mass Spectrometry*, **2002**, 216, 1-27.

Danner, S.; Belasco, J.G. T7 phage display: a novel genetic selection system for cloning RNA-binding proteins from cDNA libraries. *Proceedings of the National Academy of Sciences USA*, **2001**, 98(23), 12954-12959.

Davidovich, A.; Belousoff, M.; Bashan, A.; Yonath, A. The evolving ribosome: from non-coded peptide bond formation to sophisticated translation machinery. *Research in Microbiology*, **2009**, 18, 1-6.

de Cock, E.; Springer, M.; Dardel, F. The interdomain linker of *Escherichia coli* initiation factor IF3: a possible trigger of translation initiation specificity. *Molecular Microbiology*, **1999**, 32**,** 193-202.

Deo, R.C.; Bonanno, J.B.; Sonenberg, N.; Burley, S.K. Recognition of polyadenylate RNA by the poly(A)-binding protein. *Cell*, **1999**, 98, 835-845.

Devlin, J.J; Panganiban, L.C.; Devlin, P.E. Random peptide libraries: a source of specific protein binding molecules. *Science*, **1990**, 249, 404-6.

Diep, B.A.; Gill, S.R.; Chang, R.F.; Phan, T.H.; Chen, J.H.; Davidson, M.G.; Lin, F.; Lin, J.; Carleton, H.A.; Mongodin, E.F.; Sensabaugh, G.F.; Perdreau-Remington, F. Complete genome sequence of USA300, an epidemic clone of community-acquired meticillin-resistant *Staphylococcus aureus*. *The Lancet*, **2006**, 367, 731-739.

Dingwall, C.; Ernberg, I.; Gait, M.J.; Green, S.M.; Heaphy, S.; Karn, J.; Lowe, A.D.; Singh, M.; Skinner, M.A. HIV-1 tat protein stimulates transcription by binding to a

U-rich bulge in the stem of the TAR RNA structure. EMBO Journal, **1990**, 9(12), 4145-4153.

Djojonegoro, B.M.; Benedik, M.J.; Willson, R.C. Bacteriophage surface display of an immunoglobulin–binding domain of *Staphylococcus aureus* protein A. *Bio/Technology*, **1994**, 12, 169-172.

Doktycz, M.J.; Habibi-Goudarzi, S.; McLuckey, S.A. Accumulation and storage of ionized duplex DNA molecules in a quadrupole ion trap. *Analytical Chemistry*, **1994**, 66, 3416-3422.

Dole, M.; Mack, L.L.; Hines, R.L.; Mobley, R.C.; Ferguson, L.D.; Alice, M.B. Molecular beams of macroions. *Journal of Chemical Physics*, **1968**, 49, 2240-2249.

Doorbar, J.; Winter, G. Isolation of a peptide antagonist to the thrombin receptor using phage display. *Journal of Molecular Biology*, **1994**, 244, 361-9.

Döring, T.; Mitchell, P.; Osswald, M.; Bochkariov, D.; Brimacombe, R. The decoding region of 16S RNA; a cross-linking study of the ribosomal A, P and E sites using tRNA derivatized at position 32 in the anticodon loop. *EMBO Journal*, **1994**, 13(11), 2677-2685.

Dorsey, B.D.; Levin, R.B.; McDaniel, S.L.; Vacca, J.P.; Guare, J.P.; Darke, P.L.; Zugay, J.A.; Emini, E.A.; Schleif, W.A.; Quintero J.C. et al. L-735,524: the design of a potent and orally available HIV protease inhibitor. *Journal of Medicinal Chemistry,* **1994**, 37, 3443-3451.

Dunham, C.M.; Selmer, M.; Phelps, S.S.; Kelley, A.C.; Suzuki, T.; Joseph, S.; Ramakrishnan, V. Structures of tRNAs with an expanded anticodon loop in the decoding center of the 30S ribosomal subunit. *RNA*, **2007**, 13(6), 817-823.

Durant, P.C.; Davis, D.R. Stabilization of the anticodon stem-loop of $tRNA^{lys,3}$ by an A^{+}-C base pair and by pseudouridine. *Journal of Molecular Biology*, **1999**, 285, 115-131.

Ellington, A.D.; Szostak, J.W. *In vitro* selection of RNA molecules that bind specific ligands. *Nature*, **1990**, 346, 818-822.

Elrod-Erickson, M.; Benson, T.E.; Pabo, C.O. High resolution structures of variant Zif268-DNA complexes: implications for understanding zinc finger-DNA recognition. *Structure*, **1998**, 6, 451-464.

Elwell, L.P.; Roberts, M.; Mayer, L.W.; Falkow, S. Plasmid-mediated beta-lactamase production in *Neisseria gonorrhoeae. Antimicrobial Agents and Chemotherapy*, **1977**, 11(3), 528-533.

Enyedy, I.J.; Ling, Y.; Nacro, K.; Tomita, Y.; Wu, X.; Cao, Y.; Guo, R.; Li, B.; Zhu, X.; Huang, Y.; Long, Y.; Roller, P.P.; Yang, D.; Wang, S. Discovery of small-molecule inhibitors of Bcl-2 through structure-based computer screening. *Journal of Medicinal Chemistry,* **2001**, 44, 4313-4324.

Faber, C.; Sticht, H.; Schweimer, K.; Rösch, P. Structural rearrangements of HIV-1 Tat-responsive RNA upon binding of neomycin B. *Journal of Biological Chemistry*, **2000**, 275, 20660-20666.

Fändrich, M.; Tito, M.A.; Leroux, M.R.; Rostom, A.A.; Hartl, F.U.; Dobson, M.C.; Robinson, C.V. Observation of the noncovalent assembly and disassembly pathways of the chaperone complex MtGimC by mass spectrometry. *Proceedings of National Academy Sciences USA, 2000***,** 97, 14151-14155.

Fenn, J.B.; Mann, M.; Meng, C.K.; Wong, S.F.; Whitehouse, C.M. Electrospray ionization for mass spectroscopy of large biomolecules. *Science*, **1989**, 246, 64-71.

Fernandez de la Mora, J. Electrospray ionization of large multiply charged species proceeds via Dole's charged residue mechanism. *Analytica Chimica Acta*, **2000**, 406, 93-104.

Fierro-Monti, I.; Mathews, M.B. Proteins binding to duplexed RNA: one motif, multiple functions. *Trends in Biochemical Sciences,* **2000**, 25, 241-246.

Forbes, G.B. Infection with penicillin-resistant *Staphylococci* in hospital and general practice. *British Medical Journal*, **1949**, 2, 569-571.

Fourmy, D.; Recht, M.I.; Blanchard, S.C.; Puglisi, J.D. Structure of the A-site of *Escherichia coli* 16 S ribosomal RNA complexed with an aminoglycoside antibiotic. *Science*, **1996**, 274, 1367-1371.

Fourmy, D.; Recht, M.I.; Puglisi, J.D. Binding of neomycin-class aminoglycoside antibiotics to the A-site of 16 S rRNA. *Journal of Molecular Biology*, **1998**, 277, 347-362.

Fourmy, D.; Yoshizawa, S.; Puglisi, J.D. Paromomycin binding induces a local conformational change in the A-site of 16 S rRNA. *Journal of Molecular Biology,* **1998**, 277, 333-345.

Franceschi, F.; Duffy, E.M. Structure-based drug design meets the ribosome. *Biochemical pharmacology*, **2006**, 71, 1016-1025.

Frank, J *et al.*; Agrawal, R.K. A model of protein synthesis based on cryo-electron microscopy of the *E. coli* ribosome. *Nature,* **1995***,* 376**,** 441-444.

Frank, J.; Penczek, P.; Grassucci, R.; Srivastava, S. Three-dimensional reconstruction of the 70 S Escherichia coli ribosome in ice: the distribution of ribosomal RNA. *The Journal of Cell Biology,* **1991***,* 115, 597-605.

Frank, J.; Sengupta, J.; Gao, H.; Li, W.; Valle, M.; Zavialov, A.; Ehrenberg, M. The role of tRNA as a molecular spring in decoding, accommodation, and peptidyl transfer. *FEBS Letters,* **2005**, 579, 959-962.

Frankel, A.D. Activation of HIV transcription by Tat. *Current Opinion in Genetics & Development*, **1992**, 2, 293-298.

Franklin, R.E.; Gosling, R. Molecular configuration in sodium thymonucleate. *Nature*, **1953,** *171*, 740-741.

Freistroffer, D.V., Pavlov, M.Y., MacDougall, J., Buckingham, R.H., Ehrenberg, M. Release factor RF3 in *E. coli* accelerates the dissociation of release factors RF1 and RF2 from the ribosome in a GTP dependent manner. *The EMBO Journal*, **1997**, 16, 4126-4133.

Friesen, W.J; Darby, M.K. Phage display of RNA binding zinc fingers from transcription factor IIIA. *Journal of Biological Chemistry*, **1997**, 272, 10994-10997.

Friesen, W.J; Darby, M.K. Specific RNA binding proteins constructed from zinc fingers. *Nature Structural Biology*, **1998**, 5, 543-546.

Fuh, G.; Pisabarro, T. M.; Li, Y.; Quan, C.; Lasky, L.A.; Sidhu, S.S. Analysis of PDZ domain-ligand interactions using carboxyl-terminal phage display. *Journal of Biological Chemistry,* **2000**, 275, 21486-21491.

Fuh, G.; Sidhu, S.S. Efficient phage display of polypeptides fused to the carboxy-terminus of the M13 gene-3 minor coat protein. *FEBS Letters*, **2000**, 480, 231-4.

Gabelica, V.; De Pauw, E. Comparison between solution-phase stability and gas-phase kinetic stability of oligodeoxynucleotide duplexes. *Journal of Mass Spectrometry*, 2001, 36, 397-402.

Gabelica, V.; Galic, N.; Rosu, F.; Houssier, C.; De Pauw, E. Influence of response factors on determining equilibrium association constants of non-covalent complexes by electrospray ionization mass spectrometry. *Journal of Mass Spectrometry*, **2003**, 38, 491-501.

Gale, D. C.; Goodlett, D. R.; Light-Wahl, K. J.; Smith, R. D. Observation of duplex DNA-drug noncovalent complexes by electrospray ionization mass spectrometry. *Journal of American Chemical Society*, **1994**, 116, 6027-6028.

Gamero-Castaño, M.; Fernandez de la Mora, J. Kinetics of small ion evaporation from the charge and mass distribution of multiply charged clusters in electrosprays. *Journal of Mass Spectrometry*, **2000**, 35, 790-803.

Ganem, B.; Li, Y.T.; Henion, J.D. Detection of noncovalent receptor-ligand complexes by mass spectrometry. *Journal of American Chemical Society,* **1991**, 113, 6294-6296.

Gao, C.; Mao, S.; Lo, C.L.; Wirsching, P.; Lerner, R.A.; Janda, K.D. Making artificial antibodies: A format for phage display of combinatorial heterodimeric arrays. *Proceedings of the National Academy of Sciences USA*, **1999**, 96(11), 6025-6030.

Gao, J., Cheng, X., Chen, R., Sigal, G. B., Bruce, J. E., Schwartz, B. L., Hofstadler, S. A., Anderson, G. A., Smith, R. D., and Whitesides, G. M. Screening derivatized peptide libraries for tight binding inhibitors to carbonic anhydrase II by

electrospray ionization-mass spectrometry. *Journal of Medicinal Chemistry*, **1996**, 39, 1949-1955.

Garner, M.M.; Revzin, A. A gel electrophoresis method for quantifying the binding of proteins to specific DNA regions: application to components of the *Escherichia coli* lactose operon regulatory system. *Nucleic Acids Research*, **1981**, 9, 3047-60.

Garrey, S.M.; Cass, D.M.; Wandler, A.M.; Scanlan, M.S; Berglund, J.A. Transposition of two amino acids changes a promiscuous RNA binding protein into a sequence-specific RNA binding protein. *RNA*, **2008**, 14(1), 78-88.

Gelman, M.A.; Richter, S.; Cao, H.; Umezawa, N.; Gellman, S.H.; Rana, T.M. Selective binding of tar rna by a tat-derived β-peptide. *Organic Letters*, **2003**, 5, 3563-3565.

Gidden, J.; Baker, E.S.; Ferzoco, A.; Bowers, M.T. Structural motifs of DNA complexes in the gas phase. *International Journal of Mass Spectrometry*, **2005**, 240, 183-193.

Gissel, B.; Jensen, M.R.; Gregorius, K.; Elsner, H.I.; Svendsen, I.; Mouritsen, S. Identification of avidin and streptavidin binding motifs among peptides selected from a synthetic peptide library consisting solely of D-amino acids. *Journal of Peptide Science*, **1995**, 1, 217-226.

Goldman, E.R.; Balighian, E.D.; Mattoussi, H.; Kuno, M.K.; Mauro, J.M.; Tran, P.T.; Anderson, G.P. Avidin: A natural bridge for quantum dot-antibody conjugates. *Journal of American Chemical Society,* **2002**, 124, 6378-6382.

Goodford, P. A computational procedure for determining energetically favorable binding sites on biologically important macromolecules. *Journal of Medicinal Chemistry,* **1985**, 28, 849-857.

Gravel, M.; Melancon, P.; Brakier-Gingras, L. Cross-linking of streptomycin to the 16 S ribosomal RNA of *Escherichia coli*. *Biochemistry*, **1987**, 26, 6227-6232.

Greco, F.; Lugiori, A.; Sidona, G.; Uccella, N. Gas-phase proton affinity of deoxyribonucleosides and related nucleobases by fast-atom-bombordment tanden mass-spectroscopy. *Journal of American Chemical Society*, **1990**, 112, 9092-9096.

Green, R.; Noller, H.F. Ribosomes and translation. *Nature*, **1997**, 66, 679-716.

Green, S.R.; Mathews, M.B. Two RNA-binding motifs in the double-stranded RNA activated protein kinase, DAI. *Genes & Development*, **1992**, 6, 2478-2490.

Green-Church, K.B..; Limbach, P.A. Mononucleotide gas-phase proton affinities as determined by the kinetic method. *Journal of American Society for Mass Spectrometry*, **2000**, 11, 24-32.

Greig, M. J., Gaus, H., Cummins, L. L., Sasmor, H., and Griffey, R. H. Measurement of macromolecular binding using electrospray mass spectrometry. Determination of dissociation constants for oligonucleotide: Serum albumin complexes. *Journal of American Chemical Society,* **1995**, 117, 10765-6.

Greig, M.; Griffey, R.H. Utility of organic bases for improved electrospray mass spectrometry of oligonucleotides. *Rapid Communication in Mass Spectrometry*, **1995**, 9, 97-102.

Greig, M.J.; Gaus, H,; Cummins, L.I.; Sasmor, H.; Griffey, R.H. Measurement of macromolecular binding using electrospray mass spectrometry. Determination of dissociation constants for oligonucleotide: serum albumin complexes. *Journal of American Chemical Society*, **1995**, 117, 10765-10766.

Grentzmann, G., Brechemier-Baey, D., Heurgue, V., Mora, L., and Buckingham, R.H. Localisation and characterisation of the gene encoding release factor RF3 in *Escherichia coli. Proceedings of the National Academy of Science USA*, **1994**, 91, 5848-5852.

Griep, R.A., van Twisk, C.; van der Wolf, J.M.; Schots, A. Fluobodies: green fluorescent single-chain Fv fusion proteins. *Journal of Immunological Methods*, **1999**, 230, 121-30.

Griffey, R.H.; Greig, M. In detection of base pair mismatches in duplex DNA and RNA oligonucleotides using electrospray mass spectrometry. *Proceedings of SPIE-International Society for Optical Engineering,* **1997**, 9605.

Griffey, R.H.; Greig, M.; An, H.; Sasmor, H.; Manalili, S. Targeted site-specific gas-phase cleavage of oligoribonucleotides. Application in mass spectrometry-based identification of ligand binding sites. *Journal of American Chemical Society*, **1999,** *121*, 474-475.

Griffey, R.H.; Sannes-Lowery, K.A.; Drader, J.J.; Mohan, V.; Swayze, E.E.; Hofstadler, S.A. Characterization of low-affinity complexes between RNA and small molecules using electrospray ionization mass spectrometry. *Journal of American Chemical Society,* **2000,** 122*,* 9933-9938.

Griffith, M.C.; Risen, L.M.; Greig, M.J.; Lesnik, E.A.; Sprankle, K.G.; Griffey, R.H.; Kiely, J.S.; Freier, S.M. Single and bis peptide nucleic acids as triplexing agents: binding and stoichiometry. *Journal of American Chemical Society*, **1995**, 117, 831-832.

Gromadski, K.B.; Rodnina, M.V. Streptomycin interferes with conformational coupling between codon recognition and GTPase activation on the ribosome. *Nature Structural & Molecular Biology*, **2004**, 11, 316-322.

Gualerzi, C.O.; Brandi, L.; Caserta, E.; Garofalo, C.; Lammi, M.; LATeana, A.; Petrelli, D.; Spurio, R.; Tomsic, J.; Pon, C.L. Initiation factors in the early event of mRNA translation in bacteria *The Ribosome. Cold Spring Harbor Symposia in Quantitative Biology Volume LXVI*, **2001**, Cold Spring Harbor Laboratory Press, Cold Spring Harbor, 363-376.

Gualerzi, C.O.; Pon, C.L. Initiation of mRNA translation in prokaryotes. *Biochemistry*, **1990**, 29, 5881-5889.

Gupta, A.; Onda, M.; Pastan, I.; Sankar Adhya, S.; Chaudhary, V.K. High-density functional display of proteins on bacteriophage lambda. *Journal of Molecular Biology*, **2003**, 334, 241-254.

Gutell, R.R. Collection of small subunit (16 S- and 16 S-like) ribosomal RNA structures. *Nucleic Acids Research*, **1993**, 21, 3051-3054.

Gutell, R.R.; Fox, G.E. A compilation of large subunit RNA sequences presented in a structural format. *Nucleic Acids Research,* **1988**, 16(Suppl), r175-r269.

Haddad, J.; Kotra, L.P.; Llano-Sotelo, B.; Kim, C.; Azucena, E.F.; Liu, M.; Vakulenko, S.B.; Chow, C.S.; Mobashery, S. Design of novel antibiotics that bind to the

ribosomal acyltransfer site. *Journal of American Chemical Society*, **2002**, 124, 3229-3237.

Hall, R.M.; Collis, C.M.; Kim. M.; Partridge, S.R.; Recchia, G.D.; Stokes, H.W. Mobile gene cassettes and integrons in evolution. *Annals of the New York Academy of Sciences*, **1999**, 870, 68-80.

Hamy, F.; Felder, E.R.; Heizmann, G.; Lazdins, J.; Aboul-ela, F.; Varani, G.; Karn, J.; Klimkait, T. An inhibitor of the Tat/TAR RNA interaction that effectively suppresses HIV-1 replication. *Proceedings of the National Academy of Sciences USA*, **1997**, 94, 3548-3553.

Handa, N.; Nureki, O.; Kurimoto, K.; Kim, I.; Sakamoto, H.; Shimura, Y.; Muto, Y.; Yokoyama, S. Structural basis for recognition of the *tra* mRNA precursor by the Sex-lethal protein. *Nature,* **1999**, 398, 579-585.

Hansen, J.L.; Ippolito, J.A.; Ban, N.; Nissen, P.; Moore, P.B.; Steitz, T.A. The structures of four macrolide antibiotics bound to the large ribosomal subunit. *Molecular Cell*, **2002**, 10, 117-128.

Hansen, J.L.; Moore, P.B.; Steitz, T.A. Structures of five antibiotics bound at the peptidyl transferase center of the large ribosomal subunit. *Journal of Molecular Biology*, **2003**, 330, 1061-1075.

Hanson, C.L.; Fucini, P.; Ilag, L.L.; Nierhaus, K.H.; Robinson, C.V. Dissociation of intact *Escherichia coli* ribosomes in a mass spectrometer. *Journal of Biological Chemistry*, **2003**, 278(2), 1259-1267.

Harms, J. et al. High resolution structure of the large ribosomal subunit from a mesophilic eubacterium. *Cell*, **2001**, 107(5), 679-688.

Harms,J.; Schluenzen, F.; Fucini, P.; Bartels**,** H.; Yonath A. Alterations at the peptidyl transferase centre of the ribosome induced by the synergistic action of the streptogramins dalfopristin and quinupristin. *BMC Biology*, **2004**, 2, 1741- 47.

Harper, K.; Kerschbaumer, R.J.; Ziegler, A. et al. A scFv-alkaline phosphatase fusion protein which detects potato leafroll luteovirusin plant extracts by ELISA. *Journal of Virological Methods*, **1997**, 63, 237-42.

Hawkins, R.E.; Russell, S.J.; Winter, G. Selection of phage antibodies by binding affinity- Mimicking affinity maturation. *Journal of Molecular Biology*, **1992**, 226, 889-96.

Hecht, L.I.; Stephenson, M.L.; Zamecnik, P.C. Binding of amino acids to the end group of a soluble ribonucleic acid. *Proceedings of the National Academy of Science USA*, **1959**, 45(4), 505-518.

Hertzberg, R.P.; Dervan, P.B. Cleavage of DNA with methidiumpropyl-EDTA-iron(II): reaction conditions and product analyses. *Biochemistry*, **1984**, 23, 3934-3945.

Hill, H.R.; Stockley, P.G. Phage presentation. *Molecular Microbiology*, **1996**, 20, 685-92.

Hirabayashi, N., Sato, N.S., and Suzuki, T. Conserved loop sequence of helix 69 in *Escherichia coli* 23 S rRNA is involved in A-site tRNA binding and translational fidelity. *Journal of Biological Chemistry*, **2006**, 281, 17203-17211.

Hofstadler, S.A.; Griffey, R.H. Analysis of noncovalent complexes of DNA and RNA by mass spectrometry. *Chemical Reviews*, **2001**, 101, 377-390.

Hofstadler, S.A.; Sannes-Lowery, K.A.; Crooke, S.T.; Ecker, D.J.; Sasmor, H.; Manalili, S.; Griffey, R.H. Multiplexed screening of neutral mass-tagged RNA targets against ligand libraries with electrospray ionization FTICR MS: A paradigm for

high-throughput affinity screening. *Analytical Chemistry*, **1999**, 71(16), 3436–3440.

Houghten, R.A.; Pinilla, C.; Blondelle, S.E.; Appel, J.R.; Dooley, C.T.; Cuervo, J.H. Generation and use of synthetic peptide combinatorial libraries for basic research and drug discovery. *Nature*, **1991**, 354, 84-86.

Hubbard, J.M.; Hearst, J.E. Computer modeling 16 S ribosomal RNA. *Journal of Molecular Biology,* **1991**, 221, 889-907.

Hunter, W.N.; Brown, T.; Anand, N.N.; Kennard, O. Structure of an adenine-cytosine base pair in DNA and its implications for mismatch repair. *Nature*, **1986**, 320, 552-555.

Huq, I.; Ping, Y.; Tamilarasu, T.; Rana, T.M. Controlling human immunodeficiency virus type 1 gene expression by unnatural peptides. *Biochemistry*, **1999**, 38, 5172-5177.

Huq, I.; Wang, X.; Rana, T.M. Specific recognition of HIV-1 TAR RNA by a D-Tat peptide. *Nature Structural Biology*, **1997**, 11, 881-882.

Hwang, S.; Tamilarasu, N.; Ryan, K.; Huq, I.; Richter, S.; Still, W.C.; Rana, T.M. Inhibition of gene expression in human cells through small molecule-RNA interactions. *Proceedings of the National Academy of Science USA*, **1999**, 96, 12997-13002.

Iavarone, A.T.; Udekwu, O.A.; Williams, E.R. Buffer loading for counteracting metal salt-induced signal suppression in electrospray ionization. *Analytical Chemistry*, **2004**, 76 (14), 3944-3950.

Iribarne, J.V.; Thomson, B.A. On the evaporation of small ions from charged droplets. *Journal of Chemical Physics*, **1976**, 64, 2287-2294.

Jamieson, A.C.; Kim, S.; Wells, J.A. In vitro selection of zinc fingers with altered DNA-binding specificity. *Biochemistry*, **1994**, 33, 5689-5695.

Jiang, F.; Gorin, A.; Hu, W.; Majumdar, A.; Baskerville, S.; Xu, W.; Ellington, A.; Patel, D.J. Anchoring an extended HTLV-1 Rex peptide within an RNA major groove containing junctional base triples. *Structure*, **1999**, 7 (12), 1461-1472.

Johansson, C.; Finger, L.D.; Trantirek, L.; Mueller, T.D.; Kim, S.; Laird-Offringa, I.A.; Feigon, J. Solution structure of the complex formed by the two N-terminal RNA-binding domains of nucleolin and a pre-rRNA target. *Journal of Molecular Biology*, **2004**, 337, 799-816.

Johansson, D.; Jessen, C.H.; Pøhlsgaard, J.; Jensen, K.B.; Vester, B.; Pedersen, E.B.; Nielsen, P. Design, synthesis and ribosome binding of chloramphenicol nucleotide and intercalator conjugates. *Bioorganic & Medicinal Chemistry Letters*, **2005**, 15, 2079-2083.

Jones, K.A.; Peterlin, M.B. Control of RNA initiation and elongation at the HIV-1 promoter. *Annual Review of Biochemistry*, **1994**, 63, 717-743.

Kaminishi, T., Wilson, D.N., Takemoto, C., Harms, J.H., Kawazoe, M., Schluenzen, F., Hanawa-Suetsugu, K., Shirouzu, M., Fucini, P., Yokoyama, S. A snapshot of the 30 S ribosomal subunit capturing mRNA via the shine-dalgarno interaction. *Structure*, **2007**, 15(3), 289-297.

Karimi, R.; Pavlov, M.Y.; Buckingham, R.H.; Ehrenberg, M. Novel roles for classical factors at the interface between translation termination and initiation. *Molecular Cell*, **1999**, 3, 601-609.

Kaul, M.; Barbieri, C.M.; Pilch, D.S. Fluorescence-based approach for detecting and characterizing antibiotic-induced conformational changes in ribosomal RNA: comparing aminoglycoside binding to prokaryotic and eukaryotic ribosomal RNA sequences. *Journal of the American Society,* **2004**, 126, 3447-453.

Kebarle, P. A brief overview of the present status of the mechanisms involved in electrospray mass spectrometry. *Journal of Mass Spectrometry***, 2000**, 35, 804-817.

Kebarle, P.; Peschke, M. On the mechanisms by which the charged droplets produced by electrospray lead to gas phase ions. *Analytica Chimica Acta*, **2000**, 406, **11**-35.

Kebarle, P.; Tang, L. From ions in solution to ions in the gas phase - the mechanism of electrospray mass spectrometry. *Analytical Chemistry*, **1993**, 65 (22), 972A-986A.

Khanna, H.; Akimoto, M.; Siffroi-Fernandez, S.; Friedman, J.S.; Hicks, D.; Swaroop, A. Retinoic acid regulates the expression of photoreceptor transcription factor NRL. *Journal of Biological Chemistry*, **2006**, 281, 27327-27334.

Kieltyka, J.W.; Chow, C.S. Probing RNA hairpins with cobalt(III)hexammine and electrospray ionization mass spectrometry. *Journal of the American Society for Mass Spectrometry*, **2006**, 17, 1376-1382.

Kipper, K.; Het´enyi, C.; Sild, S.; Remme, J.; Liiv, A. Ribosomal intersubunit bridge B2a is involved in factor-dependent translation initiation and translational processivity. *Journal of Molecular Biology,* **2009**, 382, 405-422.

Kisselev, L.L.; Buckingham, R.H. Translation termination comes of age. *Trends in Biochemical Sciences*, **2000**, 25, 561-566.

Klaholz, B.P.; Myasnikov, A.G.; Heel, M.V. Visualization of release factor 3 on the ribosome during termination of protein synthesis. *Nature*, **2004**, 427, 862-865.

Klaholz, B.P.; Pape, T.; Zavialov, A.V.; Myasnikov, A.G.; Orlova, E.V.; Vestergaard, B.; Ehrenberg, M.; Heel, M.V. Structure of the *Escherichia coli* ribosomal termination complex with release factor 2. *Nature*, **2003**, 421, 90-94.

Klein, D.J.; Moore, P.B.; Steitz, T.A. The roles of ribosomal proteins in the structure assembly, and evolution of the large ribosomal subunit. *Journal of Molecular Biology*, **2004**, 340(1), 141-77.

Klingeren, B.V.; Embden, J.D.A.; Dessens-Kroon, M. Plasmid-mediated chloramphenicol resistance in *Haemophilus influenzae. Antimicrobial Agents and Chemotherapy*, **1977**, 11(3), 383-387.

Knapp, G. Enzymatic approaches to probing of RNA secondary and tertiary structure. *Methods Enzymol*ogy, **1989**, 180, 192-212.

Knowles, J. R. Penicillin resistance: the chemistry of beta-lactamase inhibition. *Accounts of Chemical Research,* **1985***,* 18, 97-105.

Konings, D.A.; Gutell, R.R. A comparison of thermodynamic foldings with comparatively derived structures of 16 S and 16 S-like rRNAs. *RNA*, **1995**, 1, 559-574.

Korostelev, A.; Trakhanov, S.; Laurberg, M.; Noller, H.F. Crystal structure of a 70 S ribosome-tRNA complex reveals functional interactions and rearrangements. *Cell*, **2006**, 126 (6), 1065-1077.

Kothe, U.; Wieden, H.; Mohr, D.; Rodnina, M.V. Interaction of helix D of elongation factor Tu with helices 4 and 5 of protein L7/12 on the ribosome. *Journal of Molecular Biology*, **2004**, 336, 1011-10 21.

Kowalak, J.A., Bruenger, E., Hashizume, T., Peltier, J.M., Ofengand, J., McCloskey, J.A. Structural characterization of U*-1915 in domain IV from *Escherichia coli* 23 S ribosomal RNA as 3-methylpseudouridine. *Nucleic Acids Research,* **1996***,* 24, 688-693.

Kuimelis, R.G.; McLaughlin, L.W. Mechanisms of ribozyme mediated RNA cleavage. *Chemical Reviews*, **1998**, 98, 1027-1044.

Kuntz, I., Blaney, J., Oatley, S., Langridge, R., and Ferrin, T. A geometric approach to macromolecular-ligand interactions. *Journal of Molecular Biology,***1982**, 161, 269-288.

Ladner, R.C. et al. Phage display-derived peptides as therapeutic alternatives to antibodies. *Drug Discovery Today*, **2004**, 9, 525-529.

Laird-Offringa, I.A.; Belasco, J.G. Analysis of RNA-binding proteins by in vitro genetic selection: identification of an amino acid residue important for locking U1A onto its RNA target. *Proceedings of the National Academy of Sciences USA*, **1995**, 92, 11859-11863.

Lam, K.S.; Lebl, M. Streptavidin and avidin recognize peptide ligands with different motifs. *Immunomethods*, **1992**, 1, 11-15.

Lam, K.S.; Salmon, S.E.; Hersh, E.M.; Hruby, V.J.; Kazmierski, W.M.; Knapp, R.J. A new type of synthetic peptide library for identifying ligand-binding activity. *Nature*, **1991**, 354, 82-84.

Lam, K.S.; Wu, J.; Lou, Q. Identification and characterization of a novel synthetic peptide substrate specific for Src-family protein tyrosine kinases. *International Journal of Peptide and Protein Research,* **1995**, 45 (6), 587- 592.

Lancaster, L.; Kiel, M.C.; Kaji, A.; Noller, H.F Orientation of ribosome recycling factor in the ribosome from directed hydroxyl radical probing. *Cell*, **2002**, 111, 129-140.

Latham, J.A.; Cech, T.R. Defining the inside and outside of a catalytic RNA molecule. *Science,* **1989**, 245, 276-282.

Lau, D. H.; Guo, L.; Liu, R.; Song, A.; Shao, C.; Lam, K.S. Identifying peptide ligands for cell surface receptors using cell-growth-on-bead assay and one-bead one-compound combinatorial library. *Biotechnology Letters*, **2002**, 24, 497-500.

Lazinski, D.; Grzadzielska, E.; Das, A. Sequence-specific recognition of RNA hairpins by bacteriophage antiterminators requires a conserved arginine-rich motif. *Cell*, **1989**, 59, 207-218.

Legault, P.; Li, J.; Mogridge, J.; Kay, L.E.; Greenblatt, J. NMR Structure of the bacteriophage*l*N peptide/*boxB* RNA complex: recognition of a GNRA fold by an arginine-rich motif. *Cell*, **1998**, 93, 289-299.

Leontis, N.B.; Lescoute, A.; Westhof, E. The building blocks and motifs of RNA architecture. *Current Opinion in Structural Biology*, **2006b**, 16, 279–287.

Lescoute, A.; Westhof, E. The A-minor motifs in the decoding recognition process. *Biochimie*, **2006**, 88, 993-999.

Levy, S.B. The challenge of antibiotic resistance *Scientific American*, **1998**, 278, 46-53.

Levy, S.B. Balancing the drug-resistance equation. *Trends in Microbiology*, **1994**, 2, 341-342.

Levy. S.B. Microbial resistance to antibiotics. An evolving and persistent problem. *Lancet*, **1982**, 2, 83-88.

Liiv, A., Karitkina, D., Maivali, U., Remme, J. Analysis of the function of *E. coli* 23 S rRNA helix-loop 69 by mutagenesis. *BMC Molecular Biology*, **2005**, 6, 18.

Lim, H.K.; Hsieh, Y.I.; Ganem, B.; Henion, J. Recognition of cell-wall peptide ligands by vancomycin group antibiotics-studies using ion-spray mass spectroscopy. *Journal of Mass Spectrometry*, **1995**, 30, 708-714.

Lind, K.E.; Du, Z.; Fujinaga, K.; Peterlin, B.M.; James, T.L. Structure-based computational database screening, in vitro assay, and NMR assessment of compounds that target TAR RNA. *Chemistry & Biology*, **2002**, 9, 185-193.

Lipovsek, D.; Plückthun, A. *In-vitro* protein evolution by ribosome display and mRNA display. *Journal of Immunological Methods*, **2004**, 1-2, 51-67.

Litovchick, A.; Evdokimov, A.G.; Lapidot, A. Aminoglycoside−arginine conjugates that bind TAR RNA: synthesis, characterization, and antiviral activity. *Biochemistry*, **2000**, 39, 2838-2852.

Litovchick, A.; Evdokimov, A.G.; Lapidot, A. Arginine-aminoglycoside conjugates that bind to HIV transactivation responsive element RNA in vitro. *FEBS Letters*, **1999**, 445, 73-79.

Liu, G.; Bryant, R.T.; Hilderman, R.H. Isolation of a tripeptide from a random phage peptide library that inhibits P1, P4-diadenosine 50-tetraphosphate binding to its receptor. *Biochemistry,* **1996**, 35, 197-201.

Liu, Q.; Rand, T.A.; Du Kalidas, S.F.; Kim, H-E.; Smith, D.P.; Wang, X. R2Dr, a bridge between the initiation and effector steps of the Drosophila RNAi pathway. *Science*, **2003**, 301, 1921-1925.

Llano-Sotelo, B.; Azucena, E.F.; Jr, Kotra, L.P.; Mobashery, S.; Chow, C.S. Aminoglycosides modified by resistance enzymes display diminished binding to the bacterial ribosomal aminoacyl-tRNA site. *Chemistry & Biology,* **2002**, 9, 455-463

Llano-Sotelo, B.; Chow, C.S. RNA-aminoglycoside antibiotic interactions: Fluorescence detection of binding and conformational change. *Bioorganic & Medicinal Chemistry Letters*, **1999**, 9 (2), 213-216.

Loo, J. A., Sannes-Lowery, K. A., Hu, P., Mack, D. P., and Mei, H.-Y. Studying noncovalent protein–RNA interactions and drug binding by electrospray ionization mass spectrometry. *NATO ASI Series C,* **1998**, 510, 83-99.

Loo, J.A. Electrospray ionization for mass spectroscopy: a technology for studying noncovalent macromolocular complexes. *International Journal of Mass Spectrometry*, **2000**, 200, 175-186.

Loo, J.A. Studying noncovalent protein complexes by electrospray ionization mass spectrometry. *Mass Spectrometry Reviews*, **2000**, 16, 1-23.

Loo, J.A.; Holler, T.P.; Foltin, S.K.; McConnell, P.; Banotai, C.A.; Horne, N.M.; Mueller, W.T.; Stevenson, T.I.; Mack, D.P. Application of electrospray ionization mass

spectrometry for studying human immunodeficiency virus protein complexes. *Proteins: Structure, Function, Bioinformatics*, **1998**, 2, 33 (S2), 28-37.

Loo, J.A.; Loo, R.R.O.; Udseth, H.R.; Edmonds, C.G.; Smith, R.D. Solvent-induced conformational changes of polypeptides probed by electrospray-ionization mass spectrometry. *Rapid Communications in Mass Spectrometry*, **1991**, 5, 101-105.

Loo, J.A.; Peifeng, H.; McConnell, P.; Mueller, W.T.; Sawyer, T.K.; Thanabal, V. A study of Src SH2 domain protein-phosphopeptide binding interactions by electrospray ionization mass spectrometry. *Journal of the American Society for Mass Spectrometry*, **1997**, 8, 234-243.

Lowman, H.B. Bacteriophage display and discovery of peptide leads for drug development. *Annual Review of Biophysics & Biomolecular Structure*, **1997**, 26, 401-24.

Lowman, H.B.; Bass, S.H.; Simpson, N.; Wells, J.A. Selecting high-affinity binding proteins by monovalent phage display. *Biochemistry*, **1991**, 30, 10832-38.

Lu, D.; Searles, M.A.; Klug, A. Crystal structure of a zinc-finger-RNA complex reveals two modes of molecular recognition. *Nature*, **2003**, 426, 96-100.

Lynch, S.R.; Gonzalez, R.L.; Puglisi, J.D. Comparison of X-Ray crystal structure of the 30S subunit-antibiotic complex with NMR structure of decoding site oligonucleotide-paromomycin complex. *Structure*, **2003**, 11, 43-53.

Maitra, U.; Stringer, E.A.; Chaudhuri, A. Initiation factors in protein synthesis. *Annual Review of Biochemistry,* **1982**, 51, 869-900.

Maivali, U.; Remme, J. Definition of bases in 23 S rRNA essential for ribosomal subunit association. *RNA*, **2004**, 10, 600-604.

Malhotra, A.; Harvey, S. C. A quantitative model of the *Escherichia coli* 16 S RNA in the 30 S ribosomal subunit. *Journal of Molecular Biology,* **1994***,* 240, 308-340.

Malmborg, A.C.; Duenas, M.; Ohlin, M.; Soderlind, E.; Borrebaeck, C.A. Selection of binders from phage displayed antibody libraries using the BIAcore biosensor. *Journal of Immunological Methods*, **1996**,198, 51-7.

Marks, J.D.; Hoogenboom, H.R.; Bonnert, T.P.; McCafferty, J.; Griffiths, A.D.; Winter, G. By-passing immunization. Human antibodies from V-gene libraries displayed on phage. *Journal of Molecular Biology*, **1991**, 222, 581-97.

Maruyama, K.; Sato, N.; Ohta, N. Conservation of structure and cold-regulation of RNA-binding proteins in cyanobacteria: probable convergent evolution with eukaryotic glycine-rich RNA-binding proteins. *Nucleic Acids Research*, **1999**, 27, 2029-2036.

Marvin, D.A. Filamentous phage structure, infection and assembly. *Current Opinion in Structural Biology*, **1998**, 8, 150-158.

Mattaj, I.W. RNA recognition: a family matter? *Cell*, **1993**, 73, 837-840.

Mattick, S.J.; Makunin, I.V. Non-coding RNA. *Human Molecular Genetics*, **2006**, 15, R17-R29.

Mazza, C.; Segref, A.; Mattaj, I.W.; Cusack, S. Large-scale induced fit recognition of an m(7)GpppG cap analogue by the human nuclear cap-binding complex. *EMBO Journal*, **2002**, 21, 5548-5557.

McAlpine, S.R.; Schreiber, S.L. Visualizing functional group distribution in solid-support beads by using optical analysis. *Chemistry European Journal*, **1999**, 5, 3528-3532.

McCutcheon, J.P.; Agrawal, R.K.; Philips, S.M.; Grassucci, R.A.; Gerchman, S.E.; Clemons, W.M.; Ramakrishnan, V.; Frank.J. Location of translational initiation factor IF3 on the small ribosomal subunit. *Proceedings of the National Academy of Science USA*, **1999**, 96, 4301-4306.

McDowell, R.S.; Blackburn, B.K.; Gadek, T.R.; McGee, L.R.; Rawson, T., et al. From peptide to non-peptide: 2. the de novo design of potent, non-peptidal inhibitors of platelet aggregation based on a benzodiazepinedione scaffold. *Journal of American Chemical Society,* **1994**,116, 5077-83.

McLafferty, F.W.; Aaserud, D.J.; Guan, Z.; Little, D.P.; Kelleher, N.L. Double stranded DNA sequencing by tandem mass spectrometry. *International Journal of Mass Spectrometry*, **1997**, 165/166, 457-466.

Mead, D.A.; Kemper, B. Chimeric single-stranded DNA phage-plasmid cloning vectors. *Biotechnology,* **1988**, 10, 85-102.

Mei, H-Y.; Cui,M.; Heldsinger, A.; Lemrow, S.M.; Loo, J.A.; Sannes-Lowry, K.A.; Sharmeen, L.; Czarnik, A.W. Inhibitors of protein-RNA complexation that target the RNA: specific recognition of human immunodeficiency virus type 1 TAR RNA by small organic molecules. *Biochemistry*, **1998**, 37 (40), 14204-14212.

Meroueh, M.; Grohar, P. J.; Qiu, J.; SantaLucia, J., Jr.; Scaringe, S. A.; Chow, C. S. Unique structural and stabilizing roles for the individual pseudouridine residues in the 1920 region of *Escherichia coli* 23 S rRNA. *Nucleic Acids Research*, **2000**, *28*, 2075-2083.

Merryman, C.; Moazed, D.; Daubresse, G.; Noller, H.F. Nucleotides in 23 S rRNA protected by the association of 30 S and 50 S ribosomal subunits. *Journal of Molecular Biology*, **1999**, 285, 107-113.

Milman, G., Goldstein, J., Scolnick, E., Caskey, T. Peptide chain termination: III. Stimulation of in vitro termination. *Proceedings of the National Academy of Science USA*, **1969**, 63, 183-190.

Mingeot-Leclercq, M.; Glupczynski, Y.; Tulkens, P.M. Aminoglycosides: activity and resistance. *Antimicrobial Agents and Chemotherapy*, **1999**, 43(4), 727-737.

Mitchell, P.; Osswald, M.; Brimacombe, R. Identification of intermolecular RNA cross-links at the subunit interface of the *Escherichia coli* ribosome. *Biochemistry,* **1992**, 31, 3004-3011.

Mitzutani, M., Tomioka, N., and Itai, A. Rational automatic search method for stable docking models of protein and ligand. *Journal of Molecular Biology*, **1994**, *243*, 310-326.

Mizushima, S.; Nomura, M. Assembly mapping of 30 S ribosomal proteins from *E. coli. Nature,* **1970**, 226, 1214-1218.

Moazed, D.; Noller, H. F. Interaction of antibiotics with functional sites in16 S ribosomal RNA. *Nature*, **1987**, 327, 389-394.

Moore, P.B. The three-dimensional structure of the ribosome and its components. *Annual Review of Biophysics and Biomolecular Structure*, **1998,** 27, 35-58.

Mucha, P.; Szyk, A.; Rekowski, P.; Weiss, P.A.; Agris, P.F. Anticodon domain methylated nucleosides of yeast tRNAPhe are significant recognition

determinants in the binding of a phage display selected peptide. *Biochemistry*, **2001**, 40, 14191-14199.

Mujeeb, A.; Bishop, K.; Peterlin, B.M.; Turck, C.; Parslow, T.G.; James, T.L. NMR structure of a biologically active peptide containing the RNA-binding domain of human immunodeficiency virus type 1 Tat. *Proceedings of the National Academy of Sciences USA,* **1994,** 91(17), 8248-8252.

Murray, C.B.; Norris, D.J.; Bawendi, Synthesis and characterization of nearly monodisperse CdE (E = sulfur, selenium, tellurium) semiconductor nanocrystallites*. Journal of American Chemical Society,* **1993**, 115, 8706-8715.

Nagano, K.; Harel, M.; Takezawa, M. Prediction of three dimensional structure of *E. coli* ribosomal RNA. *Journal of Theoretical Biology*, **1988**,134, 199-256.

Nakamura, Y.; Ito, K.; Ehrenberg, M. Mimicry grasps reality in translation termination. *Cell*, **2000**, 101, 349-352.

Nakamura, Y.; Uno,. M.; Toyoda, T.; Fujiwara, T.; Ito, K. Protein tRNA mimicry in translation termination. *The Ribosome Cold Spring Harbor Symposia in Quantitative Biology Volume LXVI*, **2001**, Cold Spring Harbor Laboratory Press, Cold Spring Harbor, 469-475.

Nakayama, G.R.; Valkirs, G.; McGrath, D.; Husea, W.D. Improving the copy numbers of antibody fragments expressed on the major coat protein of bacteriophage M13. *Journal of Molecular Biology*, **1996**, 2, 197-207.

Nandi, S.; Maurer, J.J.; Hofacre, C.; Summers, A.O. Gram-positive bacteria are a major reservoir of Class 1 antibiotic resistance integrons in poultry litter. *Proceedings of the National Academy of Science USA*, **2004**, 101(18), 7118-7122.

Nelson, M.L., Park, B.H.; Levy, S.B. Molecular requirement for the inhibition of the tetracycline antiport protein and the effect of potent inhibitors on the growth of tetracycline-resistant bacteria. *Journal of Medicinal Chemistry,* **1994**, 37, 1355-1361.

Nesatyy, V.J. Mass spectrometry evaluation of the solution and gas-phase binding properties of noncovalent protein complexes. *International Journal of Mass Spectrometry*, **2002**, 221, 147-161.

Nissen, P.; Hansen, J.; Ban, N.; Moore, P.B.; Steitz, T.A. The structural basis of ribosome activity in peptide bond synthesis. *Science*, **2000**, 289, 920-930.

Nissen, P.; Ippolito, J.A.; Ban, N.; Moore, P.B.; Steitz, T.A. RNA tertiary interactions in the large ribosomal subunit: The A-minor motif. *Proceedings of the National Academy of Science USA*, **2001**, 98, 4899-4903.

Noll, M.; Noll, H. Structural dynamics of bacterial ribosomes : V. Magnesium-dependent dissociation of tight couples into subunits: Measurements of dissociation constants and exchange rates. *Journal of Molecular Biology*, **1976**, 105, 111-127.

Noller, H.F.; Kop, J.; Wheaton, V.; Brosius, J.; Gutell, R.R.; Kopylov, A.M.; Dohme, F.; Herr, W.; Stahl, D.A.; Gupta, R.; Waese, C.R. Secondary structure model for 23 S ribosomal RNA. *Nucleic Acids Research*, **1981**, 9(22), 6167-89.

Nord, K.; Gunneriusson, E.; Ringdahl. J.; Stahl, S.; Uhlen, M.; Nygren, P Binding proteins selected from combinatorial libraries of an α-helical bacterial receptor domain. *Nature Biotechnology*, **1997**, 15, 772-777.

Nordhoff, E.; Kirpeker, F.; Roepstorff, P. Mass spectrometry of nucleic acids. *Mass Spectrometry Reviews*, **1996**, 15, 67-138.

O'Connor, M.; Dahlberg, A.E. The involvement of two distinct regions of 23 S ribosomal RNA in tRNA selection. *Journal of Molecular Biology*, **1995**, 254, 838-847.

Oberstrass, F.C.; Auweter, S.D.; Erat, M.; Hargous, Y.; Henning, A.; Wenter, P.; Reymond, L.; Amir-Ahmady, B.; Pitsch, S.; Black, D.L. et al. Structure of PTB bound to RNA: specific binding and implications for splicing regulation. *Science*, **2005**, 309, 2054-2057.

O'Brien, W.A.; Sumner-Smith, M.; Mao, S.H.; Sadeghi, S.; Zhao, J.Q.; Chen, I.S. Anti-human immunodeficiency virus type 1 activity of an oligocationic compound mediated via gp120 V3 interactions. *The Journal of Virology*, **1996**, 70, 2825-2831.

Ogle, J.M.; Brodersen, D.E.; Clemons, W.M.; Tarry, M.J.; A.P. Carter, A.P.; Ramakrishnan, V. Recognition of cognate transfer RNA by the 30 S ribosomal subunit. *Science*, **2001**, 292**,** 897-902.

Ogle, J.M.; Murphy, F.V.; Tarry, M.J.; Ramakrishnan, V. Selection of tRNA by the ribosome requires a transition from an open to a closed form. *Cell*, **2002**, 111, 721-732.

Ogle, J.M.; Ramakrishnan, V. Structural insights into translational fidelity. *Annual Review of Biochemistry*, **2005**, 74, 129-177.

Okeke, I.N.; Lamikanra, A.; Edelman, R. Socioeconomic and behavioral factors leading to acquired bacterial resistance to antibiotics in developing countries. *Emerging Infectious Diseases*, **1999**, 5, 18-25.

Ortiz-Meoz, R.F.; Green, R. Functional elucidation of a key contact between tRNA and the large ribosomal subunit rRNA during decoding. *RNA*, **2010**, 16,

Osborne, S.E.; Ellington, A.E. Nucleic acid selection and the challenge of combinatorial chemistry. *Chemical Reviews*, **1997**, *97* (2), 349-370.

Overbye, K.M.; Barrett, J.F. Antibiotics: Where did we go wrong? *Drug Discovery Today*, **2005**, 10 (1), 45-52.

Pai, R.D.; Zhang, W.; Schuwirth, B.S.; Hirokawa, G.; Kaji, H.; Kaji, A.; Cate, J.H.D. Structural insights into ribosome recycling factor interactions with the 70 S ribosome. *Journal of Molecular Biology*, **2008**, 376, 1334-1347.

Park, S.I.; Renil, M.; Vikstrom, B.; Amro, N.; Song, L.; Xu, B.; Kit S. Lam, K.S. The use of one-bead one-compound combinatorial library method to identify peptide ligands for α4β1 integrin receptor in non-Hodgkin's lymphoma. *Letters in Peptide Science*, **2001**, 8, 171-178.

Patel, R.C.; Sen, G.C. Identification of the doublestranded RNA-binding domain of the human interferon-inducible protein kinase. *Journal of Biological Chemistry*, **1992**, 267, 7671-7676.

Pattabiraman, S. On-bead screening of RNA-binding ligands *Wayne State University, Detroit, MI*, **2006**.

Pavletich, N.P.; Pabo, C.O. Zinc finger-DNA recognition: crystal structure of a Zif268-DNA complex at 2.1 Å. *Science*, **1991**, 252, 809-817.

Peattie, D.A. Direct chemical method for sequencing RNA. *Proceedings of the National Academy of Sciences USA*, **1979**, 76, 1760-1764.

Pelham, H.; Brown, D. A specific transcription factor that can bind to either the 5 S RNA gene or 5 S RNA. *Proceedings of the National Academy of Sciences USA*, **1980**, 77, 4170-4174.

Peske, F.; Rodnina, M.V.; Wintermeyer, W. Sequence of steps in ribosome recycling defined by kinetic analysis. *Molecular Cell*, **2005**, 18, 403-412.

Petry, S.; Brodersen, D.E.; Murphy, F.V.; Dunham, C.M.; Selmer, M.; Tarry, M.J.; Kelley, A.C.; Ramakrishnan, V. Crystal structure of the ribosome in complex with release factors RF1 and RF2 bound to a cognate stop codon. *Cell*, **2005**, 123, 1255-1266.

Pfeifer, R.J.; Hendricks, C.D Parametric studies of electrohydrodynamic spraying. *American Institute of Aeronautics and Astronautics,* **1968**, 6, 496.

Phelps, C.E Bug/drug resistance. Sometimes less is more. *Medical Care*, **1989**, 27, 194-203.

Pillutla, R.C. et al. Peptides identify the critical hotspots involved in the biological activation of the insulin receptor. *Journal of Biological Chemistry*, **2002**, 277, 22590-22594.

Pinard, R.; Payant, C.; Melancon, P.; Brakier-Gingras, L. The 5' proximal helix of 16 S rRNA is involved in the binding of streptomycin to the ribosome. *FASEB Journal*, **1993**, 7, 173-176.

Pinilla, C.; Appel, J.R.; Houghten, R.A. Investigation of antigen-antibody interactions using a soluble, non-support-bound synthetic decapeptide library composed of four trillion (4 x 10(12)) sequences. *Biochemical Journal*, **1994**, 301(Pt 3), 847–853.

Pioletti, M.; Schlünzen, F.; Harms, J.; Zarivach, R.; Glühmann, M.; Avila, H.; Bashan, A.; Bartels, H.; Auerbach, T.; Jacobi, C. et al. Crystal structures of complexes of the

small ribosomal subunit with tetracycline, edeine and IF3. *The EMBO Journal*, **2001**, 20, 1829-1839.

Pleij, C.W.A.; Rietveld, K.; Bosch, L. A new principle of RNA folding based on pseudoknotting. *Nucleic Acids Research,* **1985**, 13, 1717-1731.

Poehlsgaard, J.; Douthwaite, S. The bacterial ribosome as a target for antibiotics. *Nature Reviews Microbiology*, **2005**, 3(11), 870-881.

Poulsen, S.M.; Kofoed, C.; Vester, B. Inhibition of the ribosomal transferase reaction by the mycarose moiety of the antibiotics carbomycin, spiramycin and tylosin. *Journal Molecular Biology*, **2000**, 304, 471-481.

Prammananan, T.; Sander, P.; Brown, B.A.; Frischkorn, K.; Onyi, G.O.; Zhang, Y.; Böttger, E.C.; Wallace, Jr. R.J. A single 16 S ribosomal RNA substitution is responsible for resistance to amikacin and other 2-deoxystreptamine aminoglycosides in *Mycobacterium abscessus* and *Mycobacterium chelonae. The Journal of Infectious Diseases*, **1998**, 177, 1573-81.

Price, S.R.; Evans, P.R.; Nagai, K Crystal structure of the spliceosomal U2B"-U2A' protein complex bound to a fragment of U2 small nuclear RNA. *Nature*, **1998**, 394, 645-650.

Puglisi, J.D.; Chen, L.; Blanchard, S.; Frankel, A.D. Solution structure of a bovine immunodeficiency virus Tat-TAR peptide-RNA complex. *Science*, **1995**, 270, 1200-1203.

Pyle, A.M.; McSwiggen, J.A.; Cech, T.R. Direct measurement of oligonucleotide substrate binding to wild-type and mutant ribozymes from Tetrahymena. *Proceedings of the National Academy of Science USA,* **1990**, 87, 8187-8191.

Quarrell, R.; Claridge, T.D.W.; Weaver, G.W.; Lowe, G. Structure and properties of TentaGel resin beads: Implications for combinatorial library chemistry. *Molecular Diversity*, **1996**, 1, 223-232.

Quarrell, R.; Claridge, T.D.W.; Weaver, G.W.; Lowe, G. Structure and properties of Tentagel resin beads: Implications for combinatorial library chemistry. *Molecular Diversity*, **1995**, 1, 223-232.

Quattro LC User's guide. 2nd ed.; Micromass UK Limited, United Kingdom.

Ramos, A.; Grunert, S.; Adams, J.; Micklem, D.R.; Proctor, M.R.; Freund, S.; Bycroft, M.; St Johnston, D.; Varani, G. RNA recognition by a Staufen double-stranded RNA-binding domain. *EMBO Journal*, **2000**, 19, 997-1009.

Rawat, U.B.S.; Zavialov, A.V.; Sengupta, J.; Valle, M.; Grassucci, R.A.; Linde, J.; Vestergaard, B.; Ehrenberg, M.; Frank, J. A cryo-electron microscopic study of ribosome-bound termination factor RF2. *Nature*, **2003**, 421, 87-90.

Raychaudhuri, S.; Conrad, J.; Hall, B.G.; Ofengand, J. A pseudouridine synthase required for the formation of two universally conserved pseudouridines in ribosomal RNA is essential for normal growth of *Escherichia coli. RNA*, **1998**, 4, 1407–1417.

Raychaudhuri, S.; Conrad, J.; Hall, B.G.; Ofengand, J. A pseudouridine synthase required for the formation of two universally conserved pseudouridines in ribosomal RNA is essential for normal growth of *Escherichia coli*. *RNA*, **1998**, 4, 1407-1417.

Richter, S.; Cao, H.; Rana, T.M. Specific HIV-1 TAR RNA loop sequence and functional groups are required for human cyclin T1−Tat−TAR ternary complex formation. *Biochemistry*, **2002**, 41, 6391-6397.

Roberts, N.A.; Martin, J.A.; Kinchington, D.; Broadhurst, A.V.; Craig, J.C.; Duncan, I.B.; Galpin, S.A.; Handa, B.K.; Kay, J.; Krohn, A. and et al. Rational design of peptide-based HIV proteinase inhibitors. *Science*, **1990**, 248, 358-361.

Rodgers, M.T.; Campbell, S.; Marzluff, E.M.; Beauchamp, J.L. Site-specific protonation directs low-energy dissociation pathways of dinucleotides in the gas phase. *International Journal of Mass Spectrometry* and *Ion Processes*, **1995**, 148, 1-23.

Rodnina, M.V.; Savelsbergh, A.; Katunin, V.I.; Wintermeyer, W. Hydrolysis of GTP by elongation factor G drives tRNA movement on the ribosome. *Nature*, **1997**, 385, 37-41.

Rodnina, M.V.; Wintermeyer, W. Fidelity of a aminoacyl-tRNA selection on the ribosome: Kinetic and structural mechanisms. *Annual Review of Biochemistry*, **2001**, 70, 415-435.

Romano, P.R.; Zhang, F.; Tan, S-L.; Garcia-Barrio, M.T.; Katze, M.G.; Dever, T.E.; Hinnebusch, A.G. Inhibition of double-stranded RNA-dependent protein kinase PKR by vaccine virus E3: Role of complex formation and the E3 N-terminal domain. *Molecular and Cellular Biology*, **1998**, 18, 7304-7316.

Rostom, A.A.; Fucini, P.; Benjamin, D.R.; Juenemann, R.; Nierhaus, K.H.; Hartl, F.U.; Dobson, C.M.; Robinson, C.V Detection and selective dissociation of intact ribosomes in a mass spectrometer. *Proceedings of National Academy of Sciences USA,* **1999**, 97, 5185-5190.

Rosu, F.; Gabelica, V.; Houssier, C.; Pauw, E.D. Determination of affinity, stoichiometry and sequence selectivity of minor groove binder complexes with double-stranded oligodeoxynucleotides by electrospray ionization mass spectrometry. *Nucleic Acids Research*, **2002**, 30(16), e82.

Roy, S.; Delling, U.; Chen, C.H. et al. A bulge structure in HIV-1 TAR RNA is required for tat binding and tat-mediated trans-activation. *Genes & Development*, **1990**, 4, 1365-1373.

Rubin, R.J.; Harrington, C.A.; Poon, A.; Dietrich, K.; Greene, J.A.; Moiduddin. A. The economic impact of *Staphylococcus aureus* infection in New York City hospitals. *Emerging Infectious Diseases,* **1999**, 5(1), 9-17.

Russel M. Moving through the membrane with filamentous phages. *Trends in Microbiology,* **1995**, 3, 223-8.

Russell, R.J.; Murray, J.B.; Lentzen, G.; Haddad, J.; Mobashery, S. The complex of a designer antibiotic with a model aminoacyl site of the 30 S ribosomal subunit revealed by X-ray crystallography. *Journal of American Chemical Society*, **2003**, 125, 3410-1.

Ryter, J.M.; Schultz, S.C. Molecular basis of double-stranded RNA–protein interactions: structure of a dsRNA-binding domain complexed with dsRNA. *EMBO Journal,* **1998**, 17, 7505-7513.

Sannes-Lowery, K.A.; Mei, H.-Y.; Loo, J.A. Studying aminoglycoside antibiotic binding to HIV-1 TAR RNA by electrospray Ionization mass spectrometry. *International Journal of Mass Spectrometry*, **1999**, 193, 115-122.

Sannes-Lowry, K.A.; Griffey, R.H.; Hofstadler, S.A. Measuring dissociation constants of RNA and aminoglycoside antibiotics by electrospray ionization mass spectroscopy. *Analytical Biochemistry*, **2000**, 280, 264-271.

Sannes-Lowry, K.A.; Griffey, R.H.; Hofstadler, S.A. Measuring dissociation constants of RNA and aminoglycoside antibiotics by electrospray ionization mass spectroscopy. *Analytical Biochemistry*, **2000**, 280, 264-271.

Sannes-Lowry, K.A.; Hu, P.; Mack, D.P.; Mei, H.-Y.; Loo, J.A. HIV-1 Tat Peptide Binding to TAR RNA by electrospray Ionization mass spectrometry. *Analytical Chemistry*, **1997**, 69, 5130-5135.

Scaringe, S.A.; Wincott, F.E.; Caruthers, M.H. Novel RNA synthesis method using 5‘-*O*-Silyl-2‘-*O*-orthoester protecting groups. *Journal of American Chemical Society*, **1998**, 120, 11820-11821.

Scaringe, S.A.; Wincott, F.E.; Caruthers, M.H. Novel RNA synthesis method using 5'-o-silyl-2'-o-orthoester protecting groups. *Journal of American Chemical Society*, **1998**,120, 11820-11821.

Scheunemann, A.E.; Graham, W.D.; Vendeix, F.A.P.; Paul F. Agris, P.F. Binding of aminoglycoside antibiotics to helix 69 of 23 S rRNA. *Nucleic Acids Research,* **2010**, 38, 3094-3105.

Schluenzen, F. et al. Structure of functionally activated small ribosomal subunit at 3.3 angstroms resolution. *Cell*, **2000**, 102(5), 615-623.

Schluenzen, F.; Pyetan, E.; Yonath, A.; Harms, J. Inhibition of peptide bond formation by pleuromutilins: the structure of the 50 S ribosomal subunit from *Deinococcus radiodurans* in complex with tiamulin. *Molecular Microbiology,* **2004**, 54, 1287-94.

Schluenzen, F.; Zarivach, R.; Harms, J.; Bashan, A.; Tocilj, A. et al. Structural basis for the interaction of antibiotics with the peptidyl transferase centre in eubacteria. *Nature,* **2001**,413, 814-21.

Schlünzen, F.; Wilson, D.N.; Tian, P.; Harms, J.M; McInnes, S.J.; Hansen, H.A.S.; Albrecht, R.; Buerger, J.; Wilbanks, S.M.; Fucini, P. The binding mode of the trigger factor on the ribosome: implications for protein folding and SRP interaction. *Structure (Camb)*, **2005**, 13(11), 1685-1694.

Schmeing, T.M.; Ramakrishnan, V. What recent ribosome structures have revealed about the mechanism of translation. *Nature*, **2009**, 461, 1234-1242.

Schrag, S.J.; McGee, L.; Whitney, C.G.; Beall, B.; Craig, A.S.; Choate, M.E.; Jorgensen, J.H.; Facklam, R.R.; Klugman, K.P. Emergence of *Streptococcus pneumoniae* with very-high-level resistance to penicillin. *Antimicrobial Agents and Chemotherapy,* **2004**, 48, 3016-3023.

Schuwirth, B.S. et al. Structures of the bacterial ribosome at 3.5 Å resolution. *Science*, **2005**, 310(5749), 827-834.

Schweizer, H.P. Efflux as a mechanism of resistance to antimicrobials in *Pseudomonas aeruginosa* and related bacteria: unanswered questions. *Genetics and Molecular Research,* **2003**, 2 (1), 48-62.

Selmer, M.; Dunham, C.M.; Murphy, F.V.; Weixlbaumer, A.; Petry, S.; Kelley, A.C.; Weir, J.R.; Ramakrishnan, V. Structure of the 70 *S* ribosome complexed with mRNA and tRNA. *Science*, **2006**, 313, 1935-1942.

Shah, K.; Neenhold, H.; Wang, Z.; Rana, T.M. Incorporation of an artificial protease and nuclease at the HIV-1 tat binding site of trans-activation responsive RNA. *Bioconjugate Chemistry*, **1996**, 7, 283-289.

Shelimov, K.B.; Clemmer, D.E.; Hudgins, R.R.; Jarrold, M.F. Protein structure *in vacuo*: gas-phase conformations of BPTI and cytochrome *c*. *Journal of American Chemical Society*, **1997**, 119, 2240-2248.

Sidhu, S.S.; Lowman, H.B.; Cunningham, B.C.; Wells, J.A. Phage display for selection of novel binding peptides. *Methods in Enzymology*, **2000**, 328,333-363.

Sidhu, S.S.; Weiss, G.A.; Wells, J.A. High copy display of large proteins on phage for functional selections. *Journal of Molecular Biology*, **2000**, 296, 487-495.

Simon, R.J.; Kania, R.S.; Zuckermann, R.N.; Huebner, V.D.; Jewell, D.A.; Banville, S.; Ng, S.; Wang, L.; Rosenberg, S.; Marlowe, C.K *et al.* Peptoids: a modular approach to drug discovery. *Proceedings of National Academy of Sciences USA*, **1992**, 89, 9367-9371.

Siuzdak, G. The emergence of mass spectrometry in biochemical research. *Proceedings of National Academy of Sciences USA*, **1994**, 91, 11290-11297.

Siuzdak, G.; Bothner, B.; Yeager, M.; Brugkdou, C.; Faquet, C. M.; Hoey,K.; Chang, C. M. Mass spectrometry and viral analysis. *Chemistry & Biology*, **1996,** 3, 45-48.

Sivaraman, J; Iannuzzi, P.; Cygler, M.; Matte, A crystal structure of the RluD pseudouridine synthase catalytic module, an enzyme that modifies 23 S rRNA and is essential for normal cell growth of *Escherichia coli. Journal of Molecular Biology*, **2004**, 335, 87-101.

Smith, G.P. Filamentous fusion phage: Novel expression vectors that display cloned antigens on the virion surface. *Science*, **1985**, 228, 1315-1317.

Smith, G.P. Surface presentation of protein epitopes using bacteriophage expression systems. *Current Opinion in Biotechnology*, **1991**, 2, 668-673.

Smith, G.P.; Petrenko, V.A. Phage display. *Chemical Reviews*, **1997**, 97(2), 391-410.

Smith, G.P.; Scott, J.K. Libraries of peptides and proteins displayed on filamentous phage. *Methods in Enzymology,* **1993**, 217:228-257.

Smith, R.D.; Bruce, J.E.; Wu, Q.Y.; Lei, Q.P. New mass spectrometric methods for the study of noncovalent associations of biopolymers. *Chemical Society Reviews*, **1997**, 26, 191-202.

Soukup, G.A.; Breaker, R.R. Relationship between internucleotide linkage geometry and the stability of RNA. *RNA,* **1999**, 5, 1308-1325.

Stark, H. *et al.*; van Heel, M. The 70 S *E. coli* ribosome at 23 Å resolution: fitting the ribosomal RNA. *Structure*, **1995**, 3, 815-821.

Stark, H.; Rodnina, M.V.; Rinke-Appel, J.; Brimacombe, R.; Wintermeyer, W.; Heel, M. Visualization of elongation factor Tu on the *Escherichia coli* ribosome. *Nature*, **1997**, 389, 403-406.

Stefl, R.; Skrisovska, L.; Allain, F.H.T. RNA sequence- and shape-dependent recognition by proteins in the ribonucleoprotein particle. *EMBO reports*, **2005**, 6, 33-38.

Steitz, J.A.; Jakes, K. How ribosomes select initiator regions in mRNA: base pair formation between the 3' terminus of 16 S rRNA and the mRNA during initiation

of protein synthesis in *Escherichia coli. Proceedings of the National Academy of Science USA*, **1975**, 72, 4734-4738.

Stephens, C. & Shapiro, L. Bacterial protein secretion-a target for new antibiotics? *Chemistry & Biology*, **1997**, 4, 637-641.

Stern, S.; Weiser, B.; Noller, H. F. Model for the three-dimensional folding of 16 S ribosomal RNA. *Journal of Molecular Biology, **1988**,* 204, 447-481.

Stover, C. K. *et al.* Complete genome sequence of *Pseudomonas aeruginosa* PA01, an opportunistic pathogen. *Nature,* **2000**, 406, 959-964.

Stubbe, J.; Kozarich, J.W. Mechanisms of bleomycin-induced DNA degradation. *Chemical Reviews,* **1987**, 87, 1107-1136.

Szymański, M.; Barciszewska, M.Z.; Erdmann, V.A.; Barciszewski, J. 5 S rRNA: structure and interactions. *Biochemical Journal*, **2003**, 371(Pt 3), 641-651.

Tabara, H.; Yigit, E.; Siomi, H.; Mello, C.C. The dsRNA-binding protein RDE-4 interacts with RDE-1, DCR-1, and a DExH-box helicase to direct RNAi in *C. elegans*. *Cell*, **2002**, 109, 861-871.

Tan, R.; Chen, L.; Buettner, J.A.; Hudson, D.; Frankel, A.D. RNA recognition by an isolated α-helix. *Cell*, **1993**, 73, 1031-1040.

Tang, L.; Kebarle, P. Dependence of ion intensity in electrospray mass spectrometry on the concentration of the analytes in the electrosprayed solution. *Analytical Chemistry*, **1993**, 65, 3654-3668.

Taylor, G.I. Disintegration of water drops in an electric field. *Proceedings of the Royal Society, London, Ser. A.,* **1964**, 280, 383-397.

Tenson, T.; Mankin, A. Antibiotics and the ribosome. *Molecular Microbiology,* **2006**, 59 (6), 1664-1677.

Tettelin, H.; Nelson, K.E. et al Complete genome sequence of a virulent isolate of *Streptococcus pneumonia. Science*, **2001**, 293, 498-506.

Thomas, J.R; Hergenrother, P.J. Targeting RNA with small molecules. *Chemical Reviews*, **2008**, 108, 1172-1220.

Thomson, B.A.; Iribarne, J.V. Field induced ion evaporation from liquid surfaces at atmospheric pressure. *Journal of Chemical Physics*, **1979**, 71, 4451-4463.

Tito, M.A.; Tars, K.; Valegard, K.; Hajdu, J.; Robinson, C.V. Electrospray time-of-flight mass spectrometry of the intact MS2 virus capsid. *Journal of American Chemical Society*, **2000**, 122, 3550–51.

Trepel, M. et al. In vivo phage display and vascular heterogeneity: implications for targeted medicine. *Current Opinion in Chemical Biology*, **2002**, 6, 399-404.

Tullius, T.D.; Dombroski, B.A. Iron(II) EDTA used to measure the helical twist along any DNA molecule. *Science,* **1985**, 230, 679-681.

Turner J.; Crossley M. Mammalian Kruppel-like transcription factors: more than just a pretty finger. *Trends in Biochemical Sciences*, **1999**, 24, 236-240.

Udaka, K.; Wiesmüller, K.; Kienle, S.; Jung, G.; Walden, P. Tolerance to amino acid variations in peptides binding to the major histocompatibility complex class I protein H-2K^{b}. *Journal of Biological Chemistry*, **1995**, 270**,** 24130-24134.

Vakulenko, S.B.; Mobashery, S. Versatility of aminoglycosides and prospects for their future. *Clinical Microbiology Reviews,* **2003,** 16(3), 430-450.

Valentine, S.J.; Anderson, J.G.; Ellington, A.D.; Clemmer, D.E. Disulfide-Intact and -reduced lysozyme in the gas phase: conformations and pathways of folding and unfolding. *Journal of Phyical Chemistry B*, **1997**, 101, 3891-3900.

Varney, M.; Marzoni, G.; Palmer, C.; Deal, J.; Webber, S.; Welsh, K.; Bacquet, R.; Bartlett, C.; Morse, C.; Booth, C. et al. Crystal structure-based drug design and synthesis of benz[c-d]indole-containing inhibitors of thymidylate synthase. *Journal of Medicinal Chemistry,* **1992**, 35, 663–676.

Vincen, Q.; Westhof, E. Crystal structure of paromomycin docked into the eubacterial ribosomal decoding A site. *Structure*, **2001**, 9, 647-658.

Wan, C.; Guo, X.; Liu, Z.; Liu, S. Studies of the intermolecular DNA triplexes of C^{+}·GC and T·AT triplets by electrospray ionization Fourier-transform ion cyclotron resonance mass spectrometry. *Journal of Mass Spectrometry*, **2008**, 43, 164-172.

Wan, K.X.; Gross, M.L.; Shibue, T. Gas-phase stability of double-stranded oligodeoxynucleotides and their noncovalent complexes with DNA-binding drugs as revealed by collisional activation in an ion trap. *Journal of the American Society for Mass Spectrometry*, **2000**, 11(5), 450-7.

Wang, H.; Dzink-Fox, J.L.; Chen, M.; Levy, S.B. Genetic characterization of highly fluoroquinolone-resistant clinical *Escherichia coli* strains from China: role of acrR mutations. *Antimicrobial Agents and Chemotherapy*, **2001**, 45, 1515-1521.

Wang, L.F. and Yu, M. Epitope identification and discovery using phage display libraries: applications in vaccine development and diagnostics. *Current Drug Targets*, **2004**, 5, 1-15.

Wang, Y.; Hamasaki, K.; Rando, R.R. Specificity of aminoglycoside binding to RNA constructs derived from the 16 S rRNA decoding region and the HIV-RRE activator region. *Biochemistry,* **1997,** 36*,* 768-779.

Wang, Y.; Killian, J.; Hamasaki, K.; Rando, R.R. RNA molecules that specifically and stoichiometrically bind aminoglycoside antibiotics with high affinities. *Biochemistry*, **1996**, 35, 12338-12346.

Watanabe, T.; Fukasawa, T. Episome-mediated transfer of drug resistance in *Enterobacteriaceae* I transfer of resistance factors by conjugation. *The Journal of Bacteriology*,**1961**, 81(5), 669–678.

Watson, J.D.; Crick, F.H., Molecular structure of nucleic acids: a structure for deoxyribose nucleic acid. *Nature*, **1953,** 171, 737-738.

Weeks, K.M.; Ampe, C.; Schultz, S.C.; Steitz, T.A.; Crothers, D.M. Fragments of the HIV-1 Tat protein specifically bind TAR RNA. *Science*, **1990**, 249, 1281-1285.

Weeks, K.M.; Crothers, D.M. RNA recognition by Tat-derived peptides: Interaction in the major groove? *Cell*, **1991**, 66, 577-588.

Weigel, L.M.; Clewell, D.B.; Gill, S.R.; Clark, N.C.; McDougal, L.K.; Flannagan, S.E.; Kolonay, J.F.; Shetty, J.; Killgore, G.E.; Tenover, F.C. Genetic analysis of a high-level vancomycin-resistant isolate of *Staphylococcus aureus. Science* **2003**, 302, 1569-1571.

Weiss, M.A.; Narayana, N. RNA recognition by arginine-rich peptide motifs. *Biopolymers (Nucleic Acid Sciences)*, **1998**, 48, 167-180.

Wendt, S.; McCombie, M.; Daniel, J.; Kienhöfer, A.; Hilvert, D.; Zenobi, R. Quantitative evaluation of noncovalent chorismate mutase-inhibitor binding by ESI-MS. *Journal of the American Society for Mass Spectrometry*, **2003**, 14, 1470-1476.

Westhof, E.; Fritsch, V. RNA folding: beyond Watson–Crick pairs. *Structure*, **2000**, 8, R55-R65.

White, A.R.; Kaye, C.; Poupard, J.; Pypstra, R.; Woodnutt, G.; Wynne, B. Augmentin® (amoxicillin/clavulanate) in the treatment of community-acquired respiratory tract infection: a review of the continuing development of an innovative antimicrobial agent. *Journal of Antimicrobial Chemotherapy,* **2004**, 53, *Suppl. S1*, i3–i20.

Wilkins, M.H.; Stokes, A.R.; Wilson, H.R. Molecular structure of deoxypentose nucleic acids. *Nature*, **1953,** 171, 738-740.

Wilson, D.N., Schluenzen, F., Harms, J.M., Yoshida, T., Ohkubo, T., Albrecht, R., Buerger, J., Kobayashi, Y., and Fucini, P. X-ray crystallography study on ribosome recycling: the mechanism of binding and action of RRF on the 50 S ribosomal subunit. *The EMBO Journal,* **2005**, 24, 251-260.

Wimberley, B.T.; Guymon, R.; McCutcheon, J.P.; White, S.W.; Ramakrishnan, V. A detailed view of a ribosomal active site: the structure of the L11-RNA complex. *Cell*, **1999**, 97, 491-502.

Wimberly, B.T. et al. Structure of the 30S ribosomal subunit. *Nature*, **2000**, 407 (6802), 327-339.

Woese, C.R.; Winkler, S; Gutell, R.R. Architecture of ribosomal RNA: constraints on the sequence of “tetra-loops”. *Proceedings of the National Academy of Science USA,* **1990**, 87**,** 8467-8468.

Wolfe, S.A.; Nekludova, L.; Pabo, C.O. DNA recognition by Cys_2His_2 zinc finger proteins. *Annual Reviews of Biophysics and Biomolecular Structure,* **2000**, 29, 183-212.

Wong, C.H.; Hendrix, M.; Priestley, E.S.; Greenberg, W.A. Specificity of aminoglycoside antibiotics for the A-site of the decoding region of ribosomal RNA. *Chemisty & Biology,* **1998**, 5, 397-406.

Wright, G.D. The antibiotic resistome: the nexus of chemical and genetic diversity. *Nature Reviews Microbiology*, **2007**, 5, 175-186.

Wu, H.; Yang, W.P.; Barbas, III C.F. Building zinc fingers by selection: toward a therapeutic application. *Proceedings of the National Academy of Science USA*, **1995**, 92, 344-48.

Wu, Q.; Gao, D.; Joseph-McCarthy, D.; Sigal, G.B.; Bruce, J.E.; Whitesides, G.M.; Smith, R.D. Carbonic anhydrase-inhibitor binding: from solution to the gas phase. *Journal of American Chemical Society*, **1997**, 119, 1157-1158.

Yarian, C.S.; Basti, M.M.; Cain, R.J.; Ansari, G.; Guenther, R.H.; Sochacka, E.; Czerwinska, G.; Malkiewicz, A.; Agris,P.F Structural and functional roles of the N1- and N3-protons of psi at tRNA's position 39. *Nucleic Acids Research*, **1999**, 27(17), 3543-3549.

Ye**,** X., Kumar, R.A.; J. Patel, D.J. Molecular recognition in the bovine immunodeficiency virus Tat peptide-TAR RNA complex. *Chemistry & Biology*, **1995**, 2, 827-840

Yonath, A. Large facilities and the evolving ribosome, the cellular machine for genetic-code translation. *Journal of Royal Society Interface*, **2009**, 6, S575-S585.

Yonath, A. Ribosomal tolerance and peptide bond formation. *Journal of Biological Chemistry,* **2003**, 384, 1411-1419.

Yonath, A.; Bashan, A. Ribosomal crystallography: initiation, peptide bond formation, and amino acid polymerization are hampered by antibiotics. *Annual Review of Microbiology,* **2004**, 58, 233-251.

Yusupov, M.M.; Yusupova, G.Z.; Baucom, A.; Lieberman, K.; Earnest, T.N.; J. Cate, H.D.; Noller, H.F. Crystal structure of the ribosome at 5.5 Å Resolution. *Science*, **2001**, 292, 883-896.

Zavialov, A.V.; Hauryliuk, V.V.; Ehrenberg, M. Splitting of the posttermination ribosome into subunits by the concerted action of RRF and EF-G. *Molecular Cell*, **2005**, 18, 675-686.

Zucconi, A.; Dente, L.; Santonico, E.; Castagnoli, L; Cesareni,G. Selection of ligands by panning of domain libraries displayed on phage lambda reveals new potential partners of synaptojanin 1. *Journal of Molecular Biology*, **2001**, 307, 1329-1339.

ABSTRACT

ISOLATION AND ANALYSIS OF PEPTIDES BINDING TO HELIX 69 OF *E. coli* 23 S rRNA FROM M13 PHAGE DISPLAY

by

MONINDERPAL KAUR

May 2011

Advisor: Dr. Christine. S. Chow

Major: Chemistry (Biochemistry)

Degree: Doctor of Philosophy

Peptides binding to helix 69 (H69) of domain IV or residues 1906 to1924 of *E. coli* 23 S rRNA were selected from a heptapeptide phage library. An experimental system including biotin labeling of RNA and then affinity selection through multiple rounds was followed. After sequencing phage clones of the fourth round, two peptide sequences dominated the phage pool, STYTSVS and NQVANHQ. The later sequence was a unique sequence that contained an abundance of amino acid residues that are also present in the ribosome recycling factor, RRF, and known to make contacts with H69. The phage-display methodology demonstrated the feasibility of rapid ligand identification, and isolation of small peptides that bind to 23 S rRNA in an effort to discover new RNA-binding motifs that have potential therapeutic applications.

For evaluating the preliminary binding affinity of these peptides with H69, fluorescence assays were applied. For this assay, the fluorescence intensity of NQVANHQ Tentagel beads was observed to be higher than STYTSVS Tentagel beads, indicating that peptide NQVANHQ has a higher affinity for H69 as compared to

STYTSVS. The higher binding of the NQVANHQ peptide was further validated with a more sensitive method known as electrospray ionization (ESI) mass spectroscopy (MS). The apparent dissociation constant (K_d) obtained for H69 and NQVANHQ-NH_2 was in the low micromolar range (11 $\pm$ 1 μM) at pH 7.0 in 150 mM ammonium acetate buffer. This value is comparable to that of aminoglycoside antibiotics binding to the A-site RNA and H69 (1 to 10 μM).

The ESI-MS experiments with H69 variant UUU RNA and peptide NQVANHQ-NH_2 gave a relative dissociation constant (K_d) at 1:1 stoichiometry as 19 $\pm$ 2 μM at pH 7.0. The higher value of K_d for this complex revealed that the presence of pseudouridine residues positively contributes towards binding of this peptide to H69. Consequently, to learn about the role of individual pseudouridines at positions 1911 and 1915 towards binding of the peptide, ESI-MS experiments were performed with two H69 variants, UΨΨ and ΨUΨ. The apparent dissociation constants (K_ds) for the 1:1 complex for these two RNAs decreased by 2.5-fold, suggesting that peptide binding site is located at or near the loop region of H69, which contains the pseudouridines at positions 1911 and 1915. In addition, the effect of pH on the complex formation of H69 and UUU RNA with NQVANHQ-NH_2 was studied at two different values (7.0 and 5.2). There was a three-fold decrease of the apparent dissociation constant for the 1:1 complex of RNA and the peptide, indicating that either protonation of the RNA or the peptide structure influenced this change in binding of the two species.

The specificity of the peptide for H69 was tested with related RNA such as human H69 and unrelated RNAs such as helix 31 and A-site rRNA. The peptide showed three-fold lower affinity for all these RNAs compared to the target H69, suggesting that

the peptide has features that are desirable for developing it as a lead compound for novel antimicrobials.

AUTOBIOGRAPHICAL STATEMENT

MONINDERPAL KAUR

BIRTHDATE AND LOCATION: September 1, 1975 in Punjab, India

EDUCATION:

B.Sc. (Hons.) Chemistry, 1997
Guru Nanak Dev University
Punjab, India

M.Sc. (Hons.) Chemistry, 1999
Guru Nanak Dev University
Punjab, India

Ph.D. Biochemistry, 2011
Wayne State University
Detroit, MI 48202
Dissertation title: "Isolation and analysis of peptides binding to helix 69 of *E. coli* 23 S rRNA from M13 phage display"

PUBLICATIONS:

Kaur, M., Klosi, E., Pattabiraman, S., and Chow, C. S. "Isolation and analysis of peptides binding to helix 69 of *E. coli* 23 S rRNA from M13 phage display" *Manuscript in preparation*